Aerosol Black Carbon Measurements In Fort Collins, Colorado

Lorraine Calame and Jeffrey L. Collett, Jr.

Department of Atmospheric Science
Colorado State University
Fort Collins, CO

March, 1999

Colorado State University

DEPARTMENT OF ATMOSPHERIC SCIENCE

PAPER NO. 677

Aerosol Black Carbon Measurements In Fort Collins, Colorado

Lorraine Calame and Jeffrey L. Collett, Jr.

Department of Atmospheric Science
Colorado State University
Fort Collins, Colorado 80523

March, 1999

ABSTRACT

AEROSOL BLACK CARBON MEASUREMENTS IN FORT COLLINS, COLORADO

Aerosol black carbon concentrations were measured in Fort Collins, a small city in northern Colorado. A Magee Scientific aethalometer was used to obtain real time data. In 1997 a gradual build-up in monthly BC concentrations over the late spring and summer was observed to peak in August and then decline. The number of days featuring high concentrations (> 2000 ng/m^3 for 30 minutes) was also observed to rise and fall with an August peak. The monthly trends in aerosol black carbon concentrations suggest some seasonality. Observations of aerosol black carbon concentrations made during this study reveal monthly mean concentrations that vary from 487 to 1004 ng/m^3. The BC concentration timelines showed there are usually two daily peaks in the data. These peaks usually occur between 0600 – 0800 and 1600 – 2100, hours associated with peak traffic. Concentrations of BC were found to correlate reasonably well with CO concentrations over time scales of up to a week. The covariance in our data set suggests they were emitted from a common set of combustion sources. The results of this study indicate there is little relationship between measured BC concentrations and long range transport patterns, as back-trajectory results indicated that long range transport of air masses from particular regions does not influence whether BC concentrations in Ft. Collins are high or low. The observed BC concentrations tended to decrease with increasing wind speed which is consistent with emissions from a local source that would tend to be diluted at higher wind speeds.

On shorter timescales of minutes to hours, the study revealed the importance of individual sources on BC concentrations. Passages of diesel locomotives near the site were shown to increase BC concentrations on many occasions when local winds were favorable to transporting locomotive emissions to the aerosol sample site. The impact of this source, however, was fairly limited in its duration, with concentration spikes typically lasting only about 10 minutes. Train passage also exerted an indirect effect on BC concentrations, perhaps associated with a period of increased BC emissions by vehicles idled at train crossings. Fires were also shown to influence

BC concentrations during the study. The large fires associated with the July 1997 flood and smaller fires associated with a CSU student riot were observed to increase BC concentrations. The number of fires during the study period, however, was very low. Impacts of two prescribed burns along the Front Range on Ft. Collins BC concentrations were observed to be fairly minor.

Correlation of BC concentrations with "total" particle number concentrations (as measured by a Condensation Nucleus Counter), and number concentrations of particles with diameters greater than 0.3 μm (as measured by a Climet Optical Particle Counter) were extremely weak on long time scales and often weak on time scales as short as a day. This reflected the diverse sources of the aerosols. Some of these were probably primary combustion aerosol (and therefore are likely to correlate with BC), but others were the secondary aerosol fraction of CN or particles larger than 0.3 μm that are not expected to correlate strongly with BC concentrations.

BC concentrations were independent of the diurnal pressure patterns, but were affected by synoptic pressure patterns. Frontal passages were marked by low BC concentrations. BC concentrations were not found to be depressed on summer days featuring precipitation, as the duration of summer thunderstorms is typically too short to scavenge enough aerosol particles to significantly influence the daily average BC concentration. In addition, primary aerosol particles that are generated locally by vehicle emissions would be replenished rapidly in the atmosphere following precipitation.

Absorption coefficients were derived from the aethalometer and the difference between transmissometer and nephelometer data. The monthly mean values ranged from 0.005 - 0.009 km^{-1} for the aethalometer, and 0.036 – 0.038 km^{-1} for the transmissometer and nephelometer. The aethalometer derived absorption coefficients are on the order of 10 – 20% of the absorption coefficients determined from the paired nephelometer and transmissometer measurements, and only 6 – 11% of the total extinction measured by the transmissometer.

ACKNOWLEDGEMENTS

We are grateful to many individuals at CSU for their assistance in the conduct of this work. D. E. Sherman was very helpful in the operation of the aethalometer and other aerosol measurement instruments. This work would not have been possible without him. We thank S. Kreidenweis for her generous loan of the condensation particle counter and many helpful comments. T. McKee, W. Massman, D. Rogers, and P. Demott are acknowledged for their many helpful suggestions.

We thank S. Burns and W. Kotasek of the Colorado Department of Public Health and Environment for permission to use the sampling trailer and for providing air quality data. We thank S. Caplan and B. Woodruff of the Fort Collins Natural Resource Department and Fred Jones of the Fort Collins Traffic Department for providing visibility and train data, respectively. We are also grateful to Magee Scientific Inc. for their loan of a second aethalometer and to A. D. A. Hansen of Magee Scientific for his technical assistance. We thank L. Sherman of Air Resource Specialists Inc. for providing us with transmissometer and nephelomter data and for technical advice.

Finally, we are grateful to Colorado State University and the Atmospheric Science Department for financial support of Lorraine Calame during completion of her M.S. program.

TABLE OF CONTENTS

APPENDICES

LIST OF TABLES

APPENDIX A

APPENDIX C

LIST OF FIGURES

FIGURES IN APPENDICES

1. Background

The atmosphere interacts both with incoming as well as outgoing light. Two main processes take place: light scattering and light absorption. Light scattering redistributes light energy in the atmosphere, while light absorption converts light energy to internal energy of the absorbing molecules and eventually transfers it to the surrounding atmosphere (Horvath, 1993).

The atmospheric aerosol gives an important contribution to the atmospheric light absorption in the visible and near ultraviolet (UV) and near infra-red (IR). Aerosol "black" carbon (BC, sometimes referred to as elemental carbon, EC), the main constituent of soot, is responsible for much of the light absorption by particles. Black carbon is produced by all combustion processes. It is usually found in the nucleation or accumulation mode with particles well under 1μm in equivalent dimensions, i.e., if chain aggregates were consolidated into a single sphere (Moosmuller et al., 1997). Since most fires on earth are due to humans, then indirectly humans are a major source of light absorbing aerosol particles. The small sizes of black carbon particles, coupled with their relative chemical inertness, prolong their atmospheric residence time. Consequently, they can serve as useful tracers for long-distance transport of polluted continental air masses (Jennings et al., 1996). Examples of typical BC concentrations are 0.0001 – 0.002 $\mu g/m^3$ at the South Pole, 0.07 – 0.5 $\mu g/m^3$ in the Arctic, 0.3 – 1.6 $\mu g/m^3$ in rural Europe, 0.6 – 1.3 $\mu g/m^3$ in rural U.S.A., 4.6 – 25 $\mu g/m^3$ in urban Europe, and 2.2 – 6.4 $\mu g/m^3$ in urban U.S.A. (Pinnick et al., 1993; Hitzenberger et al., 1996).

Previous studies on the vertical distribution of BC concentrations show concentrations generally decrease with height. The WATOX program, conducted off the eastern seaboard of the United States, showed BC concentration values typically ranged from 200 – 500 ng/m^3 in the boundary layer, decreasing to 50 – 100 ng/m^3 at higher altitudes (Hansen and Novakov, 1988). AGASP 3 conducted in Barrow Alaska showed 50 – 500 ng/m^3 of BC in the boundary layer, decreasing to 10 – 100 ng/m^3 at higher

altitudes (Hansen and Rosen, 1984). Hansen et al. (1996) found typical BC concentrations over the East Siberian Sea ranged from 120 – 500 ng/m^3 up to 850 mb. Above that these authors reported a polluted layer (BC = 500 – 750 ng/m^3) between 750 and 800 mb, followed by a clean layer (BC = 0 – 50 ng/m^3) extending up to 650 mb.

1.1 Atmospheric effects of aerosol black carbon

Although light absorbing particles are a minor component of the total atmospheric aerosol, their effects on radiative transfer and visibility cannot be neglected. BC has a specific absorption cross-section (σ_{ap}) of approximately 10 m^2/g which is higher by a factor of two or more than the scattering cross-section of transparent particles (Hansen et al., 1993). These light absorbing particles have several effects in the atmosphere. These include optical effects on transmission of visible light, effects on the radiative balance of the atmosphere and related climate consequences, and other effects not related to the light absorbing properties of BC.

The easiest detectable effect of particles in the atmosphere is reduced visibility. The standard visibility V_{st} is defined as the maximum distance an observer, being able to see contrasts larger than a threshold value of 0.02, can recognize a black target against the horizon as a background. An atmosphere that contains light absorbing particles will give a horizon radiance less than an atmosphere without light absorbing particles. Light transmitted from the target to the observer will also be absorbed by BC and other light-absorbing particles. The overall result is a decrease in contrast that reduces the visual range.

Absorbing aerosol particles can also affect the color of the sky and haze layer. The sky in a clean environment is usually blue at the zenith and white or slightly blue at the horizon. With increasing pollution the color fades to white or gray, or sometimes even to brown. If the aerosol contains substances which have a higher absorption in the blue than in the red (true for BC) the color of the haze layer changes to yellow or red, and if the haze layer is darker than the surroundings, its color appears brown.

Absorbing aerosol particles can also interact with the atmosphere's radiative balance. Light absorption by aerosol particles such as BC provides a mechanism for capture of

light energy which is transformed into thermal energy. This transformation will tend to cause a temperature increase of the local atmosphere. Increased BC content incorporated into Arctic snows can cause a decrease of the albedo of the ice cap, which may trigger a temperature increase resulting from increased absorption of light energy at Earth's surface. There is, at the same time, some suggestion that increased BC particles in the atmosphere can catalyze the oxidation of sulfur dioxide to sulfate (Muhlbaier et al., 1989). Increases in light-scattering sulfate particle concentrations can enhance backscatter of incoming solar radiation back toward space, thereby tending to cool the Earth atmosphere (Horvath, 1993).

Atmospheric elemental carbon also has some other effects that are not directly related to its light absorbing properties. As mentioned above BC surfaces may act as sites for catalytic oxidation of SO_2. Toxic substances can also be transported on the surfaces of BC particles. During combustion, partly oxidized, nitrated and/or polyaromatic hydrocarbons can be formed. When the combustion products cool, these compounds condense on available particles, often BC particles. Since BC particles have a size which permits deposition deep in the lung, they transport these substances to the lung and can promote lung cancer (Cuddihy et al., 1984).

BC can also cause soiling of buildings and materials. The dirty and dark appearance of old buildings is caused by deposition of particles on the surface. Fine black carbon particles are the main cause, since they adhere well on surfaces and are not readily washed off (Creighton et al., 1990) due to their low solubility. Furthermore, deposited carbon particles may act as a catalyst for the formation of gypsum (Del Monte et al., 1984).

1.2 Characterization of aerosol light absorption

Attenuation by a medium interacting with light is given by the Lambert or Bouguer law. If I_o is the incident flux of monochromatic light, the flux I after passing a distance x through the medium is obtained by means of the transmission T by

$$I = I_o * T \qquad (1)$$

with $T = \exp(-b_{ext} x)$,

where b_{ext} is the extinction coefficient, the constant due to the attenuation of a parallel beam of light by scattering and absorption at the same time (Horvath, 1993). The extinction is due to both absorption and scattering by gases and aerosol particles, so we can write:

$$b_{ext} = b_{sp} + b_{sg} + b_{ag} + b_{ap} \qquad (2)$$

where b_{sg} and b_{sp} are the light scattering coefficients for gas molecules and particles, and b_{ag} and b_{ap} are the coefficients of light absorption by gases and particles. It may be assumed that the light extinction due to gaseous contribution is not significant in polluted environments (Groblicki et al., 1981). Then the dominant contribution to light extinction is due to absorption and scattering, so Equation (1) can be rewritten as:

$$\ln (I/ I_o) = -(b_{ap} + b_{sp}) x \qquad (3)$$

A linear relationship exists between the absorption coefficient of a sample b_{ap}, and the mass content of the absorbing material (BC), through σ_{atn}, the specific attenuation cross-section:

$$b_{ap} = \sigma_{atn} * BC \qquad (4)$$

The specific attenuation cross-section σ_{atn} relates light attenuation to BC mass loadings in the case of filter based measurement methods while the specific absorption cross-section σ_{ap} is used to relate light absorption by particles suspended in air to particle mass concentration (Petzold et al., 1997).

Findings by Liousse et al. (1993) and Petzold and Niessner (1995a, b) show that σ_{atn} is not constant for all BC samples. They report that σ_{atn} varies depending on regional variations in the predominant aerosol type. The value of σ_{atn} is typically 1.9 – 2.5 times the normally accepted specific absorption cross-section σ_{ap} for airborne black carbon particles of 6 – 10 m^2/g in the visible spectral region (Horvath, 1993). The observed variability in σ_{atn} ranges from 5 m^2/g (remote areas) to 14 m^2/g at urban locations, and to 20 m^2/g at near-street measuring sites (Petzold et al., 1997). Liousse et al. (1993) relate the variability in the value of σ_{atn} to variability in the nature of the BC itself resulting

from aging during transport and mixing with other particles. The aging of the aerosol and mixing with other particles lead to a decrease of σ_{atn}.

Examples of measured aerosol light absorption coefficients are 0.00001 - 0.00004 km^{-1} at the South Pole, 0.000045 – 0.0035 km^{-1} in the Arctic, 0.004 - 0.023 km^{-1} in rural Europe, 0.0007 – 0.005 km^{-1} in the rural U.S.A., 0.02 – 2.4 km^{-1} in urban Europe, and 0.02 – 0.06 km^{-1} in the urban U.S.A. (Horvath, 1993).

Several methods have been developed to measure light absorption by suspended particles. They can be separated into two groups, depending on the effect or methodology they use. No standard procedure has been adopted so far for making a definitive measurement. The different methods used can be grouped into those which measure an effect which is caused by light absorption and those utilizing optical analysis.

1.2.1 Absorption characterized by measuring effects due to absorption

One method for measuring aerosol particle absorption is termed the photoacoustic method. The principle of operation of this method is based on the photoacoustic effect (Pao, 1977; Rosencwaig, 1980). Radiation from a laser beam is absorbed by the sample contained in a sample cell and transferred as heat energy to the surrounding gas. An increase in the pressure in the sample cell results from the thermal expansion. By modulating the laser beam, the oscillating pressure forms a sound wave which can be detected by a microphone. The microphone signal is directly proportional to the optical absorption.

1.2.2 Optical analysis of aerosol absorption

Several methods designed to characterize aerosol absorption employ a measurement of transmission through an aerosol sample and compensate for losses of scattered light. These methods include the integrating sphere method, the laser integrating plate method, the laser transmission method, the subtraction method, and the aethalometer. An overview of these measurement approaches has been given by Horvath (1993).

In the integrating sphere method (Campbell et al., 1995) a sample of aerosol particles collected by impaction on a glass slide is placed in an integrating sphere. Both the light scattered by and transmitted through the sample reaches the diffusely reflecting surface of the sphere and is scattered in the direction of a photodetector. The signal of the photodetector is proportional to the transmitted plus the scattered light. The difference between the measurement made using a clean glass slide and a slide loaded with particles yields the amount of light absorbed by the particles.

The integrating plate method (IPM) (Campbell et al., 1995) is a simplification of the integrating sphere method. The integrating plate system consists of a light source, interference filter, opal glass plate, and photodetector. A filter is placed in the apparatus with the aerosol laden side away from the laser beam. Light from the laser passes the interference filter (diffuser and variable mask) to select the desired spectral range, and then passes through the filter. The opal glass plate receives the transmitted light. The light intensity transmitted through the filter is measured before and after sampling. The difference between the measurement yields the amount of light absorbed by the particles.

In the laser transmission method (Rosen and Novakov, 1983) a filter loaded with particles is placed with the particle laden face towards the laser beam. After passing the filter sample, the transmitted radiation is focused on the active area of a photodiode. To obtain an accurate value of the reference signal, I_0, blank filters are measured before sampling. The difference of the two measurements yields the amount of light absorbed by the particles.

In the subtraction method the extinction coefficient is measured with, for example, an extinction cell or a transmissometer; the light scattering coefficient of the aerosol is measured with an integrating nephelometer. The difference between the two measured quantities is the absorption coefficient (Lewis and Dzubay, 1986; Horvath and Habenreich, 1989).

The aethalometer method was developed at the Lawrence Berkley Laboratory by Drs. Hansen, Rosen, and Novakov. This method is based on the laser transmission method. The instrument was named the aethalometer, which translated from Greek means "to blacken with soot". The aethalometer operates on the principle of continuous measuring of the attenuation of a beam of light transmitted through a spot on a suitable

filter on which aerosol is being continuously collected. The rate of deposition of BC on the filter is proportional to its concentration in the aerosol and gives a rate of increase of optical attenuation.

1.2.3 Obtaining the specific absorption/attenuation cross-section from aerosol absorption measurements

Values for σ_{ap} or σ_{atn} can be obtained from experimental measurements. Optical analysers assume that BC is primarily responsible for the measured absorption and thus the attenuation of light. If the BC content of the sample is obtained by an independent measurement (e.g. by thermal analysis), then b_{ap} and BC give access to the specific attenuation cross-section as indicated by equation 2. In the case of filter based techniques, the fibrous filter may lead to an enhancement of the attenuation, and consequently an enhancement of σ_{atn}. The photoacoustic method of determining the absorption coefficient coupled with the BC content of the sample similarly give access to the specific absorption cross-section.

1.3 Measuring concentrations of aerosol black carbon

The most common ways for determining concentrations of aerosol black carbon are through aethalometer measurements and through thermal analysis. Measurement of BC using the aethalometer relies on a calibrated attenuation cross-section for carbon deposited on the quartz tape. The BC concentration is derived from the amount of light attenuation using equation 4.

$$BC = b_{ap} / \sigma_{atn}$$

The thermal analysis method (Chow et al., 1993) is based on the preferential volatilization and oxidation of organic compounds and elemental carbon at different temperatures. The analysis operates by: (1) liberating carbon compounds under different temperatures and oxidation environments from a small sample punch taken from a quartz-fiber filter, (2) converting these compounds to CO_2 by passing the volatilized

compounds through an oxidizer (MnO_2 at 912°C), (3) reduction of the CO_2 to methane by passing the flow through a methanator (firebrick impregnated with nickel catalyst at ~ 550°C in a steam of hydrogen), and (4) quantification of CH_4 by flame ionization detection (FID). The EC mass obtained can also be converted to an absorption coefficient by equation (4), using an appropriate value of σ_{ap} in place of σ_{atn}.

1.4 Study objectives

Because BC concentration and aerosol absorption measurements are far from routine, little is known about their typical ranges in most environments. In this study we were interested in developing a record to characterize aerosol black carbon concentrations in the city of Ft. Collins, Colorado. Along with documenting typical BC concentration values and their range, we were interested in determining whether these values were significantly influenced by local or distant emission sources. We were also interested in determining the amount of visibility extinction due to light absorption by Ft. Collins aerosol.

Specifically, the objectives during this study were (1) to document typical BC concentrations (and their range) in Fort Collins, Colorado using an aethalometer, (2) to determine whether elevated BC concentrations are associated with particular source regions using back trajectory analysis, (3) to examine whether elevated BC concentrations are strongly correlated with local vehicle emissions as represented by carbon monoxide concentrations, and (4) to compare derived aerosol absorption with the difference between atmospheric extinction and scattering measured by the city of Fort Collins.

2. Experiment

2.1 Sites

Aerosol black carbon concentrations were measured in Fort Collins, a small city in northern Colorado. Fort Collins has a population of approximately 100,000, and is located 111 km north of Denver. Sampling was performed in an air quality monitoring trailer operated by the Colorado Department of Public Health and Environment (CDPHE). The trailer is located on the northeastern corner of the Colorado State University (CSU) campus near the intersection of Mason and Laurel streets. The trailer is one block west of College Avenue (U.S. highway 287), the major north-south thoroughfare in Fort Collins. The trailer is situated at the southwestern corner of a small parking lot. There are several other parking lots within a few hundred meters of the trailer. The CSU Industrial Sciences laboratory is located approximately 20 meters west of the trailer. The CSU heating plant is approximately 200 meters south of the trailer. The Burlington Northern Santa Fe Railroad runs through Fort Collins along a track located approximately 10 meters west of the trailer. Typically 5 – 10 trains with diesel engines pass the site daily. This site met the aethalometer operation specifications (it has to be shielded from direct sunlight, and the instrument should not be placed in an environment where ambient temperatures exceed 100°F, nor where high relative humidity may cause condensation). The CDPHE trailer is temperature and controlled.

2.2 Instrumentation

The instruments used in this study were a Magee Scientific aethalometer, a CliMet Innovation CI-500 optical particle counter (OPC), and a TSI, Inc. Condensation Nucleus Counter (CNC Model 3020). Data were also used from a nephelometer, and a transmissometer operated by Air Resource Specialists, Inc. for the city of Ft. Collins and

a CO monitor operated by CDPHE. The aethalometer, OPC, CNC, and CO monitor were located in the monitoring trailer. The nephelometer and the receiver of the transmissometer are located on top of a 37 meter building in downtown Fort Collins. The transmitter of the transmissometer is located 2 km away at an elevation of 37 meters on the University Park Holiday Inn on Prospect Avenue.

2.2.1 Aethalometer

The aethalometer is a self contained instrument that determines black carbon concentrations based on measured optical transmission through a spot on a quartz fiber tape on which aerosol is being continuously collected. The measurements are performed in real time. The light source is an incandescent lamp, approximate wavelength range 500 –1000 nm (Hansen, 1996).

The instrument measures the transmitted light intensities through the 'sensing' portion of the filter (a spot of 0.95 cm^2 on the quartz fiber tape which is collecting aerosols), and a 'reference' portion of the filter (similar size spot on the quartz fiber tape where aerosol is not collected). Light transmission through the particle-free reference part of the filter is used to correct for variations in lamp brightness and drifts in electronic response. Two light guides placed beneath the filter support, under the collecting and reference portions of the filter, convey the transmitted light to a pair of matched photodetectors.

The attenuation of the intensity, I, transmitted through the collecting part of the filter relative to the intensity, I_0, through the reference part is

$$ATN = 100 * \ln (I_0 / I) \qquad (5)$$

and is proportional to the concentration of BC. This measurement is made at successive regular half hour intervals. A flow rate of 5 standard liters per minute (slpm) regulated by a mass flow controller, is used for sampling.

The electronics connected to the photodetectors convert the optical signals to voltages that are digitized and passed to the computer program for calculation. The increase in optical attenuation from one period to the next is due to the increment of BC deposited on the tape during the period. The BC concentration is derived from the

amount of light attenuation using a calibrated attenuation cross-section (19 m^2/g) for carbon deposited on the quartz tape (Hansen, 1996).

The filter must be changed periodically to avoid overloading and saturation of the optical absorption. As the aerosol deposit accumulates, the optical transmission through the spot diminishes exponentially. However, the resolution of the measuring electronics and the amplitude of the electronic noise remain constant. Thus, the relative importance of noise and measurement error increase exponentially as the aerosol deposit loading increases. For this reason, the computer program automatically advances the tape to a fresh filtration spot before the aerosol black carbon loading becomes large. When a value of ATN = 75 is reached the program halts temporarily to advance the filter tape, and resumes automatically when the fresh spot is in place (Hansen, 1996). The value of ATN = 75 is recommended by the manufacturer based on an optical absorption depth of 0.75 integrated across the visible spectrum. This corresponds to a surface loading of aerosol BC of approximately 4 $\mu g/cm^2$ on the collected spot.

The aethalometer calculates the BC concentration from the measured attenuation and the flow rate recorded by the internal mass flow meter. The flow meter is calibrated at standard temperature and pressure (STP): 25°C and 1 atmosphere. The BC concentration is reported in nanograms per standard cubic meter. A correction is applied to the data for both pressure and ambient temperature to convert STP data to ambient geometric volumes. This correction is made according to the formula

$$BC_{ambient} = BC_{STP} * (537°R / T°R) * (Pmb / 1013mb) \qquad (6)$$

where T and P are the ambient temperature and pressure. As mentioned above, the aethalometer halts temporarily to advance to a fresh spot when a value of ATN = 75 is reached. When that happens the instrument doesn't record data in that time interval, and the subsequent time interval (i.e., no data for 1 hour when the time interval is ½ hour, 10 minutes when time interval is 5 minutes). This results in a gap in the data that typically occurs once per day. On days with high BC concentrations, the gaps in the data are more frequent.

Due to installation of the wrong tubing in the aethalometer at the time of manufacture, oxidants in the sampled air eventually caused the internal tubing to crack and leak at stress points. This problem was identified during a comparison with a second aethalometer in May 1998. Because the study aethalometer data compared well with data from a second aethalometer in late October and early November 1997, we are confident the leaks developed after that time. Unfortunately it is not possible to define the beginning of the problem any more precisely than to say it occurred between the second week of November 1997 and May 1998. Accordingly data from this period will not be reported here. The tubing was replaced in May 1998 and the aethalometer again showed good agreement when compared with a second unit. Sampling at the CSU campus site resumed in August, 1998 and continued through September, 1998.

2.2.2 Optical Particle Counter

The CliMet Instruments CI-500 Innovation optical particle counter is a laser diode based aerosol particle counter. It is a fully self-contained, battery-powered 0.1 CFM (cubic feet per minute flow rate) instrument in a stainless steel enclosure. The CI-500 counts particles by detecting light scattered by the particles as they pass through a laser diode beam that is focused directly under the inlet nozzle. The amount of light scattered is proportional to the size of the particle passing through the laser beam. An elliptical mirror based optical system collects the scattered light over a wide solid angle and reflects it onto a solid state photo detector. Since the detector receives scattered light from a wide solid angle, variation in response due to particle shape and refractive index is minimized.

The solid state photo detector and associated electronic circuitry convert the collected light to an electric pulse with an amplitude proportional to particle size. These electrical pulses are sent to voltage comparators which compare the amplitude of each voltage pulse to a reference voltage determined at calibration. If the amplitude of each pulse is greater than the predetermined reference voltage, the pulse will be counted as a particle greater than or equal to the size threshold assigned to the comparator. Particles that enter the inlet tube are trapped in a HEPA filter after passing through the sensor so

that they are not exhausted into the trailer. The particles are sized and counted in six channels: 0.3-0.4, 0.4-0.56, 0.56-1.0, 1.0-1.8, 1.8-3.2, and > 3.2 microns diameter. The OPC was operated to collect particle size distributions over 30 minute sample intervals. The flow through the CI-500 was controlled by an internal mass flow controller.

2.2.3 Condensation Nucleus Counter

The condensation nucleus counter (CNC) used in this study was a TSI, Inc. model 3020. The CNC measures the number concentration of submicron aerosol particles by passing each particle through a heated zone saturated with n-butyl alcohol vapor. As the particle-laden flow leaves the heated zone and begins to cool, high n-butyl alcohol vapor supersaturations are generated, leading to condensation of alcohol onto particle surfaces, thereby forming droplets. Each droplet is large enough to scatter a detectable amount of light when it passes through a light beam, although the dry particle would have been too small to be detected. The droplet size is nearly independent of the size of the original particle over a wide range of particle sizes, so the light scattered is a function of number concentration only, not of the size distribution. TSI, Inc. specifies a lower particle size limit of 10 nm diameter that can be efficiently detected by the model 3020. The instrument operates at a flow rate of 0.3 slpm. Measured particle concentrations in the sampled air were determined over 30 minute sample intervals selected to match the OPC and aethalometer sample intervals. In order to vent butanol vapors from CNC (butanol is flammable and harmful if inhaled), a vent was run from the CNC outside the trailer.

2.2.4 Nephelometer

The Optec NGN-2 integrating nephelometer is a field proven instrument for monitoring ambient air optical scattering (b_{scat}) in remote and urban environments. The NGN-2 employs an open air design that minimizes modification of the ambient aerosol and allows accurate point measurement of the ambient scattering coefficient (b_{scat}) at 550 nm. The instrument estimates b_{scat} by directly measuring the light scattered by aerosols and gases in an enclosed sample volume. Scattered radiation from the illumination

source is integrated over a large range of scattering angles in the defined band of visible wavelength. Since the total light scattered out of path is the same as the reduction of light along a path due to scattering, the integrating nephelometer gives a direct estimate of b_{scat}. The one minute average values are then averaged by the nephelometer program to create hourly averaged values of b_{scat} (Molenar et al., 1992).

Possible limitations can be caused by instrument related modification of the sampled air due to chamber heating, aerosol sizing by the inlet, large scattering angle truncation error, poorly defined optical response, and unstable electronics. The NGN-2 is designed to overcome these deficiencies. The key features of the NGN-2 that overcome these deficiencies include:

- An unobstructed inlet that replaces complex sample trains and allows ambient air to directly enter the measurement chamber as a laminar flow.
- The high flow rate (280 liters per minute) and specially designed chamber manifold wall assure laminar flow through the measurement chamber and minimum residence time (less than 0.25 seconds)
- The heat generated by the 25 watt quartz halogen lamp is drawn away from the measurement chamber with a 700 nm heat absorbing glass filter and heat sink in the sample fan chamber.
- The solid state detector and control electronics minimize temperature dependence, power consumption, and heat dissipation in the electronics chamber.
- A layer of insulation isolates the measurement chamber from heat generated in the electronics and sample fan chamber.
- The single-board computer controls all nephelometer functions, provides input and output via an RS-232 serial interface and analog lines, and allow user-defined operational parameters(integration time, zero air interval, etc).
- Rugged physical design and solid state electronics in a sealed chamber allow the instrument to operate in ambient conditions over a broad temperature range (-20°C to 40°C) with no documented temperature dependence.
- Reflective exterior white paint minimizes solar heating.

An ideal nephelometer would measure scattering from 0 to 180°. The integrating angles for the NGN-2 are at 5° and 175° making the truncation angles 5° in both the

forward and backward scattering directions. Because large particles scatter more efficiently in the extreme forward direction, small truncation angles are important. The small truncation angles of the NGN-2 measure more scattering in the forward and backward directions, thus providing a more accurate estimate of total scattering (Cismoski et al., 1994).

2.2.5 Transmissometer

The Optec LPV-2 transmissometer directly measures the irradiance of a light source after the light has traveled over a finite atmospheric path. The transmissometer consists of a constant output light source transmitter and computer-controlled photometer receiver. It continuously measures ambient extinction at 550 nm over a path length of 2km. The transmittance of the path is calculated by dividing the measured irradiance with the calibrated initial intensity of the light source. The average extinction of the path is calculated from the transmittance and the length of the path. It is attributed to the average concentration of atmospheric gases and ambient particles along the path. The transmitter signal is processed at the receiver by an internal computer with the output voltage made proportional to irradiance, extinction or visual range (Molenar et al., 1992).

The transmissometer makes a completely ambient measurement of b_{ext} without perturbing or selectively sampling the atmospheric aerosol. However, it requires a path length of a few kilometers to achieve the sensitivity to resolve extinctions near the Rayleigh limit. Extinction measurements from transmissometers also are affected by any meteorological or optical interferences present along the path which are independent from the ambient aerosol (Molenar et al., 1992).

2.2.6 Meteorological, Carbon Monoxide, and Train Data

Meteorological data and CO data at the CDPHE trailer site were obtained from the CDPHE. Additional meteorological data were also obtained from the Fort Collins Weather Station located 400m west of the CDPHE trailer on the Colorado State

University campus. CO concentrations were measured using a TECO Model 48 CO analyzer. The analyzer is a Gas Filter Correlation (GFC) spectrometer. GFC spectroscopy is based upon comparison of the detailed structure of the infrared absorption spectrum of the measured gas to that of other gases also present in the sample analyzed. The technique is implemented by using a high concentration sample of the measured gas, i.e., CO, as a filter for the infrared radiation transmitted through the analyzer. Radiation from an infrared source is chopped and then passed through a gas filter alternating between CO and N_2 due to rotation of the filter wheel. The CO gas filter acts to produce a reference beam that cannot be further attenuated by CO in the sample cell. The chopped detector signal is modulated by the alternation between the two gas filters with an amplitude related to the concentration of CO in the sample cell. The radiation then passes through a narrow bandpass interference filter and enters a multiple optical pass cell where absorption occurs. The IR radiation then exits the sample cell and falls on an IR detector. The sample and reference signals are sent to a micro-computer which returns the CO concentration in ppm.

Train passage data were obtained from the city of Fort Collins Traffic Department. We wanted the data to examine what effect, if any, diesel locomotive passage so near to the site had on the BC concentration measured. The data for the nearest traffic crossing to the site was used to ascertain the time and duration of each passage. This crossing is at Mulberry and Mason Streets which is a block north of the site. The direction of the passage (whether going north or south) could not be ascertained from these data.

2.3 Aerosol Sample Inlets

The aethalometer, the OPC and the CNC were set up in the CDPHE trailer according to the schematic in Fig.1 in and on top of the metal racks respectively. A separate inlet was made for the CNC due to the low flow rate of the instrument. Conductive tubing was used for the inlets to reduce particle losses due to electrostatic attraction. The inlet lengths were 30 inches for the CNC, and 99 inches for the OPC/aethalometer. A ¼"

internal diameter (ID) plastic tubing was used for the CNC inlet which was teed off of an existing ozone sample inlet present in the trailer. The OPC/aethalometer inlet was a ½" diameter stainless steel tube. A ¼" ID conductive black plastic tubing of length 54 inches was teed off to the aethalometer. A TSI Incorporated aerosol calculation program was used to calculate diffusional and gravitational particle losses through the inlets. The program used equations and constants from Willeke and Baron (1993), and Hinds (1982). Tables 1-5 illustrating results of particle number loss calculations are located in Appendix A. The results show a maximum of 10-20% diffusional loss in the CNC inlet, 10% for the aethalometer, and 6% for the OPC inlet for 0.01μm. Gravitational losses were 11 and 17% respectively for 10 μm diameter particles in the OPC and aethalometer inlet. Gravitational losses were negligible for particles less than 3μm.

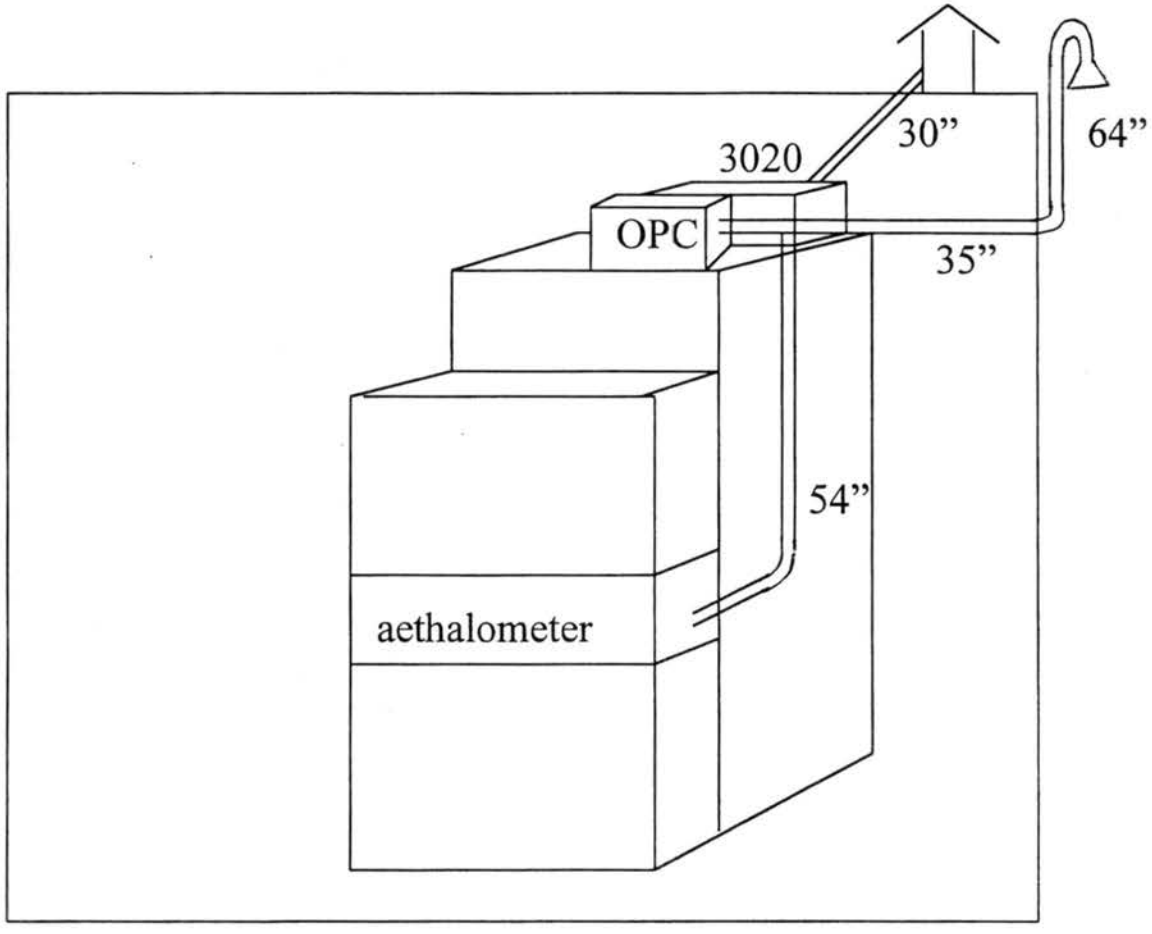

Figure 1. A schematic of instrument set-up and inlet lengths. Not to scale.

2.4 Measurement strategy

The study was planned to measure BC concentrations over a year. The colocated instruments in the CDPHE trailer were set up to sample at half hour time intervals. The sampling time was chosen to obtain enough data points to observe daily fluctuations.

In mid-October 1997 we were able to obtain a second aethalometer on loan from Magee Scientific with which we were able to do a spatial variation study of BC concentrations in Fort Collins. First, we colocated the two aethalometers from October 17th – 23rd, 1997 in the CDPHE trailer to ensure good agreement between the two instruments. The second aethalometer inlet was teed off of the inlet to the first. The second aethalometer, which hereafter will be referred to as "loaner", was then colocated with the nephelometer and the receiver end of the transmissometer from October 23rd – 31st. The "loaner" was again colocated at the CDPHE trailer site from October 31st – November 3rd. It was then moved to a second floor office in the First Choice bank building on the southwest corner of Horsetooth and College Avenues, Fort Collins' busiest intersection, for a traffic study. This study took place November 3rd – 5th. Normally the two aethalometers sampled at half hour intervals. During the traffic study, however, the sample interval for both aethalometers was changed to 5 minutes to enable us to better examine short time scale fluctuations in BC concentrations.

The study of train passage influence on BC concentration measured at the CSU campus site was conducted in August – September, 1998. Typical train passages are 3-5 minutes in duration. The aethalometer sample time was reduced to 5 minutes during the train study. This time scale was chosen to observe the fluctuations in BC concentrations associated with train passages (train passages were often obscured in the half hour sample data).

2.5 Trajectories

Back-trajectory calculations from the CDPHE trailer measurement site (40.576° N, 105.079° W, and 1525m in elevation) were performed using NOAA's Air Resources Laboratory HYSPLIT4 (Hybrid Single-Particle Lagrangian Integrated Trajectory) model. The HYSPLIT4 model is the newest version of a complete system for computing simple air parcel trajectories (HYSPLIT4, 1997). Trajectories are computed kinematically from gridded wind fields assuming that a parcel passively follows the horizontal motion of the wind. The trajectory approach is a revised version of the method used by Draxler (1991). All the meteorological fields are first remapped to a terrain-following coordinate system that is defined by a normalized variable

$$\sigma = 1 - Z / Z_t \qquad (7)$$

where Z is the height above ground level (AGL) and Z_t represents the top of the model domain. A parcel trajectory is computed from the time integration of the three-dimensional position vector S,

$$d\,S/dt = \mathbf{V}\,(x, y, z, t) \qquad (8)$$

where **V** is the horizontal velocity vector at a point in space and time. The integral is solved numerically through the improved Euler-Cauchy method where the velocity vector is represented by the average of the velocities at the initial location and time and the velocity at the first-guess position at time $t + \Delta t$. The velocity at a point is linearly interpolated from the values at the adjacent grid points and time periods. The time steps can range from 1 minute to 1 hour.

The trajectory path is computed in both the horizontal and vertical directions such that the vertical integration of the position vector is computed in a manner similar to the horizontal component. The model uses the archived field of the total derivative of

pressure (the vertical wind component) to compute vertical motion (Draxler, 1996). The archived data field used is EDAS –Eta Data Assimilation System. The EDAS is an intermittent assimilation system consisting of successive 3h Eta model forecasts and Optimum Interpolation (IO) analyses for a pre-forecast period on a 38 level, 48 km grid. The 3h analysis updates allow for the use of high frequency observations, such as wind profiler, NEXRAD, and aircraft data (HYSPLIT4, 1997). The input parameters for the model are location (in fraction of degrees), starting year, day, hour (UTC), starting height, and duration of the trajectory.

Daily 3-dimensional back-trajectories were computed with an end time of 06 UTC daylight or 07 UTC standard time. Additional trajectories were calculated during periods of elevated and low BC concentrations. Elevated BC concentrations were identified as those periods when the BC concentration exceeded 2000 ng/m^3, and low BC concentrations were identified as those periods when the BC concentration is less than 200 ng/m^3.

Trajectories are primarily used as a diagnostic tool to evaluate the flow field at various levels of the atmosphere and to compare the fields between different meteorological models. The error in a trajectory calculation is primarily due to the fact that meteorological fields, which vary continuously in space and time, are at times poorly represented by a field defined at fixed locations (grid resolution) and at fixed temporal intervals. Clearly, any error in the Eta weather forecasting model is passed along into the HYSPLIT trajectory model. Trajectories only represent the flow path of a single particle at the time of the initial release (HYSPLIT4, 1997).

3. Results

3.1 Black carbon concentrations

Monthly BC concentration timelines for the period June to October, 1997 are shown in Figure (2). The timelines reveal a peak in the number of high BC concentration days in August with the lowest number of high BC days in June. The months of July, September, and October have concentration peaks in excess of 10,000 ng/m^3. There are 3.5 days of data missing in September due to problems with the instrument. The periods of low BC concentrations in late July and October were associated with adverse weather conditions. Strong convective activity and considerable precipitation dominated late July while late October featured blizzard conditions.

The data for each month were averaged to produce monthly average diurnal concentration profiles, shown in Figure (3). The monthly average hourly BC concentrations ranged from 200 – 2428 ng/m^3. The daily pattern shows a morning and late afternoon/evening peak. Weekday concentrations are higher than weekend concentrations. Weekend evening peaks occur later than on weekdays. August and September typically have higher BC concentrations than are observed in other months. The late evening peak in July (BC concentrations ~ 50,000 ng/m^3) associated with fires near the CSU campus site during the disastrous Fort Collins flood on July 28th, 1997 and possibly overturned diesel engines and emergency vehicles a few meters south of the monitoring site were removed from the data to show typical concentration patterns. Also, the afternoon peak on October 1st, 1997 (BC concentrations ~ 44,000 ng/m^3 which could not be linked to a particular source) were removed (see weekly timelines in Appendix G). August and September have a peak around midnight that is more prominent in the weekend plot. June has the lowest concentrations of these months.

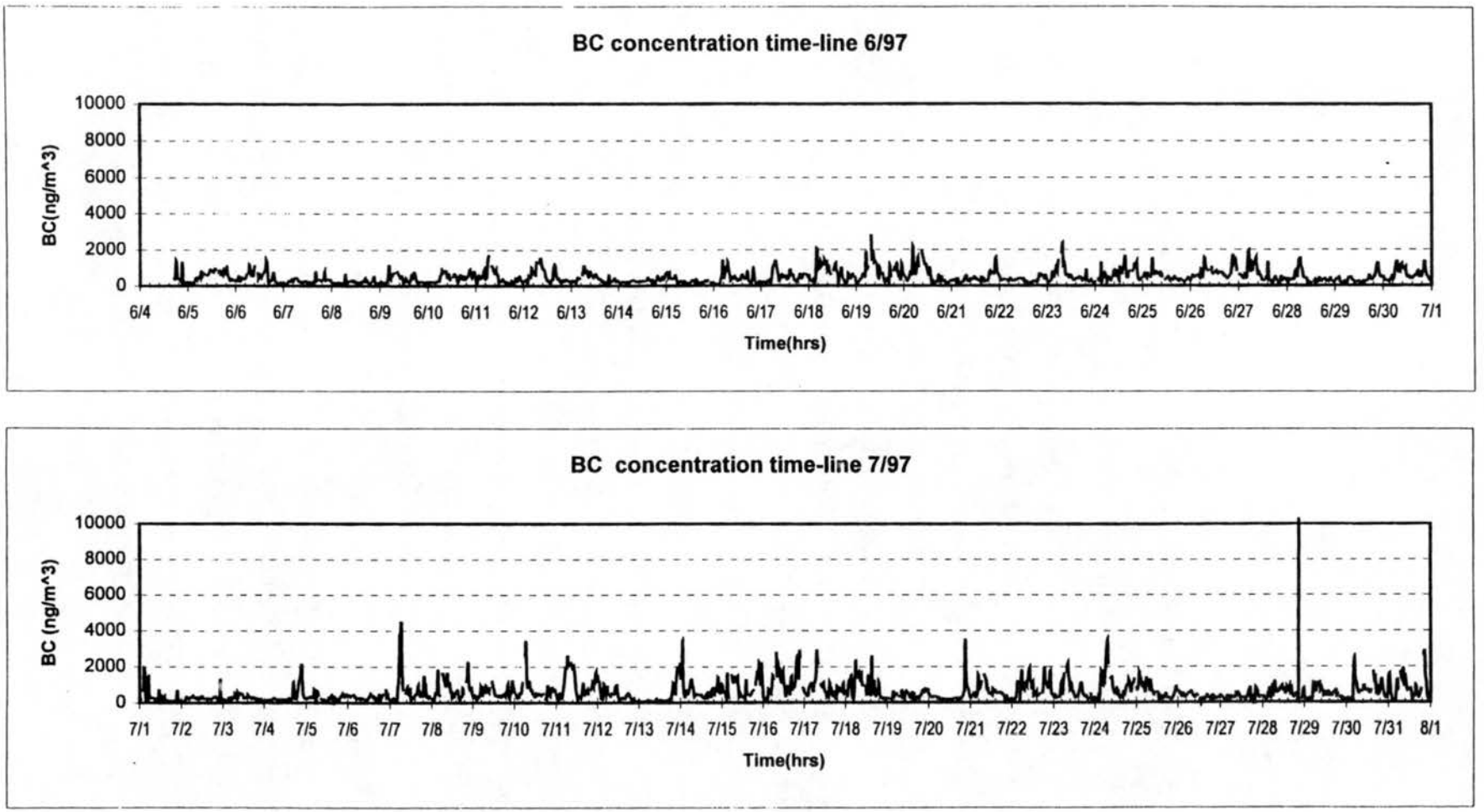

Figure 2a. June and July monthly BC concentration time-line.

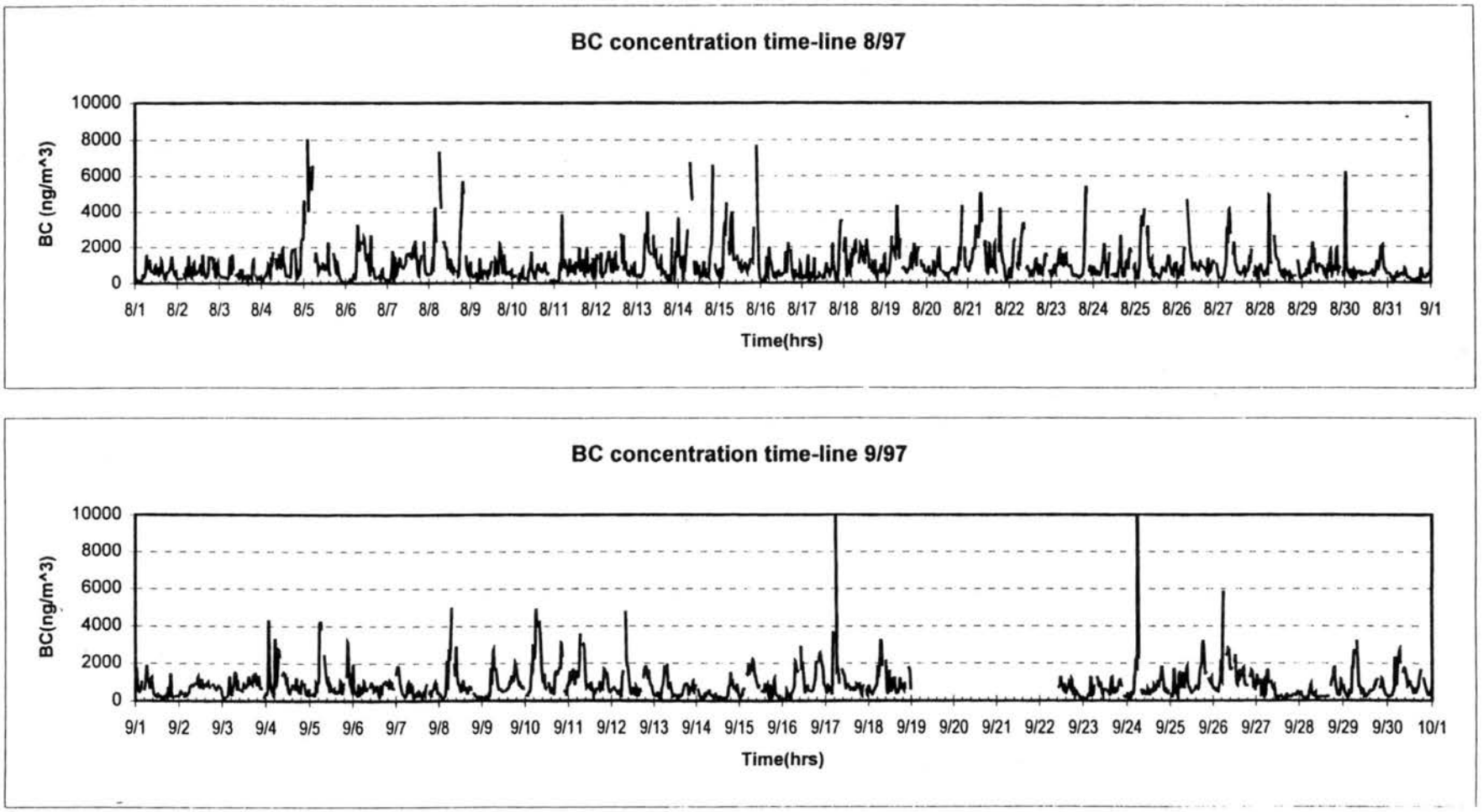

Figure 2b. August and September monthly BC concentration time-line.

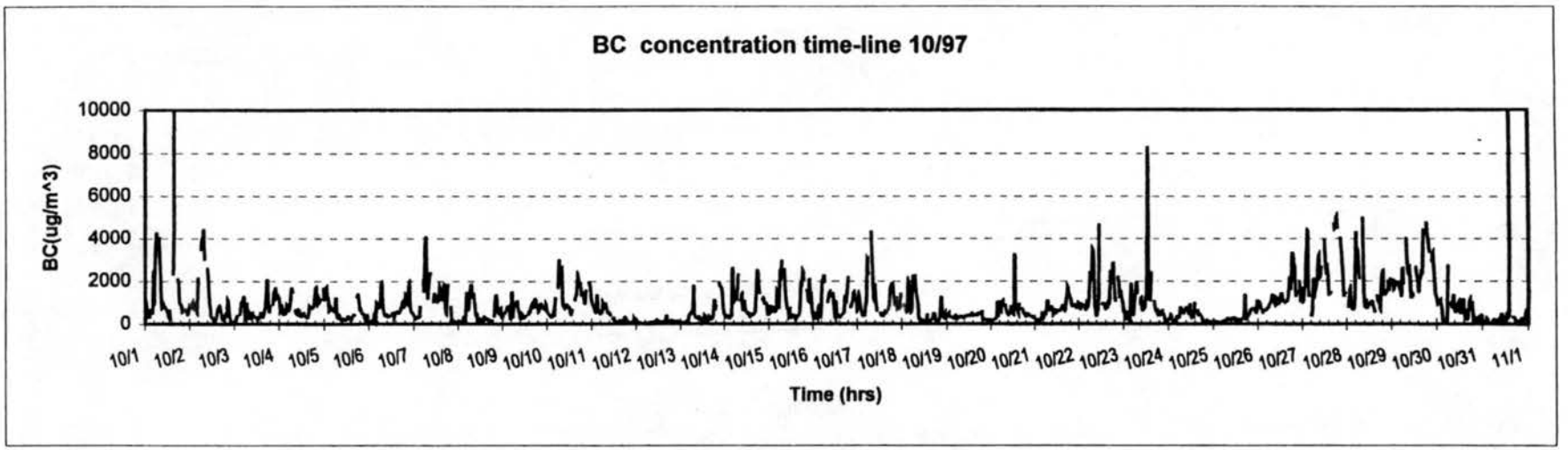

Figure 2c. October monthly BC concentration time-line.

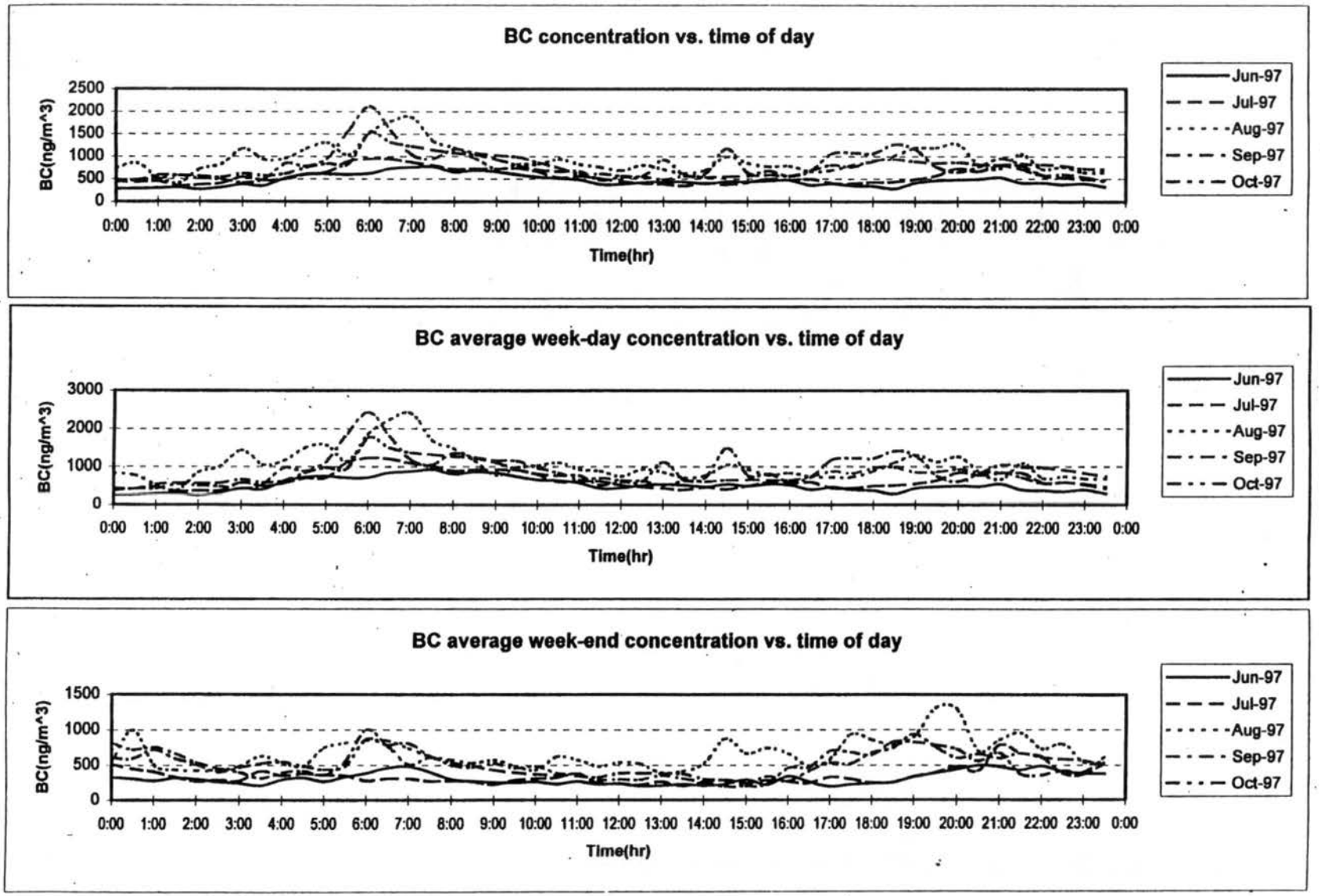

Fig. 3. Monthly average diurnal BC concentration profiles for June - October, 1997.

3.2 Trajectories

A sample air mass source trajectory is shown in Figure 4. This trajectory illustrates the likely history of air arriving at the CSU campus site at 12 a.m. local time on September 13th, 1997 (all calculated trajectories are available in electronic form, see Appendix B). Air at the sampling site appears to have come from the southwestern U. S. at this time. Air mass back-trajectories from June-November 1997 and August-September 1998 are grouped into nine categories indicating the air mass source region in Figure (5). The data are broken into summer (June, July and August) and autumn (September, October, and November) periods. The categories are NW, SW, SE, NE, Mixed (N), Mixed (W), Mixed (S), Mixed (E), and none. These quadrants are designated to indicate the general direction from which the trajectories arrived at the site. Days with missing meteorological input data are classified as "none". "Mixed" categories indicate an air mass traveled through two quadrants (e.g., Mixed (N) includes NW and NE contributions). In the figure the "All" category includes daily trajectory runs ending at 12 a.m. local time. The "High" category includes trajectories ending at times with peak daily BC concentrations exceeding 2000 ng/m^3. The "Low" category includes trajectories ending at times with minimum daily BC concentrations below 200 ng/m^3. The "All", "High", and "Low" trajectory categories included 117, 67, and 64 trajectories, respectively in the summer period and 95, 56, and 57 trajectories in the autumn period. Back trajectories were computed to test whether the directions of the daily back trajectories were affected by the ending time. Back trajectories with various ending times were computed, and they showed that the ending times did not affect the directions of the back trajectories.

In summer and autumn the dominant air mass source region is southwest. SW air mass trajectories comprise approximately 40% of the daily 12 a.m. local time trajectories in both summer and autumn. The least frequent air mass source quadrant is NE in both summer and autumn. Daily trajectory source region frequencies look similar for the summer and autumn periods. The frequency distributions of air mass source regions for both high and low BC concentration periods also look very similar to the daily back-trajectory frequencies in both summer and autumn.

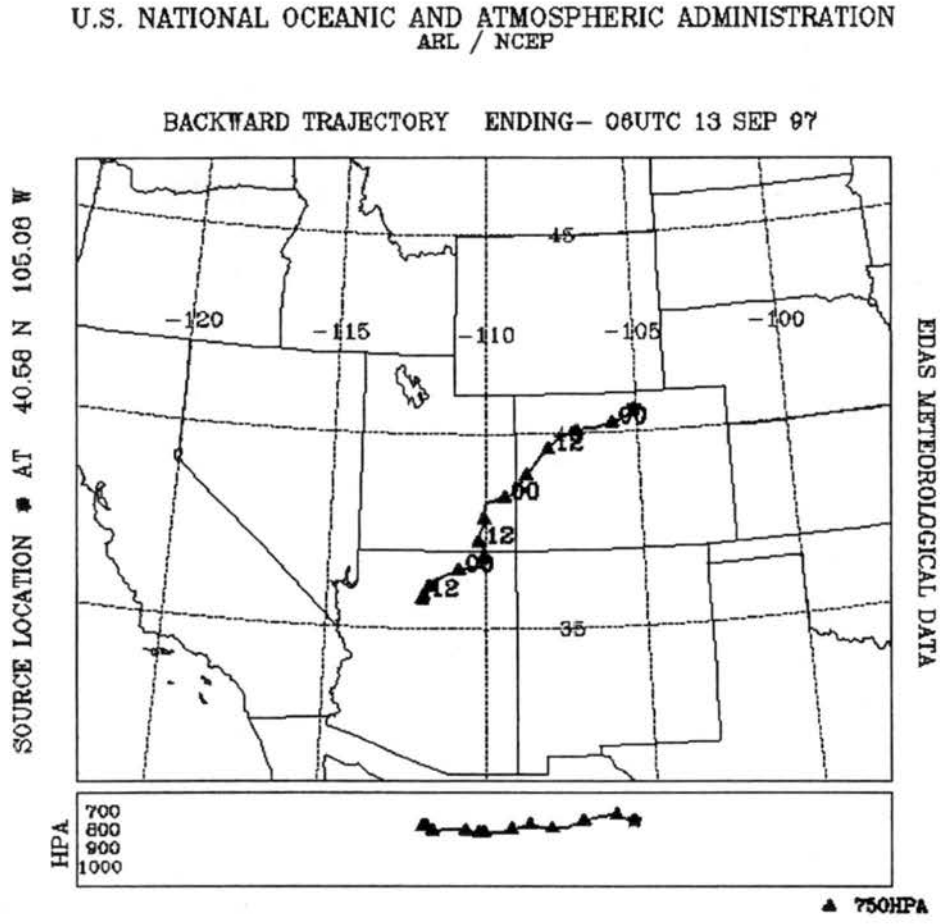

Figure 4. Back-trajectory for CDPHE trailer ending 9/13/97 06Z UTC

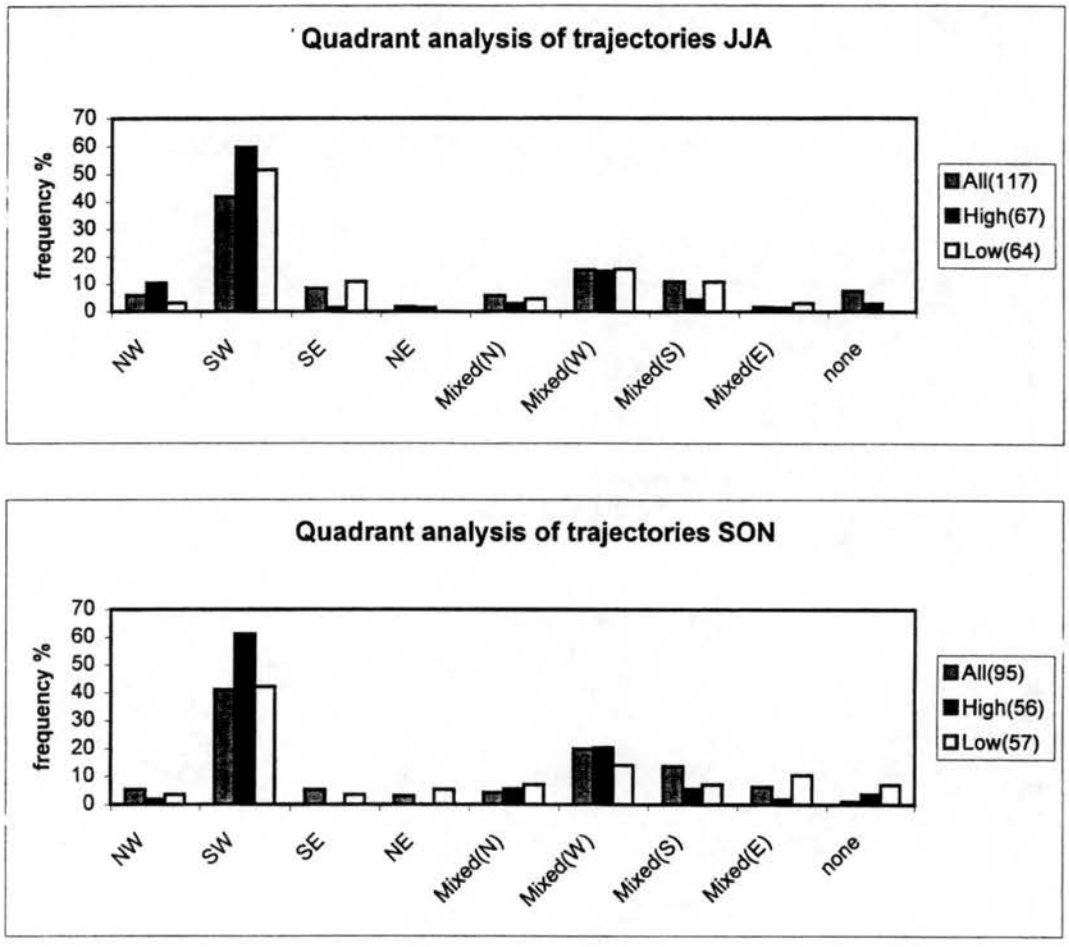

Figure 5. Quadrant analysis of a) summer (JJA) and (b) autumn (SON) trajectories

3.3 Effects of local wind direction on BC concentrations

The relationship between BC concentration and local wind direction was analyzed by comparing the frequency of different wind directions during all days and during periods of high (BC > 2000 ng/m^3) and low (BC < 200 ng/m^3) concentrations. "All" data used an average of the wind direction around 12a.m. local time (this was probably biased by down slope drainage winds at night). "High" and "Low" categories represented periods of high and low BC concentrations. The results of the wind direction quadrant analysis are shown in Figure (6) for the summer (June, July and August) and autumn (September, October, and November) study periods. Both 1997 and 1998 data

are included. The analysis shows that the NW quadrant is the most frequent in both summer and autumn. The analysis also clearly reveals that periods of high BC concentration are less likely to be associated with northwesterly winds than are periods of low BC concentration in both summer and autumn. In summer, there is a tendency for high BC periods to be associated with southwesterly flow more often than low BC periods are. In autumn there is a tendency for high BC periods to be associated with southwesterly, southeasterly, or northeasterly flow more often than low BC periods are associated with these wind directions. These results are consistent with expectations, since the region northwest of Ft. Collins and the sampling site probably feature the lowest emissions of aerosol black carbon.

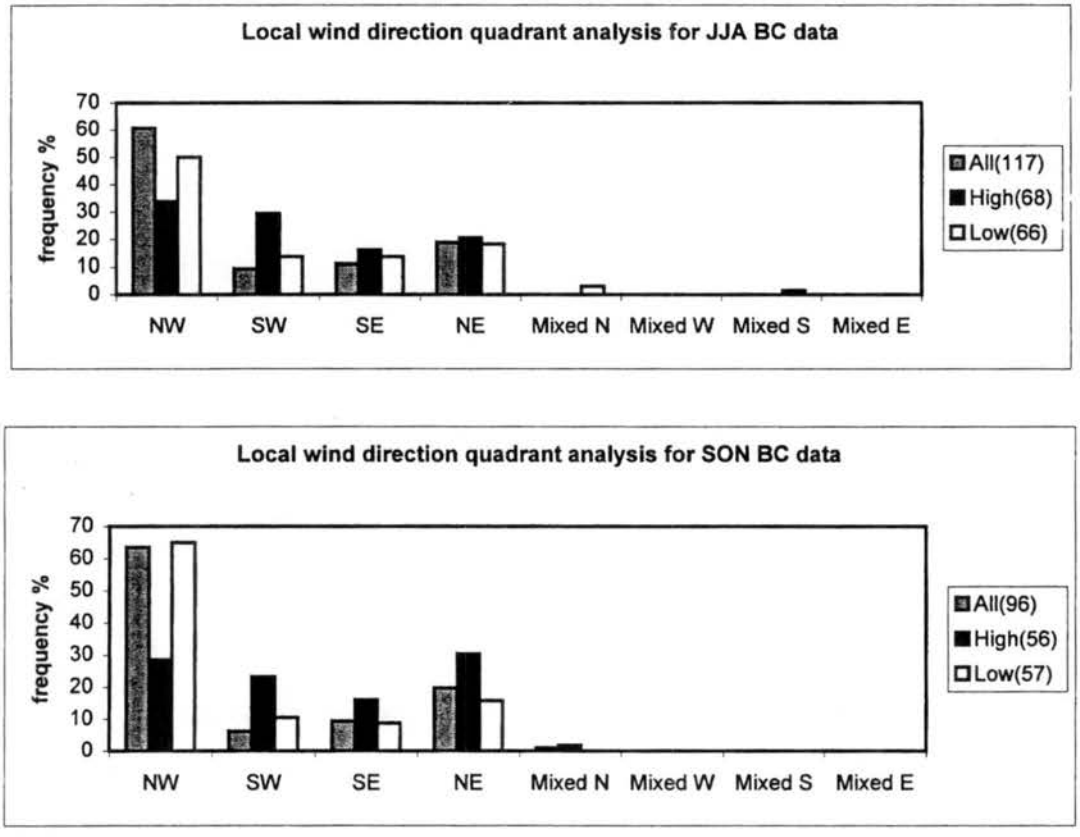

Figure 6. Quadrant analysis of (a) summer (JJA) and (b) autumn (SON) local wind directions.

3.4 Estimating aerosol particle absorption

Determination of the aerosol light absorption coefficient, b_{ap}, unfortunately is not possible by a unique direct method, i.e., a method where the signal of the instrument is proportional to the absorption coefficient and no assumptions are needed. All methods presently in use make some assumptions in order to measure the absorption coefficient. Since transmission and scattering measurements are direct ways to determine the extinction and scattering coefficient, the "b_{ap} subtraction method" is probably the only existing method which can be considered as an absolute method to obtain the absorption coefficient (Horvath and Habenreich, 1989). The aethalometer, by contrast, provides a relatively simple but indirect method of measuring optical particle absorption.

Visibility degradation is directly determined by the total extinction coefficient b_{ext}, which is given by the sum

$$b_{ext} = b_{sp} + b_{sg} + b_{ag} + b_{ap} \qquad (9)$$

where b_{sg} and b_{sp} are the light scattering coefficients for gas molecules and particles, and b_{ag} and b_{ap} are the coefficients of light absorption by gases and particles. The scattering measurements made by the nephelometer are subtracted from the extinction measurements made by the transmissometer assuming the b_{ext} and b_{sp} terms are usually dominant in the above equation for other than pristine environments (Lewis and Dzubay, 1986). The transmissometer/nephelometer data used are data that have been screened at Air Resources Specialists, Inc. The data are screened to comply with the state visibility standard. The visibility standard is an atmospheric extinction of 0.076/km. It is applicable from 8:00am to 4:00pm (8 hours) Mountain Local Time, and standard violations are any 4 contiguous hours where the average extinction is at .076/km or above. Any hour where the relative humidity is 70% or greater cannot be included in an average. The intent is to not include times when visibility impairment is dominated by natural sources (AQCC, 1993). The b_{sp} data are given in units of km^{-1}. The b_{ext} data are given in units of $km^{-1} * 1000$. In order to estimate b_{ap}, the measured value of b_{ext} is divided by 1000 and the corresponding measured value of b_{sp} data is subtracted from it.

Estimates of b_{ap} are obtained from the aethalometer data by multiplying the measured BC concentration by an airborne specific absorption cross-section (σ_{ap}) for aerosol black carbon. A value of σ_{ap} of 10 m^2/g was chosen based on its frequent use in the literature. In order to compare values of the absorption coefficient derived from the aethalometer data with those obtained from the transmissometer/nephelometer data, correction for standard-versus-actual volumes is necessary so that all three instruments are reporting in the same units. The following adjustments are made to the BC concentration reported by the aethalometer:

1. The aethalometer output data are averaged to get hourly BC_{STP} concentrations (to compare with transmissometer/nephelometer data)
2. The concentrations are multiplied by a pressure correction factor (850 mb/1013 mb) to adjust for density
3. The concentration is multiplied by an assumed airborne absorption coefficient for particulate BC: 10 m^2 / g
4. unit conversions are made from ng to g and from m to km

As an example, consider the calculation of a particle absorption coefficient for the one hour sample period ending at 17:00 local time on June 4, 1997. The hourly average BC concentration measured by the aethalometer was 345 ng/m^3. Using the calculation procedure outlined immediately above, this corresponds to a particle absorption coefficient of

345 ng /m^3 * (850 mb/1013 mb) * 10 m^2/g * 1g/10^9 ng * 10^3 m/km = 0.002895 km^{-1}

Comparisons of the aethalometer and transmissometer/nephelometer derived values of b_{ap} are shown in Figure (7). The absorption derived from the subtraction method is usually a factor of four or more greater than that derived from the aethalometer. The times when both data sets are similar, or the aethalometer derived absorption is greater, occur at high BC concentrations.

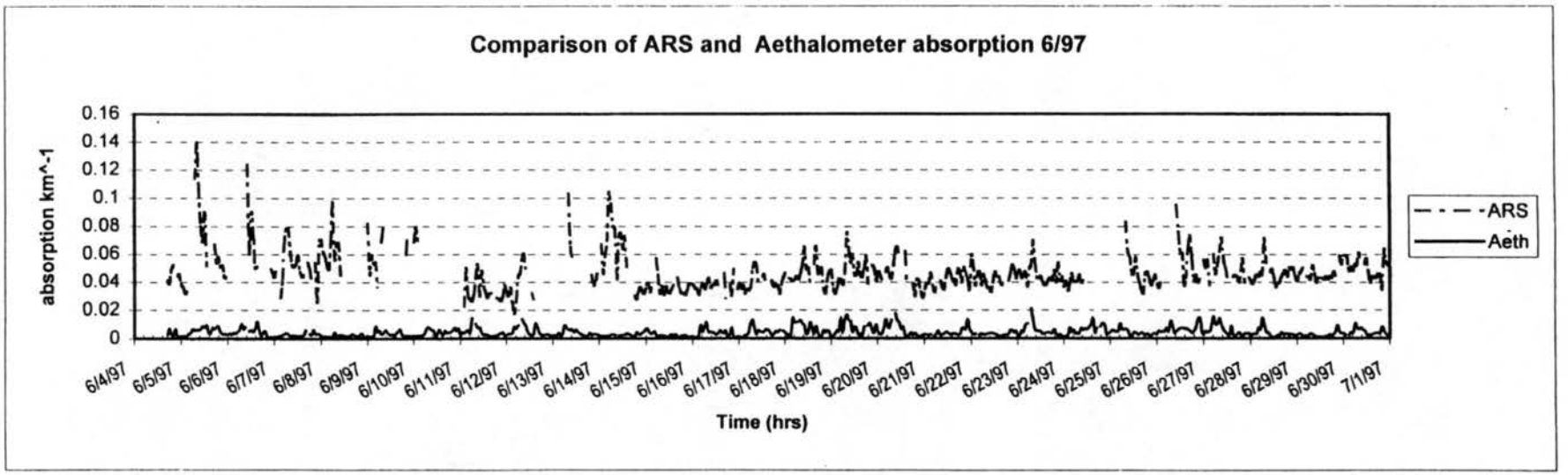

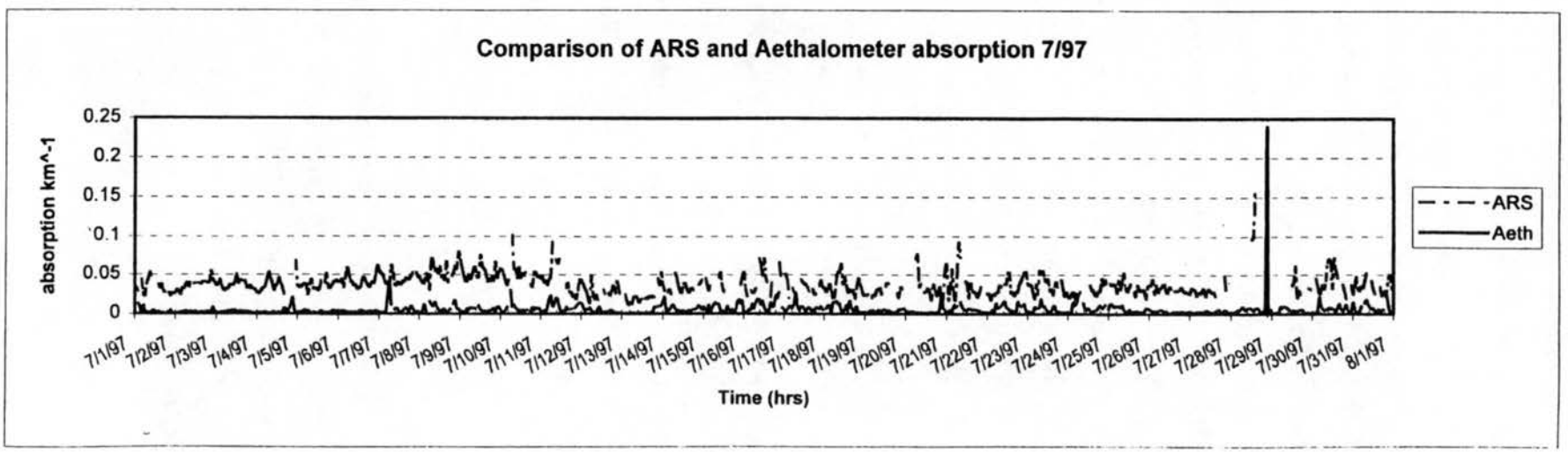

Figure 7a. June and July monthly time-lines of ARS and the Aethalometer absorption coefficients

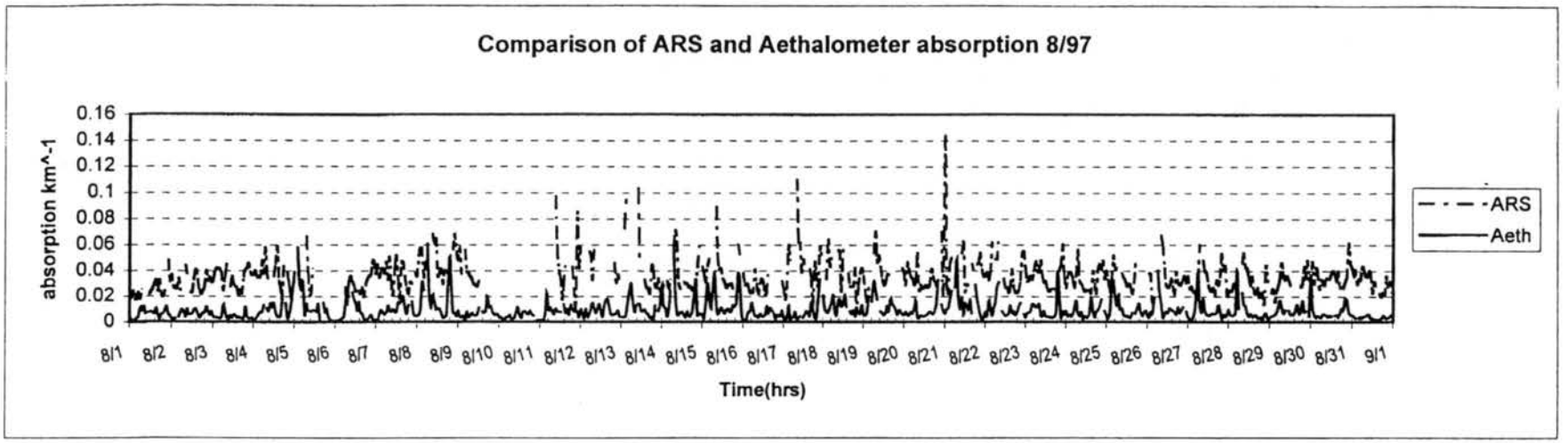

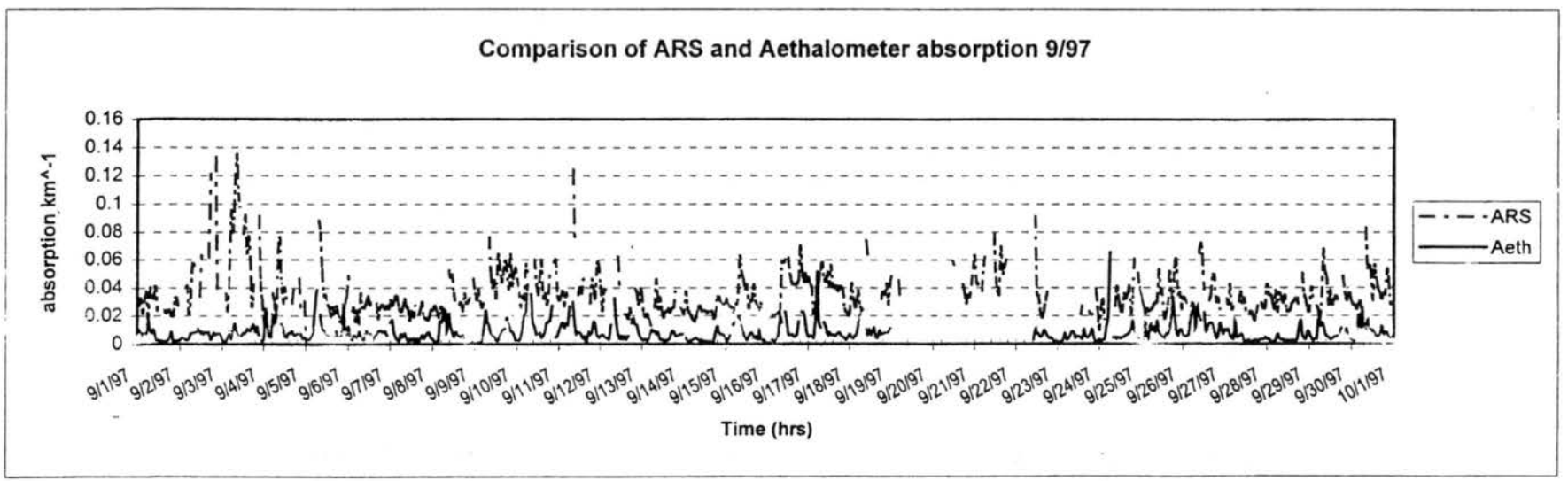

Figure 7b. August and September monthly time-lines of ARS and the Aethalometer absorption coefficients

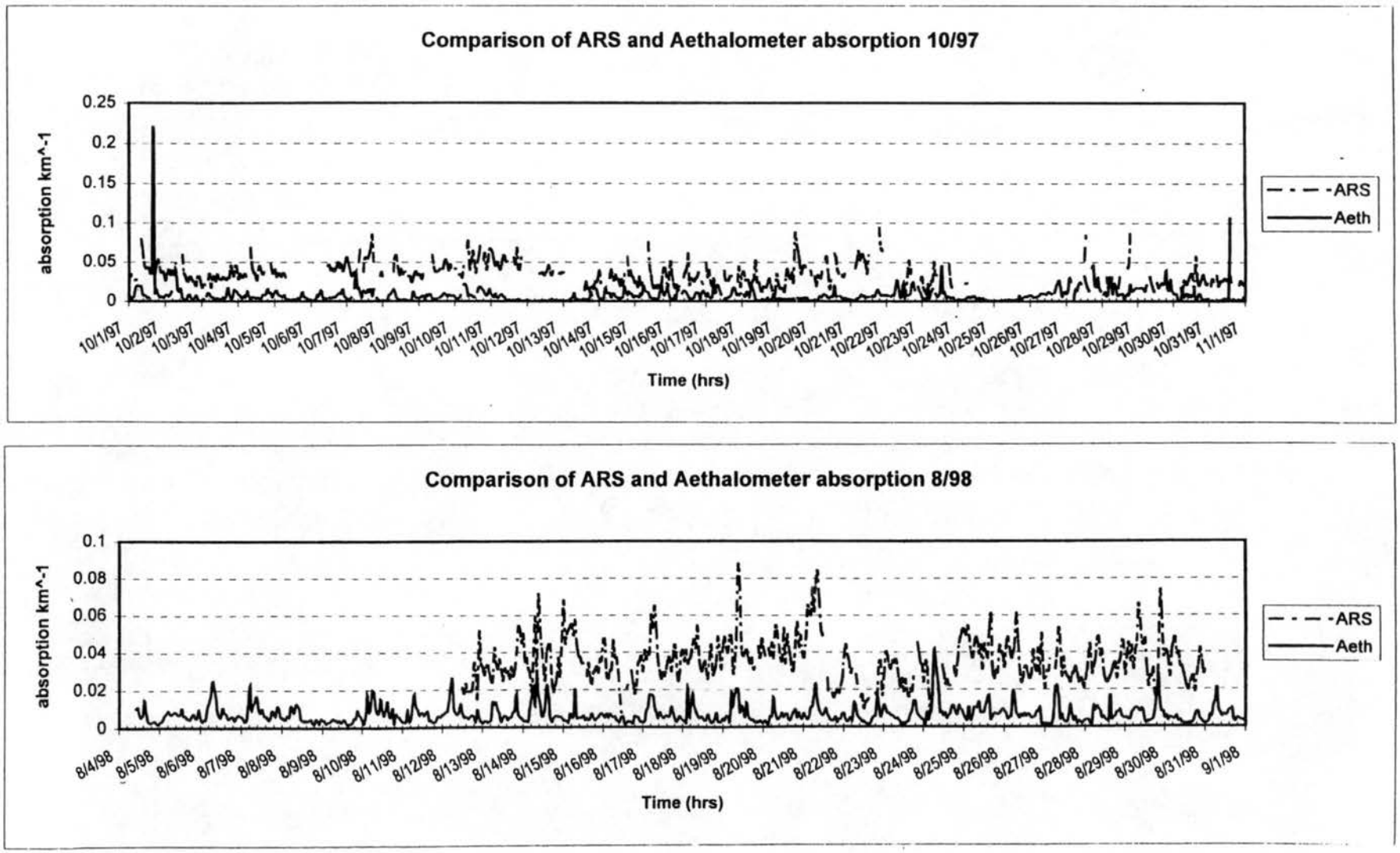

Figure 7c. October and August 1998 monthly time-lines of ARS and the Aethalometer absorption coefficients

3.5 Spatial variability in aerosol black carbon concentrations

During the spatial variation study, the colocated aethalometers were well correlated (refer to Figure 8), with a correlation coefficient of $r^2 = 0.98$. The data did not agree as closely when the "loaner" unit was moved to the downtown location, although a good correlation between the BC concentrations measured by the two instruments remained, with $r^2 = 0.7$. The campus site BC concentrations were usually higher than BC concentrations at the downtown location, perhaps due to the difference in sampling height (40m). Since BC emissions locally are probably dominated by vehicle traffic we expect them to decrease with elevation above the ground. The average BC concentrations were 885 and 644 ng/m^3 at the campus and downtown sites respectively.

The difference was more pronounced when the "loaner" instrument was measuring at the city's busiest intersection (refer to Figure 9) where average traffic count was 46,000 per day. The average BC concentrations at the intersection were similar to those at the campus site, but the overall correlation was $r^2 = 0.5$. Concentrations were sometimes higher on campus (even during heavy traffic periods) and sometimes higher at the intersection. The difference in sampling height was 6m between the two sites. The average BC concentrations were 1022 and 1016 ng/m^3 at the campus and at the intersection, respectively. High concentrations at all three of the intercomparison study sites generally occur when wind speed is low. Comparisons of BC concentrations at each of the sites with wind direction reveal no obvious patterns (see Figures D.1.1 and D.1.2 in Appendix D with meteorological data). This analysis is complicated by the fact that BC emissions from traffic vary diurnally. The longer data record available at the campus site allows us to explore the relationship between BC concentrations and wind direction at that site more fully.

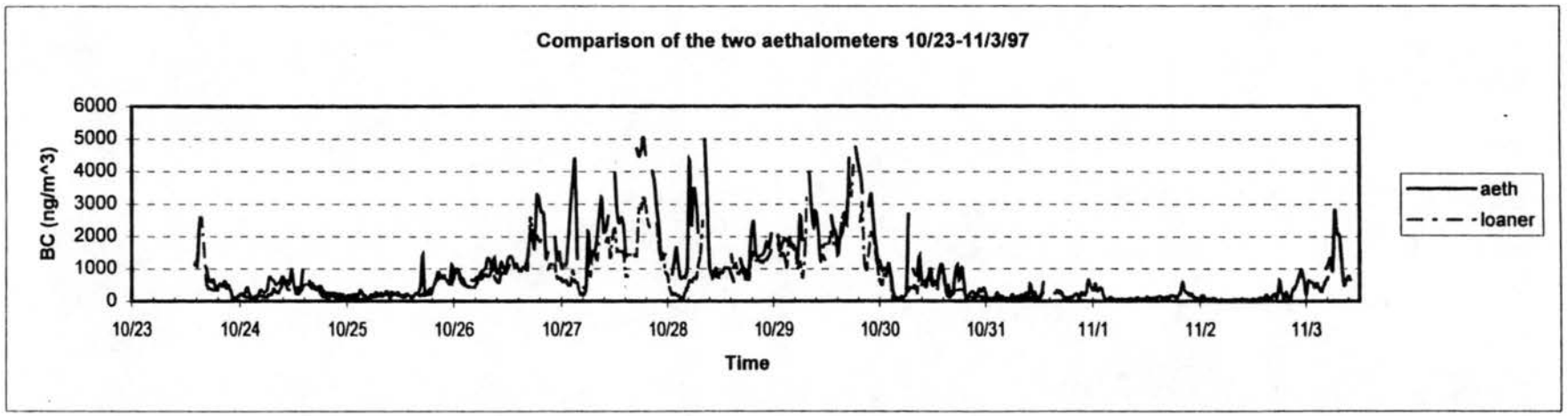

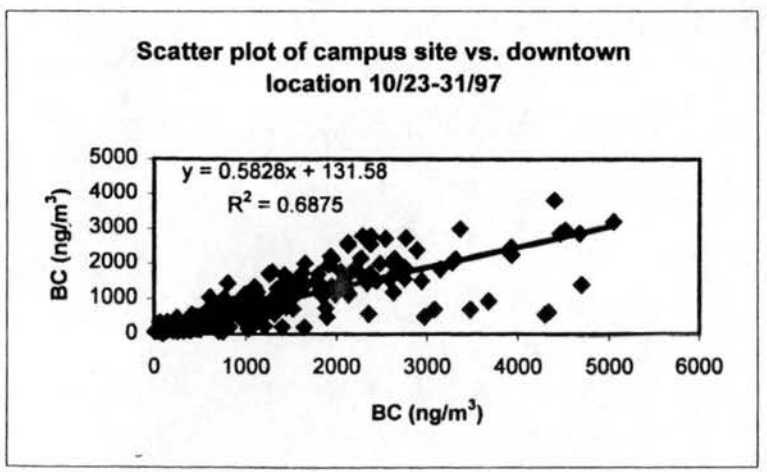

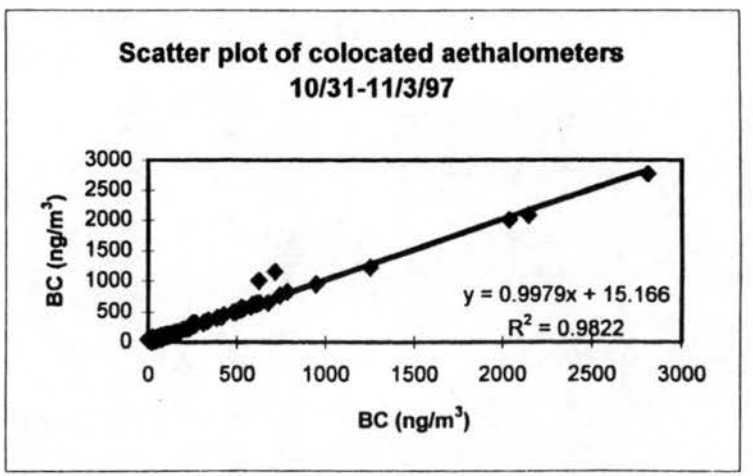

Figure 8. Spatial variation study. a) time-line comparison of the two aethalometers. b) comparison of campus and downtown location. c) comparison of colocated aethalometers.

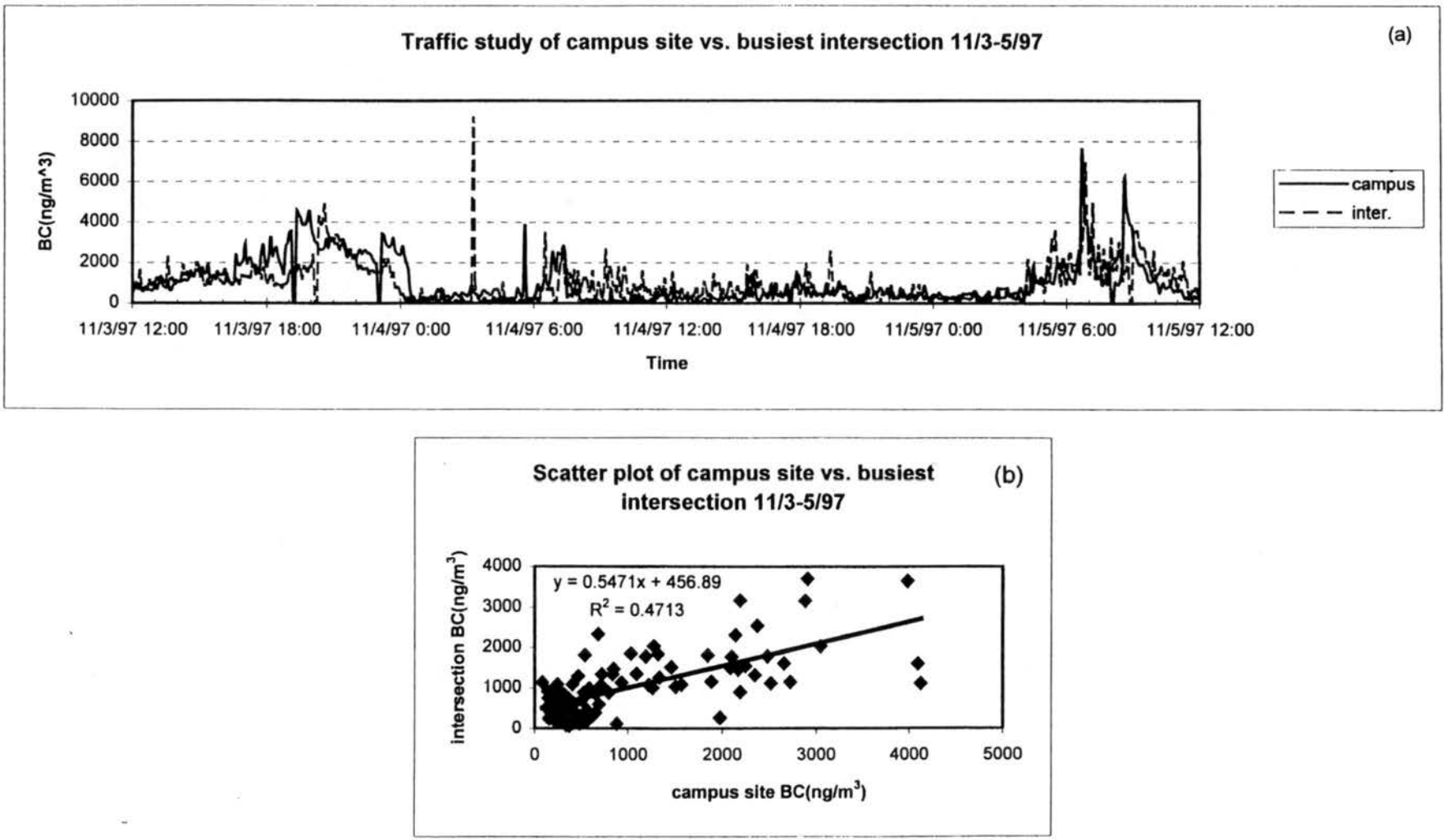

Figure 9. Spatial variation study. a) time-line comparison of campus site and busiest intersection. b) comparison of campus and intersection.

3.6 Special events influencing BC concentrations

During the measurement period several episodes which we term "special events" occurred in or near Fort Collins. These events included fires associated with the disastrous flood on July 28th, 1997, CSU student riots on August 29th and September 5th, 1997, a prescribed burn near Red Feather Lakes in northern Colorado on October 7th – 9th, 1997, a blizzard on October 24th - 25th, 1997, and a prescribed burn at Crosier in the Roosevelt National Forest on August 19th – September 18th, 1998. Passage of trains pulled by diesel locomotives along the tracks immediately west of the campus monitoring station will also be analyzed as "special events" since they don't run on a regular schedule.

Fires near the campus site associated with the July 28th 1997 flood were observed in the BC concentration data record. The aethalometer measured peak BC concentrations near 50,000 ng/m^3. These high concentrations led to rapid saturation of the collection spot on the aethalometer sampling tape so that no data were obtained for the hour following this BC peak. The blizzard on October 24th-25th, 1997 was observed in the data record. During this period the aethalometer recorded consistently low concentrations (< 250 ng/ m^3). This was not surprising given the dramatic drop in vehicle traffic during and following the snowfall, coupled with the strong upslope ventilation provided by the storm.

One of the two CSU student riots was evident in the BC concentration record while the other was not. Both riots occurred on the north side of the CSU campus, and were located approximately 400 m west northwest of the campus sampling site. During the riots students set several household objects on fire in the streets. The student riot that occurred on August 29th, 1997 between 11pm and 1am, was observed in the data (peak 30 minute average BC concentration of approximately 6300 ng/m^3). The September 5th, 1997 riot was not detected, despite the facts that winds blew from the northwest in both events. Low wind speeds in the September riot (0.9-1.4 miles per hour) may have allowed the fire plume to dilute significantly before being transported past the campus aethalometer site.

allowed the fire plume to dilute significantly before being transported past the campus aethalometer site.

The prescribed burn near Red Feather Lakes was not observed in the data. This was probably due to the distance from Fort Collins (59 km northwest of Fort Collins), low to moderate wind speeds, and varying wind directions at that time. The prescribed burn at Crosier (25 km southwest of Fort Collins) in the Roosevelt National Forest on August 19th – September 18th, 1998 was readily visible with the naked eye on September 18th, 1998; however, the burn could not be identified in the aethalometer data with any certainty. Although a lofting plume from the fire was visibly being transported eastward aloft, surface winds were from the southeast at the campus sampling site. Visual observations suggested the plume was nearing the ground several km southeast of the sampling site. Several peaks in the August 1998 monthly timeline with winds from the southwest could be associated with this event.

Figure (10) shows BC concentration timelines for August and September, 1998. BC concentrations were measured over 5 minute intervals during this period to help characterize the influence of diesel locomotives passing the site. The lettered arrows in the timelines indicate times of train passages. Table 1 in Appendix C shows the duration of each train passage and the wind speed and direction during each train passage. Typical train passages last 3 – 5 minutes. The trains pass west of the site, so only a westerly component of the wind would allow effluent from the train to reach the site. Since lengthy train passages also lead to extra automobile and truck emissions resulting from vehicles waiting at train crossings, it is conceivable that this indirect effect of train passage on BC concentrations might be evident when the wind does not possess a westerly component. From analysis of Figure (10) it appears that some BC concentration peaks are associated with train passages. Figure (11) illustrates in detail the time evolution of BC concentrations in periods surrounding train passages for several case studies. Case studies were selected by the passage of trains near spikes in BC concentrations. The case studies for long train passage were train passages 10 minutes or longer in duration. The parallel lines in the plots mark the length of the train passage. Keep in mind the times of train passage corresponds to train passing an intersection 1

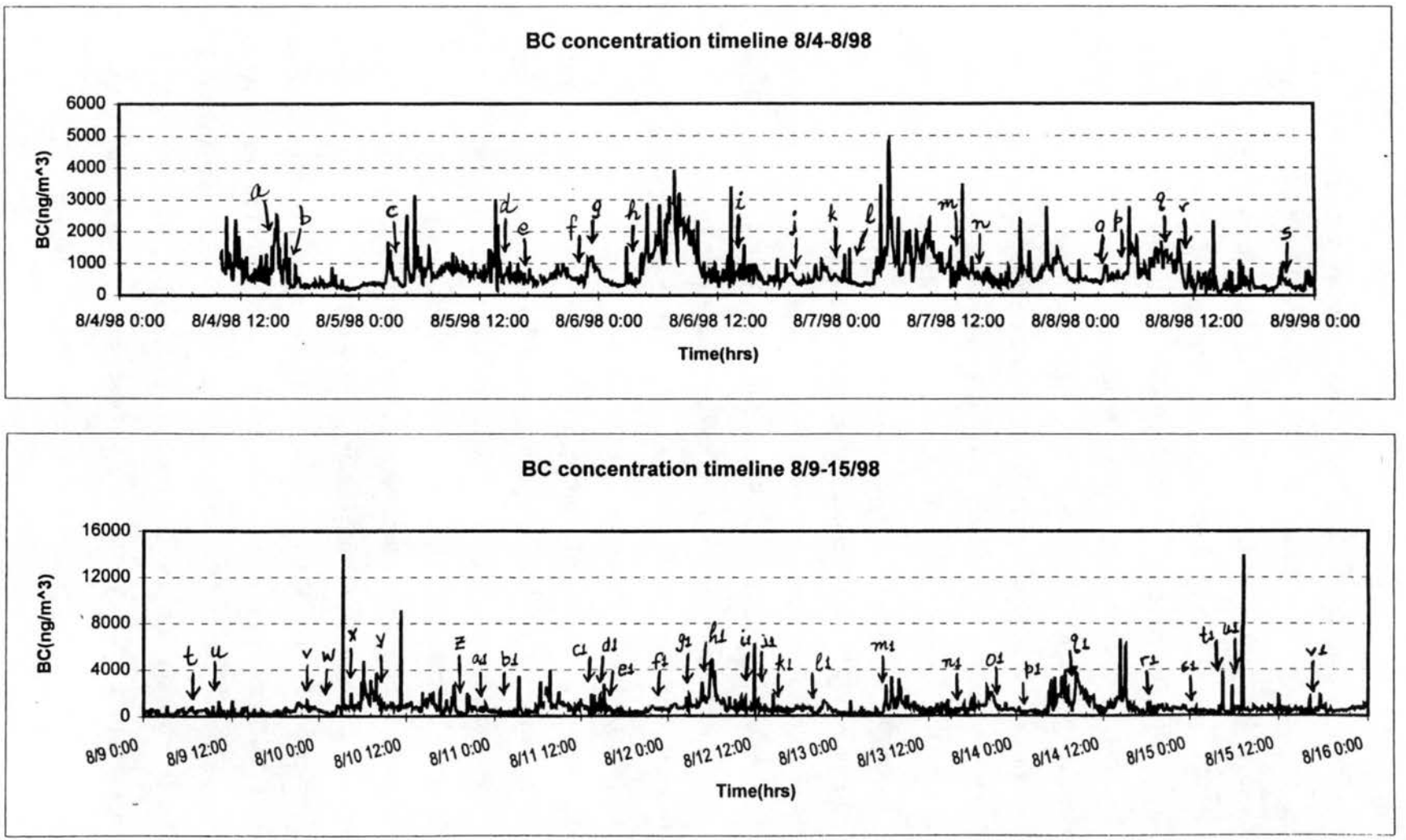

Figure 10a. Weekly BC concentration time-lines indicating train passages

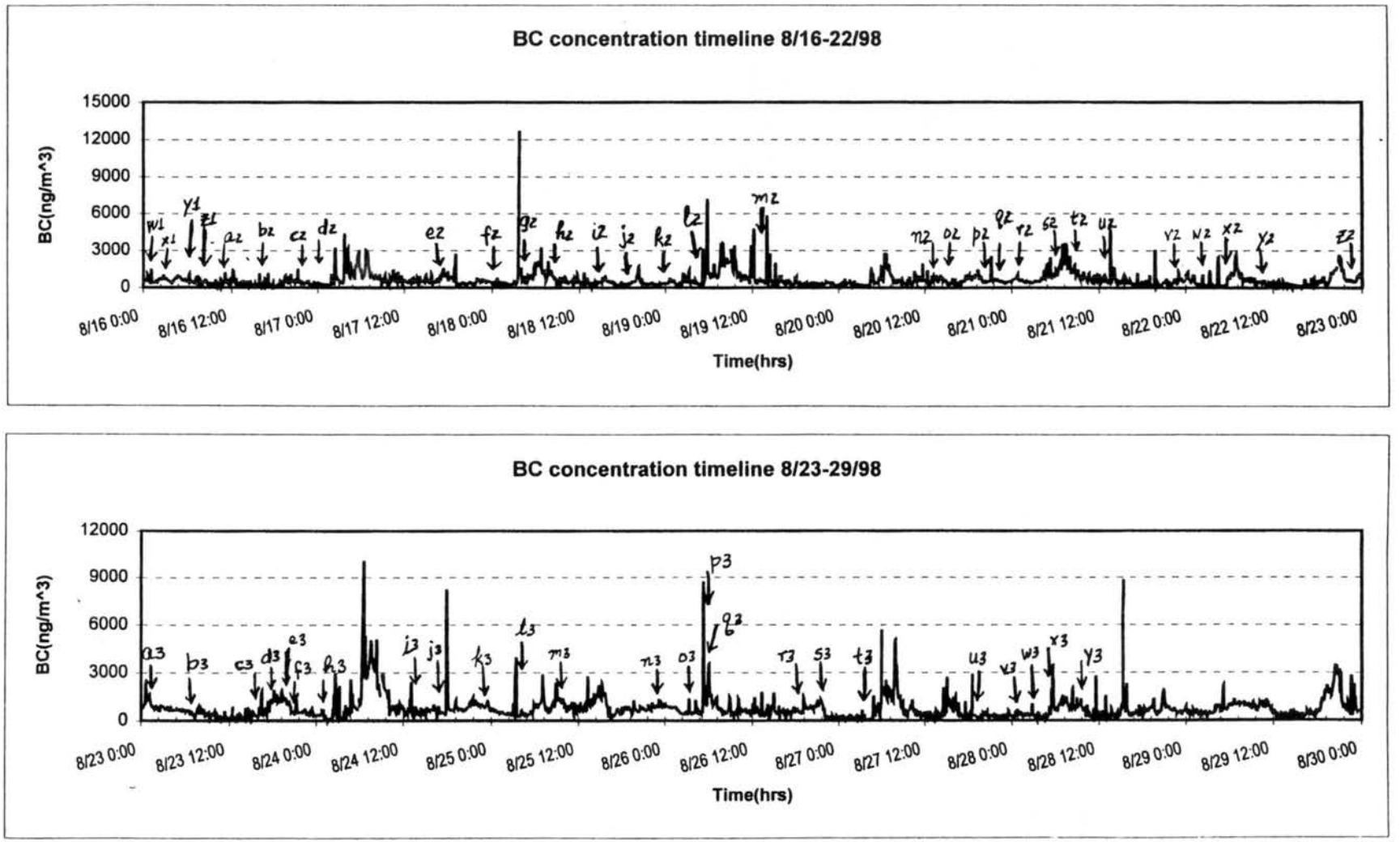

Figure 10b. Weekly BC concentration time-lines indicating train passages

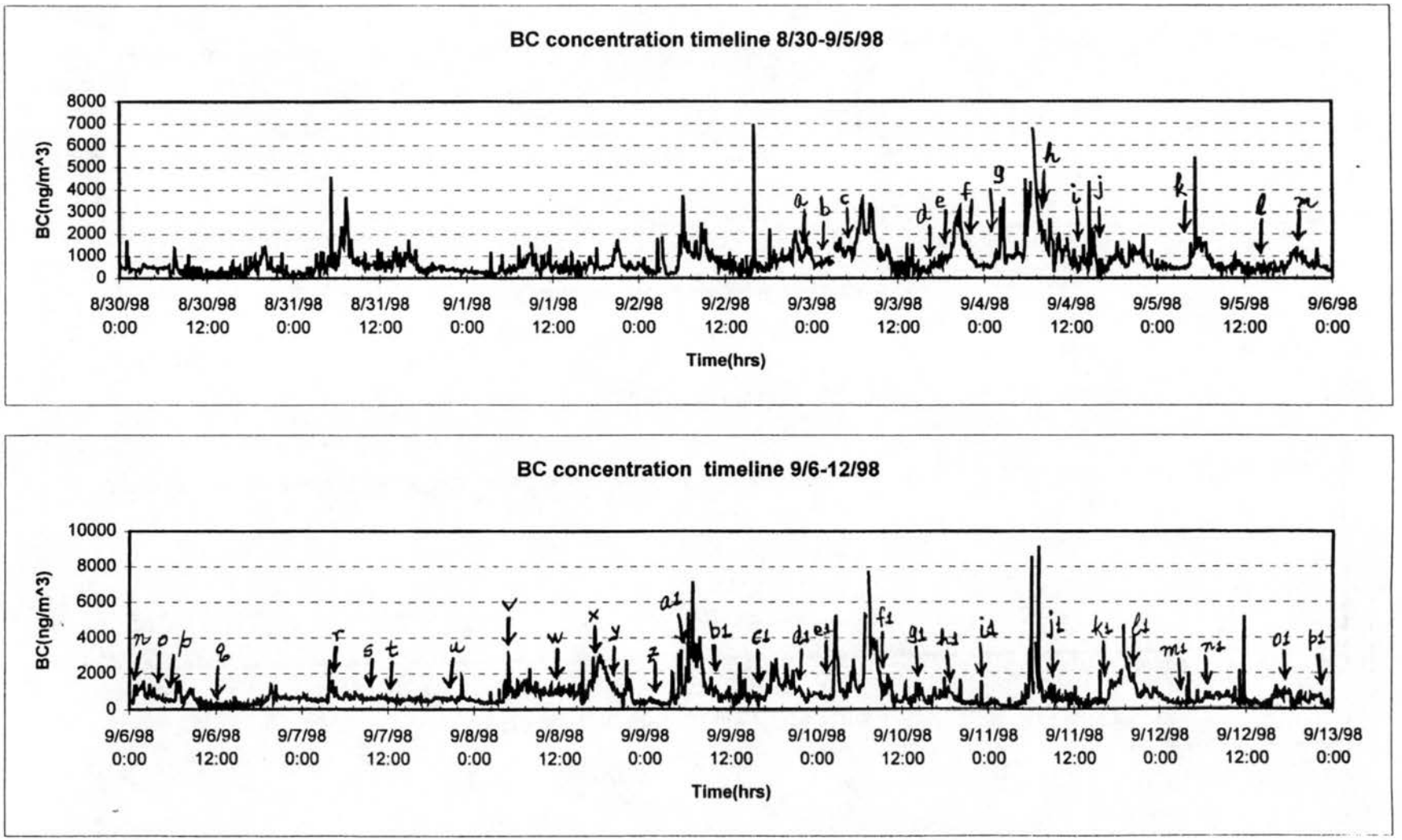

Figure 10c. Weekly BC concentration time-lines indicating train passages.

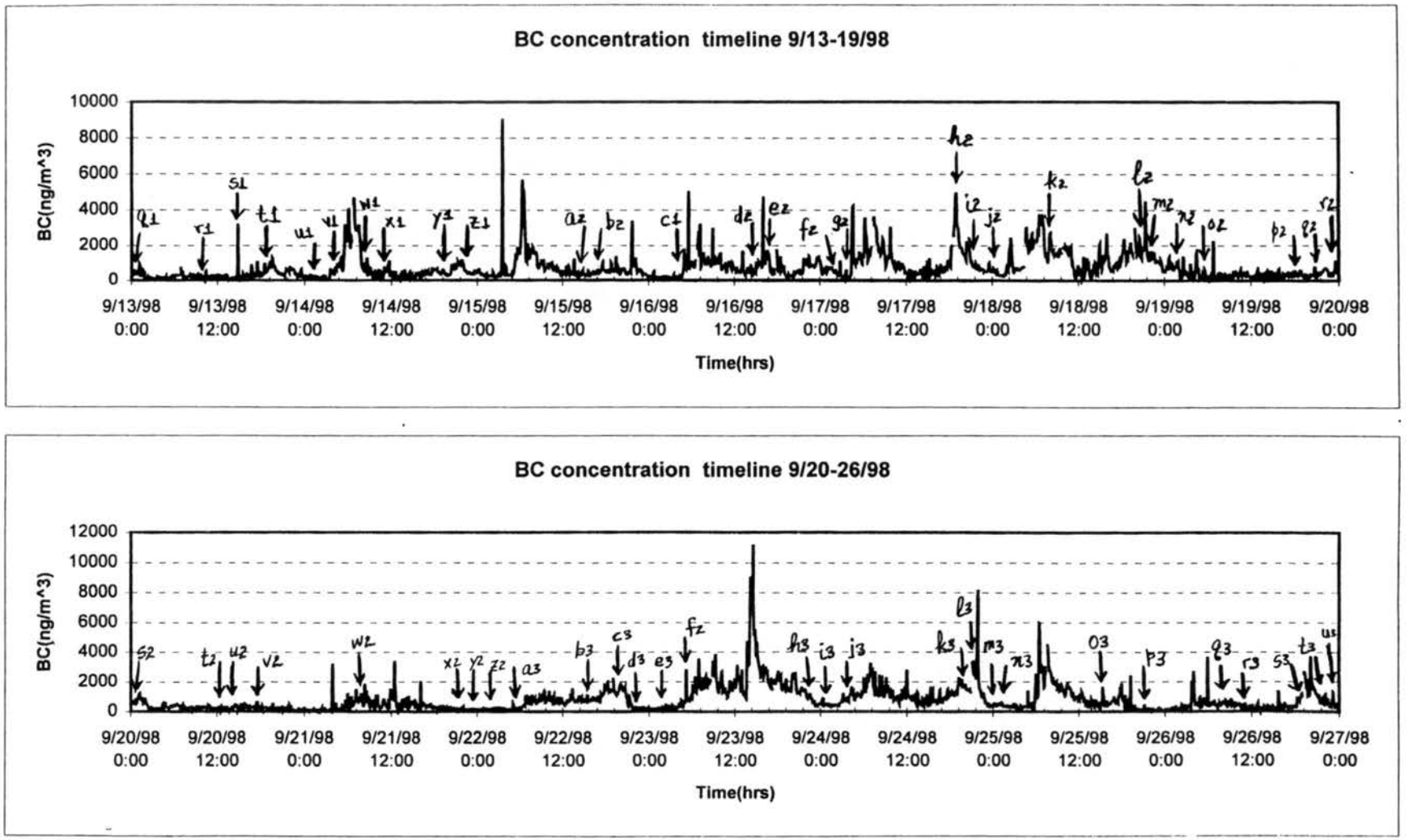

Figure 10d. Weekly BC concentration time-lines indicating train passages.

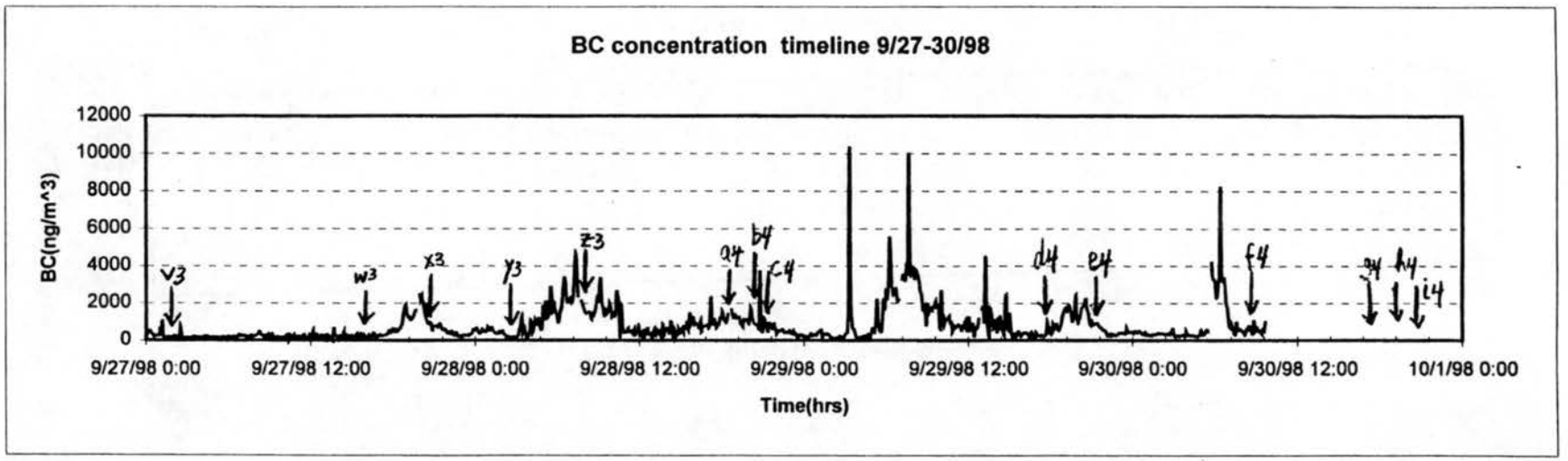

Figure 10e. Weekly BC concentration time-lines indicating train passages.

block north of the monitoring site. Also, we do not know the train speed, travel direction, or number of locomotives.

Case study 1 occurred on August 4th with two train passages at 15:30-15:36, and 16:00-16:03 hours. An increase in BC concentration (2495 ng/m^3) was seen immediately after the first passage (aethalometer sample interval 15:35-15:40). The winds at this time were from the northwest at 5 mph. The second passage at 16:00-16:03 showed no immediate increase in BC concentration. An increase in BC concentration was seen 30 minutes later. The wind during this second passage had shifted to the southwest and decreased to 1.9mph.

Case study 2 occurred on August 5th at 13:03-13:09 hours. A significant increase in BC concentration (3015 ng/m^3) was seen 30 minutes after the train passage. An immediate signal from the train was not present. The winds were from the southeast at 4 mph.

Case study 3 occurred on August 6th at 13:14-13:19 hours. An increase in BC concentration (3381 ng/m^3) was seen immediately following the train passage. The winds were from the southeast at 1.1 mph.

Case study 4 occurred on August 7th and featured two train passages at 12:43-12:46 and 13:37-13:41hours. Concentrations were increasing and reached a maximum during the train passages (3496 and 1220 ng/m^3, respectively). The winds were from the southeast at 5.3 and 4.9 mph respectively.

Case study 5 occurred on August 12th at 11:47-11:50 hours. The increase in BC concentration (6253 ng/m^3) occurred during the end of the train passage. The winds were from the northeast at 3.9 mph.

Case study 6 occurred on August 15th at 6:54-6:58 hours. No increase in BC concentration was seen during the train passage. An increase (13800 ng/m^3) was seen 10 minutes later. The winds were from the northwest at 2.3 mph.

Case study 7 occurred on August 19th at 5:31-5:36 hours. An increase in BC concentration was seen during (2775 ng/m^3) and immediately after the passage (7195 ng/m^3). The concentrations were elevated for 10 minutes after the passage. The winds were from the northwest at 0.9 mph.

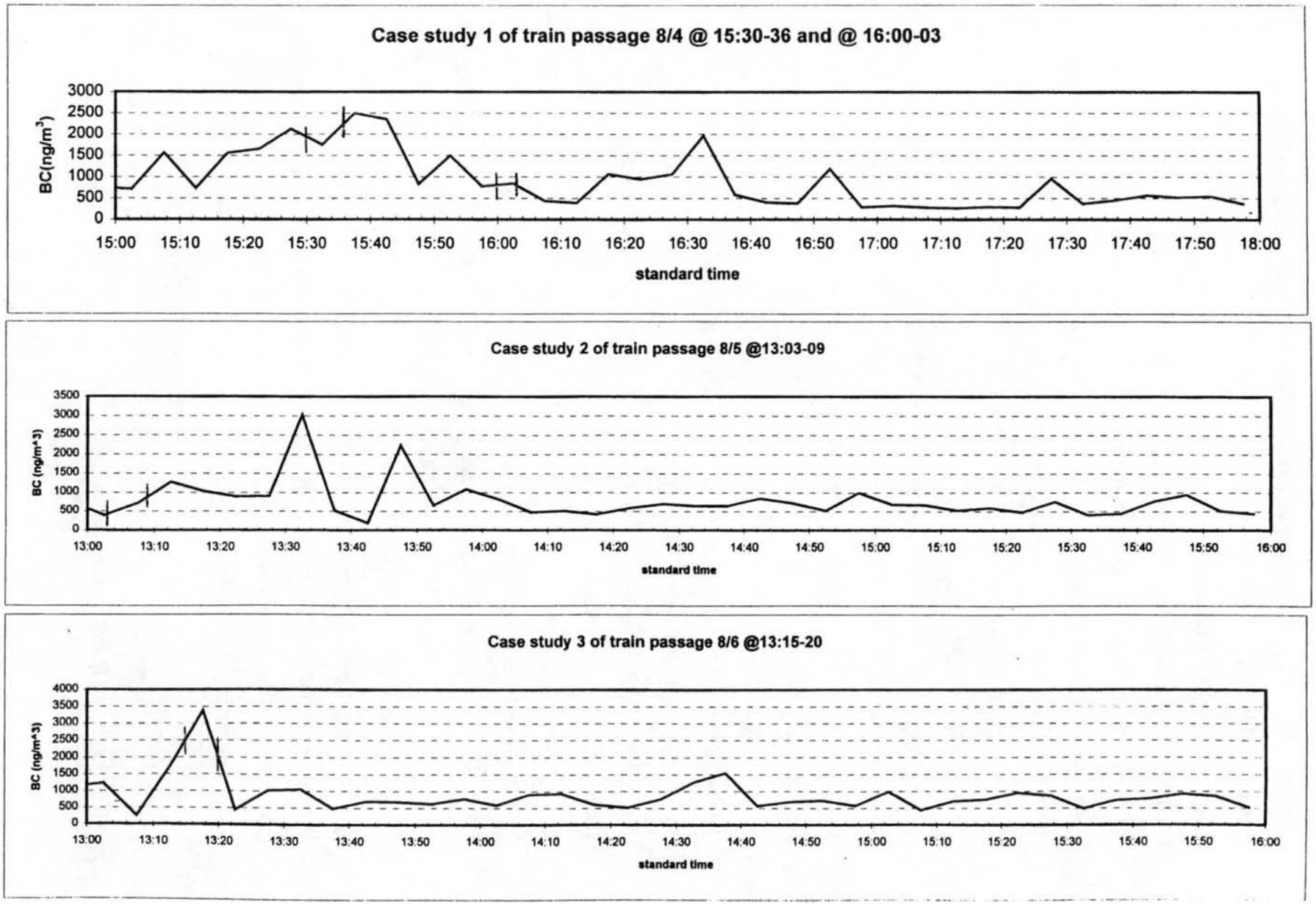

Figure 11a. Train passage case studies 1, 2, and 3.

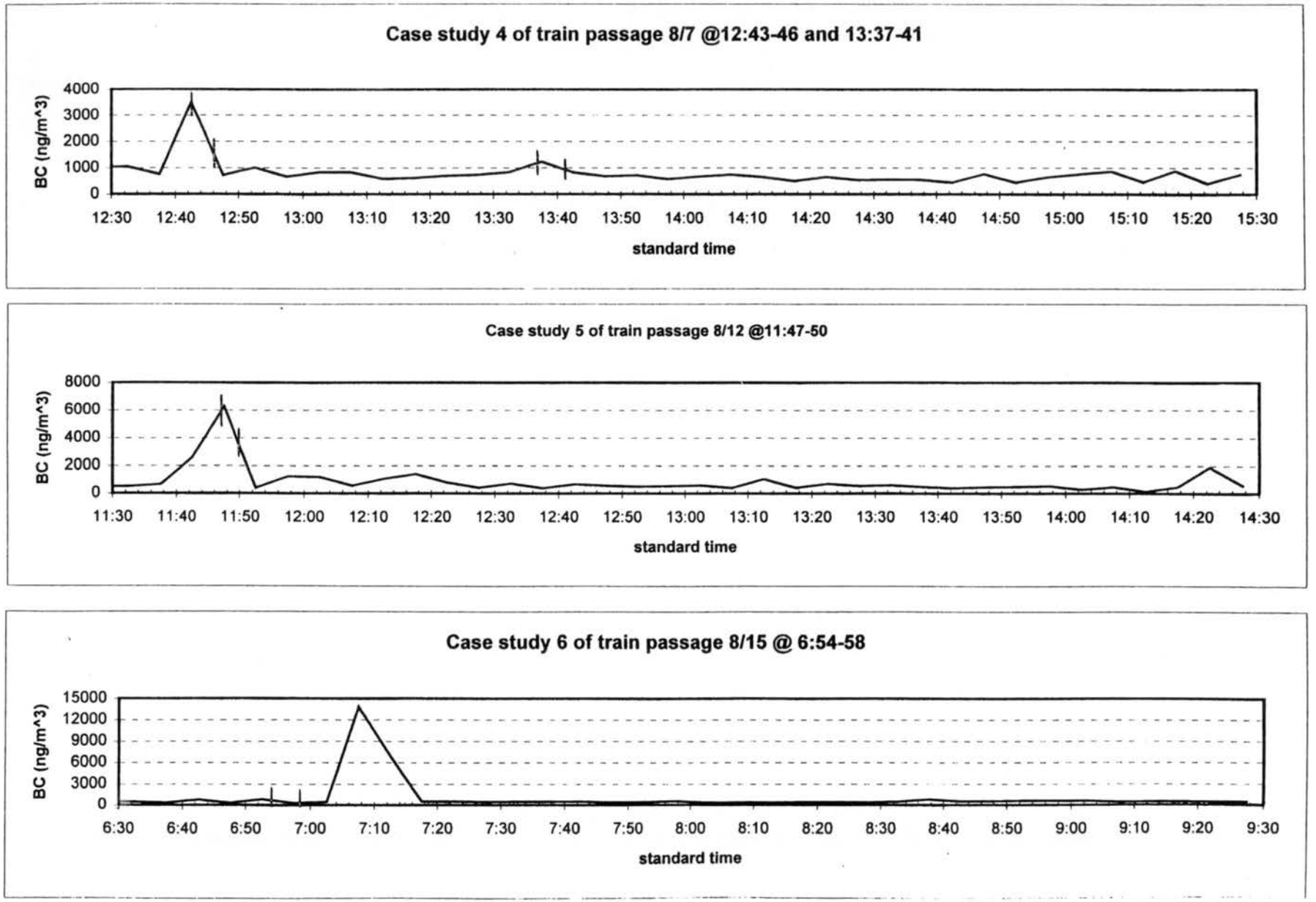

Figure 11b. Train passage case studies 4, 5, and 6.

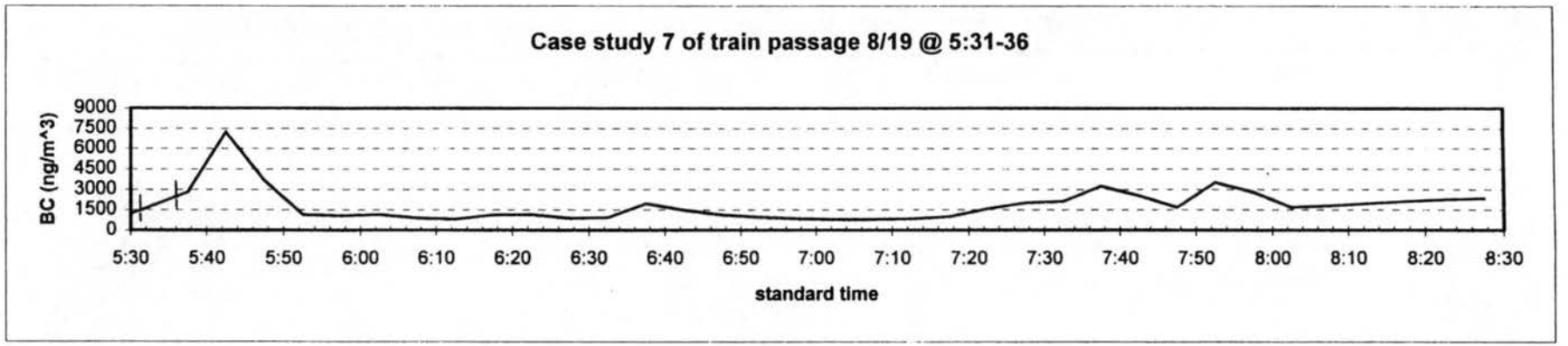

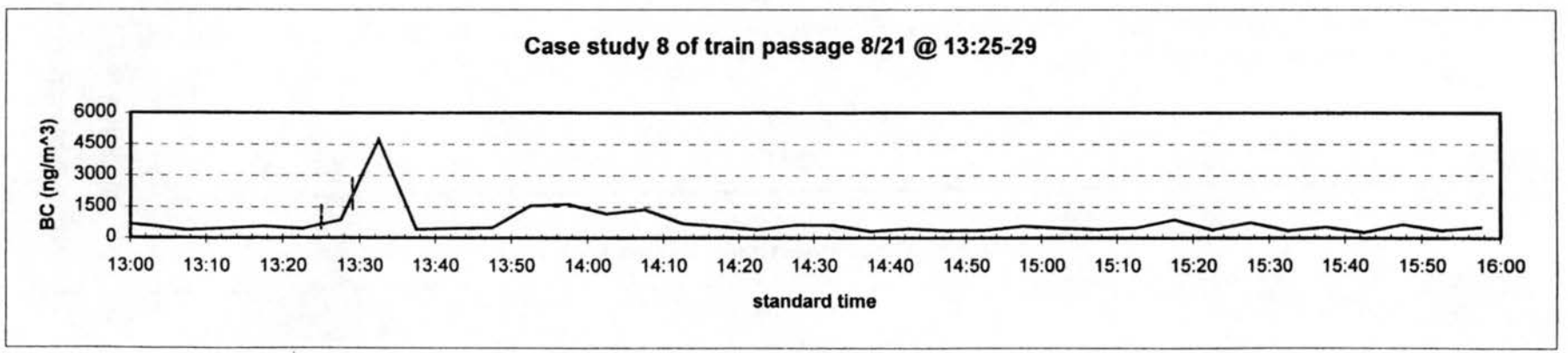

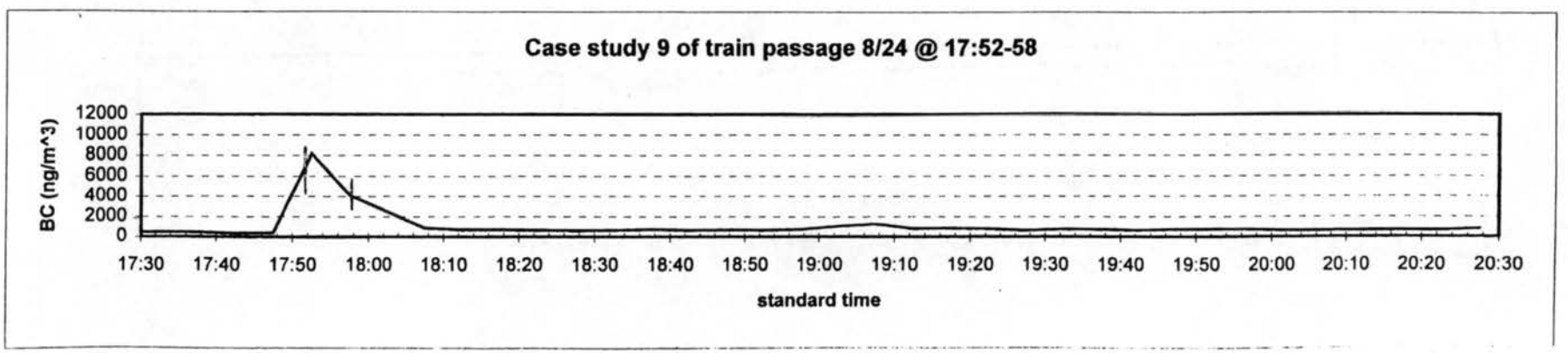

Figure 11c. Train passage case studies 7, 8, and 9.

Case study 8 occurred on August 21st at 13:25-13:29 hours. The increase in BC concentration (4718 ng/m^3) was seen during and following the train passage. Winds were from the southeast at 5.5 mph.

Case study 9 occurred on August 24th at 17:52-17:58 hours. An increase in BC (8157 ng/m^3) was seen during the train passage. The winds were from the southwest at 8 mph.

Case study 10 occurred on August 25th at 2:58-3:02 hours. A small increase was seen during the train passage and a large increase peaking 20 minutes later. The winds were from the northwest at 1.4 mph.

Case study 11 occurred on September 3rd at 5:32-5:36 hours. A small increase in concentration is seen during the passage. The winds were from the southwest at 1.2 mph. The increasing concentrations measured after 6:00 are probably the morning rush hour signal.

Case study 12 occurred on September 4th at 13:40-13:44 hours. A small increase is seen during and after the passage. The small signal may reflect strong dilution of the locomotive plume. Winds during this period blew from the southwest at 12.5 mph. An increase in BC concentration measured at 14:35 is probably traffic related.

Case study 13 occurred on September 8th and included two train passages at 17:16-17:21 and 18:51-18:54 hours. A possible small increase is seen during the first train passage, but not in the second. A further increase after the first passage may reflect a combination of train and traffic emissions. The winds were from the northwest at 0.9 and 1.4 mph, respectively, during the two train passages.

Case study 14 occurred on September 9th at 5:23-5:27 hours. There is no increase during or immediately following the passage but an increase in BC concentration is seen 15 minutes later. The winds were from the southwest at 0.8 mph.

Case study 15 occurred on September 10th at 2:20-2:23 hours. An increase in BC concentration (1995 ng/m^3) is seen immediately after the train passage. The increase in concentration from 2:20-3:05 peaked at 5184 ng/m^3 at 2:40-2:45. The winds were from the southwest at 1.8 mph. The prolonged increase in BC concentration shows the slow dissipation of the plume at that time.

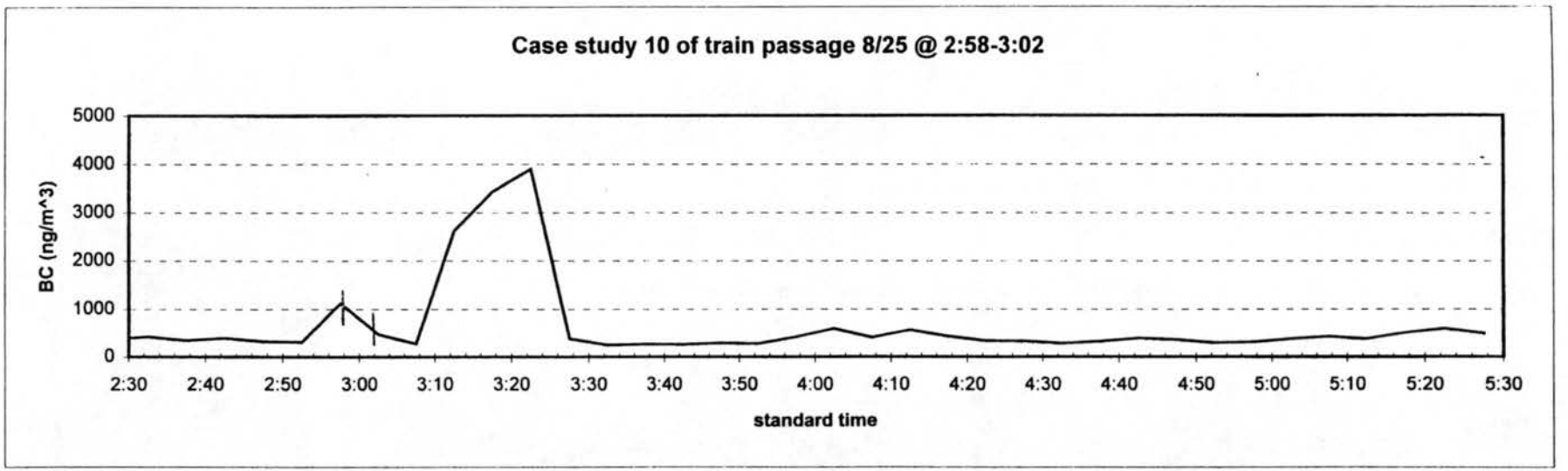

Figure 11d. Train passage case study 10.

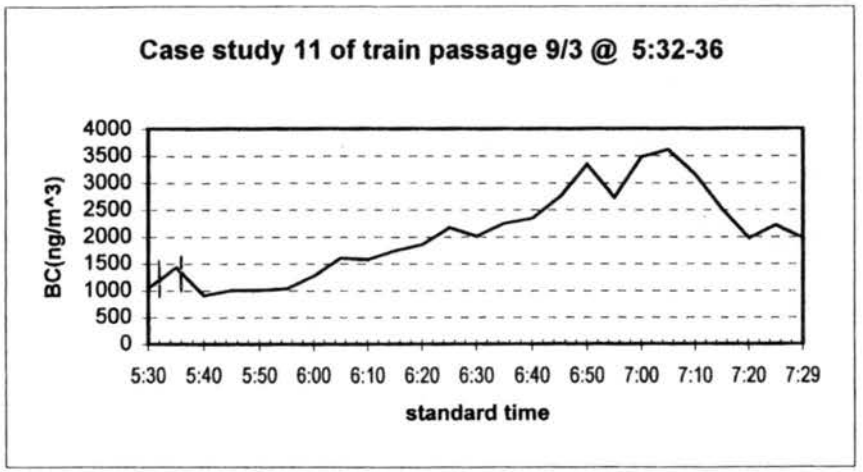

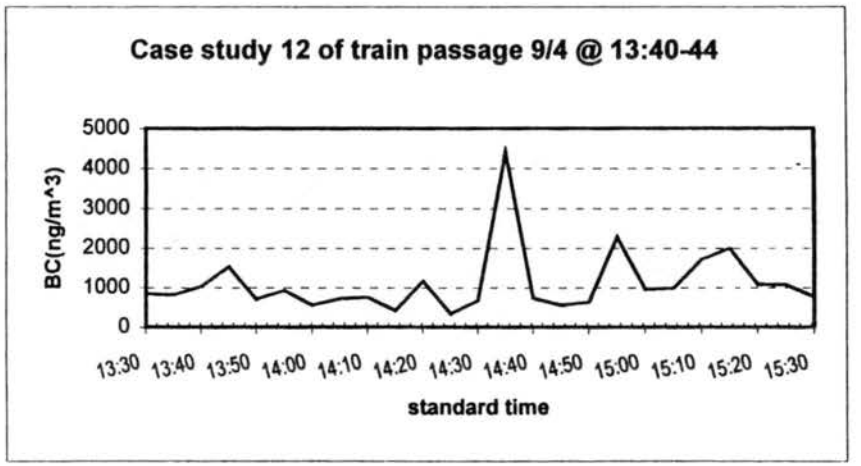

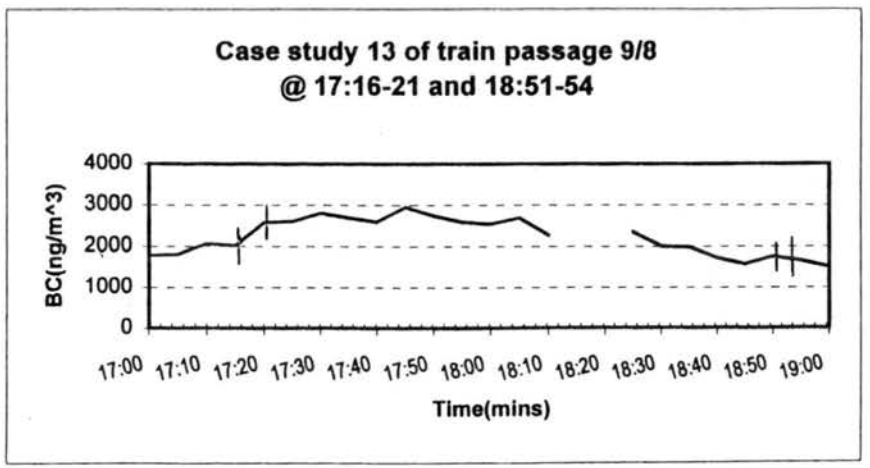

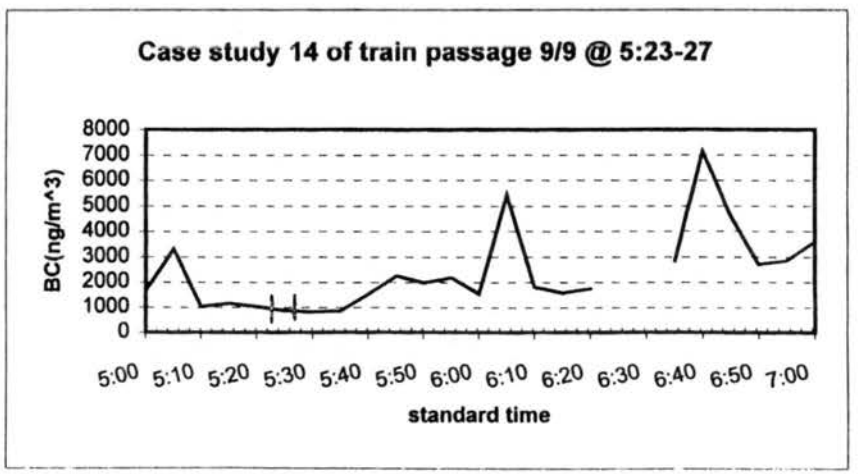

Figure 11e. Train passage case studies 11, 13, 13, and 14.

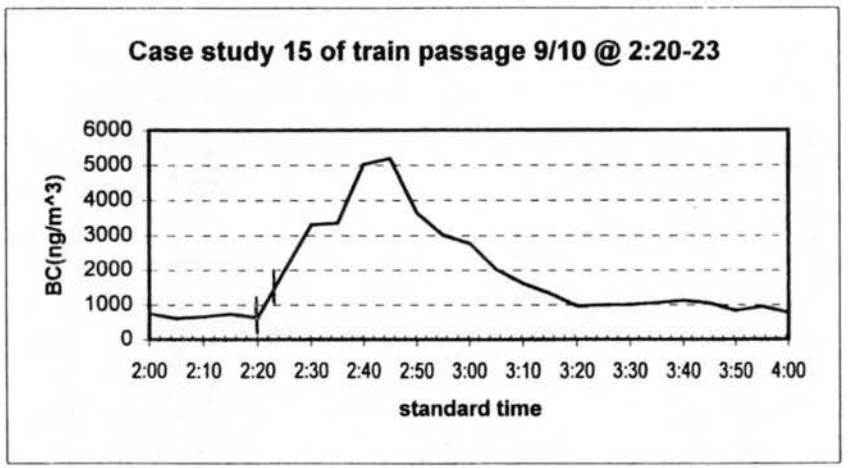

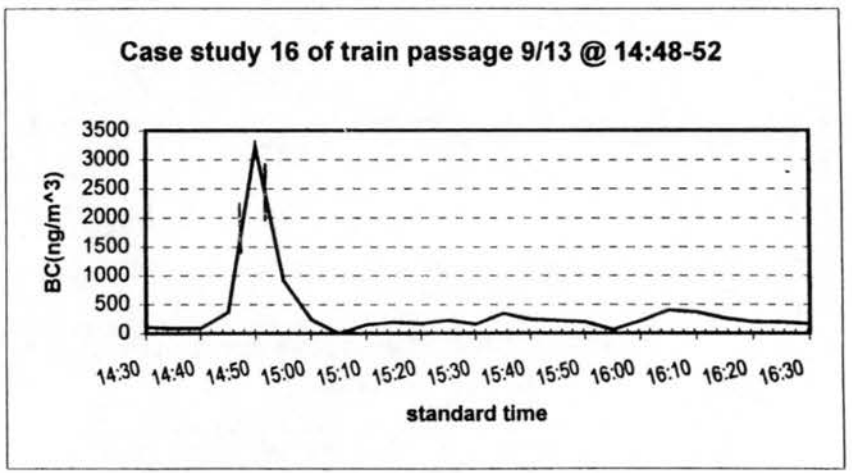

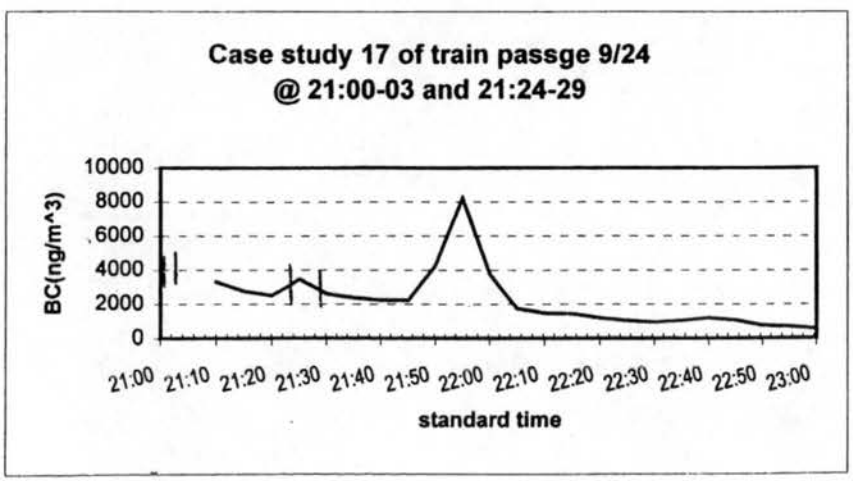

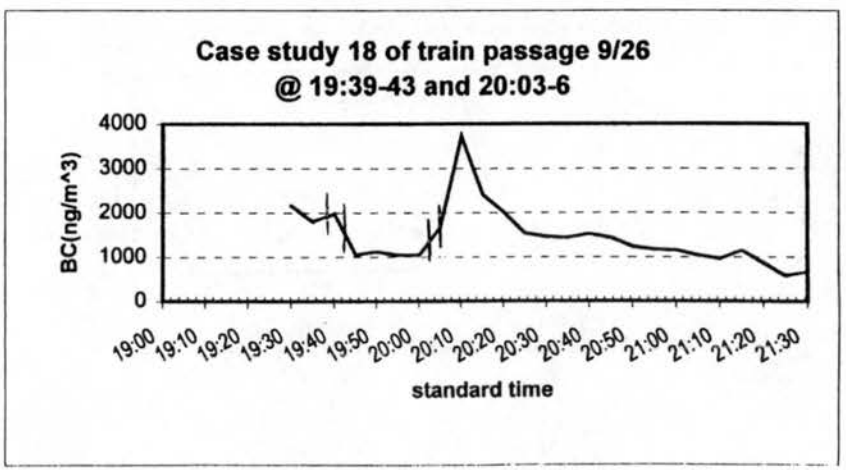

Figure 11f. Train passage case studies 15, 16, 17, and 18.

Case study 16 occurred on September 13th at 14:48-14:52 hours. An increase in BC concentration to 3220 ng/m^3 is seen during the train passage. The winds were from the northwest at 1.2 mph. Concentrations were elevated for 10 minutes (during and after the train passage).

Case study 17 occurred on September 24th and featured two train passages at 21:00-21:03 and 21:25-21:29 hours. No data were recorded during the first passage as the instrument halted to change the 'sensing' spot on the filter. A large increase was seen 25 minutes after the second train passage. Winds were from the northwest at 0.1 mph.

Case study 18 occurred on September 26th and featured two train passages at 19:40-19:43 and 20:03-20:06 hours. An increase in BC concentration is seen during the first train passage (1978 ng/m^3) and after the second train passage (3717 ng/m^3). The winds changed direction between the train passages, from northwest at 1.9mph during the first passage to southwest at 1.1mph during the second passage.

Analysis of the data described above indicates that peaks in BC concentration are often associated with train passage. This is not surprising given the BC-rich plume emitted by diesel locomotives. It seems plausible, therefore, to assume that BC concentration peaks observed shortly after train passage originate from the diesel locomotive emissions. The data even suggest that the length of time passing between train passage and observation of the plume increases with decreasing wind speed. One must keep in mind, however, that the train moves along a line extending from very near the site in a north-south direction. Depending on the exact wind direction, the along-wind distance from the locomotive plume to the sample inlet can vary considerably. This will certainly impact the time lag between train passage at the site and arrival of the plume. The time lag can be further affected by the train's direction and speed. For example, if the winds are from the NNW and the train is headed north, the time at which the train emits a plume at a point which will be transported to the aethalometer sample inlet will occur after the train itself passes the monitoring site.

It is difficult however, to separate out the impact on BC concentrations of direct locomotive emissions from increased motor vehicle emissions resulting from traffic jams created by train passage. In several cases where winds were moderately strong and contained an easterly component, we saw significant increases in BC concentrations

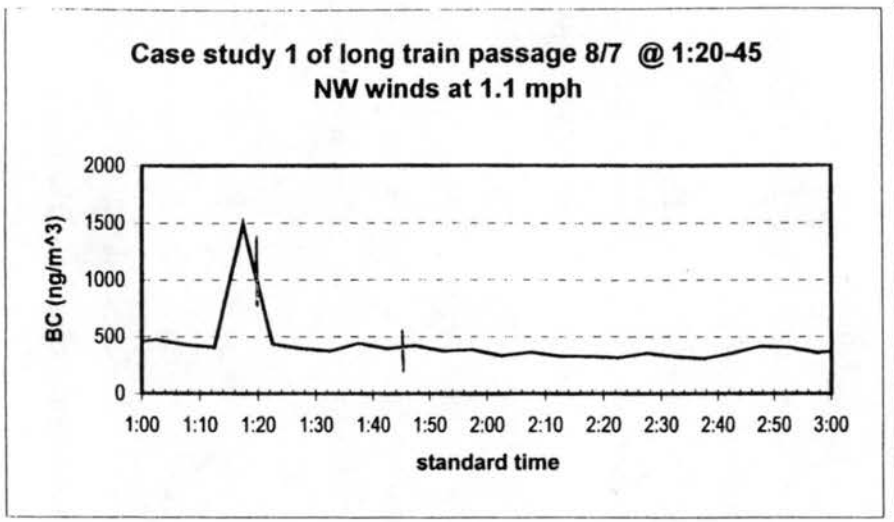

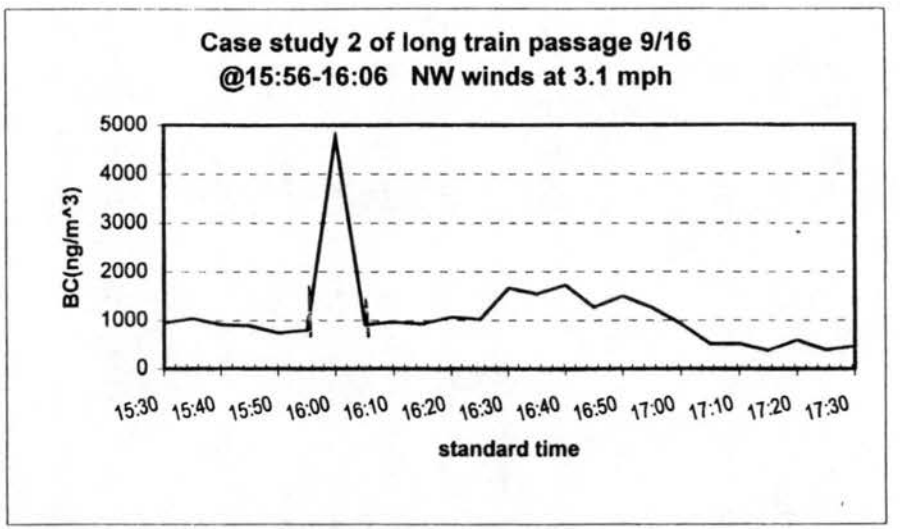

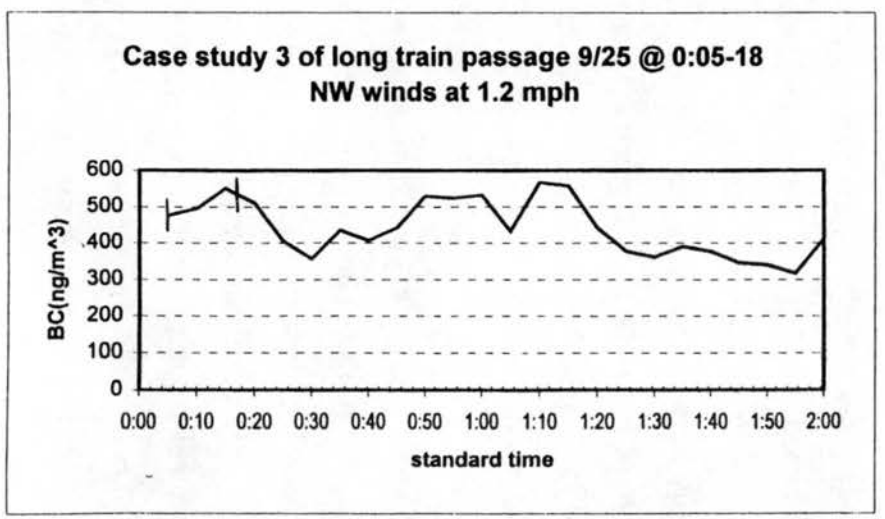

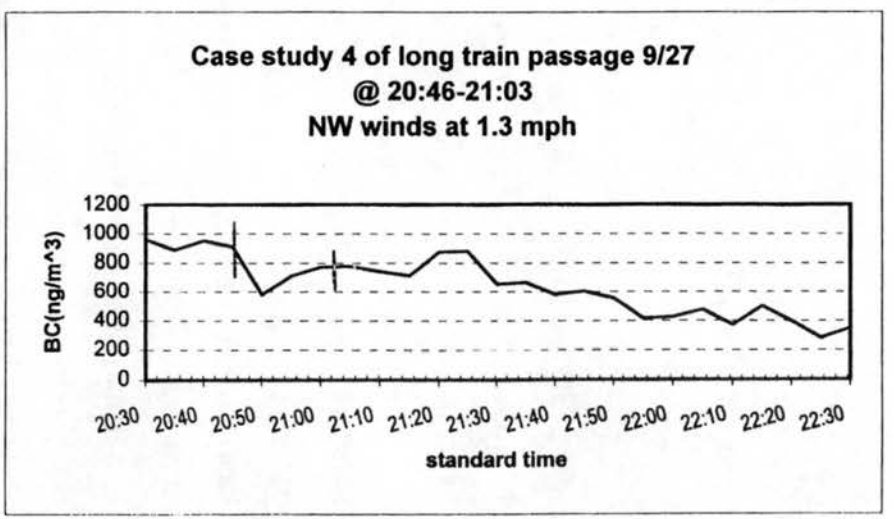

Figure 11g. Long train passage case studies 1, 2, 3, and 4.

following train passage. It seems more likely that these concentration increases reflect increased vehicle emissions than locomotive emissions. In order to examine this issue more closely we looked at several long train passages. The examined train passages, each at least 10 minutes in duration, were from August 7th at 1:20-1:45 hours, September 16th at 15:56-16:06 hours, September 25th at 0:05-0:18 hours, and September 27th at 20:46-21:03 hours. Three of these train passages (August 7th, September 25th, and September 27th) were associated with periods of light traffic. In all three of these cases the winds were from the northwest and wind speeds were between 1.1 and 1.3 mph. No increase in BC concentration was observed for the September 25th and 27th passages, suggesting increased traffic emissions during train passage might be an important component of BC concentration peaks observed by the aethalometer. This is consistent with observations on the September 16th case, during a period of moderate afternoon traffic flow, when an increase in BC concentration to 4757 ng/m^3 was observed. The winds at this time were also from the northwest at 3.1 mph.

3.7 Month-to-month variability in aerosol black carbon concentrations

Figure (12) shows the August and September, 1998 timelines. The 5-minute average data have been averaged to 30 minute periods for comparison with the August-September 1997 data. The number of high BC (> 2000 ng/m^3) days in these months is similar to the number observed in August and September 1997, but the magnitudes of the concentration peaks are typically smaller in 1998. There are no days in the August and September 1998 data with concentrations in excess of 10,000 ng/m^3. The monthly average hourly BC concentrations range from 200 – 2368 ng/m^3 in August - September 1998 and from 200 – 2428 ng/m^3 in August-September 1997(see Figure 13). Like the 1997 data, the 1998 weekend afternoon/evening peaks occur later than on weekdays and weekday BC concentrations are higher than weekend concentrations. Figure 14 show average hourly BC concentrations for August – September 1998 with and without the influence of train passages. The figure shows that the train passages make little difference overall in the average BC concentration measured. Average BC

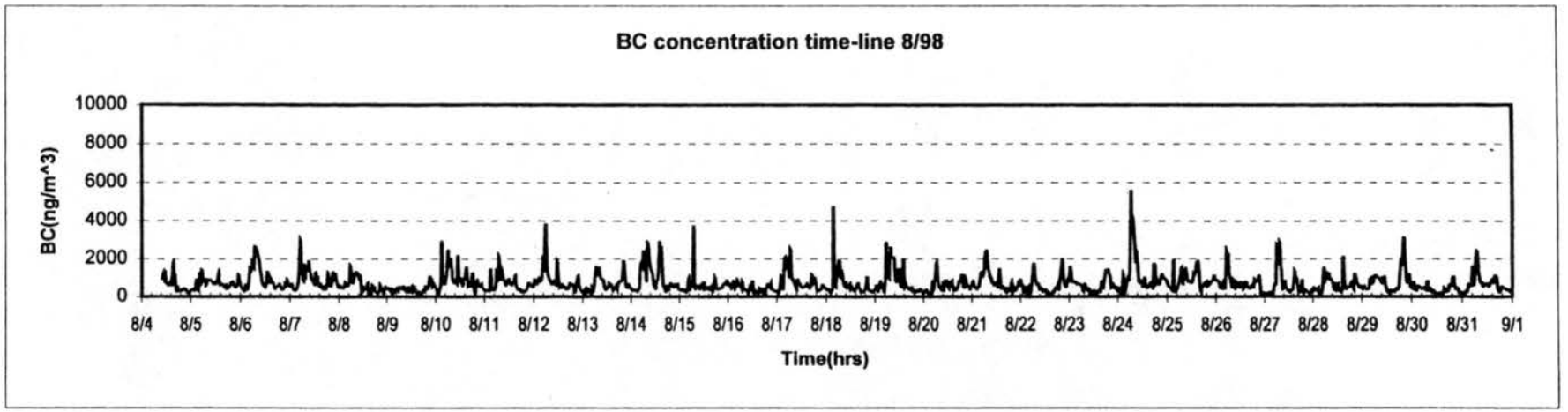

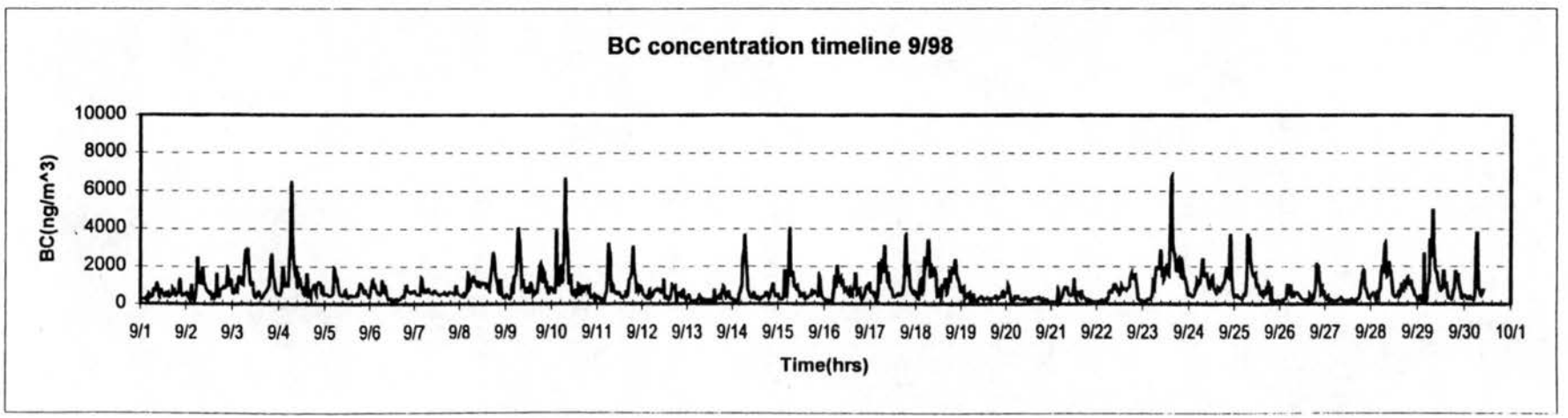

Figure 12. August and September 1998 monthly BC concentration time-lines.

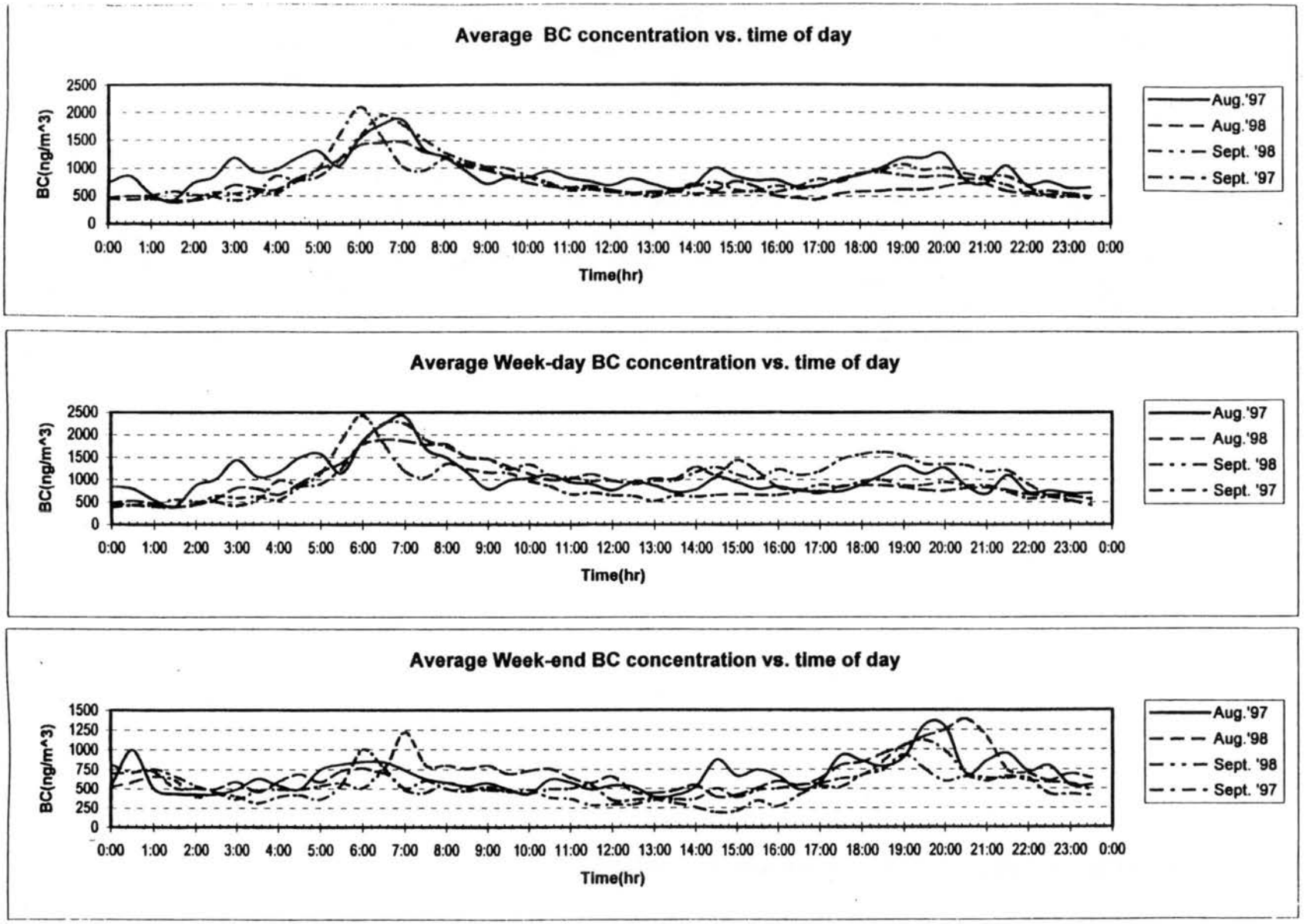

Figure 13. Monthly average diurnal BC concentration profiles for August - September 1997 and 1998.

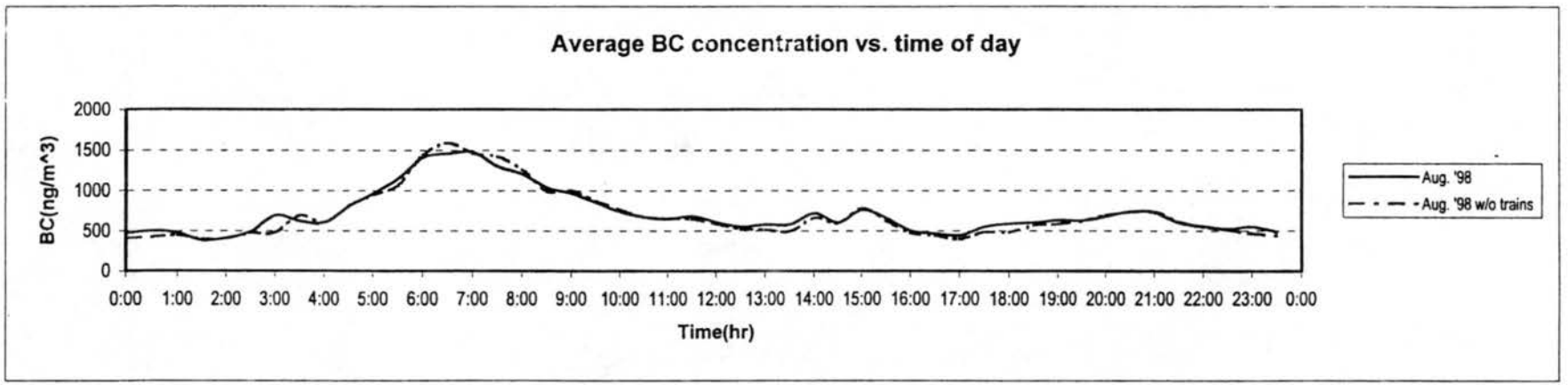

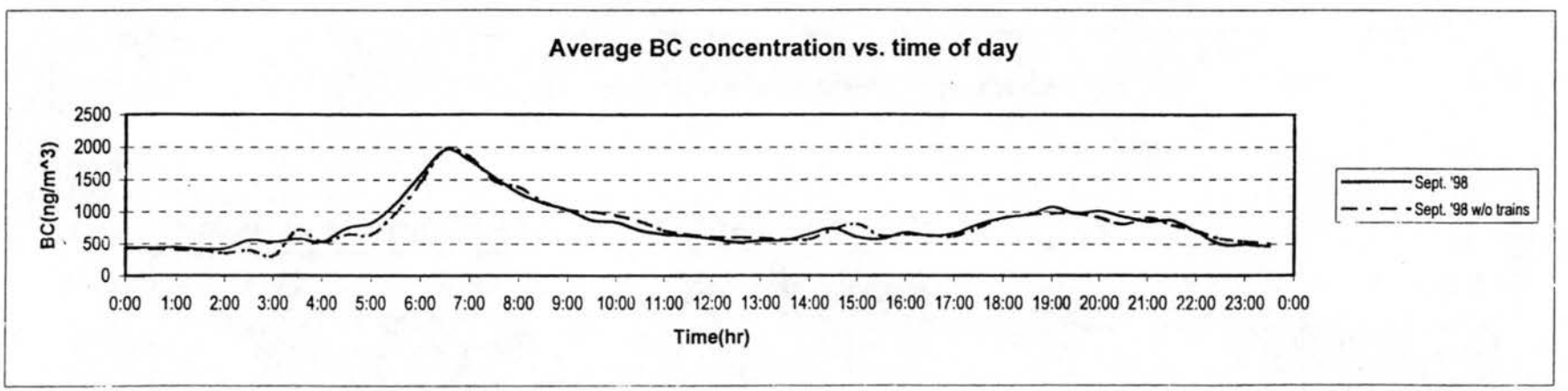

Figure 14. Monthly average diurnal BC concentration profiles for August and September 1998 including and excluding periods(30 minutes before and after) each recorded train passage.

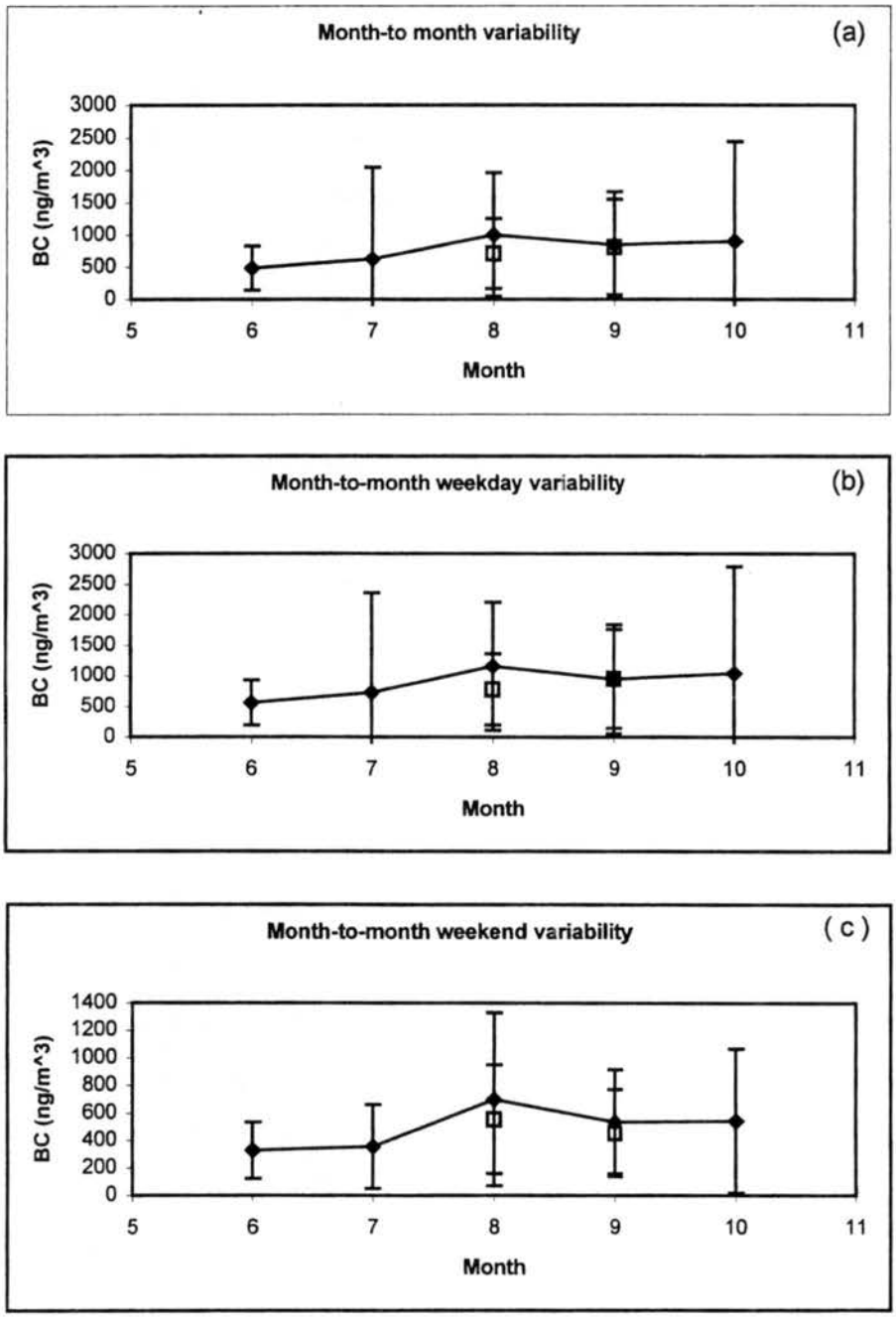

Figure 15. BC monthly mean concentrations and standard deviations for June-October, 1997 (filled symbols) and August and September 1998 (open symbols). a) all days b) weekdays, and c) weekends.

Concentrations for August and September 1998 were 712 and 815 ng/m^3 when periods of train passage are included and drop to 696 and 802 ng/m^3 when these periods are excluded. The mean and standard deviation for each month (June-October 1997 and August-September 1998) were calculated and are shown in Figure15 for all days, for weekdays, and for weekend days. The plots show that the mean monthly concentration of BC for the period June-October 1997 peaked in August for both weekdays and weekend days.

In 1998 August weekend days had higher average concentrations than September weekend days, but September weekdays had higher average BC concentrations than August weekdays. In all months the standard deviations of the measured BC concentrations are large compared to the means. The August 1998 mean and standard deviation are less than the mean concentration and standard deviation measured in August 1997 for weekdays and weekend days. The September 1998 mean BC concentration and standard deviation are similar to the September 1997 mean and standard deviation on weekdays, but not on weekends. When the train passages were removed from the August and September 1998 data the means decreased from 712 to 696 ng/m^3 and 815 to 802 ng/m^3 respectively. Student t-tests were performed on the August and September data to test whether significant differences were present between the 1997 and 1998 monthly mean values for all days, weekdays, and weekend days. These tests were formulated to test the null hypothesis: that no significant difference was present between the two means compared. The results are shown in Table 2. There is a statistical difference between the means of the August 1997 and 1998 data for all days, weekdays, and weekend days at the 99% confidence level. For the September data, there is no statistical difference at the 90% (or higher) confidence level between the 1997 and 1998 monthly means for all days or for weekdays. There is a statistical difference in the weekend day means at the 99% confidence level.

The absorption coefficient mean and standard deviation for each month were calculated and are shown in Figure (15). There is not much variability between each month in the absorption coefficient derived from the transmissometer and nephelometer measurements (ARS data). The month with the highest absorption is July, while the

Table 2a. T-test result for August 1997 and 1998

t-Test: Two-Sample Assuming Equal Variances

	August '97	*August '98*
Mean	1004.618752	711.604152
Variance	912907.953	295144.9482
Observations	1353	1324
Pooled Variance	607375.0725	
H_0 Difference	0	
df	2675	
t Stat	9.725892936	
P(T<=t) one-tail	2.69304E-22	
t Critical one-tail	1.645423708	
P(T<=t) two-tail	5.38607E-22	
t Critical two-tail	1.960852387	

x1 - x2	ts*sqrt((n1+n2)/(n1n2)	
293.0146	59.07513	95% CL
	49.57212	90% CL
	77.72836	99% CL

t-Test: Two-Sample Assuming Equal Variances

	Wkday '97	*Wkday '98*
Mean	1156.267743	775.7828659
Variance	1100640.796	337969.5363
Observations	904	939
Pooled Variance	712055.4394	
H_0 Difference	0	
df	1841	
t Stat	9.676868498	
P(T<=t) one-tail	6.13152E-22	
t Critical one-tail	1.645680641	
P(T<=t) two-tail	1.2263E-21	
t Critical two-tail	1.961252565	

x1 - x2	ts*sqrt((n1+n2)/(n1n2)	
380.4849	77.11451	95% CL
	64.70653	90% CL
	101.443	99% CL

t-Test: Two-Sample Assuming Equal Variances

	Wkend '97	*Wkend '98*
Mean	699.9396995	555.6059028
Variance	397410.1004	156968.4699
Observations	448	384
Pooled Variance	286459.3239	
H_0 Difference	0	
df	830	
t Stat	3.877747359	
P(T<=t) one-tail	5.68809E-05	
t Critical one-tail	1.64669018	
P(T<=t) two-tail	0.000113762	
t Critical two-tail	1.962825991	

x1 - x2	ts*sqrt((n1+n2)/(n1n2)	
144.3338	73.05843	95% CL
	61.29152	90% CL
	96.03029	99% CL

Table 2b. T-test result for September 1997 and 1998

t-Test: Two-Sample Assuming Equal Variances

	September '97	*September '98*	x1 - x2	ts*sqrt((n1+n2)/(n1n2)	
Mean	850.3317278	814.9297201	35.40201	60.17563	95% CL
Variance	669785.9794	549603.8185		50.49552	90% CL
Observations	1175	1413		79.17525	99% CL
Pooled Variance	604164.4747				
H_0 Difference	0				
df	2586				
t Stat	1.153607782				
P(T<=t) one-tail	0.124383807				
t Critical one-tail	1.645444172				
P(T<=t) two-tail	0.248767614				
t Critical two-tail	1.960879672				

t-Test: Two-Sample Assuming Equal Variances

	Wkday '97	*Wkday '98*	x1 - x2	ts*sqrt((n1+n2)/(n1n2)	
Mean	945.5851247	949.364244	-3.779119	75.72854	95% CL
Variance	791166.0873	650651.2963		63.54408	90% CL
Observations	901	1029		99.62283	99% CL
Pooled Variance	716244.3004				
H_0 Difference	0				
df	1928				
t Stat	-0.09787042				
P(T<=t) one-tail	0.461022681				
t Critical one-tail	1.645644261				
P(T<=t) two-tail	0.922045362				
t Critical two-tail	1.961193448				

t-Test: Two-Sample Assuming Equal Variances

	Wkend '97	*Wkend '98*	x1 - x2	ts*sqrt((n1+n2)/(n1n2)	
Mean	537.1079665	454.6872068	82.42076	53.53217	95% CL
Variance	143671.7921	101151.0149		44.90616	90% CL
Observations	274	384		70.33715	99% CL
Pooled Variance	118846.3993				
H_0 Difference	0				
df	656				
t Stat	3.023232485				
P(T<=t) one-tail	0.001299228				
t Critical one-tail	1.647179033				
P(T<=t) two-tail	0.002598456				
t Critical two-tail	1.963585419				

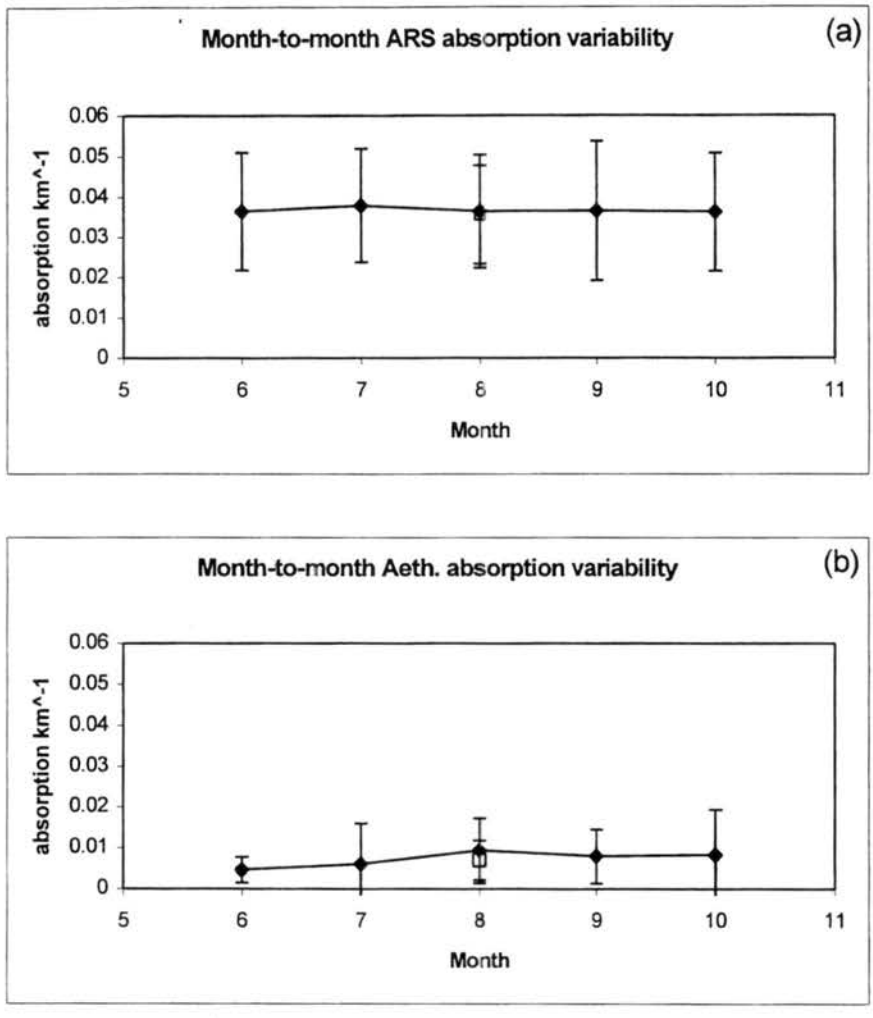

Figure 16. Absorption coefficient monthly means and standard deviations for June – October, 1997 (filled diamonds) and August, 1998 (open squares). a) ARS (transmissometer – nephelometer) b) Aethalometer

lowest absorption coefficient was found in October. The 1998 and 1997 August mean absorption coefficients are very similar (0.036 and 0.038 km^{-1}, respectively). The aethalometer-derived monthly mean absorption coefficient shows more variability. The month with the highest absorption is August, and the least absorption is found in June. The 1998 August mean absorption coefficient (0.0068 km^{-1}) is less than August 1997

($0.0094\ km^{-1}$). As noted above, the absorption coefficient derived from the aethalometer data is much lower than the absorption coefficient derived from the transmissometer and nephelometer measurements.

3.8 Meteorological Data

The local meteorological parameters used in this study were temperature, pressure, wind direction, wind speed, and precipitation. All these parameters were given by the Fort Collins Weather Station on the CSU campus, approximately 400m west southwest of the campus aethalometer site. The sampling trailer meteorological tower also provided temperature, wind direction, and wind speed measurements. A comparison was made between the two data sets (refer to Figure 17 for June, 1997 plots of these parameters; data from other months are shown in Appendix D). The comparison shows there is sometimes a difference in wind direction when the wind speed is low. There is not much difference between the temperatures measured at the two sites. The 1997 aethalometer BC concentration measurements were corrected for non-standard conditions using temperature data from the aethalometer site and pressure data from the Fort Collins weather station. The 1998 BC concentration data were corrected using temperature and pressure data from the Ft. Collins weather station, since temperature data were not yet available from the CDPHE weather station at the aethalometer site.

Timelines of BC concentration, wind direction, and pressure are included in Appendix D. As mentioned previously, the timelines of BC concentration and wind direction show no obvious pattern. The BC and pressure plots highlight the diurnal pressure patterns. In October when changes in the pressure patterns are more noticeable, the plots typically show low BC concentrations after frontal passages as marked by a greater than 10mb change in pressure. This is seen on October 8^{th}, 11^{th}, $24-25^{th}$, and 31^{st}- November 1^{st}.

In order to determine the influence of precipitation on BC concentration levels, study days were segregated into categories with and without precipitation. Days with 0.01 inches or more of precipitation measured at the Ft. Collins weather station were classified as precipitation days. Days with no recorded precipitation were classified as

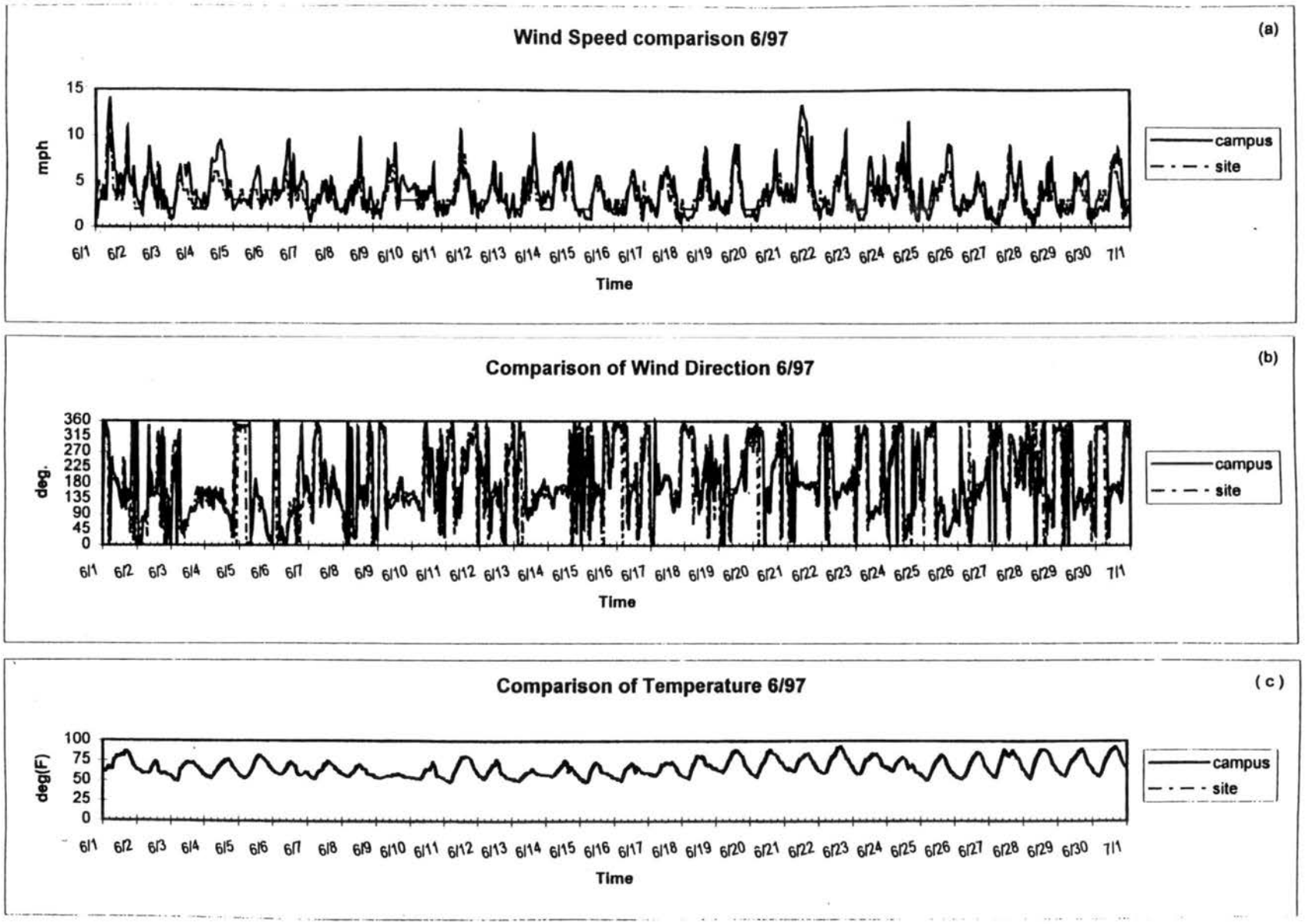

Figure 17. Comparison of CDPHE (site) and Ft. Collins Wx. Station (campus) data. a) wind speed b) wind direction and c) temperature.

non-precipitation days. Days where trace precipitation was recorded were excluded from this analysis. Frequency distributions of daily average BC concentration were constructed for all days and for days with and without precipitation. The results are shown in Figure 18. During the summer period (June, July and August) the frequency distribution of BC concentrations is very similar for days with and without precipitation. During the autumn (September-November) period, there is a clear difference between the distributions of BC concentrations on precipitating and non-precipitating days. Days with precipitation are much more likely to feature lower BC concentrations than are days without precipitation. The observation that autumn precipitation is more likely to be associated with diminished BC concentrations while summer precipitation has little effect may be related to differences in the typical precipitation types during those seasons.

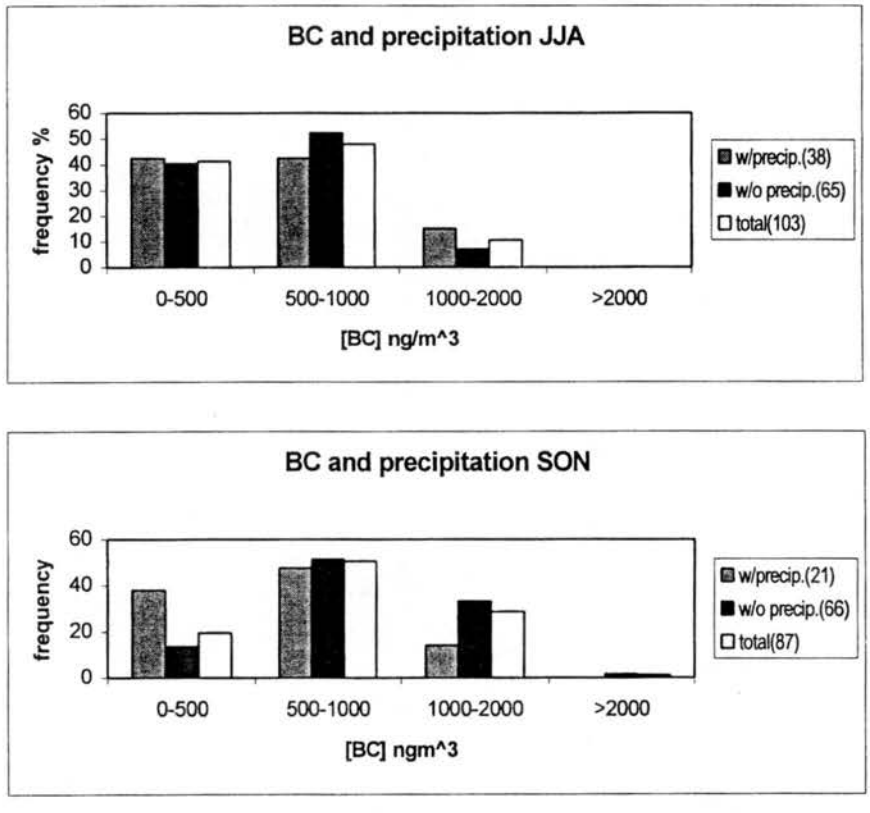

Figure 18. Precipitation and its influence on BC concentrations in a) summer and b) autumn.

Summer precipitation is much more likely to be strongly convective and of short duration while autumn precipitation is more typically stratiform precipitation and of longer duration. Short periods of local precipitation are less likely to substantially affect daily average BC concentrations than are periods of widespread precipitation of several hours duration.

3.9 Correlation of black carbon concentrations with carbon monoxide and particle number concentrations

Figure 19 shows the July 1997 timelines of CO and BC concentrations (timelines for other study months are illustrated in Appendix E). Similar patterns are observed in the CO and BC concentrations. In order to evaluate the relationship between BC and CO concentrations more quantitatively, linear regressions of BC concentrations vs. CO concentrations were performed. The results of these regressions are depicted in Table 3 and Figure 20. Figure 20 reveals that the correlation between BC and CO concentrations for the entire June - October 1997 period is poor, with variations in CO concentrations only explaining about 35% of the variability in BC concentrations ($r^2 = 0.35$). When the regression is restricted to shorter time periods, however, the correlation often improves significantly. The second panel in Figure 20 illustrates the correlation for a one week period in July 1997. During this period, variations in CO concentrations were capable of explaining approximately half of the variability observed in the BC concentrations ($r^2 = 0.53$). Results of weekly regressions for the June-October 1997study period are shown in Table 3. Correlation coefficients for the 22 weekly regressions vary from 0.12 to 0.61 with an average value of 0.4. No comparison of the BC and CO concentrations was made for the August-September 1998 study period due to delays in availability of the CO data.

Condensation nuclei (CN, measured by the TSI condensation particle counter) and optical particle counter (OPC) ($d > 0.3$ μm) particle concentrations were measured simultaneously. The July timelines of BC, CN, and OPC concentrations are shown in Figure 21. Although there are some similarities between the BC concentrations and the OPC and CN particle concentrations, the concentrations of these three particle classes don't track very tightly. The CN concentrations show the most variability. This is not

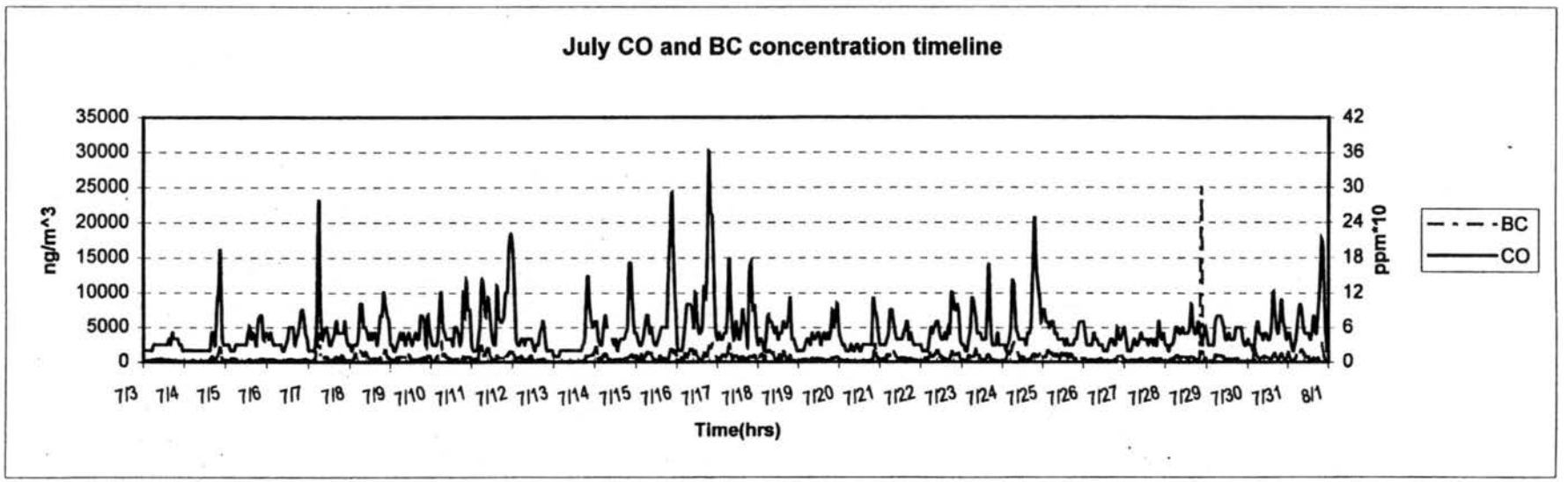

Figure 19. July BC and CO concentrations time-line

Table 1. Weekly linear regression results for CO and BC concentrations

Date(s)	Best-fit line	Correlation coefficient
6/4-7/97	y = 85.553x + 41.203	r^2 = 0.4507
6/8-14/97	y = 55.369x + 115.69	r^2 = 0.3389
6/15-21/97	y = 66.12x + 141.99	r^2 = 0.2784
6/22-28/97	y = 82.051x + 162.33	r^2 = 0.4096
6/29-7/5/97	y = 63.132x + 94.545	r^2 = 0.425
7/6-12/97	y = 99.151x + 78.733	r^2 = 0.5286
7/13-19/97	y = 68.535x + 259.28	r^2 = 0.4942
7/20-26/97	y = 79.25x + 247.42	r^2 = 0.315
7/27-8/2/97	y = 90.839x + 111.35	r^2 = 0.3993
8/3-9/97	y = 84.772x + 568.04	r^2 = 0.1192
8/10-16/97	y = 122.07x + 304.49	r^2 = 0.2544
8/17-23/97	y = 116.23x + 289.57	r^2 = 0.3755
8/24-30/97	y = 62.478x + 446.88	r^2 = 0.1973
8/31-9/6/97	y = 88.588x + 208.97	r^2 = 0.3428
9/7-13/97	y = 78.632x + 286.68	r^2 = 0.4237
9/14-20/97	y = 74.508x + 219.44	r^2 = 0.3355
9/21-27/97	y = 69.915x + 191.5	r^2 = 0.4502
9/28-10/4/97	y = 48.535x + 330.51	r^2 = 0.369
10/5-11/97	y = 67.68x + 168.82	r^2 = 0.6069
10/12-18/97	y = 46.133x + 263.65	r^2 = 0.545
10/19-25/97	y = 53.964x + 243.64	r^2 = 0.4205
10/26-11/1/97	y = 54.836x + 421.17	r^2 = 0.5694

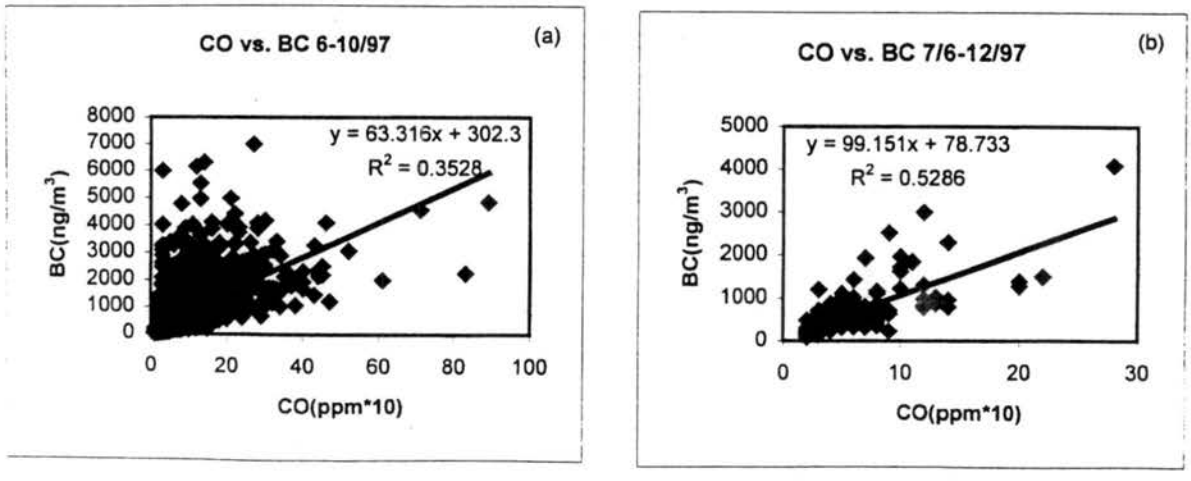

Figure 20. a) comparison of BC and CO concentrations for June-October,1997.
b) comparison of BC and CO concentrations for July 6 - 12, 1997.

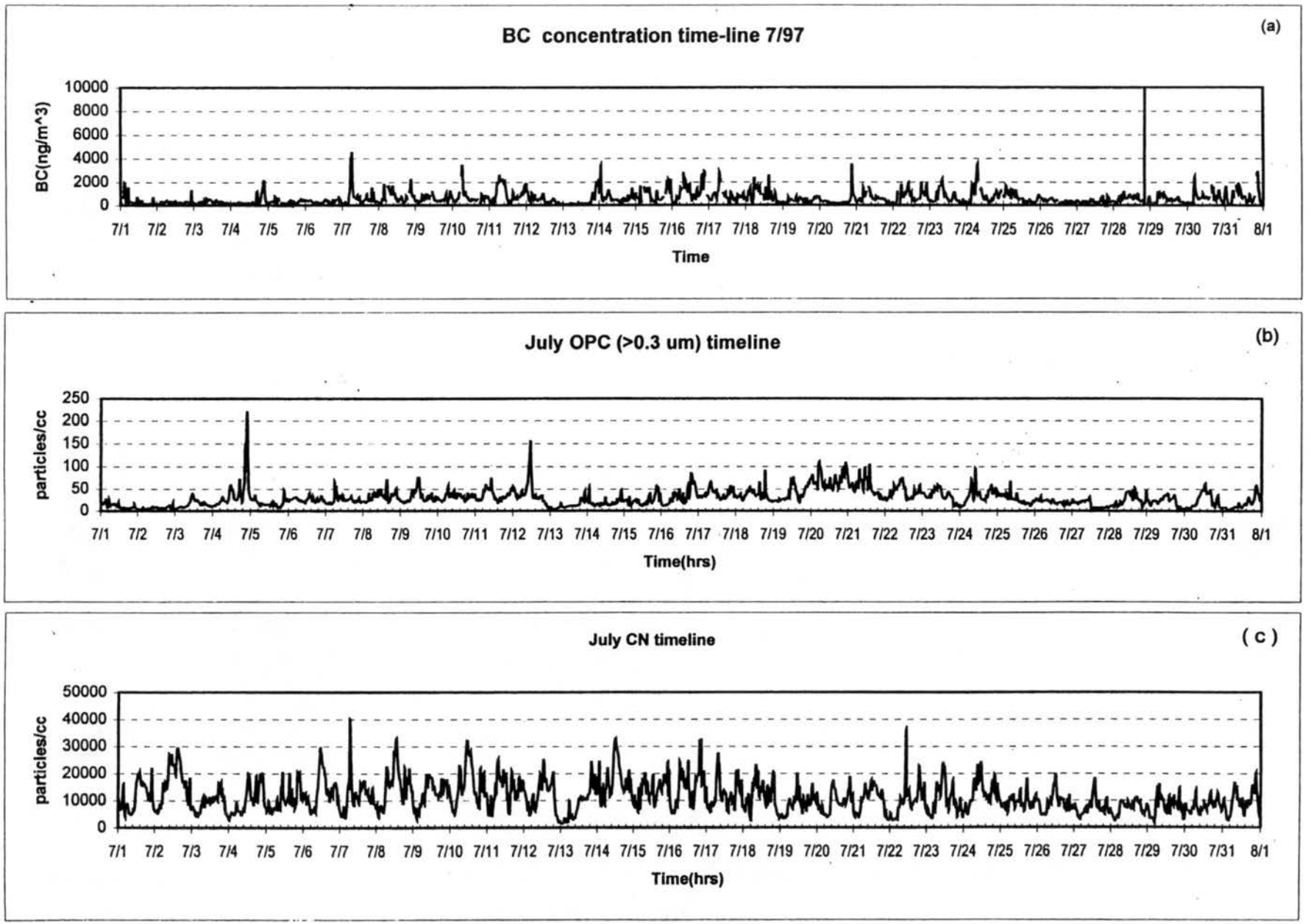

Figure 21. July concentration timelines of a) BC b) OPC c)CN

surprising given that lifetimes of the very small particles that usually dominate CN number are very short. There appear to be two peaks in the CN data corresponding to the morning and late afternoon-evening BC peaks described earlier. However, there seems to be a lag in the OPC particle concentrations compared to the others. This is seen more clearly in the weekly timelines (see Appendix F). Correlation between BC, CN, and OPC concentrations are shown in Figure 22. The results are similar to the BC and CO correlation. The overall correlation is poor, with $r^2 = 0.1$ and 0.04 for BC vs. CN and BC vs. OPC particle concentrations, respectively. As the time scale for the regression is decreased to a day the correlation generally improves. Tables 4a and 4b show the results of daily July 1997 regressions of BC concentrations vs. CN and OPC concentrations, respectively. Correlation coefficients for the 31 BC vs. CN regressions range from 0.00 to 0.44 with a mean value of 0.16, while the correlation coefficients for the BC vs. OPC regressions range from 0.01 to 0.67 with a mean value of 0.19. Analysis of these correlation coefficients reveal that the daily correlation between BC and CN or OPC concentrations typically improve or worsen together.

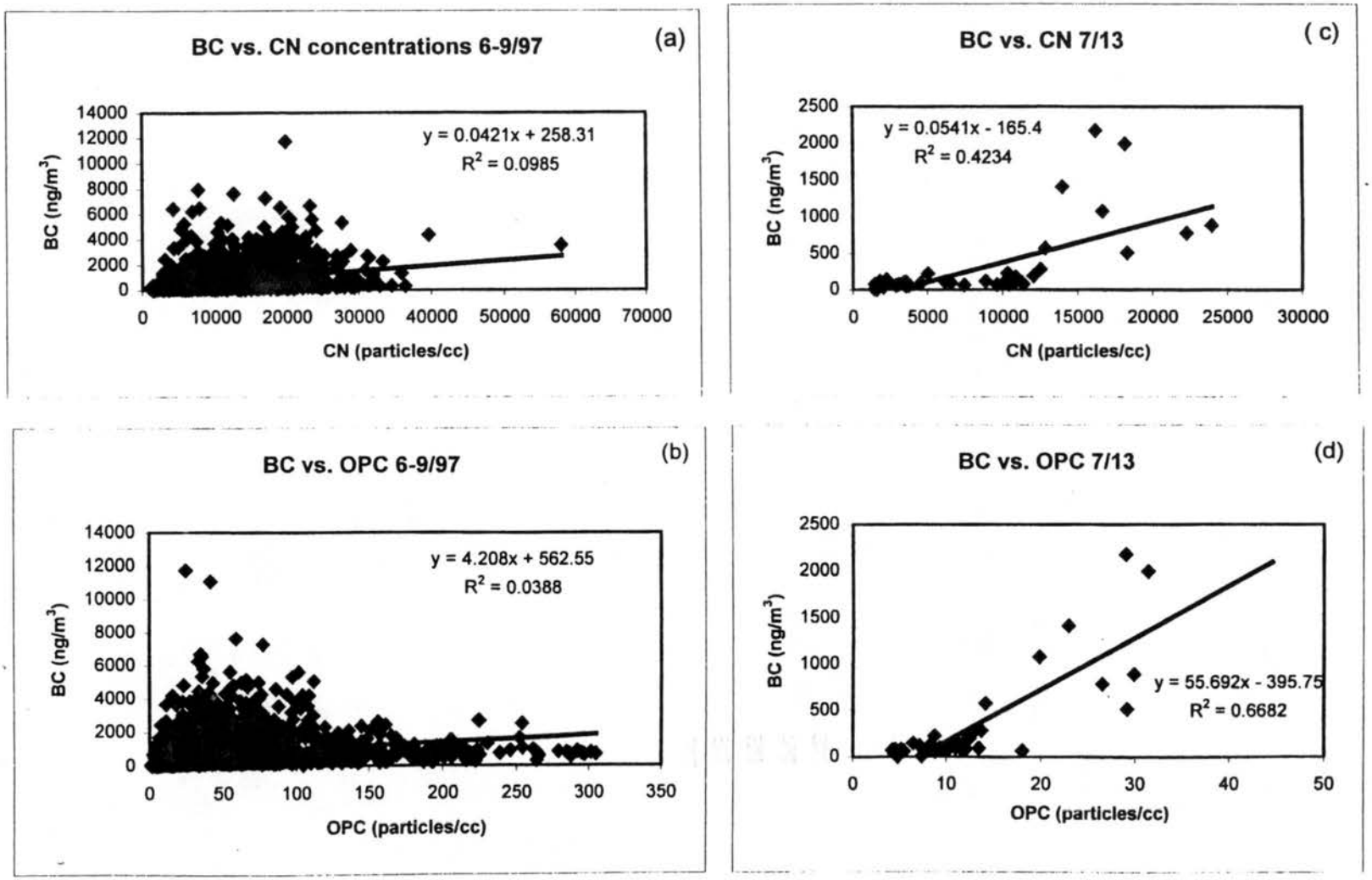

Figure 22. June-September, 1997 comparison of a) BC and CN b) BC and OPC concentrations. comparison of c) BC and CN d) BC and OPC concentrations for July 13, 1997.

Table 4a. Daily linear regression results for BC and CN concentrations for July, 1997

Date(s)	Best-fit line	Correlation coefficient
7/1	y = -0.0144x + 485.69	r^2 = 0.0305
7/2	y = 0.0025x + 224.82	r^2 = 0.0102
7/3	y = 0.0126x + 160.8	r^2 = 0.1112
7/4	y = 0.0561x - 186.01	r^2 = 0.3721
7/5	y = 0.0007x + 281.6	r^2 = 0.0005
7/6	y = 0.002x + 320.51	r^2 = 0.0002
7/7	y = 0.0892x - 349.06	r^2 = 0.3867
7/8	y = 0.0089x + 635.73	r^2 = 0.0156
7/9	y = 0.0201x + 320.51	r^2 = 0.1084
7/10	y = 0.0104x + 541.03	r^2 = 0.0197
7/11	y = 0.07x + 9.0081	r^2 = 0.3111
7/12	y = 0.0061x - 395.93	r^2 = 0.00114
7/13	y = 0.0541x - 165.4	r^2 = 0.4234
7/14	y = -0.011x + 889.81	r^2 = 0.0172
7/15	y = 0.0357x + 405.12	r^2 = 0.0823
7/16	y = 0.0737x + 77.238	r^2 = 0.4439
7/17	y = 0.0617x + 78.075	r^2 = 0.349
7/18	y = 0.0469x + 274.91	r^2 = 0.1731
7/19	y = 0.0224x + 210.36	r^2 = 0.237
7/20	y = 0.0584x - 147.01	r^2 = 0.1539
7/21	y = 0.0307x + 270.53	r^2 = 0.1661
7/22	y = 0.0421x + 387.7	r^2 = 0.2759
7/23	y = 0.0348x + 272.93	r^2 = 0.1602
7/24	y = 0.0377x + 430.89	r^2 = 0.0779
7/25	y = -0.0144x + 791.66	r^2 = 0.0077
7/26	y = -0.0056x + 397.48	r^2 = 0.0133
7/27	y = -0.0003x + 322.85	r^2 = 4E-05
7/28	y = -0.0488x + 206.74	r^2 = 0.2414
7/29	y = 0.0451x + 129.98	r^2 = 0.2922
7/30	y = 0.0295x + 468.89	r^2 = 0.0212
7/31	y = 0.1042x - 139.66	r^2 = 0.4195

Table 4b. Daily linear regression results for BC, and OPC concentrations for July, 1997

Date(s)	Best-fit line	Correlation coefficient
7/1	y = 22.711x + 51.3	r^2 = 0.0935
7/2	y = 9.6279x + 196.54	r^2 = 0.0238
7/3	y = 7.5222x + 156.98	r^2 = 0.2802
7/4	y = 6.6075x + 119.15	r^2 = 0.3202
7/5	y = 5.8158x + 180.53	r^2 = 0.1114
7/6	y = 7.8103x + 120.26	r^2 = 0.0972
7/7	y = 58.999x - 787.74	r^2 = 0.3276
7/8	y = 8.3384x + 490.21	r^2 = 0.035
7/9	y = 6.1032x + 370.4	r^2 = 0.1168
7/10	y = 29.689x - 267.5	r^2 = 0.1484
7/11	y = 42.445x - 548.64	r^2 = 0.5478
7/12	y = 5.0726x + 260.67	r^2 = 0.1848
7/13	y = 55.692x - 395.75	r^2 = 0.6682
7/14	y = 17.282x + 350.57	r^2 = 0.0879
7/15	y = 21.324x + 365.4	r^2 = 0.2146
7/16	y = 25.092x + 335.7	r^2 = 0.416
7/17	y = 29.924x - 322.88	r^2 = 0.2729
7/18	y = 12.677x + 370.61	r^2 = 0.0722
7/19	y = 5.1282x + 211.74	r^2 = 0.2438
7/20	y = 6.8069x - 91.004	r^2 = 0.0471
7/21	y = 6.9542x + 200.21	r^2 = 0.1355
7/22	y = 17.438x + 67.28	r^2 = 0.2508
7/23	y = 18.285x - 16.427	r^2 = 0.2285
7/24	y = 15.036x + 394.31	r^2 = 0.1434
7/25	y = 22.177x + 39.639	r^2 = 0.3928
7/26	y = 14.9x + 44.505	r^2 = 0.2196
7/27	y = -3.1176x + 366.4	r^2 = 0.0216
7/28	y = 5.4651x + 428.52	r^2 = 0.0743
7/29	y = 7.7545x + 301.74	r^2 = 0.0733
7/30	y = 6.0806x + 562.6	r^2 = 0.0455
7/31	y = -6.7074x + 929.74	r^2 = 0.0115

4. Discussion

4.1 Temporal and spatial variability in aerosol black carbon concentrations

Observations of aerosol black carbon concentrations made during this study reveal monthly mean concentrations that vary from 0.5 to 1.0 $\mu g/m^3$. Typical BC concentrations are 0.3 – 1.6 $\mu g/m^3$ in rural Europe, and 0.6 – 1.3 $\mu g/m^3$ in rural U.S.A. The values for Ft. Collins fall within a range of concentrations typically seen in rural and urban areas:1.0 to 10.0 $\mu g/m^3$. This is not surprising given the status of Fort Collins as a small city.

BC concentrations measured in this study were also of comparable magnitude to elemental carbon (EC) concentrations measured in Ft. Collins during the Northern Front Range Air Quality Study (NFRAQS). The average BC concentration measured by the aethalometer in July 1997 was 626 ng/m^3 and in August 1997 and August 1998 it was 1004 and 711 ng/m^3. This compares to an average elemental carbon (EC) concentration of approximately 1300 ng/m^3 measured at Ft. Collins during 5 days in the summer 1996 NFRAQS study period (July 17 – August 31, 1996) (Chow et al, 1998).

Analysis of monthly trends in aerosol black carbon concentrations suggest some seasonality. In 1997 a gradual build up in monthly BC concentrations over the late spring and summer was observed to peak in August and then decline. In addition to changes in monthly mean values, the number of days featuring high (> 2000 ng/m^3 for 30 minutes) concentrations was also observed to rise and fall with an August peak. The numbers of high BC concentration (peak BC > 2000 ng/m^3 for 30 minutes) days observed in June through October 1997 were 4, 20, 25, 20, and 20, respectively.

4.2 Factors influencing aerosol black carbon concentrations

The occurrence of high BC concentrations can result from a combination of high local emissions and air stagnation or high emissions at a distant location coupled with transport suitable to bringing those emissions to Ft. Collins. The results of this study indicate there is little relationship between measured BC concentrations and long range transport patterns. The trajectory results shown earlier in Figure 5 indicate that long range transport of air masses from particular regions does not strongly influence whether BC concentrations in Ft. Collins are high or low. By contrast, analysis of the available data does indicate an association between BC concentrations and local emissions.

The BC concentration timelines show there are usually two peaks in the data (see Figure 3 and the weekly timelines in Appendix G). These peaks usually occur between 0600 – 0800 and 1600 – 2100, hours associated with peak traffic. In addition, concentrations of BC were found to correlate reasonably well with CO concentrations over time scales of up to a week (see Figure 18 and Table 3). CO and aerosol black carbon both are conserved tracers of continental emissions from the combustion of fossil fuels and biomass. The fact that they covary in our data set suggests they are emitted from a common set of combustion sources. Finally, observed BC concentrations tend to decrease with increasing wind speed. This is again consistent with emissions from a local source which would tend to be diluted at higher wind speed.

Together these results suggest that aerosol BC concentrations measured in Ft. Collins during the study were probably dominated by local emissions. The timing of BC concentration peaks suggests that local motor vehicle emissions probably dominate observed BC concentrations. At the same time, however, it is clear that the local emissions impact BC concentrations across a large section of the city. The spatial variability study shows high BC concentrations are not confined to a particular site in the city of Fort Collins. BC concentrations measured at the campus site, in downtown Ft. Collins and at a busy intersection in the city's shopping district were observed to be quite similar. These observations suggest that the CSU campus site provides a representative measure of typical aerosol BC concentrations in the city of Ft. Collins.

The city of Fort Collins traffic department has indicated that vehicular traffic increased from 1997 to 1998. Although this increase is not reflected by an increase in

measured BC concentrations in the months of August and September, it will be interesting to continue monitoring BC concentrations as the city grows to determine what impact increased vehicular traffic may exert on BC concentrations and associated impacts on PM-2.5 and visibility.

On shorter timescales of minutes to hours, the study revealed the important influence individual sources can have on BC concentrations. Passages of diesel locomotives near the site were shown to increase BC concentrations on many occasions when local winds were favorable to transporting locomotive emissions to the aerosol sample site. The impact of this source, however, is fairly limited in its duration, with concentration spikes typically lasting only about 10 minutes. Train passage may also exert an indirect effect on BC concentrations. East-west traffic is blocked by passage of trains through the city. At times the traffic is backed up and idling for several minutes. There is some suggestion in the BC concentration data record of an increase in BC concentrations several minutes after train passage, perhaps associated with a period of increased BC emissions by vehicles idled at train crossings.

Fires were also shown to influence BC concentrations during the study. The large fires associated with the July 1997 flood and smaller fires associated with a CSU student riot were observed to increase BC concentrations. One of the goals of this study was to document impacts of wildfires and prescribed burns on Ft. Collins BC concentrations. The number of fires during the study period, however, was very low. Impacts of two prescribed burns along the Front Range on Ft. Collins BC concentrations were observed to be fairly minor. It remains to be seen over a longer time period whether some fires exert a much greater influence on BC and PM-2.5 concentrations along the Front Range urban corridor. This is an issue of great current interest in deciding how to account for impacts of forest fires on the ability of urban areas to meet federal particulate matter concentration limits.

Comparisons of BC concentrations and atmospheric pressure show that BC concentrations are independent of the diurnal pressure patterns. However, BC concentrations are affected by synoptic pressure patterns. Frontal passages are marked by low BC concentrations, as the precipitation accompanying these systems remove pollutants that have accumulated in the atmosphere, and clean air is advected into the

region. BC concentrations were not found to be depressed on summer days featuring precipitation. Most likely this reflects the sporadic nature of summer convective precipitation. The duration of summer thunderstorms is typically too short to scavenge enough aerosol particles to significantly influence the daily average BC concentration. In addition, primary aerosol particles that are generated locally by vehicle emissions will be replenished rapidly in the atmosphere following precipitation.

Although the aethalometer is designed to measure absorption by aerosol black carbon, it will in fact respond to collection of any absorbing aerosol. For example, soil dust, which can absorb visible light, will cause a response by the aethalometer. At rural, windy, dry locations it is conceivable that soil dust may comprise a significant fraction of the absorbing aerosol. Evidence from the current study, however, suggests that the response of the aethalometer is probably primarily due to aerosol BC. This evidence includes the observations that the aethalometer response seems to track diurnal patterns in vehicle traffic and that higher aethalometer response is generally associated with low, rather than high, wind speeds.

4.3 The relation between aerosol black carbon and particle number concentrations

Comparisons of BC concentrations with "total" particle number concentrations (as measured by the CNC) and number concentrations of particles with diameters greater than 0.3 μm (as measured by the Climet OPC) revealed the correlations to be extremely weak on long time scales and often weak on time scales as short as a day. This is not surprising since particles in these various measurement categories can have quite diverse sources. As stated earlier, BC particles are dominated by primary combustion aerosol. The number of CN will be dominated by fine and ultra-fine particles. Some of these may be primary combustion aerosol (and therefore likely to correlate with BC), but others will be secondary aerosol particles that originate from gas phase photochemical reactions that produce condensable products. While a portion of the CN, therefore, might be expected

to be well correlated with BC, the secondary aerosol fraction of CN is not expected to show a significant correlation.

Particles larger than 0.3 μm can come from many sources. They can be secondary particles formed from gas-to-particle conversion that have grown by further condensation and/or coagulation into the accumulation mode. Sulfate, nitrate and carbonaceous (including some aged BC) particles will all be found in this category. Emissions that produce BC directly will, after aging, also produce particles in the size range measured by the OPC. Therefore, it is not surprising to see in our data record that peaks in particles counted by the OPC sometimes lag peaks in BC and CN concentrations. Particles larger than 0.3 μm may also be mechanically generated primary aerosol particles, including products of soil erosion, street sweeping, and industrial activity. These particles, which are likely to be dominated by soil constituents such as calcium and silicon, are not expected to correlate strongly with BC concentrations.

4.4 Comparison of derived values of the atmospheric aerosol absorption coefficient

Aerosol absorption coefficients estimated from the aethalometer BC concentrations are generally fairly small, with monthly mean values ranging from 0.005 - 0.009 km^{-1}. These are on the order of 6 – 11% of the total extinction measured by the transmissometer and only 10 – 20% of the absorption coefficients determined from the paired nephelometer/transmissometer measurements. This result was unexpected as previous studies have shown good agreement for similar comparisons of absorption coefficients derived by these same methods at other locations (Lewis and Dzubay, 1986; Horvath and Habenreich, 1989). It is also somewhat surprising that the aethalometer derived absorption coefficients vary by nearly a factor of two while the absorption coefficients derived from the nephelometer and transmissometer measurements show little relative variation. The absolute variation in the two derived absorption coefficients is similar.

There are several possible explanations for the large discrepancy between values obtained in the present comparison. The transmissometer records extinction over a 2 kilometer path length, while the nephelometer and aethalometer make point measurements. This seems unlikely to account for a consistent bias of "excess" absorption, however, since the difference between the point and line average concentrations should be distributed randomly about zero (barring the existence of local sources in the transmissometer path). For slightly absorbing aerosols the scattering and extinction coefficients are almost equal, thus the difference of both has a large error (Horvath and Habenreich, 1989). In the nephelomter and transmissometer data, however, the absorption obtained by difference between the extinction and scattering signals was generally a significant fraction of the total extinction. There is also the possibility that the absorption coefficient derived from the aethalometer is underestimated. The σ_{ap} value used in this study was 10 m^2/g. Petzold et al. (1997) suggests that σ_{ap} is closely related to the site-specific average aerosol properties which is currently not known for Fort Collins, and so our estimate of σ_{ap} may be too low. It is unlikely to be low, however, by more than a factor of two.

The effect of gases on the absorption comparison was examined. An average Rayleigh scattering value of 0.11 km^{-1} calculated from values given in Seinfeld and Pandis (1998) and monthly average NO_2 concentration of 0.02 ppm from Denver were used. The Fort Collins NO_2 concentration is much smaller than that observed in Denver. These values along with the nephelometer values were subtracted from the extinction for each month and compared with the aethalometer derived values. The absorption derived by the subtraction method did not decrease significantly.

Conclusions

Aerosol black carbon concentrations were measured in Fort Collins, a small city in northern Colorado. A Magee Scientific aethalometer was used to obtain real time data. In 1997 a gradual build-up in monthly BC concentrations over the late spring and summer was observed to peak in August and then decline. The monthly trends in aerosol black carbon concentrations suggest some seasonality. Observations of aerosol black carbon concentrations made during this study reveal monthly mean concentrations that vary from 487 to 1004 ng/m^3. The number of days featuring high (> 2000 ng/m^3 for 30 minutes) concentrations was also observed to rise and fall with an August peak.

The occurrence of high BC concentrations can result from a combination of high local emissions and air stagnation or high emissions at a distant location coupled with transport suitable to bringing those emissions to Ft. Collins. In the current study we found little relationship between measured BC concentrations and long range transport patterns, as the trajectory results indicated that long range transport of air masses from particular regions does not significantly influence whether BC concentrations in Ft. Collins are high or low.

The BC concentration timelines showed there are usually two peaks in the diurnal data. These peaks usually occur between 0600 – 0800 and 1600 – 2100, hours associated with increased motor vehicle traffic. In addition, concentrations of BC were found to correlate reasonably well with CO concentrations over time scales of up to a week, suggesting they were emitted from a common set of combustion sources.

The observed BC concentrations tended to decrease with increasing wind speed which is consistent with emissions from a local source that would tend to be diluted at higher wind speeds. These results, coupled with the timing of BC concentration peaks suggest that aerosol BC concentrations measured in Ft. Collins during the study were probably dominated by local emissions. Examination of spatial variability of BC concentrations showed that local emissions impact BC concentrations across a large

section of the city, as high BC concentrations are not confined to a particular site in the city of Fort Collins. BC concentrations measured at the Colorado State University campus, in downtown Ft. Collins, and at a busy intersection in the city's shopping district were observed to be quite similar.

On shorter timescales of minutes to hours, the study revealed the important influence of individual sources on BC concentrations. Passages of diesel locomotives near the site were shown to increase BC concentrations on many occasions when local winds were favorable to transporting locomotive emissions to the aerosol sample site. Train passage may also exert an indirect effect on BC concentrations. There is some suggestion in the BC concentration data record of increases in BC concentrations several minutes after train passage, perhaps associated with a period of increased BC emissions by vehicles idled at train crossings. Fires were also shown to influence BC concentrations during the study. The large fires associated with the July 1997 flood and smaller fires associated with a CSU student riot were observed to increase BC concentrations. The number of fires during the study period, however, was very low. Impacts of two prescribed burns along the Front Range on Ft. Collins BC concentrations were observed to be fairly minor.

Correlation of BC concentrations with "total" particle number concentrations (as measured by a TSI Condensation Nucleus Counter), and number concentrations of particles with diameters greater than 0.3 μm (as measured by a Climet Optical Particle Counter) were extremely weak on long time scales and often weak on time scales as short as a day. This reflects the diverse sources of the aerosols. Some of these were probably primary combustion aerosol (and therefore likely to correlate with BC), but others were secondary aerosol particles or coarse particles that are not expected to correlate strongly with BC concentrations.

BC concentrations were independent of local diurnal pressure patterns. However, BC concentrations were affected by synoptic pressure patterns. Frontal passages were marked by low BC concentrations, as the precipitation accompanying these systems remove pollutants that have accumulated in the atmosphere, and as clean air was advected into the region. BC concentrations were not found to be reduced on summer days featuring precipitation, presumably because the duration of summer thunderstorms

is typically too short to scavenge enough aerosol particles to significantly influence the daily average BC concentration.

Aerosol absorption coefficients derived from the aethalometer BC concentrations were generally fairly small. The monthly mean values ranged from 0.005 - 0.009 km^{-1}. The absorption coefficients varied by nearly a factor of two while the absorption coefficients derived from the nephelometer and transmissometer measurements showed little relative variation (0.036 – 0.038 km^{-1}). The absolute variations in the two absorption coefficients are similar. The aethalometer derived absorption coefficients are on the order of 10 – 20% of the absorption coefficients determined from the paired nephelometer/transmissometer measurements, and only 6 – 11% of the total extinction measured by the transmissometer.

Future Work

This study was planned to document BC concentrations over the course of a year. Problems with instrument performance resulting from the manufacturer's use of incorrect tubing type in the aethalometer prevented us from doing so. A future study acquiring data for a year may show there is a peak in the winter months with the addition of other BC sources such as wood burning and space heating and periods of air stagnation.

Another goal of the study was to examine the impact of wild and prescribed fires on BC concentrations in Ft. Collins. This goal was difficult to realize due to the low number of fires during the seasons measured. Federal land managers are slated to significantly increase prescribed burns in the coming decade, perhaps by as much as a factor of ten. Continued monitoring of Front Range BC concentrations, coupled with back-trajectory analysis, could be one useful tool in quantifying impacts of these burns on regional air quality.

A better way to quantify the impact of individual sources like train passages on BC concentrations could be designed. The method used in this work was qualitative and only suggests the passages as a likely source. Statistical tools might accomplish this quantification. Methods such as the simple Student t-test to the more complex Fourier analysis with variables clearly defined may be able to quantify this impact.

There were uncertainties associated with the absorption coefficients estimated from the transmissometer/nephelometer and aethalometer data. Some knowledge of the aerosol properties for this region may help to reduce the uncertainties associated with the data. Knowledge of the nature of the combustion source, size distribution, and whether the aerosol is mixed (internal or external mixture) is needed as the absorption coefficient is affected by these variables. For the aethalometer data knowledge of σ_{ap} and σ_{atn} for the regional aerosol would also reduce uncertainties and permit better estimates of b_{abs}. The instrument gives us attenuation data. If the mass on the 'sensing' spot is known, from the equation

$$ATN = \sigma_{atn} * [BC]$$

we could deduce σ_{atn} . This would reduce or eliminate the uncertainties in our b_{abs} data. The mass of BC could be examined by thermal analysis.

We noticed the difference in BC concentrations between the campus site and the downtown location may be due to vertical gradients in BC concentrations. Previous studies have shown that BC concentrations are highly stratified in layers whose air temperatures may show numerous transitions (Hansen et al., 1997). Determination of the atmospheric burden of BC from the ground up to 50 meters would provide a closer look at this issue.

The results of our study indicated that BC concentrations are probably dominated by local sources. A second aethalometer placed a few miles outside of Ft. Collins could test whether the BC really is mostly coming from local sources.

References

Cismoski D.S., Dietrich D.L., and Molenar J.V. (1994) Design and field operation of the Optec NGN-2 ambient nephelometer; Air Resource Specialists, Inc.

Colorado Air Quality Control Commission (AQCC) (1993), Ambient Air Standard for Metropolitan Denver Air Quality Control Region, State Air Pollution Control Areas and the State of Colorado.

Chow J.C., Watson J.G., Pritchett L.C., Pierson W.R., Frazier C.A., and Purcell R.G. (1993) The DRI thermal/optical reflectance carbon analysis system: description, evaluation and applications in U.S. air quality studies. *Atmos. Environ.*, **27**, 1185 – 1201.

Chow J.C., Zielinska B.J., Watson J.G., Fujita E., Richards H.W., Neff W., Dietrich D., and Hering S., (1998) *Northern Front Range Air Quality Study Volume A: Ambient Measurements.* DRI Document No. 6580-685-8750.2F2

Creighton P.J., Lioy P.L., Haynie F.H., Lemmons T.J., Miller J.L. and Gerhart J. (1990) Soiling by atmospheric aerosols in an urban industrial area. *J. Air Waste Man. Ass.* **40**, 1285 – 1289.

Cuddihy R.C., Griffith W.C., and McClellan O. (1984) Health risks for light duty diesel vehicles. *Environ. Sci. Technol.*, **18**, 14 –21.

Del Monte M., Sabbione C. and Vittori G. (1984) Urban stone sulphatisation and oil fired carbonaceous particles. *Sci. Total Envir.* **36**, 369 – 376.

Draxler R.R. (1991) The accuracy of trajectories during ANATEX calculated using dynamic model analyses versus rawinsonde observations. *J. Appl. Meteor.*, **30** 1446 – 1467.

Draxler R.R. (1996) Trajectory optimization for balloon flight planning. *Weather and Forecasting* **11**, 111 – 114.

Groblicki P.J., Wolff G.T., and Countess R.J. (1981) Visibility reducing species in the Denver "brown cloud"—I. Relationships between extinction and chemical composition. *Atmos. Environ.*, **15**, 2473 – 2484.

Hansen A.D.A. and Rosen H. (1984) Vertical distributions of particulate carbon, sulfur,

and bromine in the Arctic haze and comparison with ground-level measurements at Barrow, Alaska. *Geophys. Res. Lett.* **11**, 381 – 384.

Hansen A.D.A. and Novakov T. (1988) Aerosol black carbon measurements over the Western Atlantic Ocean. *Global Biogeochem. Cycles* **2**, 41 – 45.

Hansen A.D.A., Kapustin V.N., Kopeikin V.M. Gillette D.A., and Bodhaine B.A. (1993) Optical absorption by aerosol black carbon and dust in a desert region of Central Asia. *Atmos. Environ.* **27A**, 2527 - 2531.

Hansen A.D.A., Polissar A.V., and Schnell R.C. (1997) Airborne aerosol and black carbon measurements over the East Siberian Sea, Spring 1992. *Atmos. Res.* **44**, 153 – 165.

Hansen A.D.A. (1996) *The Aethalometer*. Magee Scientific Company

Hinds W.C. (1982) *Aerosol Technology: Properties, Behavior, and Measurement of of Airborne Particles*. J. Wiley and Sons, NY.

Hitzenberger R., Dusek U., and Berner A. (1996) Black carbon measurements using an Integrating sphere. *J. Geophys. Res.* **101**, 19601 – 19606.

Horvath H. and Habenreich T.A. (1989) Absorption coefficient of the Vienna Aerosols: Comparison of two methods. *Aerosol Sci. Technol.* **10**, 506 – 514.

Horvath H. (1993) Atmospheric light absorption—a review. *Atmos. Environ.* **27A**, 293 – 317.

HYSPLIT4 (Hybrid Single-Particle Lagrangian Integrated Trajectory) Model, 1997. http://www.arl.noaa.gov/ready/hysplit4.html NOAA Air Resources Laboratory, Silver Springs, Maryland.

Jennings S.G., Spain T.G., Doddridge B.G., Maring H., Kelly B.P., and Hansen A.D.A. (1996). Concurrent measurements of black carbon aerosol and carbon monoxide at Mace Head. *J. Geophys. Res.* **101**, 19447 – 19454.

Liousse C., Cachier H., and Jennings S.G. (1993) Optical and thermal measurements of black carbon aerosol content in different environments: variation of the specific attenuation cross-section, sigma (σ). *Atmos. Environ.* **27A,** 1203 – 1211.

Lewis C.W., and Dzubay T.G. (1986) Measurement of light absorption extinction in Denver. *Aerosol Sci. Technol.* **5**, 325 –336.

Moosmuller H., Arnott W. P., and Rogers C. F. (1997) Methods for real-time, in situ

measurement of aerosol light absorption. *J. Air Waste Man. Ass.* **47**, 157 – 166.

Molenar J.V., Cismoski D.S., and Tree R.M. (1992) *Intercomparison of ambient optical monitoring techniques*; Air Resource Specialists, Inc.

Muhlbaier D.J., and Cadle S.H. (1989) Atmospheric aerosol particles in the Detroit urban area. Wintertime sources and sinks. *Aerosol Sci. Technol.* **10**, 236 – 248.

Pao Y.H. (1977) *Optoacoustic Spectroscopy and Detection.* Academic Press, NY.

Petzold A., and Niessner R. (1995a) Intercomparison study on soot-selective methods-Field study results from several polluted areas in Germany. *J. Aerosol Sci.* **26** S393 – S394.

Petzold A., and Niessner R. (1995b) Method comparison study on soot-selective techniques. *Mikrochim. Acta.* **117**, 215 – 237.

Petzold A., Kopp C., and Niessner R. (1997) The dependence of the specific attenuation cross-section on black carbon mass fraction and particle size. *Atmos. Environ.* **31**, 661 – 672.

Pinnick R.G., Fernandez G., Martinez-Andazola E., Hinds B.D., Hansen A.D.A., and Fuller K. (1993) Aerosol in arid southwestern United States: Measurements of mass loading, volatility, size distribution, absorption characteristics, black carbon content, and vertical structure to 7 km above sea level. *J. Geophys. Res.* **98**, 2651 – 2666.

Rosen H. and Novakov T. (1983) Optical transmission through aerosol deposits on diffusively reflective filters: a method for measuring the absorbing component of aerosol particles. *Appl. Opt.* **22**, 1256.

Rosencwaig A. (1980) Photoacoustics and Photoacoustic Spectroscopy. Vol.57 in *Chemical Analysis: A series of monographs on analytical chemistry and its applications.* John Wiley, NY.

Seinfeld J.H. and Pandis S.N. (1998) Atmospheric Chemistry and Physics. John Wiley and Sons, Inc. NY.

Willeke K. and Baron P.A. (1993) *Aerosol Measurement: Principles, Techniques and Applications,* Van Nostrand Reinhold, NY.

APPENDICES

APPENDIX A

Particle Loss Calculations

A TSI Incorporated aerosol calculation program was used to calculate diffusional and gravitational particle number losses through the inlets. The following tables illustrate the results of the loss calculations. The diffusional losses in the CNC inlet are shown in Table A.1. The gravitational losses in the OPC inlet are shown in Table A.2. The gravitational losses in the aethalometer inlet are shown in Table A.3. The diffusional losses in the OPC and aethalometer are shown in Tables A.4 and A.5.

Table A.1 Diffusional losses in the CNC 3020 inlet

diameter(um)	Frac. through GK	Frac. through lWB	Frac. through tWB
0.01	0.809411663	0.804542946	0.901902965
0.02	0.918093449	0.911091015	0.959143214
0.03	0.950287703	0.944823698	0.975560158
0.04	0.965054602	0.960901446	0.982969187
0.05	0.97334269	0.970101983	0.987084944
0.06	0.978576364	0.975970691	0.989665154
0.07	0.982148343	0.979997273	0.991416622
0.08	0.9847247	0.982909242	0.992674562
0.09	0.986661441	0.985100805	0.993616978
0.1	0.988164982	0.986802625	0.994346538
0.11	0.989362697	0.988157929	0.994926326
0.12	0.990337167	0.989259963	0.995397089
0.13	0.991144116	0.990171831	0.995786239
0.14	0.991822418	0.990937638	0.996112845
0.15	0.992399961	0.991589063	0.996390556
0.16	0.992897237	0.992149399	0.996629381
0.17	0.993329617	0.992636126	0.996836812
0.18	0.99370884	0.993062595	0.997018562
0.19	0.994044017	0.993439167	0.997179058
0.2	0.99434232	0.993773994	0.99732178
0.21	0.994609466	0.994073574	0.997449499
0.22	0.994850062	0.994343142	0.997564445
0.23	0.995067863	0.994586961	0.997668434
0.24	0.995265956	0.994808533	0.997762957
0.25	0.995446901	0.995010763	0.997849249
0.26	0.995612838	0.995196077	0.997928343
0.27	0.995765569	0.995366514	0.998001107
0.28	0.99590662	0.995523805	0.998068276
0.29	0.996037293	0.995669423	0.998130476
0.3	0.996158706	0.99580463	0.998188244

GK = laminar flow from Gormley and Kennedy (W&B 6-46)
lWB = laminar flow (W&B 6-42, 6-43)
tWB = turbulent flow (W&B 6-42, 6-45)

Table A.2 Gravitational losses: total fraction penetrating OPC

diameter(um)	Frac. pene.	diameter(um)	Frac. pene.
0.3	0.99918668	4.7	0.96435355
0.4	0.99883797	4.8	0.96327179
0.5	0.99845099	4.9	0.96218146
0.6	0.99802949	5	0.96108274
0.7	0.99757636	5.5	0.95546949
0.8	0.99709388	6	0.94967206
0.9	0.99658391	6.5	0.94370973
1	0.99604801	7	0.93760017
1.1	0.99548752	7.5	0.93135971
1.2	0.99490358	8	0.92500349
1.3	0.99429726	8.5	0.91854565
1.4	0.99366945	9	0.91199937
1.5	0.99302102	9.5	0.90537706
1.6	0.99235271	10	0.89869035
1.7	0.99166524		
1.8	0.99095926		
1.9	0.99023536		
2	0.98949411		
2.1	0.98873605		
2.2	0.98796165		
2.3	0.98717139		
2.4	0.98636572		
2.5	0.98554504		
2.6	0.98470976		
2.7	0.98386026		
2.8	0.9829969		
2.9	0.98212003		
3	0.98122998		
3.1	0.98032706		
3.2	0.9794116		
3.3	0.97848388		
3.4	0.97754418		
3.5	0.97659279		
3.6	0.97562998		
3.7	0.97465599		
3.8	0.97367108		
3.9	0.9726755		
4	0.97166948		
4.1	0.97065325		
4.2	0.96962703		
4.3	0.96859104		
4.4	0.96754549		
4.5	0.9664906		
4.6	0.96542655		

Table A.3 Gravitational losses: total fraction penetrating Aeth.

diameter(um)	Frac. pene.	diameter(um)	Frac. pene.
0.3	0.998517598	4.7	0.93690309
0.4	0.997882631	4.8	0.93504852
0.5	0.997178425	4.9	0.93318286
0.6	0.996411892	5	0.93130651
0.7	0.995588429	5.5	0.9217779
0.8	0.994712315	6	0.91203768
0.9	0.993787049	6.5	0.90212776
1	0.992815577	7	0.89208632
1.1	0.991800438	7.5	0.8819483
1.2	0.990743864	8	0.87174571
1.3	0.989647847	8.5	0.86150794
1.4	0.988514182	9	0.85126198
1.5	0.987344504	9.5	0.84103258
1.6	0.986140312	10	0.83084248
1.7	0.984902991		
1.8	0.98363383		
1.9	0.982334027		
2	0.98100471		
2.1	0.979646938		
2.2	0.978261713		
2.3	0.976849982		
2.4	0.975412648		
2.5	0.973950568		
2.6	0.972464564		
2.7	0.97095542		
2.8	0.96942389		
2.9	0.967870696		
3	0.966296535		
3.1	0.964702078		
3.2	0.963087973		
3.3	0.961454846		
3.4	0.959803303		
3.5	0.95813393		
3.6	0.956447297		
3.7	0.954743958		
3.8	0.953024448		
3.9	0.951289291		
4	0.949538994		
4.1	0.947774052		
4.2	0.945994949		
4.3	0.944202155		
4.4	0.942396129		
4.5	0.940577319		
4.6	0.938746164		

Table A.4 Diffusional losses:fraction through entire inlet for the OPC

diameter(um)	Frac. through GK	Frac. through lWB	Frac. through tWB
0.01	0.968179645	0.964610802	0.946007884
0.02	0.986833855	0.985294476	0.977602313
0.03	0.992117429	0.991250581	0.986616807
0.04	0.994499532	0.993931729	0.990678539
0.05	0.995823659	0.995415839	0.992933125
0.06	0.99665455	0.99634309	0.994345923
0.07	0.997219093	0.996970619	0.995304668
0.08	0.997624908	0.997420138	0.995993123
0.09	0.997929167	0.997756131	0.996508821
0.1	0.998164867	0.998015713	0.996907999
0.11	0.998352294	0.998221637	0.997225202
0.12	0.998504558	0.998388575	0.99748274
0.13	0.998630487	0.998526378	0.997695618
0.14	0.998736223	0.998641886	0.997874274
0.15	0.998826165	0.998739989	0.998026179
0.16	0.998903542	0.998824268	0.998156809
0.17	0.998970769	0.998897398	0.998270264
0.18	0.999029691	0.998961418	0.99836967
0.19	0.999081737	0.999017906	0.998457449
0.2	0.999128032	0.999068101	0.998535507
0.21	0.99916947	0.999112988	0.998605357
0.22	0.999206772	0.999153361	0.998668221
0.23	0.999240525	0.999189863	0.998725091
0.24	0.999271212	0.999223023	0.998776784
0.25	0.999299232	0.99925328	0.998823975
0.26	0.999324919	0.999280999	0.99886723
0.27	0.999348554	0.999306488	0.998907022
0.28	0.999370375	0.999330006	0.998943753
0.29	0.999390585	0.999351776	0.998977768
0.3	0.999409357	0.999371986	0.999009359

GK = laminar flow from Gormley and Kennedy (W&B 6-46)
lWB = laminar flow (W&B 6-42, 6-43)
tWB = turbulent flow (W&B 6-42, 6-45)

Table A.5 Diffusional losses:fraction through entire inlet for aethalometer

diameter(um)	Frac. through GK	Frac. through lWB	Frac. through tWB
0.01	0.951888433	0.946547687	0.905751756
0.02	0.980039835	0.977618727	0.960794717
0.03	0.988037661	0.986658516	0.976556161
0.04	0.991648011	0.990740777	0.983665774
0.05	0.993656317	0.993003528	0.98761425
0.06	0.994917127	0.994418217	0.990089244
0.07	0.995774068	0.995375974	0.991769139
0.08	0.996390227	0.996062182	0.992975598
0.09	0.996852285	0.996575148	0.993879405
0.1	0.997210285	0.996971478	0.994579053
0.11	0.997495003	0.997285893	0.995135054
0.12	0.997726333	0.997540783	0.995586493
0.13	0.99791767	0.997751186	0.995959661
0.14	0.998078341	0.997927547	0.996272851
0.15	0.998215022	0.998077331	0.996539151
0.16	0.998332615	0.998206003	0.99676816
0.17	0.99843479	0.998317653	0.996967063
0.18	0.998524348	0.998415391	0.997141339
0.19	0.998603458	0.998501628	0.997295235
0.2	0.998673829	0.998578256	0.997432087
0.21	0.998736819	0.998646779	0.997554552
0.22	0.998793526	0.998708408	0.997664769
0.23	0.998844839	0.998764128	0.99776448
0.24	0.998891491	0.998814745	0.997855113
0.25	0.998934091	0.99886093	0.997937854
0.26	0.998973145	0.99890324	0.998013693
0.27	0.999009079	0.998942144	0.998083462
0.28	0.999042257	0.99897804	0.998147866
0.29	0.999072985	0.999011266	0.998207505
0.3	0.999101529	0.999042112	0.998262896

GK = laminar flow from Gormley and Kennedy (W&B 6-46)
lWB = laminar flow (W&B 6-42, 6-43)
tWB = turbulent flow (W&B 6-42, 6-45)

APPENDIX B

Summary of Calculated Trajectories

Back trajectories were calculated daily during the study. Back trajectories were also calculated for high and low BC periods during the study. The files are stored electronically due to the large number produced during the study (452). The back trajectory files are GIF files. They are identified by the date, e.g. the daily trajectory run for September 13, 1997 at 12a.m.local time (refer to Figure 2) is stored as 9-13-97. Similarly a low BC period trajectory on the same day is stored as 9-13-97l. A high BC period trajectory for the previous day is stored as 9-12-97h. The high and low BC period trajectory for September 12 and 13,1997 are shown as examples.

U.S. NATIONAL OCEANIC AND ATMOSPHERIC ADMINISTRATION
ARL / NCEP

BACKWARD TRAJECTORY ENDING- 14UTC 12 SEP 97

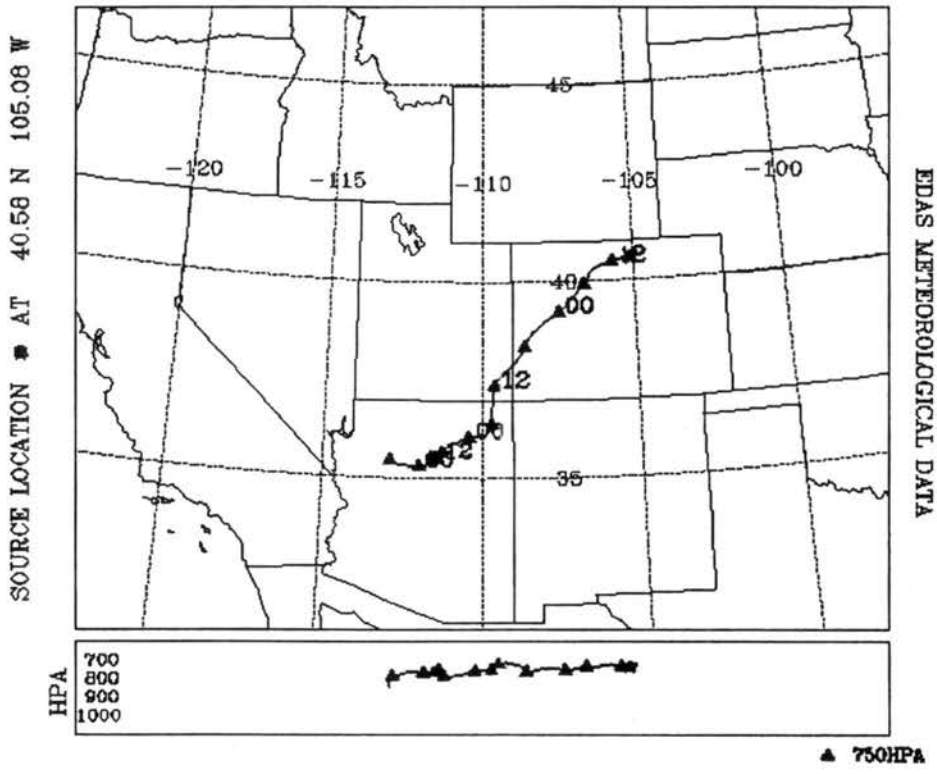

U.S. NATIONAL OCEANIC AND ATMOSPHERIC ADMINISTRATION
ARL / NCEP

BACKWARD TRAJECTORY ENDING- 09UTC 13 SEP 97

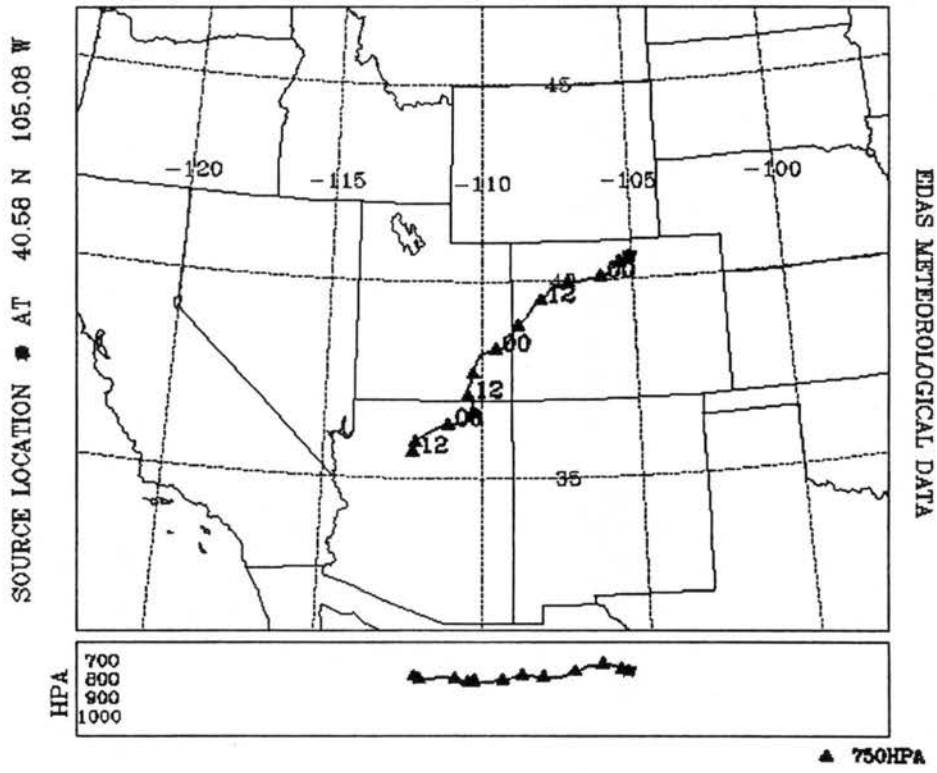

APPENDIX C

Train passage Data.

Tables 1a and 1b are presented showing train passage data presented in Figure 10a – 10e. The tables show the date and time of train passages, wind direction and wind speed during the passages.

Table 1a. Train passage duration, wind direction, and wind speed

	Time	Wind directio	Wind Speed
a	8/4 @ 15:30 - 36	NW	5 mph
b	8/4 @ 16:00 - 03	SW	1.9 mph
c	8/5 @ 3:15 - 19	NW	0.1 mph
d	8/5 @ 13:03 - 09	SE	4 mph
e	8/5 @ 16:45 - 52	SE	4.8 mph
f	8/5 @ 21:47 - 51	SE	2.4 mph
g	8/5 @ 22:37 - 40	SE	2.1 mph
h	8/6 @ 3:14 - 18	NE	0.9 mph
I	8/6 @ 13:15 - 20	SE	1.1 mph
j	8/6 @ 19:00 - 06	SE	5.4 mph
k	8/7 @ 0:38 - 44	NW	1.5 mph
l	8/7 @ 1:20 - 45	NW	1.13 mph
m	8/7 @ 12:43 - 46	SE	5.3 mph
n	8/7 @ 13:38 - 41	SE	4.9 mph
o	8/8 @ 4:16 - 21	SW	2 mph
p	8/8 @ 5:35 - 39	SW	1.1 mph
q	8/8 @ 10:02 - 06	SW	1.5 mph
r	8/8 @ 10:41 - 44	SW	1.4 mph
s	8/8 @ 20:23 - 30	NW	1.9 mph
t	8/9 @ 8:01 - 05	SE	1.7 mph
u	8/9 @ 9:20 - 24	SE	4.2 mph
v	8/9 @ 22:18 - 23	NE	1.8 mph
w	8/10 @ 1:53 - 2:01	NW	2.8 mph
x	8/10 @ 3:42 - 47	NE	0.9 mph
y	8/10 @ 8:28 - 33	NE	2.35 mph
z	8/10 @ 17:57 - 18:01	SW	1.9 mph
a1	8/10 @ 20:08 - 12	SE	3.2 mph
b1	8/11 @ 1:56 - 2:02	NW	0.0 mph
c1	8/11 @ 13:36 - 40	SW	2.8 mph

Table 1b. Train passage duration, wind direction, and wind speed

	Time	Wind directio	Wind Speed
a	9/2 @ 23:56 - 59	NE	1.7mph
b	9/3 @ 2:00 - 3:04	SE	1.0 mph
c	9/3 @ 5:32 - 36	SW	1.2 mph
d	9/3 @ 16:23 - 28	SW	5.1 mph
e	9/3 @ 19:38 - 41	NE	0.7 mph
f	9/3 @ 21:05 - 11	NW	2.6 mph
g	9/4 @ 2:41 - 45	SW	0.0 mph
h	9/4 @ 8:22 - 25	SE	1.9 mph
I	9/4 @ 13:41 - 44	SW	12.5 mph
j	9/4 @ 16:59 - 17:03	SE	0.0 mph
k	9/5 @ 5:02 - 07	N	0.0 mph
l	9/5 @ 14:49 - 53	SE	2.2 mph
m	9/5 @ 21:56 - 22:02	NW	1.1 mph
n	9/6 @ 0:58 - 1:02	NE	1.9 mph
o	9/6 @ 3:20 - 23	SE	1.2 mph
p	9/6 @ 5:56 - 59	SE	1.1 mph
q	9/6 @ 12:24 - 28	SE	5.7 mph
r	9/7 @ 4:41 - 46	SW	1.6 mph
s	9/7 @ 9:24 - 27	NE	6.9 mph
t	9/7 @ 13:21 - 26	SE	6.9 mph
u	9/7 @ 20:06 - 13	SE	4.4 mph
v	9/8 @ 4:49 - 56	NW	0.9 mph
w	9/8 @ 11:47 - 50	SW	5.9 mph
x	9/8 @ 17:16 - 21	NW	0.9 mph
y	9/8 @ 18:21 - 55	NW	1.4 mph
z	9/9 @ 2:30 - 33	NW	0.6 mph
a1	9/9 @ 5:23 - 27	SW	0.8 mph
b1	9/9 @ 10:07 - 10	SE	7.5 mph
c1	9/9 @ 16:03 - 07	SW	1.4 mph

Table 1a. Train passage duration, wind direction, and wind speed

	Time	Wind directio	Wind Speed
d1	8/11 @ 14:09 - 13	NE	6.2 mph
e1	8/11 @ 15:05 - 09	NW	7.1 mph
f1	8/11 @ 23: 06 - 09	NW	0.0 mph
g1	8/12 @ 2:26 - 29	SW	3.6 mph
h1	8/12 @ 4:00 - 04	NW	0.1 mph
I1	8/12 @ 11:47 - 50	NE	3.9 mph
j1	8/12 @ 12:10 - 15	NE	7.8 mph
k1	8/12 @ 15:00 - 03	NE	9.8 mph
l1	8/12 @ 18:47 - 52	NW	0.7 mph
m1	8/13 @ 5:52 - 55	NW	0.7 mph
n1	8/13 @ 16:01 - 04	SE	6.8 mph
o1	8/13 @ 20:49 - 53	NW	0.8 mph
p1	8/14 @ 0:15 - 20	NW	1.4 mph
q1	8/14 @ 8:26 - 32	SE	3 mph
r1	8/14 @ 18:23 - 28	SW	4.3 mph
s1	8/15 @ 0:17- 23	NE	1.5 mph
t1	8/15 @ 3:54 - 4:02	NW	1.2 mph
u1	8/15 @ 6:54 - 58	NW	2.3 mph
v1	8/15 @ 16:06 - 09	SW	3.4 mph
w1	8/16 @ 0:35 - 39	NW	0.7 mph
x1	8/16 @ 1:02 - 07	SW	0.6 mph
y1	8/16 @ 4:32 - 38	SE	1.0 mph
z1	8/16 @ 7:08 - 12	SW	1.3 mph
a2	8/16 @ 10:29 - 32	NW	2.0 mph
b2	8/16 @ 16:59 - 17:0	SW	5.0 mph
c2	8/16 @ 21:12 - 17	SW	1.5 mph
d2	8/16 @ 22:22 - 27	NE	2.1 mph
e2	8/17 @ 16:32 - 37	SE	3.5 mph
f2	8/18 @ 1:25 - 30	NE	2.8 mph

Table 1b. Train passage duration, wind direction, and wind speed

	Time	Wind directio	Wind Speed
d1	9/9 @ 21:35 - 41	SE	1.7 mph
e1	9/10 @ 2:20 - 23	SW	1.8 mph
f1	9/10 @ 8:54 - 58	SE	5.4 mph
g1	9/10 @ 14:39 - 44	NW	2.1 mph
h1	9/10 @ 20:03 - 07	NW	2.0 mph
I1	9/10 @ 23:04 - 09	NW	2.7 mph
j1	9/11 @ 9:10 - 15	NE	4.1 mph
k1	9/11 @ 16:44 - 49	SE	0.9 mph
l1	9/11 @ 20:16 - 22	SE	0.9 mph
m1	9/12 @ 4:09 - 13	NE	1.3 mph
n1	9/12 @ 7:26 - 32	SW	3.6 mph
o1	9/12 @ 17:17 - 23	NW	3.5 mph
p1	9/12 @ 22:19 - 25	NE	1.3 mph
q1	9/13 @ 1:32 - 37	NW	0.5 mph
r1	9/13 @ 10:17 - 22	SW	5.1 mph
s1	9/13 @ 14:48 - 52	NW	1.2 mph
t1	9/13 @ 19:18 - 23	SW	2.4 mph
u1	9/14 @ 2:46 - 50	NE	1.3 mph
v1	9/14 @ 3:46 - 53	SW	2.1 mph
w1	9/14 @ 8:13 - 19	NE	6.9 mph
x1	9/14 @ 11:50 - 56	NE	2.4 mph
y1	9/14 @ 18:53 - 57	SE	1.4 mph
z1	9/14 @ 22:39 - 43	NE	2.5 mph
a2	9/15 @ 15:12 - 16	SE	4.0 mph
b2	9/15 @ 17:31 - 34	SE	2.9 mph
c2	9/16 @ 5:11 - 17	NW	0.8 mph
d2	9/16 @ 15:56 - 16:06	NW	3.1 mph
e2	9/16 @ 16:30 - 34	NW	1.7 mph
f2	9/17 @ 3:38 - 45	SE	0.0 mph

Table 1a. Train passage duration, wind direction, and wind speed

	Time	Wind directio	Wind Speed
g2	8/18 @ 4:20 - 26	NW	0.8 mph
h2	8/18 @ 9:12 - 19	NW	2.3 mph
l2	8/18 @ 15:01 - 07	SW	6.6 mph
j2	8/18 @ 19:46 - 50	NE	1.2 mph
k2	8/19 @ 0:27 - 33	NE	1.3 mph
l2	8/19 @ 5:31 - 36	NW	0.9 mph
m2	8/19 @ 13:23 - 26	SE	3.2 mph
n2	8/20 @ 12:14 -19	SE	4.2 mph
o2	8/20 @ 14:51 - 55	SE	4.8 mph
p2	8/20 @ 18:57 - 19:0	SE	3.8 mph
q2	8/20 @ 22:32 - 37	SE	3.2 mph
r2	8/21 @ 0:17 - 20	NE	0.6 mph
s2	8/21 @ 5:25 - 33	NW	1.4 mph
t2	8/21 @ 8:49 - 55	NE	2.01 mph
u2	8/21 @ 13:25 - 30	SE	5.5 mph
v2	8/21 @ 23:10 - 15	NE	0.6 mph
w2	8/22 @ 3:10 - 16	NW	0.2 mph
x2	8/22 @ 6:49 - 52	NE	1.5 mph
y2	8/22 @ 9:32 - 37	SE	5.2 mph
z2	8/22 @ 23:36 - 41	NW	2.3 mph
a3	8/23 @ 0:31 - 35	NW	1.4 mph
b3	8/23 @ 6:49 - 53	NW	1.4 mph
c3	8/23 @ 16:21 - 26	SE	2.9 mph
d3	8/23 @ 17:19 - 23	NW	2.1 mph
e3	8/23 @ 18:07 - 13	NW	1.4 mph
f3	8/23 @ 19:16 - 22	NE	1.2 mph
g3	8/23 @ 19:46 - 50	NW	1.4 mph
h3	8/24 @ 0:44 - 48	NW	4.4 mph
l3	8/24 @ 13:52 - 57	SE	5.7 mph
j3	8/24 @ 17:52 - 58	SW	8.0 mph

Table 1b. Train passage duration, wind direction, and wind speed

	Time	Wind directio	Wind Speed
g2	9/17 @ 4:32 - 36	N	0.0 mph
h2	9/17 @ 18:53 - 58	NE	0.3 mph
l2	9/17 @ 19:58 - 20:01	NE	1.4 mph
j2	9/18 @ 0:07 - 11	NW	1.7 mph
k2	9/18 @ 8:21 - 26	SE	2.7 mph
l2	9/18 @ 15:28 - 33	SE	1.2 mph
m2	9/18 @ 17:12 - 17	NW	1.1 mph
n2	9/19 @ 1:23 - 27	NE	3.4 mph
o2	9/19 @ 5:43 - 48	NW	3.8 mph
p2	9/19 @ 18:13 - 18	NW	1.8 mph
q2	9/19 @ 20:44 - 50	SW	0.0 mph
r2	9/19 @ 23:51 - 55	NW	1.0 mph
s2	9/20 @ 12:29 - 32	SE	3.6 mph
t2	9/20 @ 12:54 - 58	SE	3.4 mph
u2	9/20 @ 14:45 - 49	NW	2.9 mph
v2	9/20 @ 17:33 - 37	NW	1.9 mph
w2	9/21 @ 8:22 - 27	SE	3.9 mph
x2	9/21 @ 20:01 - 04	SE	6.6 mph
y2	9/21 @ 20:31 - 36	SE	8.2 mph
z2	9/22 @ 0:56 - 1:01	SE	3.9 mph
a3	9/22 @ 3:28 - 32	SE	4.1 mph
b3	9/22 @ 15:47 - 52	SW	1.1 mph
c3	9/22 @ 20:40 - 46	NW	1.3 mph
d3	9/22 @ 21:08 - 11	NE	7.4 mph
e3	9/23 @ 3:00 - 05	NE	3.2 mph
f3	9/23 @ 5:05 - 09	NE	2.5 mph
g3	9/23 @ 20:16 - 19	NW	1.5 mph
h3	9/23 @ 21:15 - 20	NW	0.9 mph
l3	9/24 @ 0:20 - 26	NW	3.3 mph
j3	9/24 @ 3:45 - 50	NW	1.2 mph

Table 1a. Train passage duration, wind direction, and wind speed

	Time	Wind directio	Wind Speed
k3	8/24 @ 23:25 - 30	NE	1.4 mph
l3	8/25 @ 2:58 - 3:02	NW	1.4 mph
m3	8/25 @ 9:25 - 35	NE	2.6 mph
n3	8/25 @ 22:24 - 27	NE	0.3 mph
o3	8/26 @ 4:17 - 23	NW	1.4 mph
p3	8/26 @ 5:23 - 30	NW	0.5 mph
q3	8/26 @ 5:53 - 58	NE	3.1 mph
r3	8/26 @ 19:03 - 07	SW	2 mph
s3	8/27 @ 4:20 - 26	NW	2.3 mph
t3	8/27 @ 9:08 - 11	SW	1.5mph
u3	8/27 @ 19:31 - 35	NW	4.8 mph
v3	8/28 @ 0:43 - 47	NW	0.0 mph
w3	8/28 @ 2:41 - 44	SW	2.1 mph
x3	8/28 @ 5:34 - 39	NW	0.5 mph
y3	8/28 @ 9:22 - 29	SW	2.4 mph

Table 1b. Train passage duration, wind direction, and wind speed

	Time	Wind directio	Wind Speed
k3	9/24 @ 21:00 - 03	NE	2.5 mph
l3	9/24 @ 21:24 - 29	NW	0.1 mph
m3	9/25 @ 0:05 - 17	NW	1.1 mph
n3	9/25 @ 0:48 - 55	NE	1.7 mph
o3	9/25 @ 15:20 - 25	NW	2.4 mph
p3	9/25 @ 21:08 - 13	SW	11.1 mph
q3	9/26 @ 9:41 - 47	SE	5.7 mph
r3	9/26 @ 11:331 - 37	SE	2.6 mph
s3	9/26 @ 19:40 - 43	NW	1.9 mph
t3	9/26 @ 20:03 - 06	SW	1.1 mph
u3	9/26 @ 22:22 - 26	NW	1.3 mph
v3	9/27 @ 2:30 - 34	NW	2.2 mph
w3	9/27 @ 16:34 - 39	SW	0.5 mph
x3	9/27 @ 20:46 - 21:03	NW	1.3 mph
y3	9/28 @ 4:38 - 43	SW	1.1 mph
z3	9/28 @ 7:35 - 39	NW	0.8 mph
a4	9/28 @ 19:37 - 43	NW	2.1 mph
b4	9/28 @ 20:06 - 10	NW	0.7 mph
c4	9/28 @ 20:43 - 47	NE	2.2 mph
d4	9/29 @ 17:41 - 45	SW	1.3 mph
e4	9/29 @ 20:59 - 21:02	NW	2.2 mph
f4	9/30 @ 9:06 - 12	NE	8.3 mph
g4	9/30 @ 17:19 - 25	SE	4.3 mph
h4	9/30 @ 19:31 - 34	SE	5.0 mph
l4	9/30 @ 20:43 - 47	SE	9.5 mph

APPENDIX D

Summary of Meteorological Data

D.1 BC concentrations and wind direction during the spatial variation study.

Figure D.1.1 shows plots of BC concentration and wind direction. One hour averages of each variable are plotted. The panels show the downtown location and campus site during the spatial variation study. Figure D.1.2 panels show the intersection and campus sites during the spatial variation study.

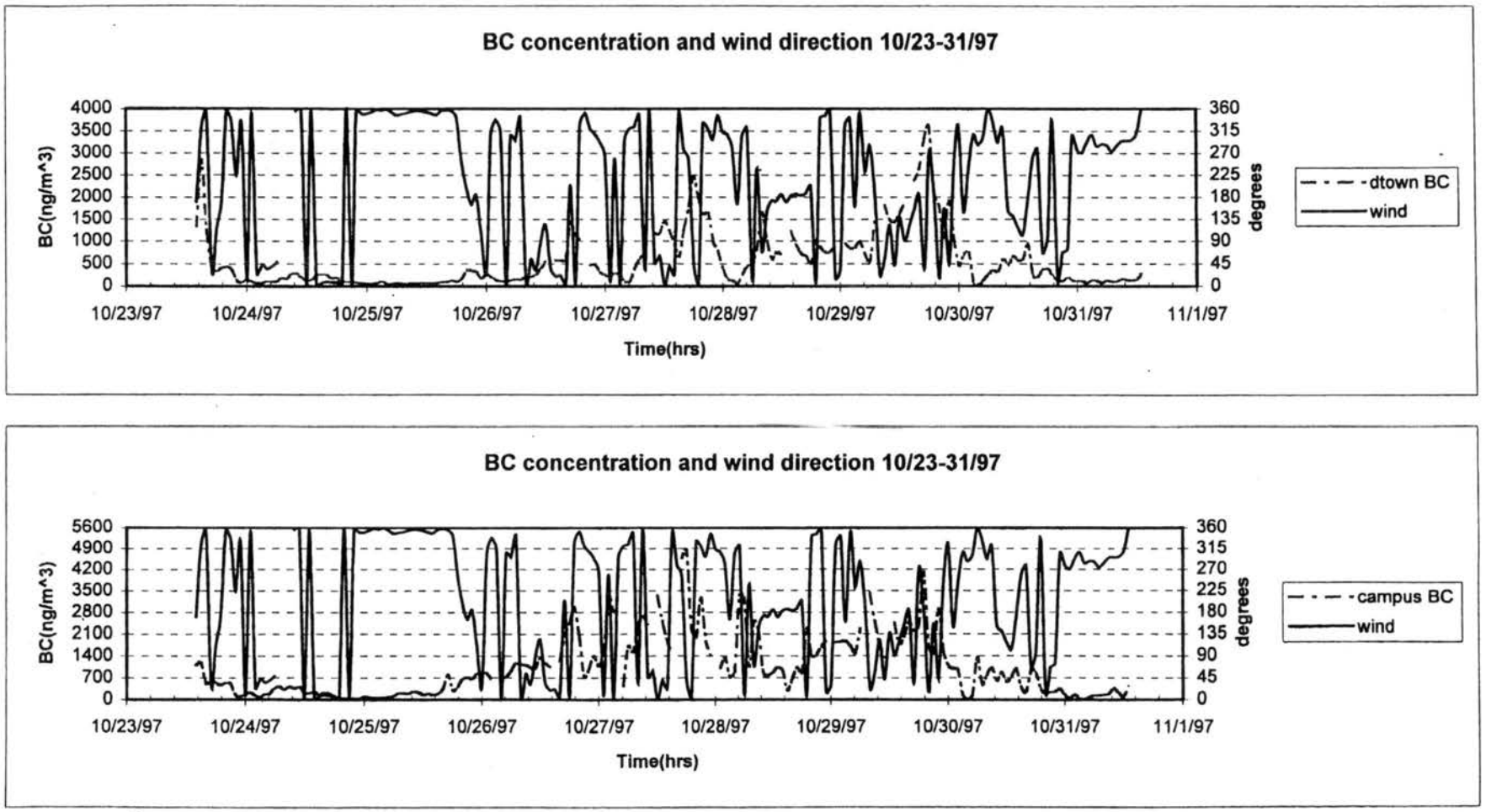

Figure D.1.1 BC concentrations and wind direction during the spatial variation study for the downtown and campus sites.

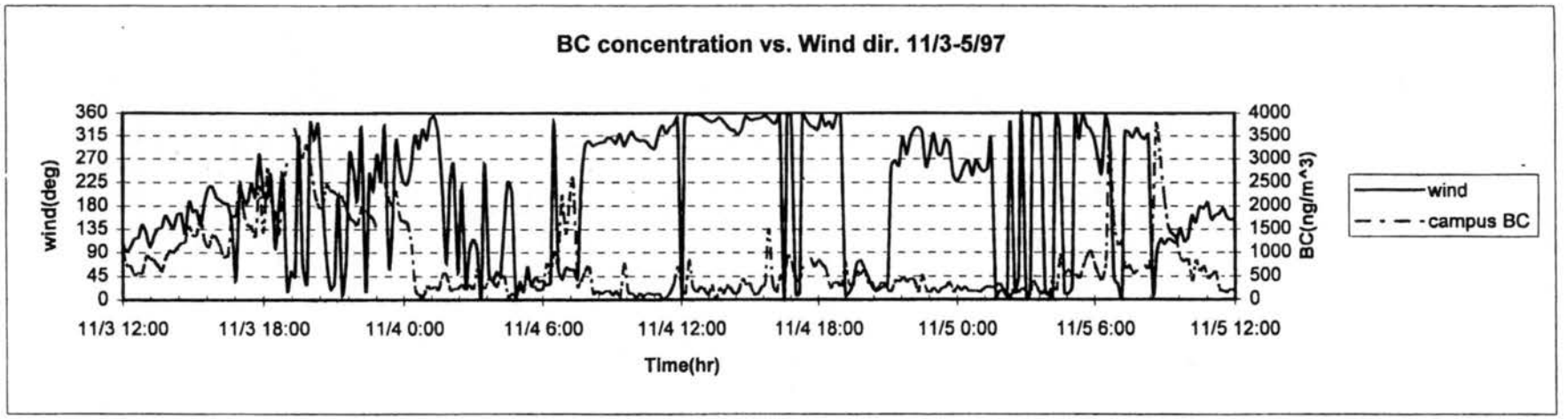

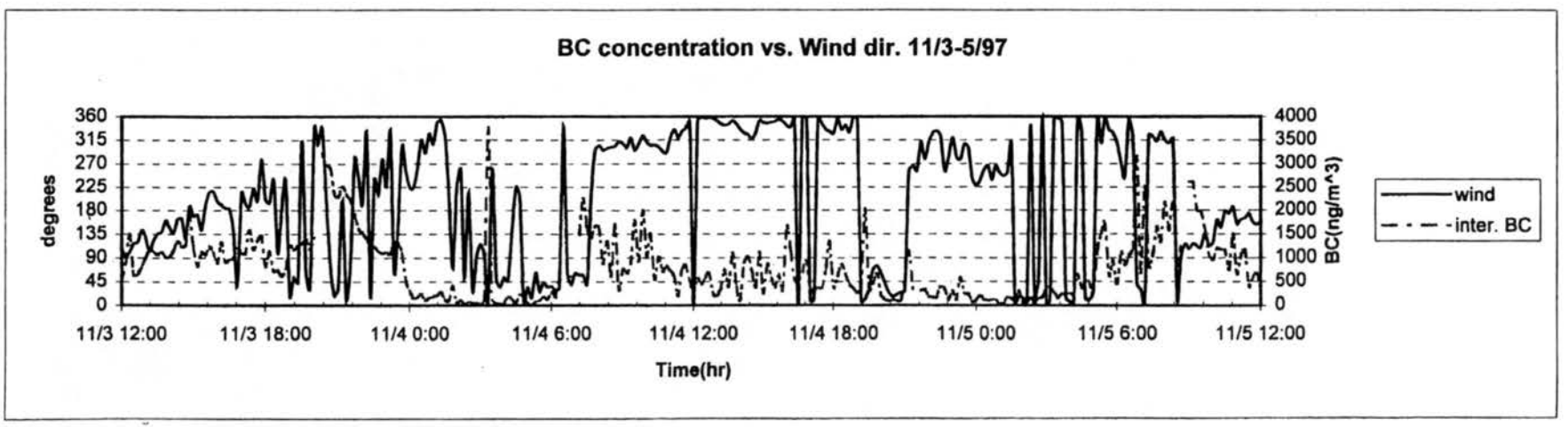

Figure D.1.2 BC concentrations and wind direction during the spatial variation study for the campus and busy intersection sites.

D.2 Comparison of Meteorological Data.

Figure D.2.1 – Figure D.2.4 show the monthly time-lines of the comparison of CDPHE and the Fort Collins Weather Station meteorological data. The parameters plotted are one hour averages of wind speed, wind direction, and temperature. The comparison for June is shown in Figure15.

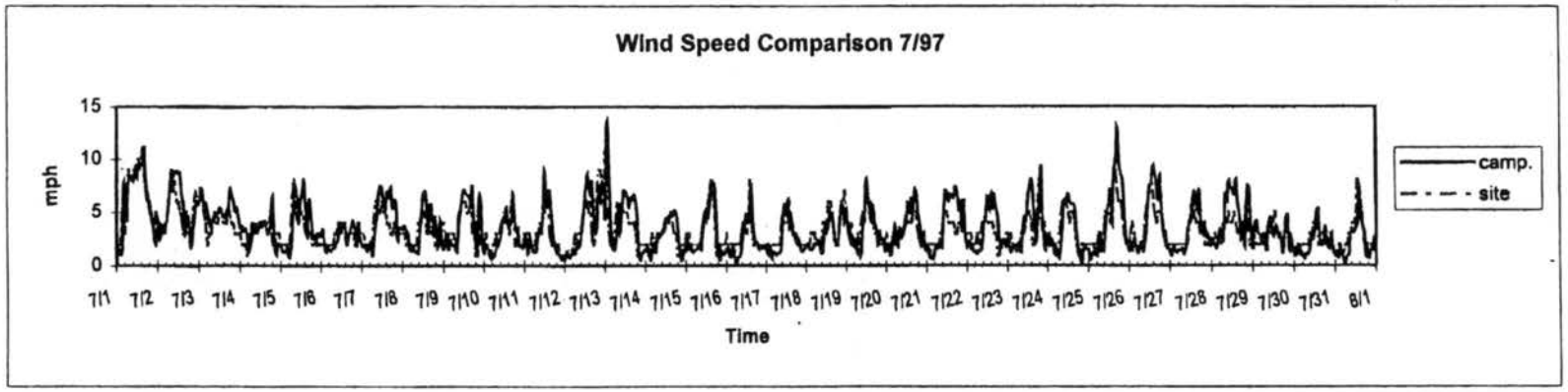

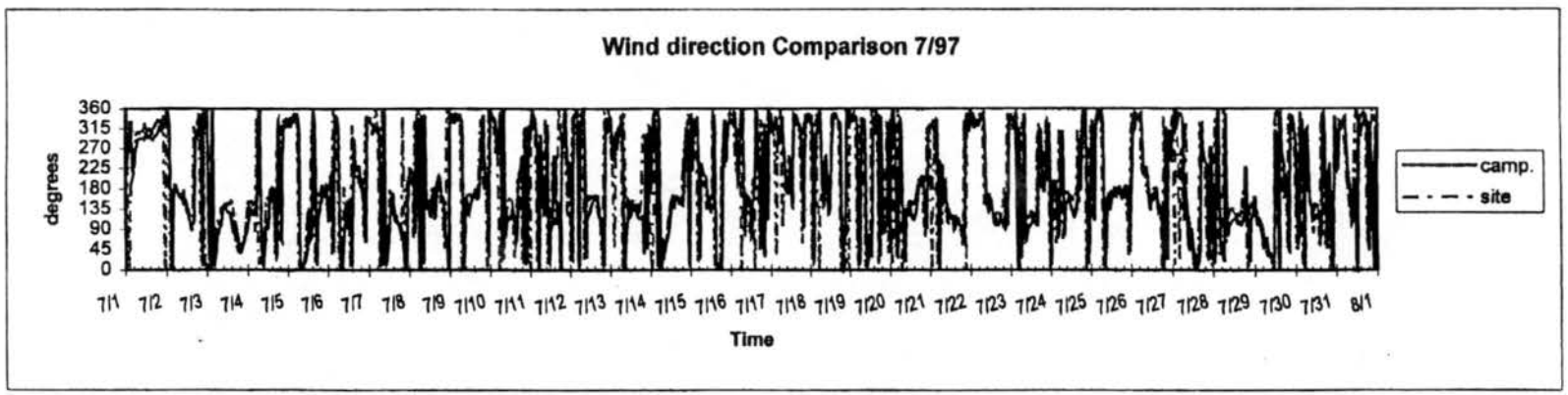

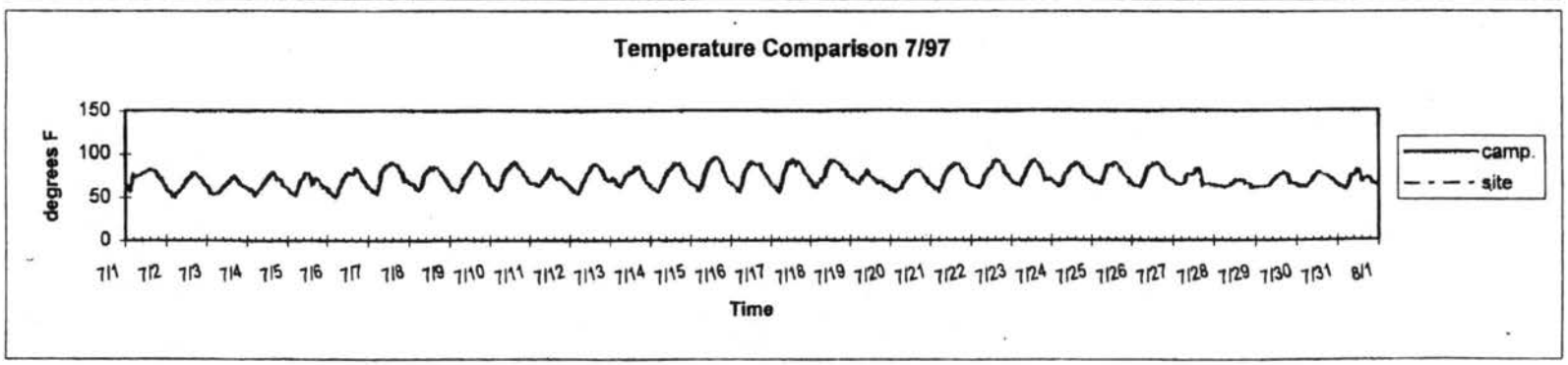

Figure D.2.1 July weather data comparison.

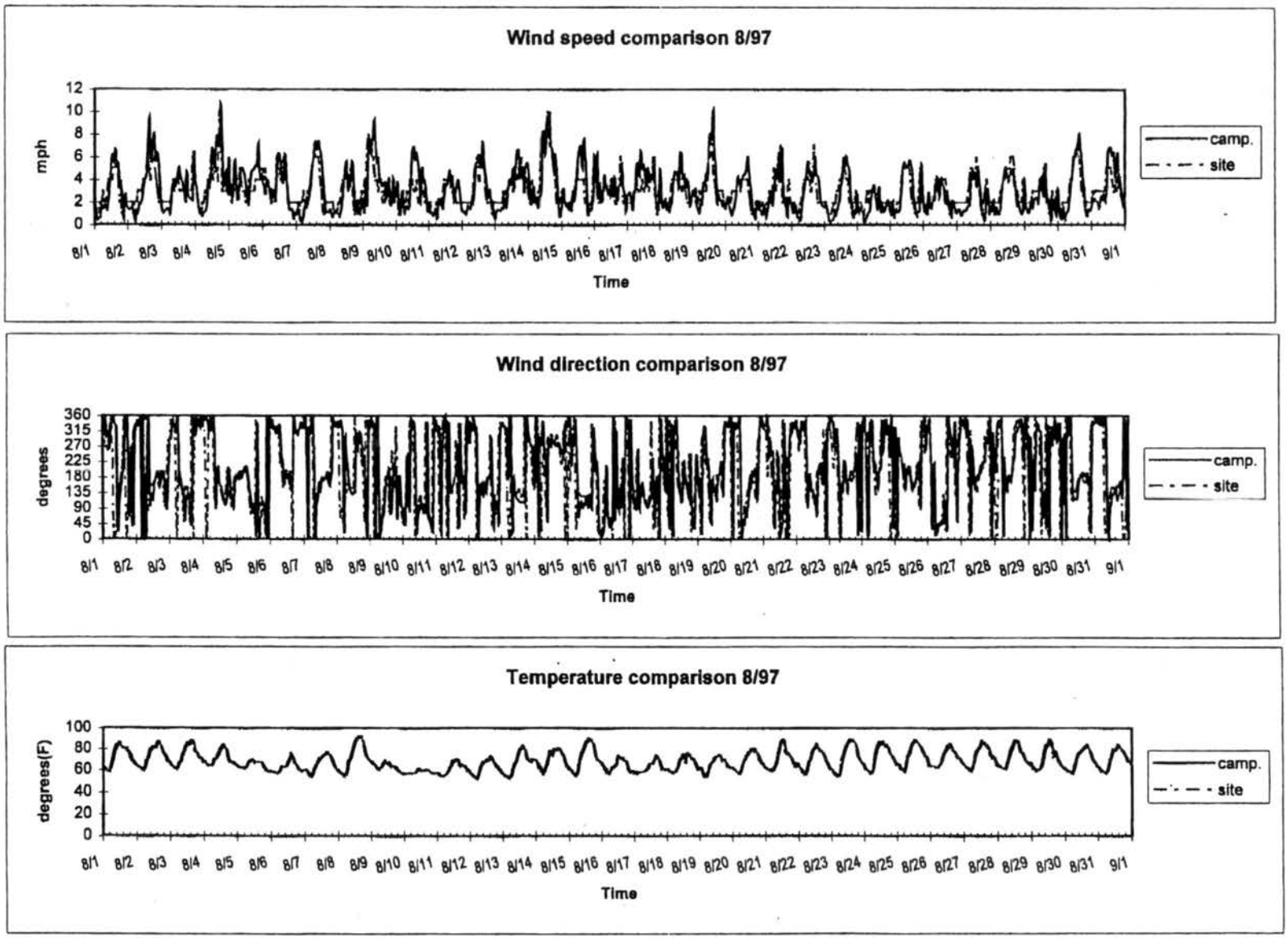

Figure D.2.2 August weather data comparison

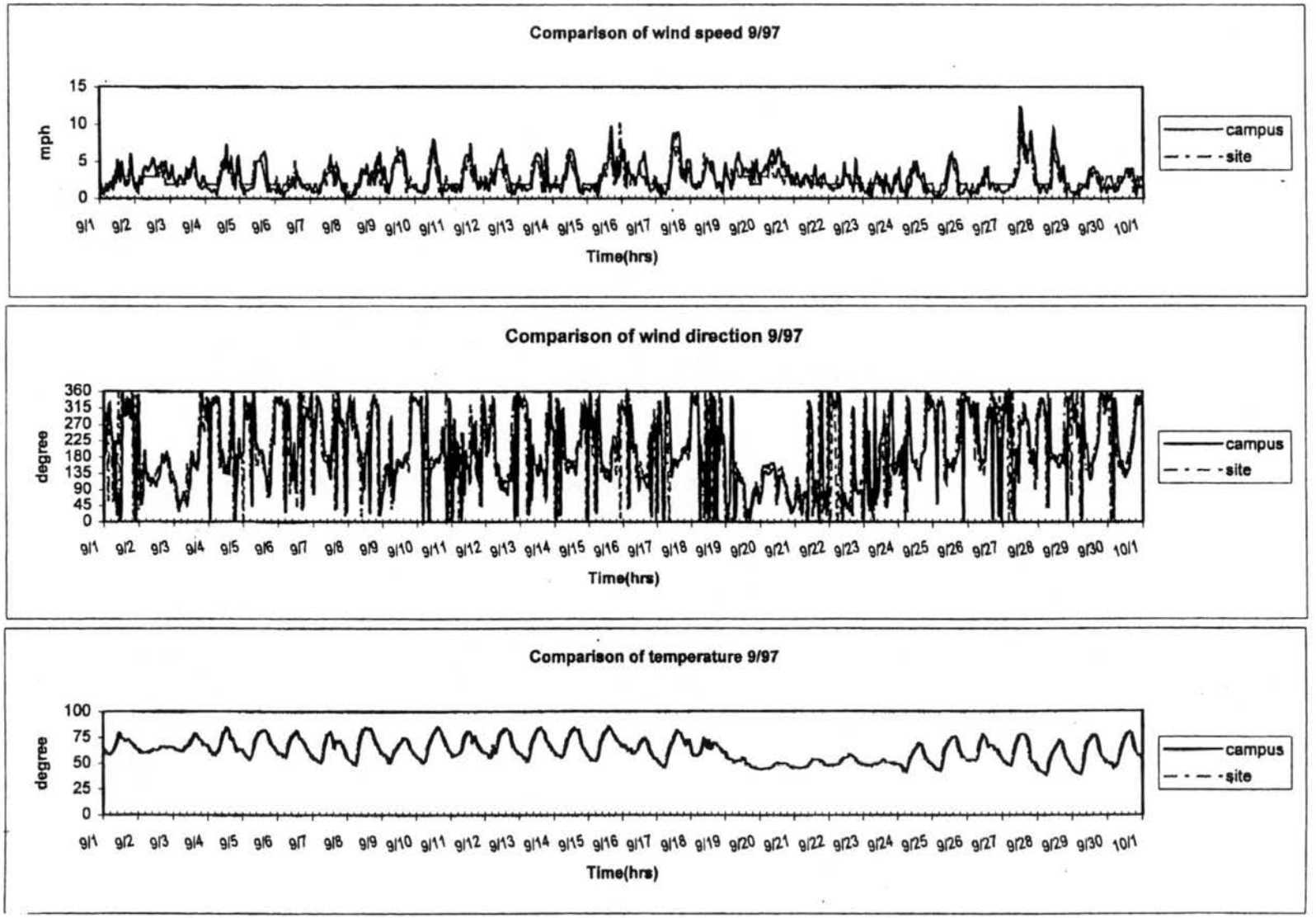

Figure D.2.3 September weather data comparison.

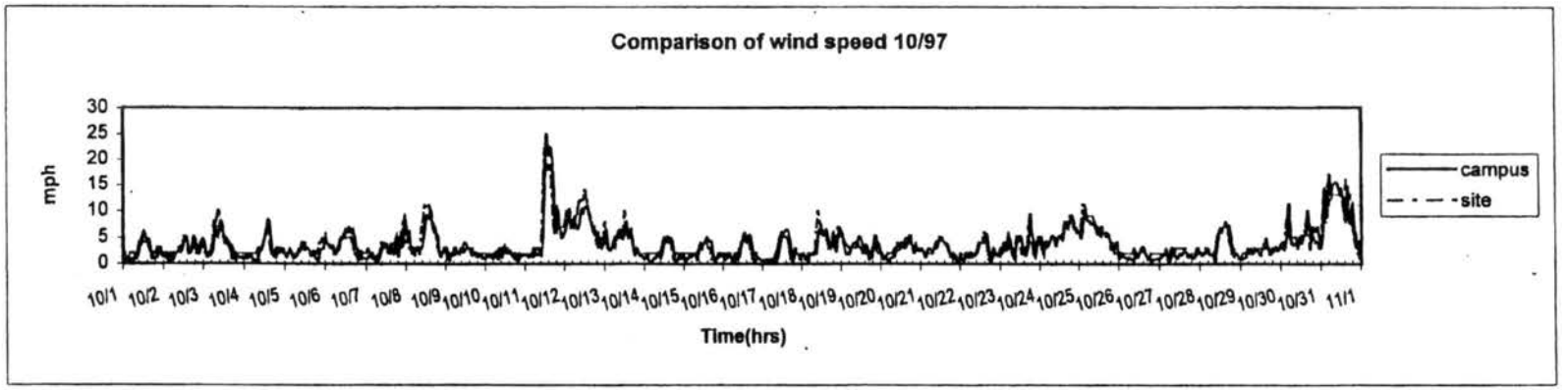

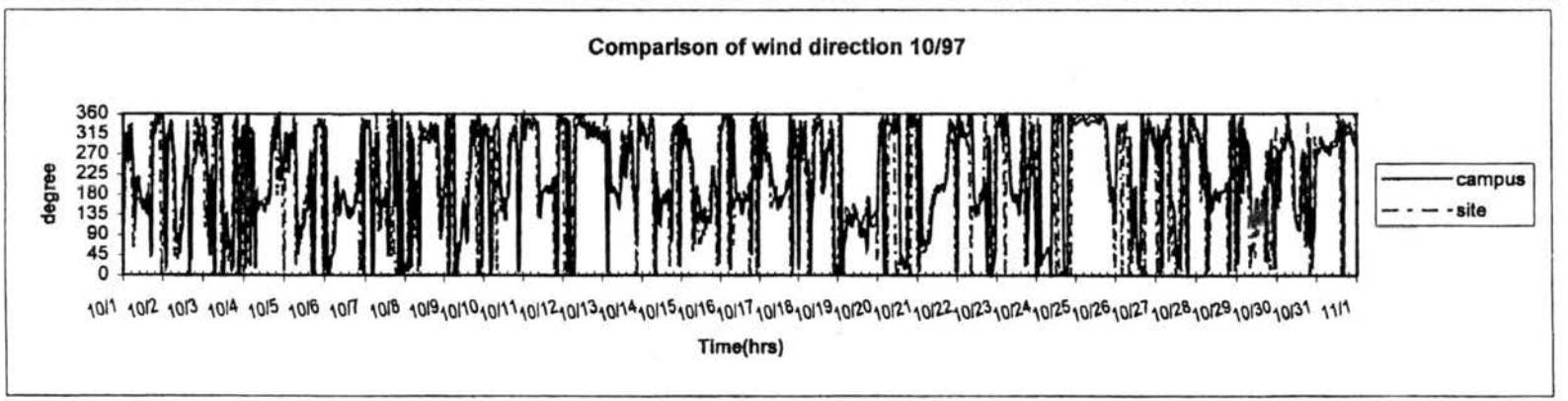

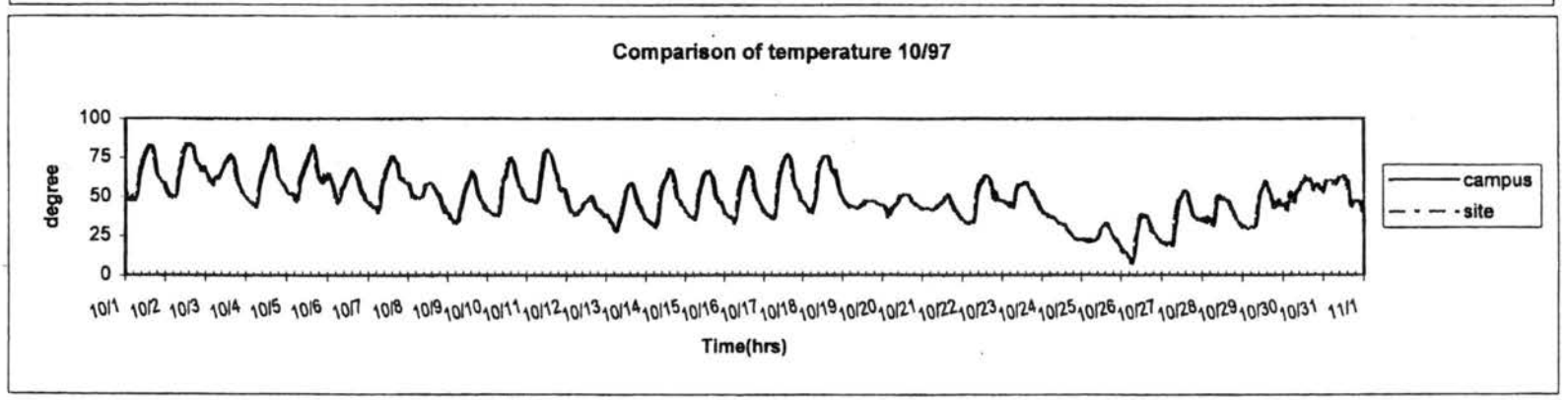

Figure D.2.4 October weather data comparison.

D.3 Meteorological Data and Black Carbon Concentrations.

Figure D.3.1 – Figure D.3.24 show the weekly timelines of BC concentrations with wind direction and pressure. One hour averages of the variables are plotted. The timelines are for the months of June – October, 1997.

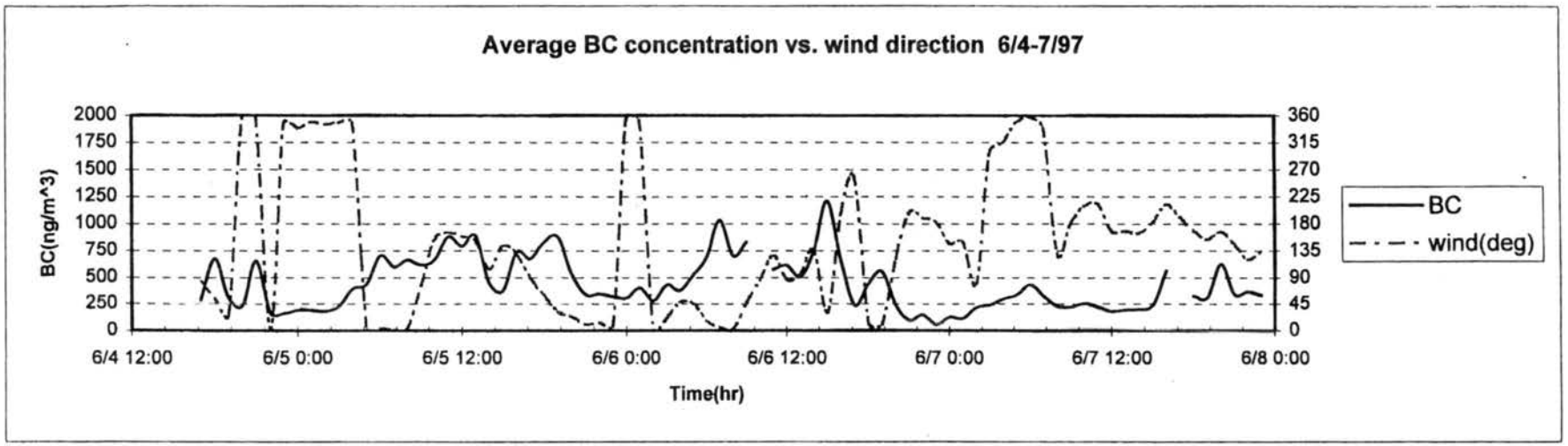

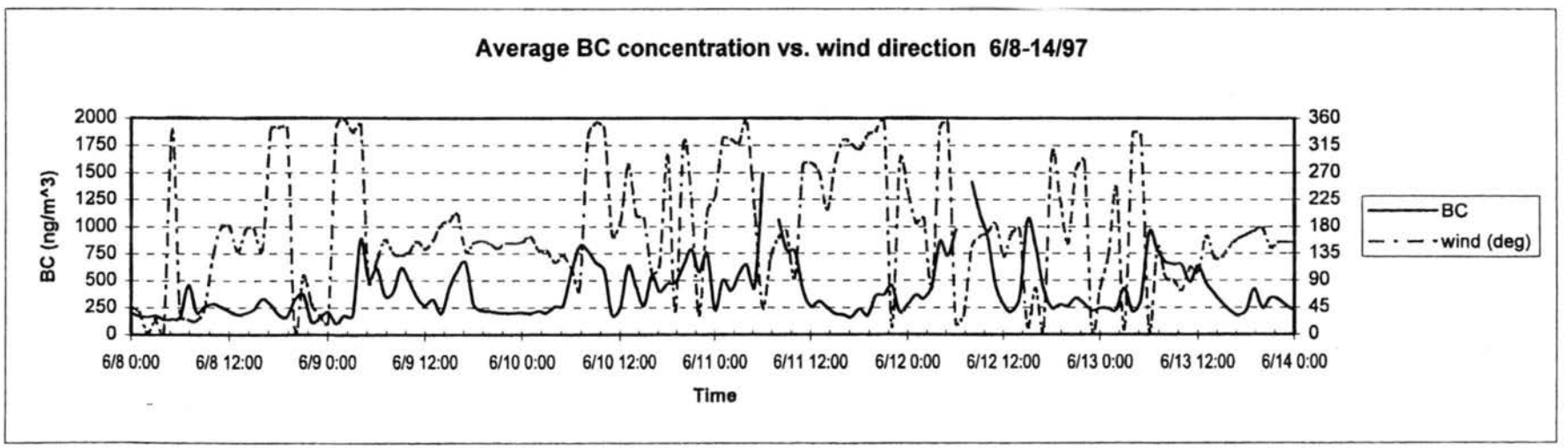

Figure D.3.1 Timeline of BC concentrations and wind direction.

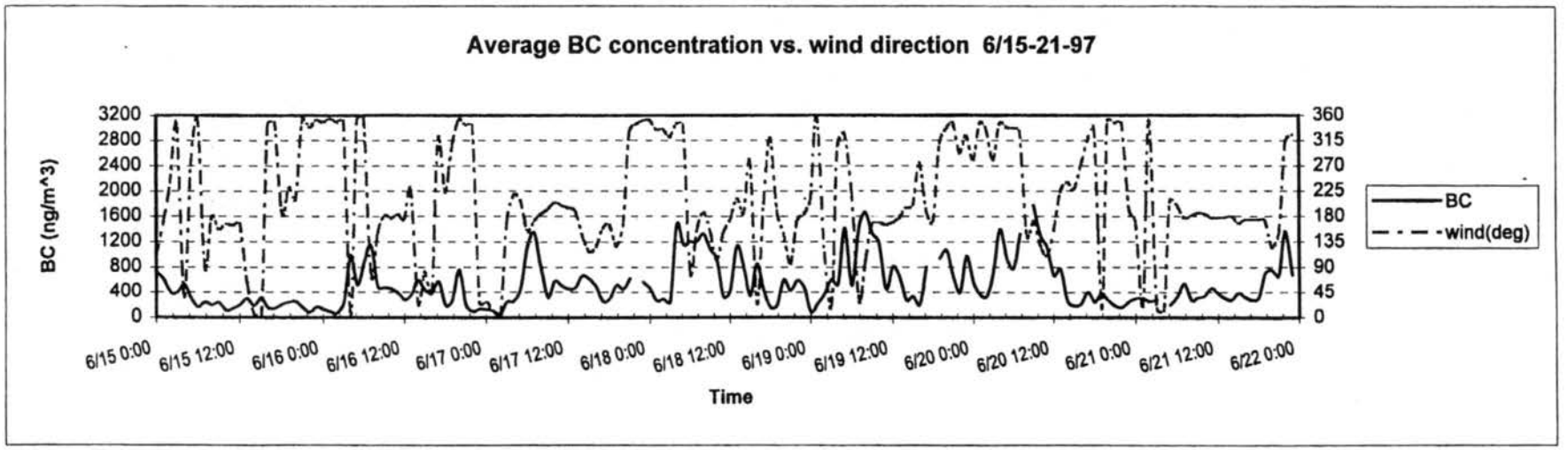

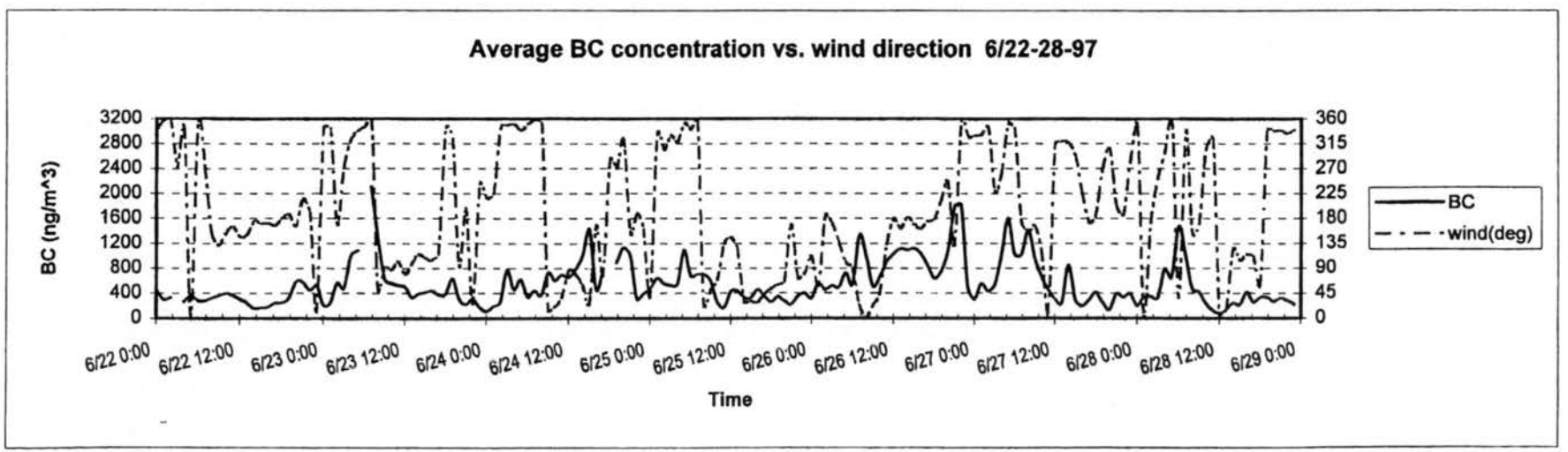

Figure D.3.2 Timeline of BC concentrations and wind direction.

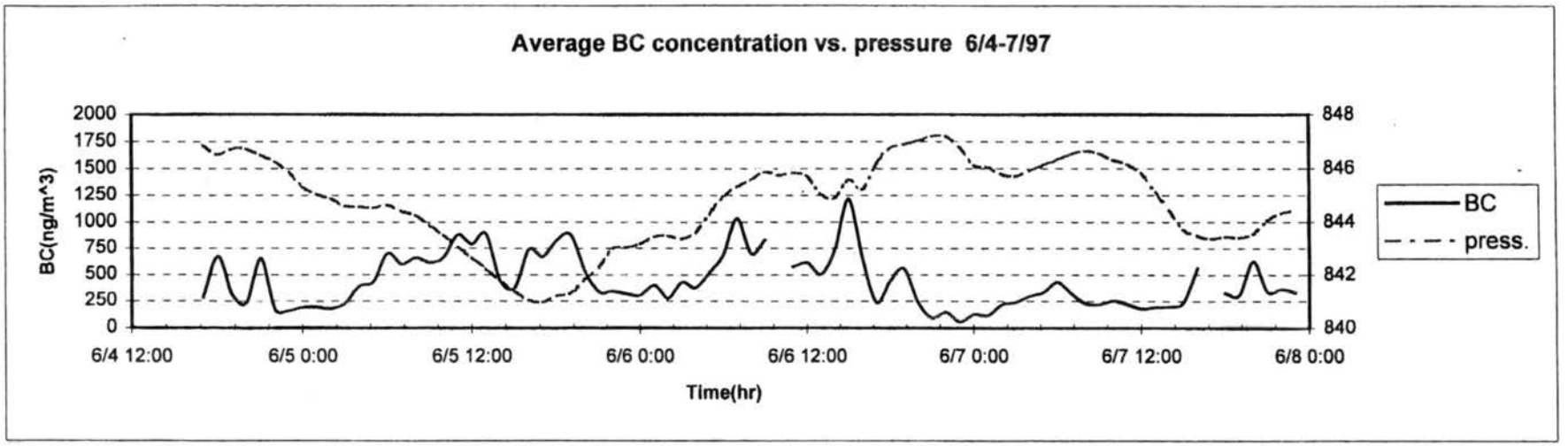

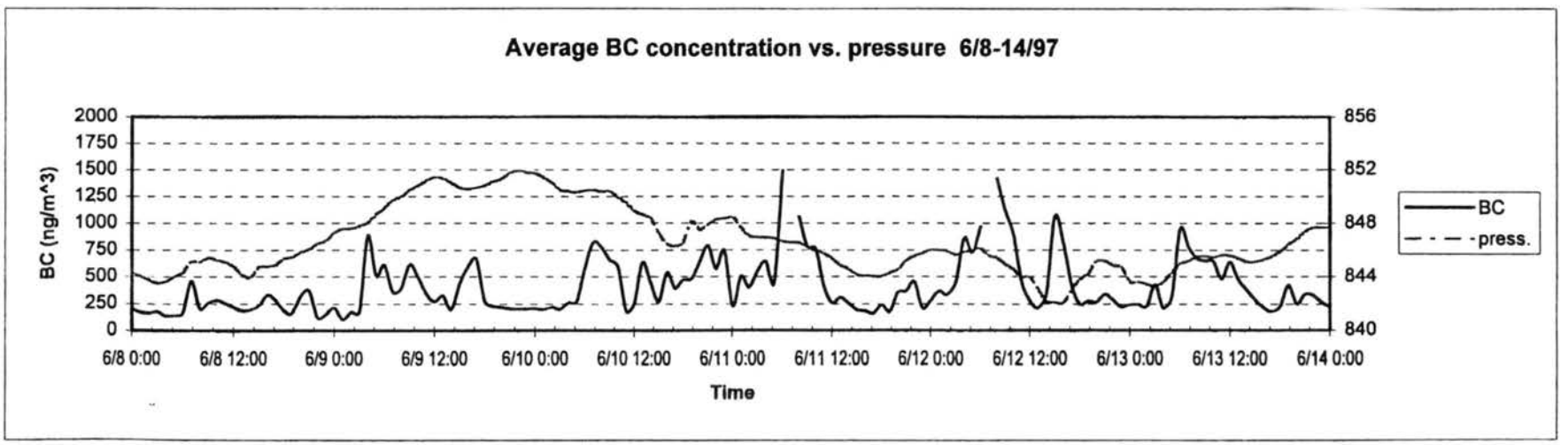

Figure D.3.3 Timeline of BC concentrations and pressure.

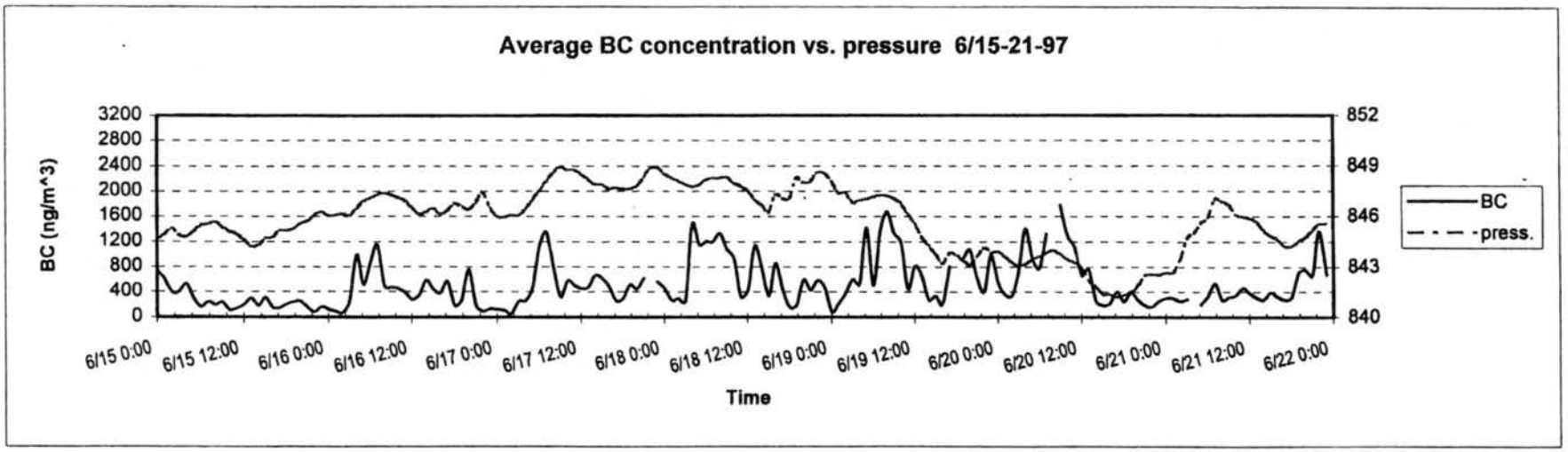

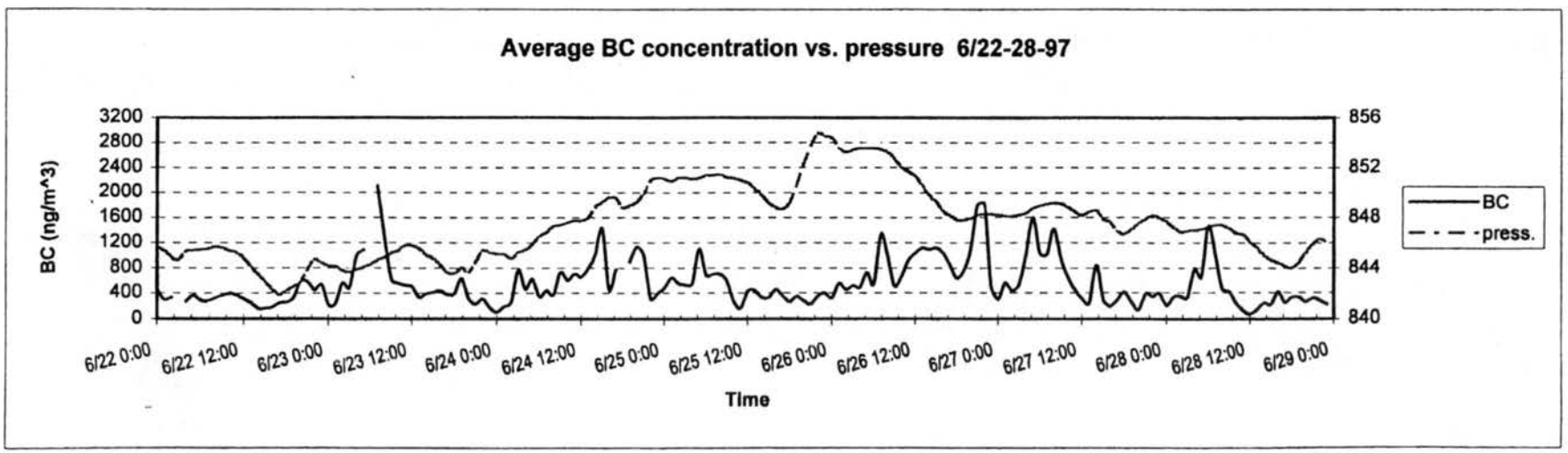

Figure D.3.4 Timeline of BC concentrations and pressure.

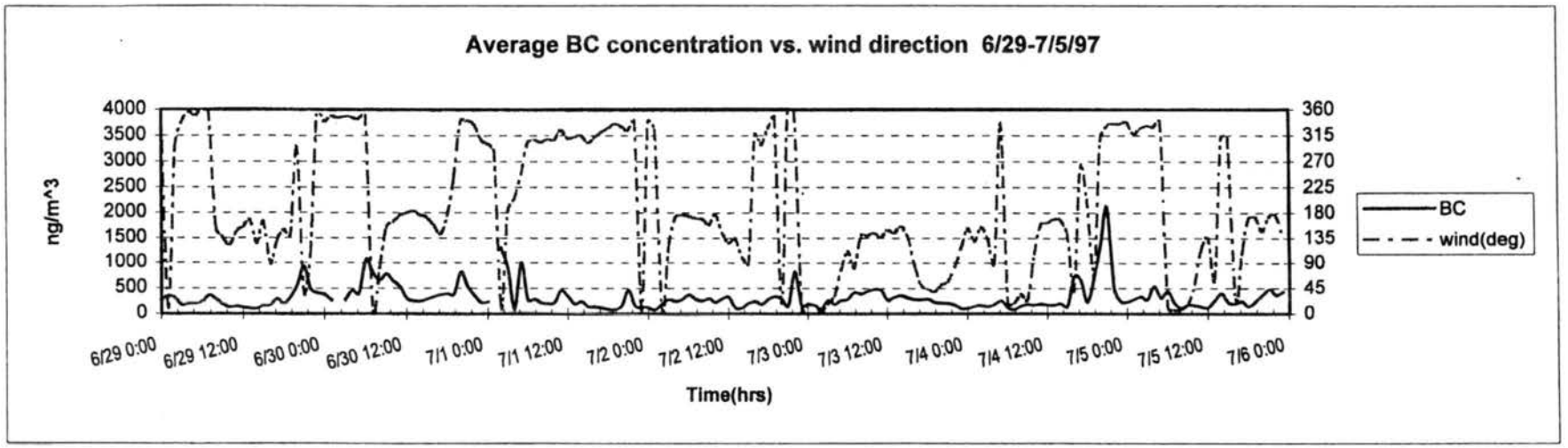

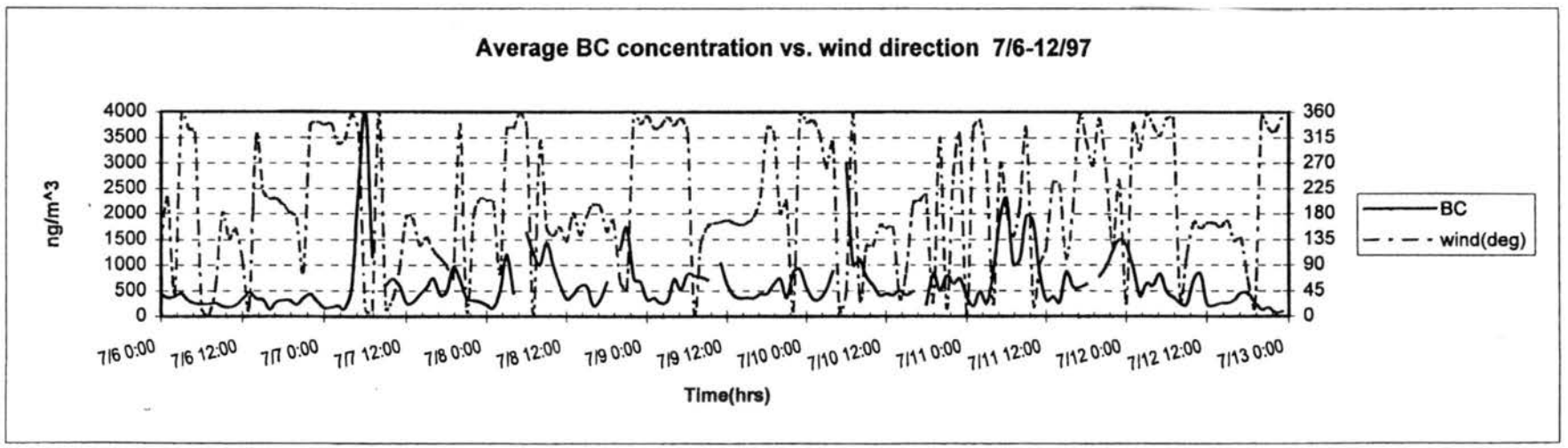

Figure D.3.5 Timeline of BC concentrations and wind direction.

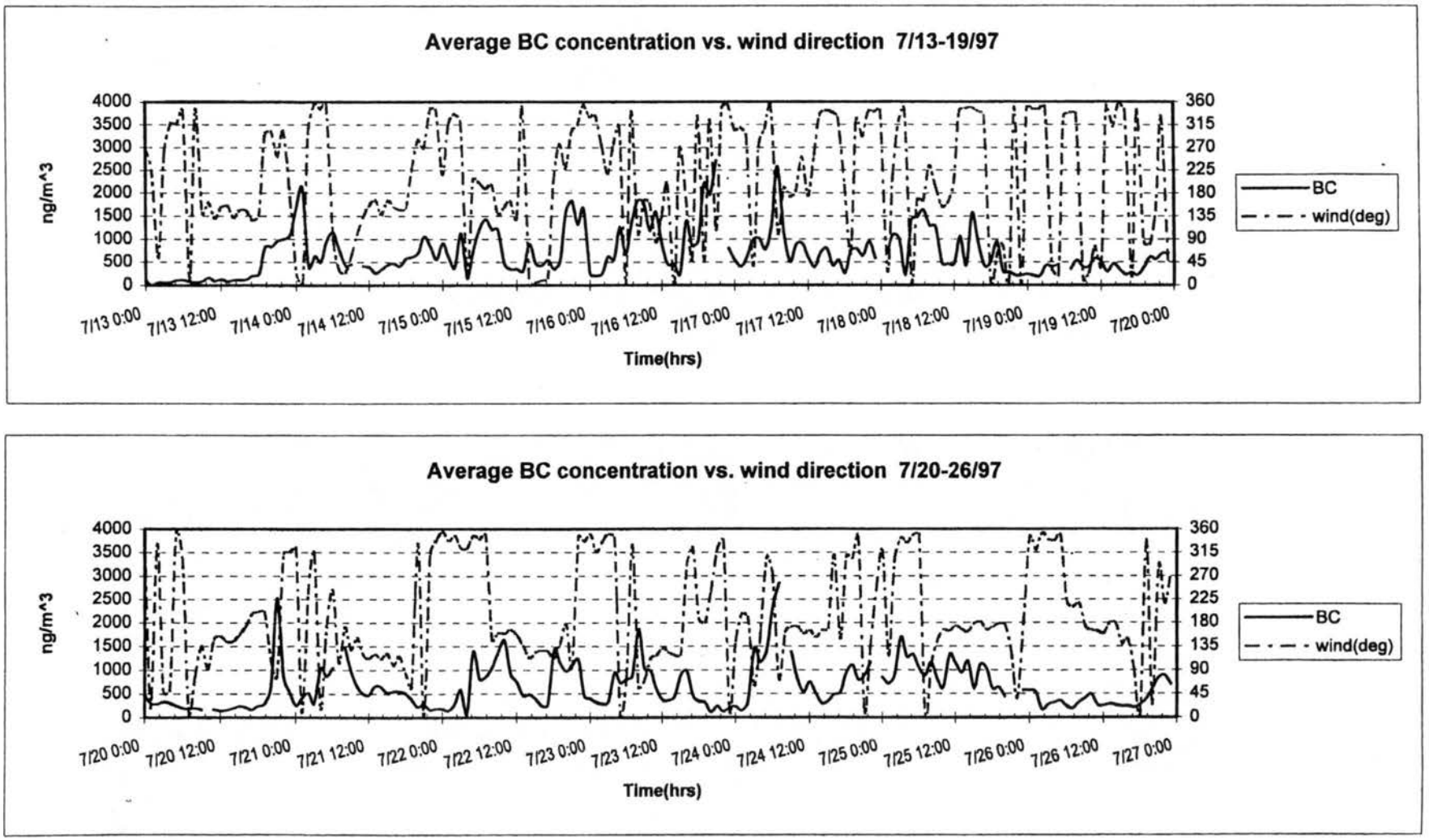

Figure D.3.6 Timeline of BC concentrations and wind direction.

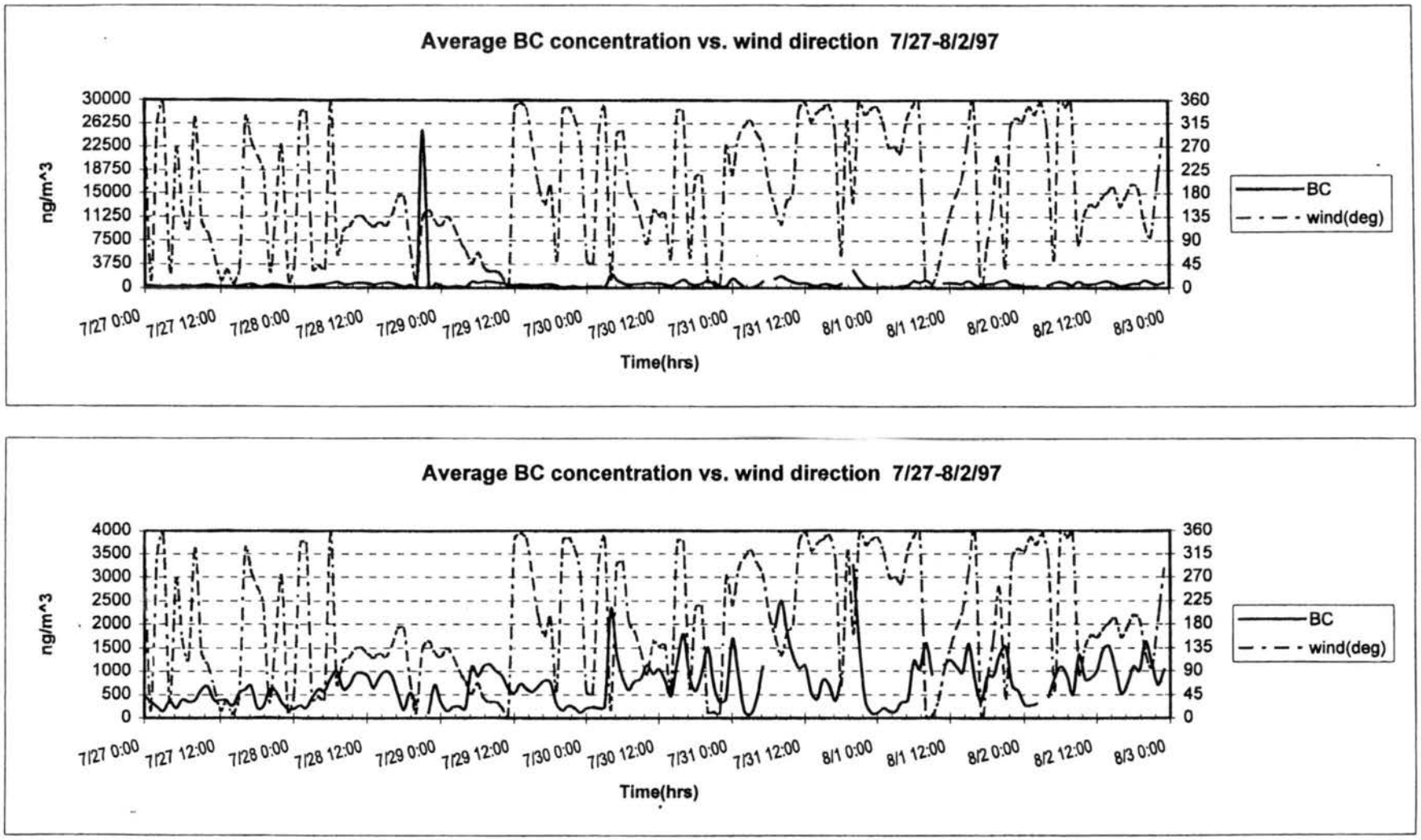

Figure D.3.7 Timeline of BC concentrations and wind direction.

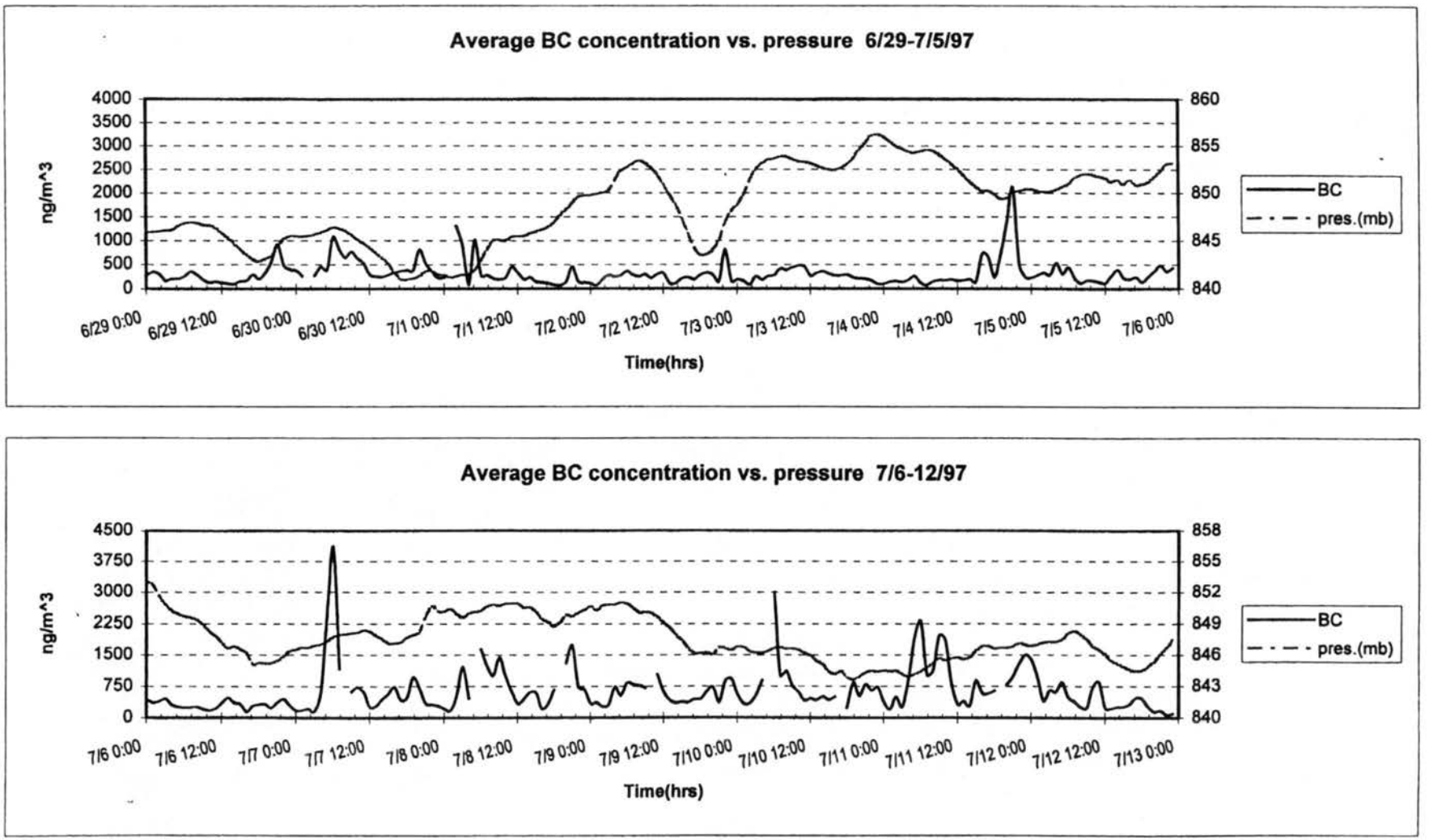

Figure D.3.8 Timeline of BC concentrations and pressure.

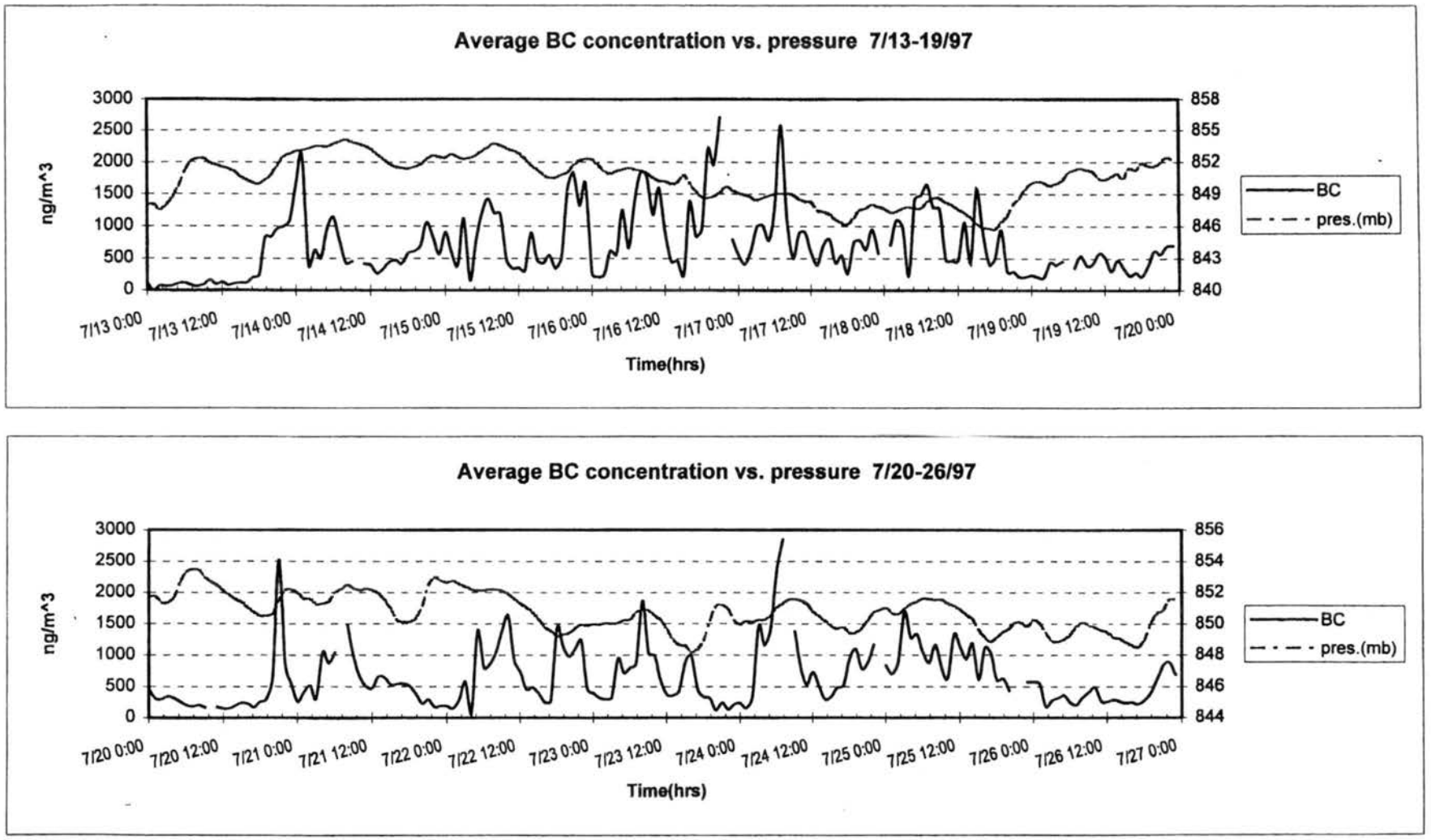

Figure D.3.9 Timeline of BC concentrations and pressure.

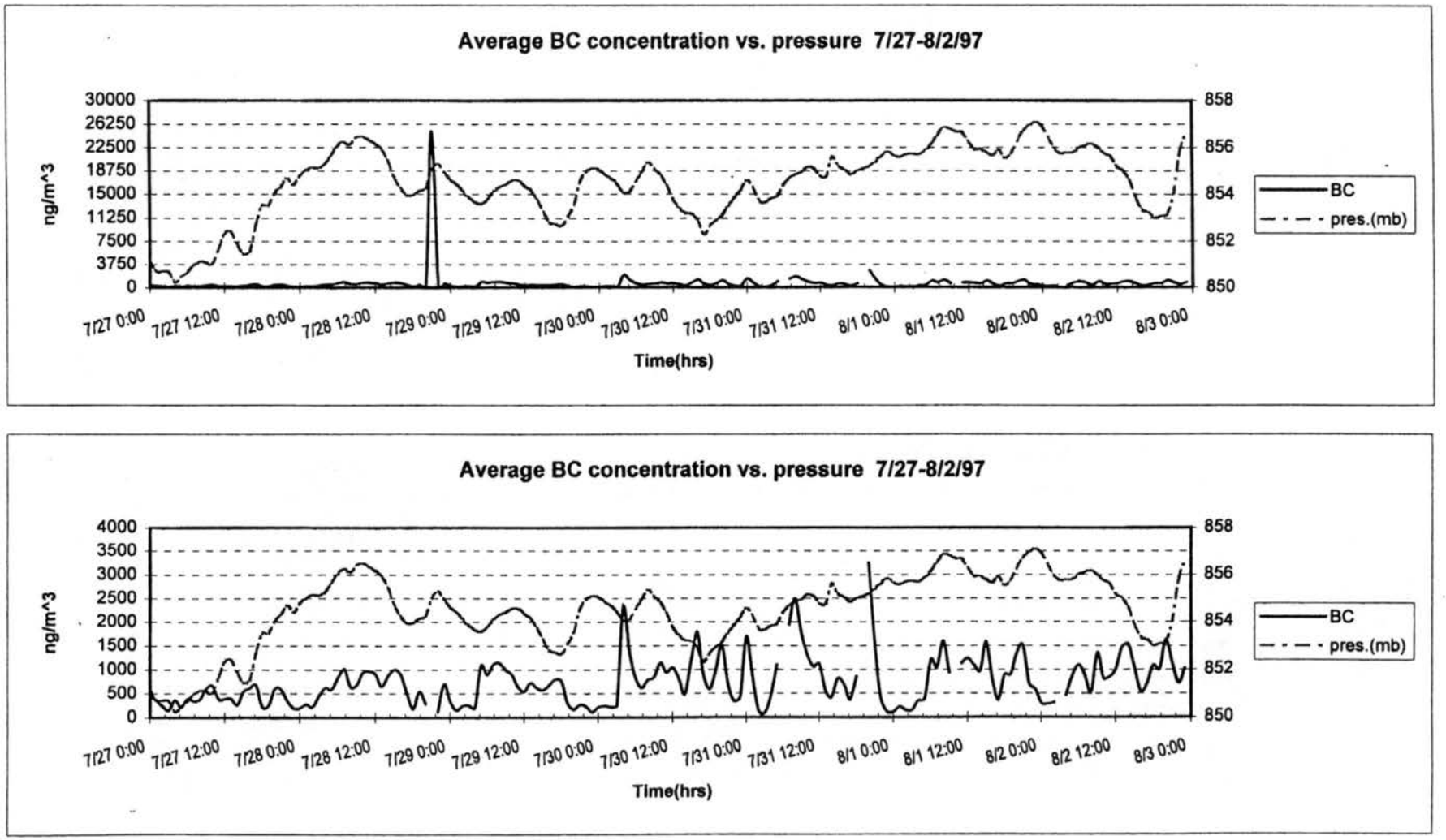

Figure D.3.10 Timeline of BC concentrations and pressure.

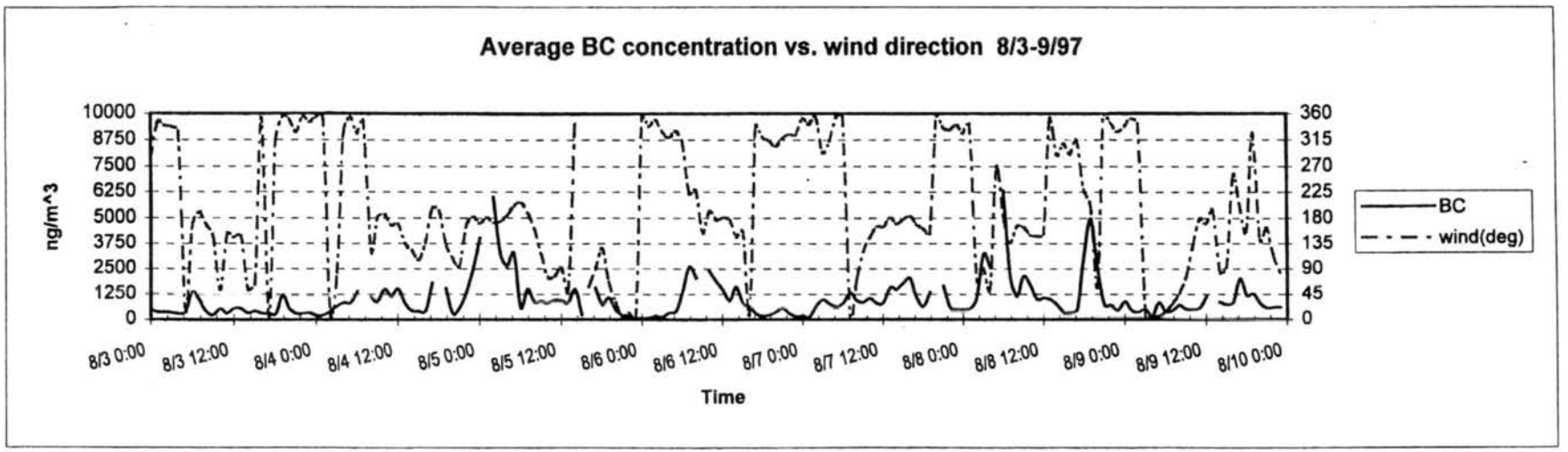

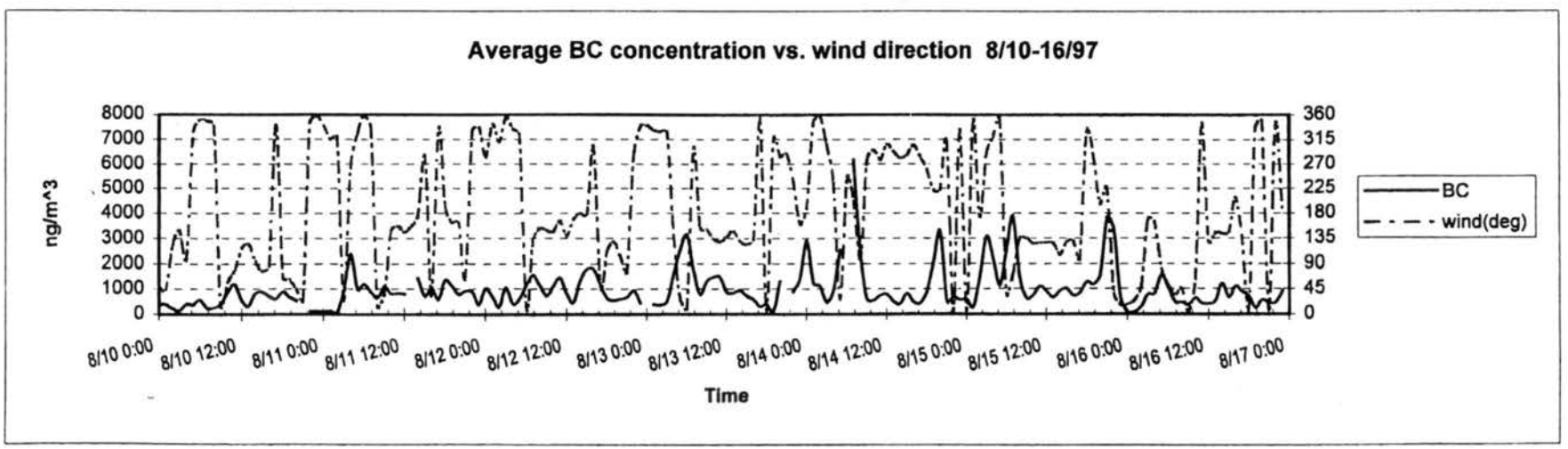

Figure D.3.11 Timeline of BC concentrations and wind direction.

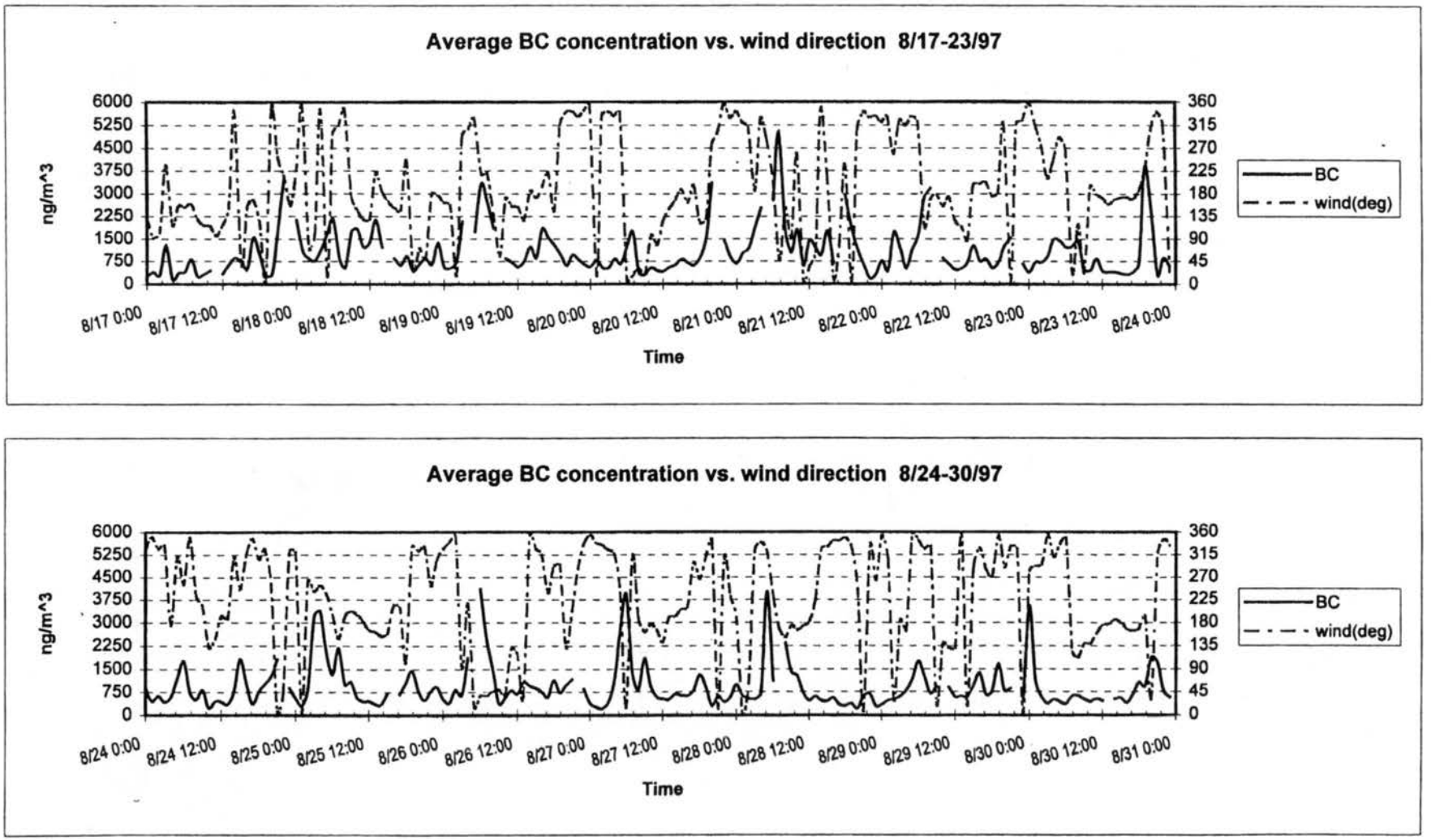

Figure D.3.12 Timeline of BC concentrations and wind direction.

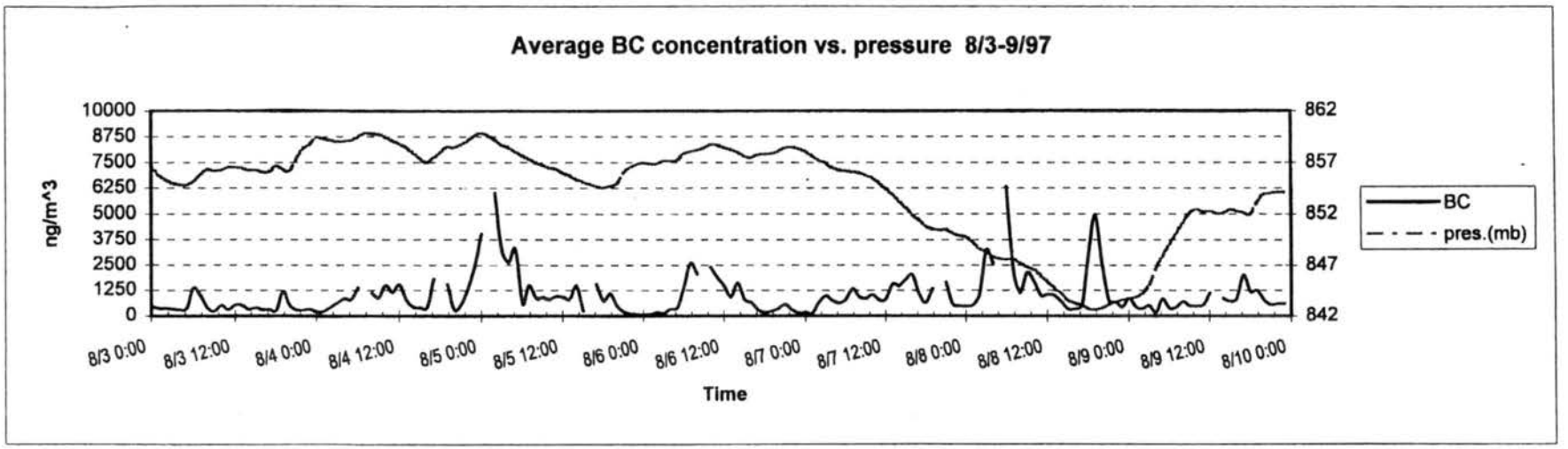

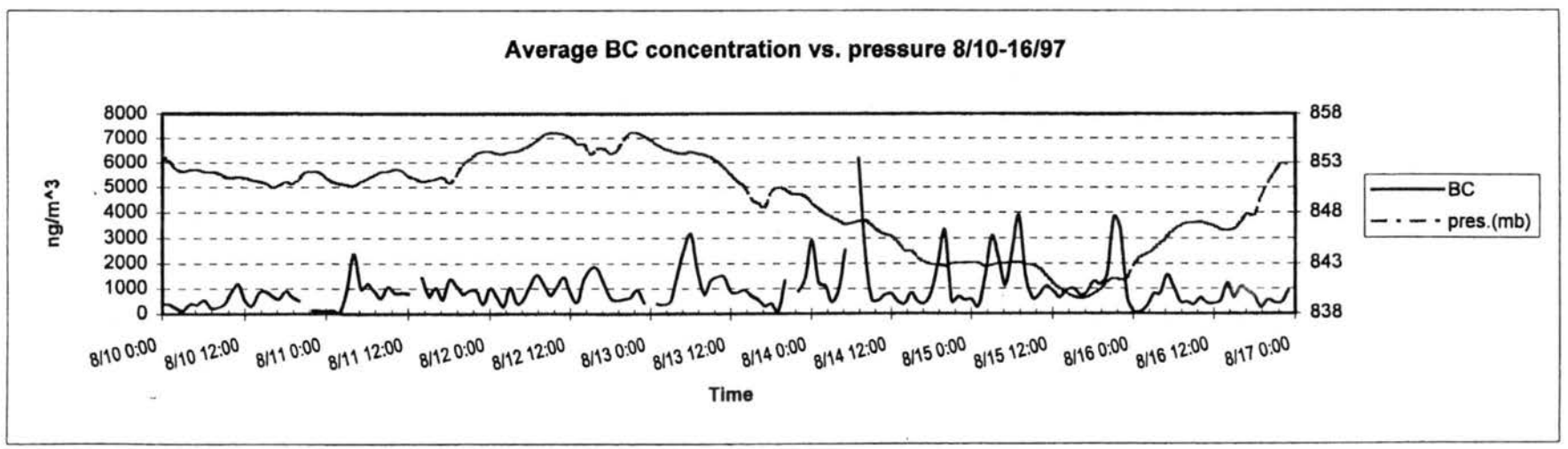

Figure D.3.13 Timeline of BC concentrations and pressure.

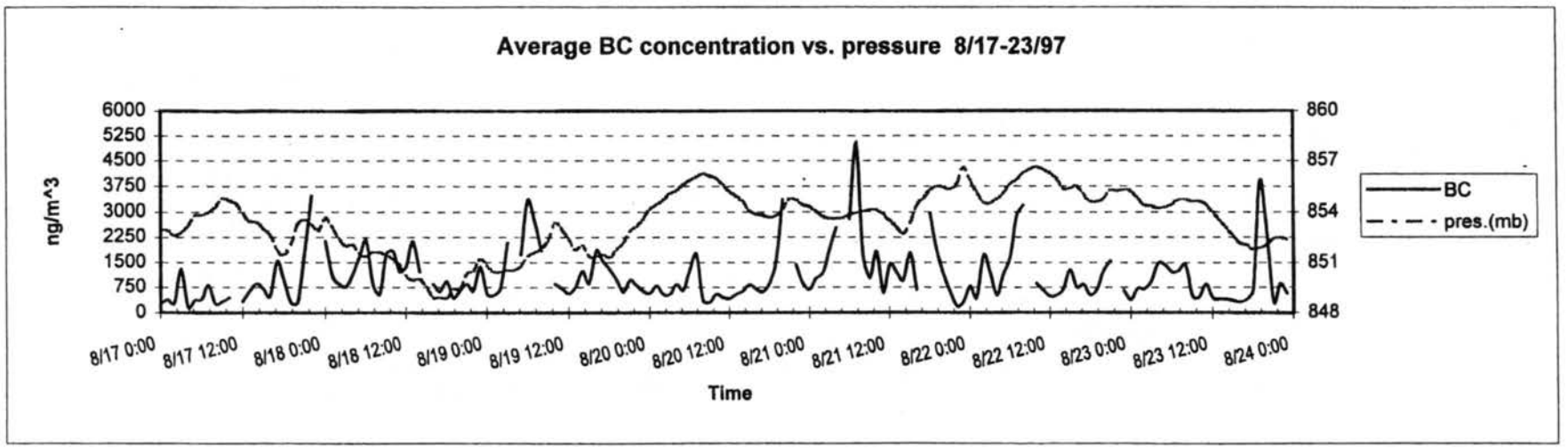

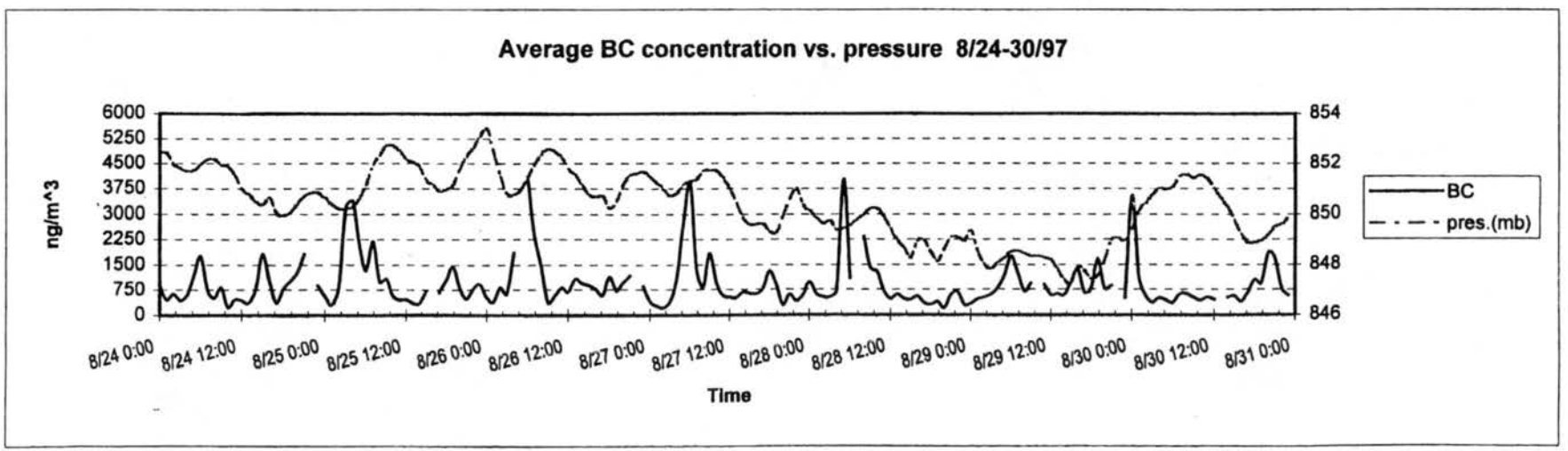

Figure D.3.14 Timeline of BC concentrations and pressure.

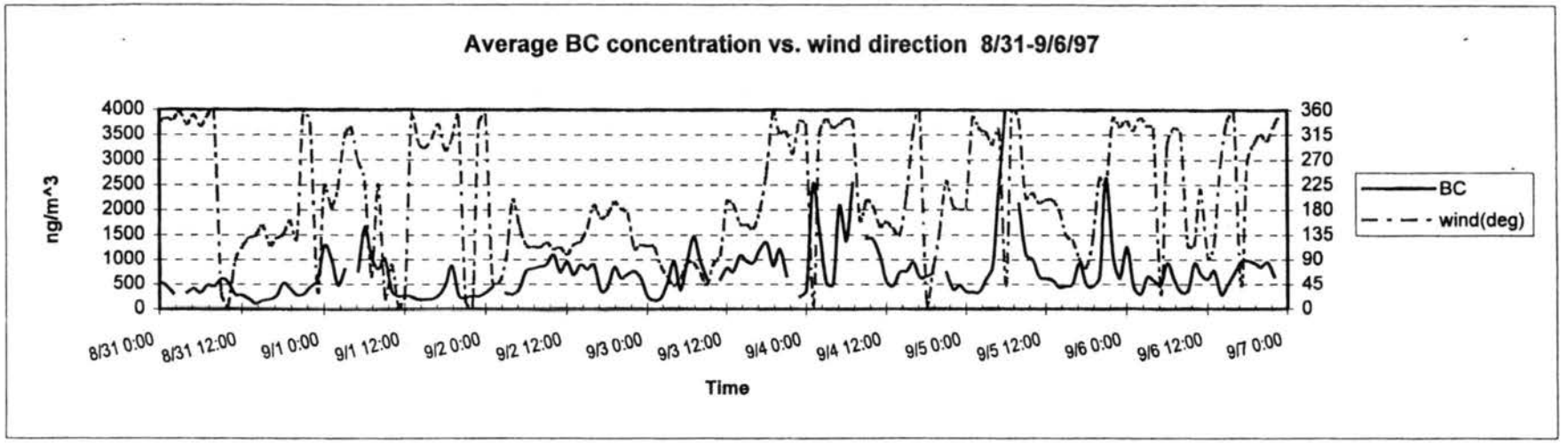

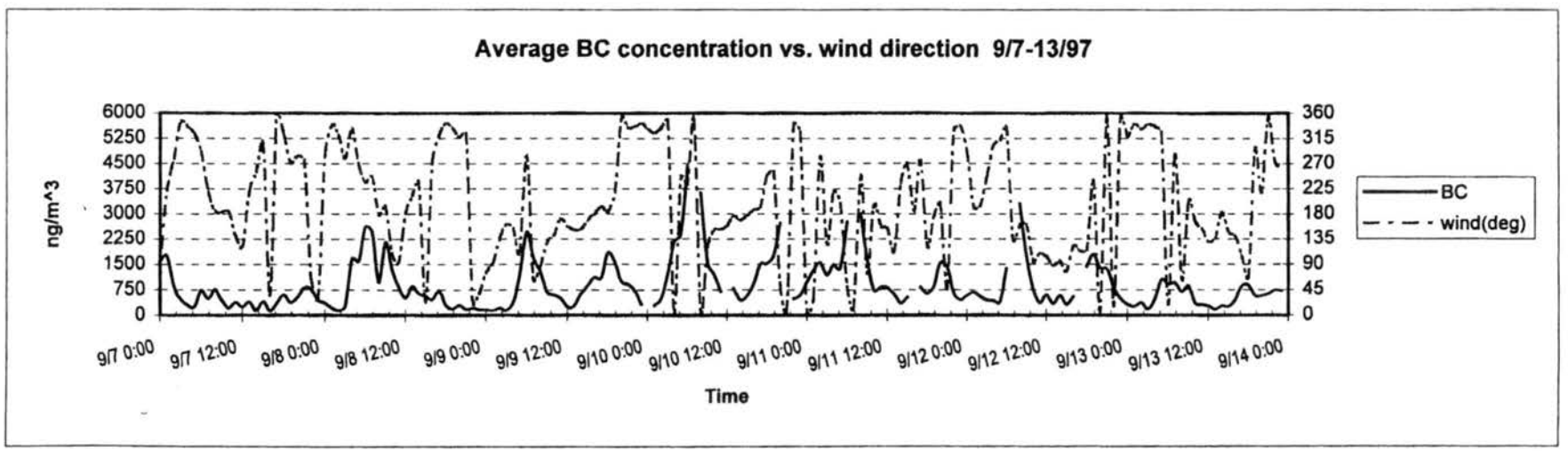

Figure D.3.15 Timeline of BC concentrations and wind direction.

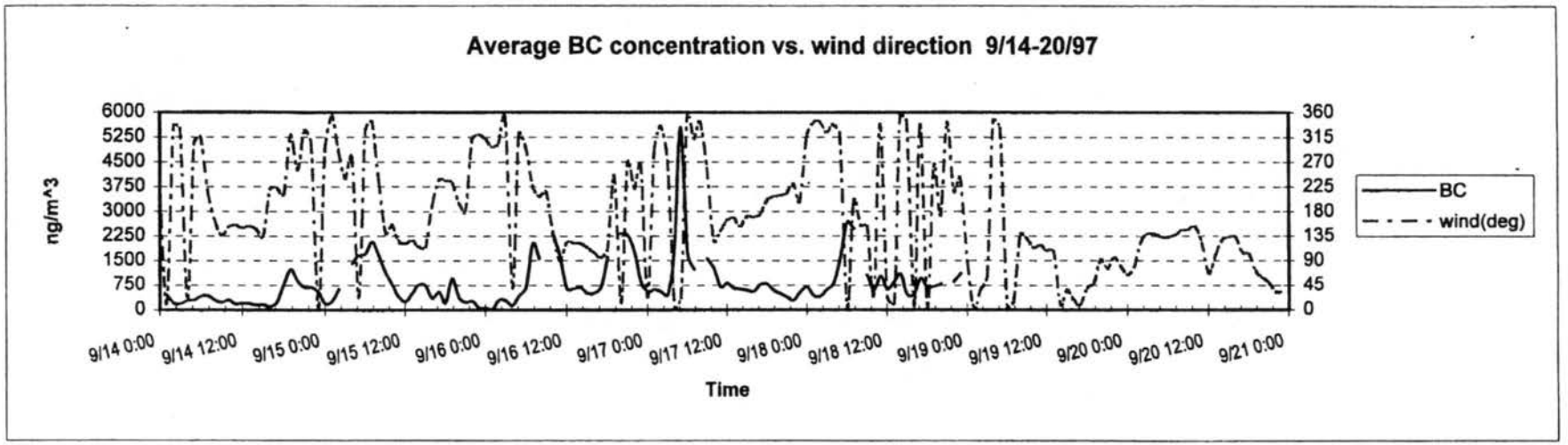

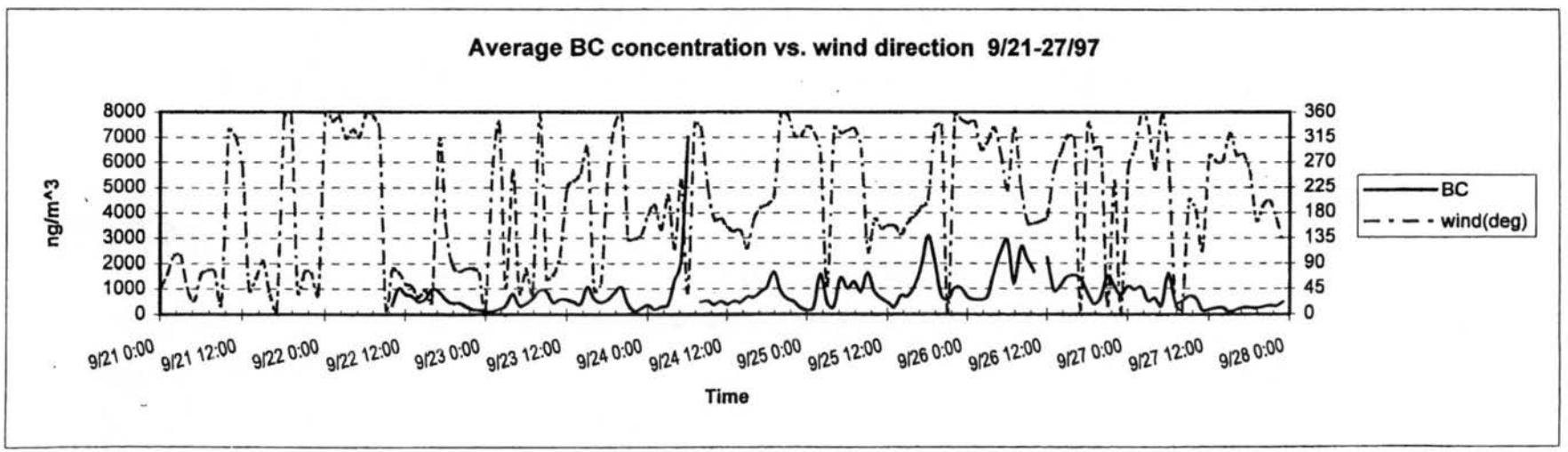

Figure D.3.16 Timeline of BC concentrations and wind direction.

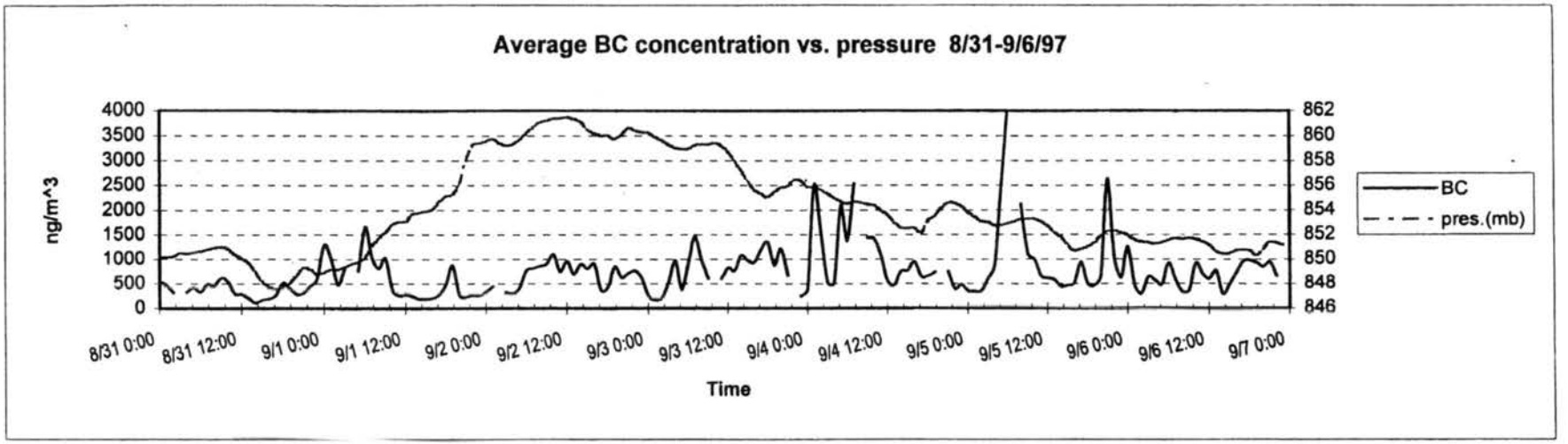

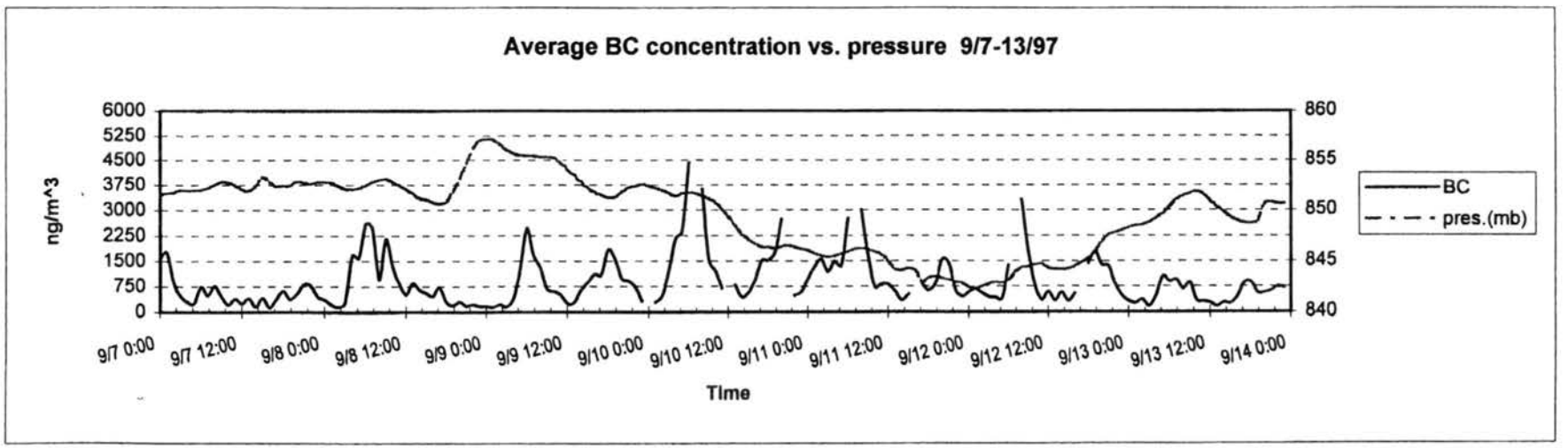

Figure D.3.17 Timeline of BC concentrations and pressure.

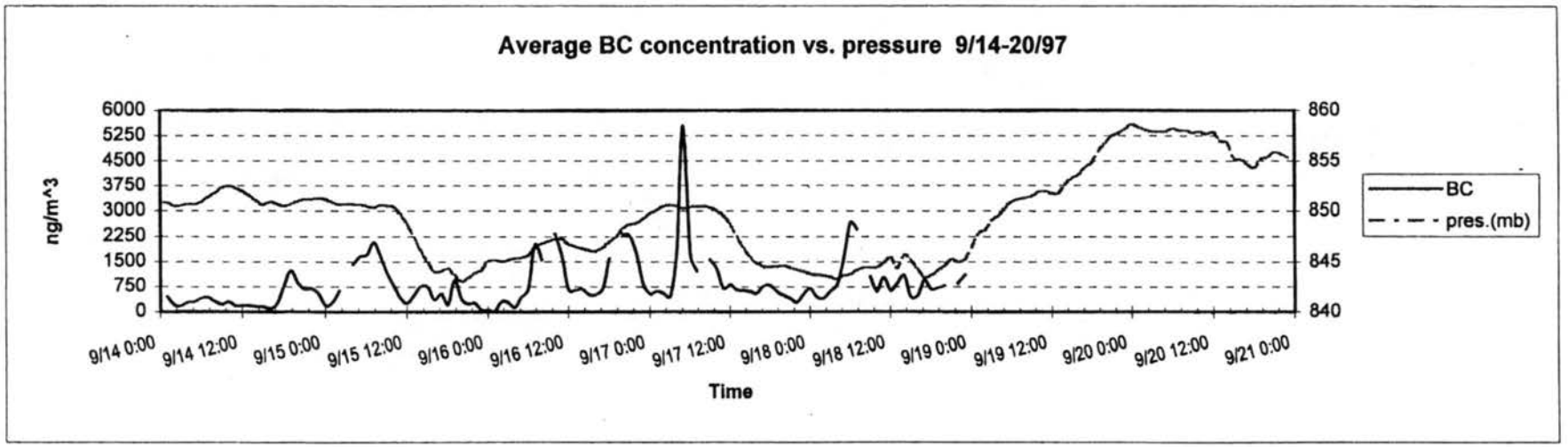

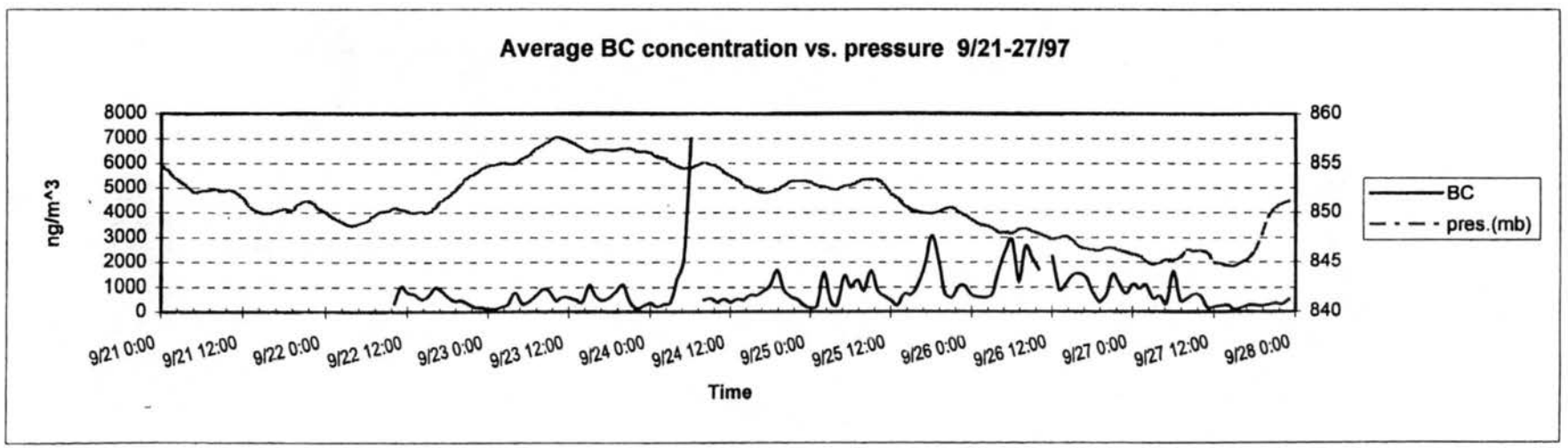

Figure D.3.18 Timeline of BC concentrations and pressure.

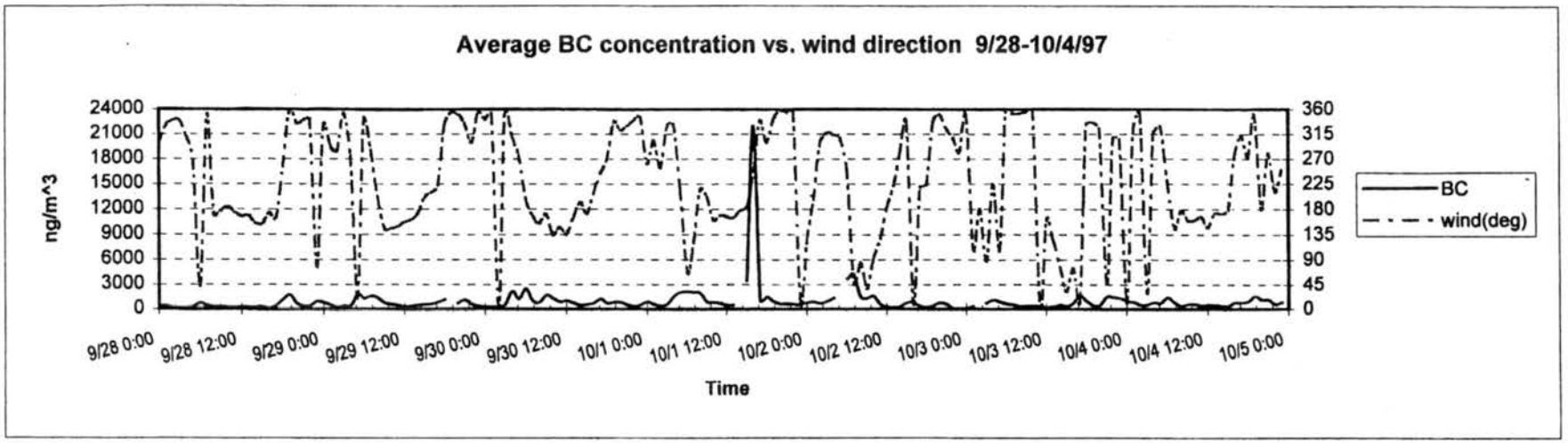

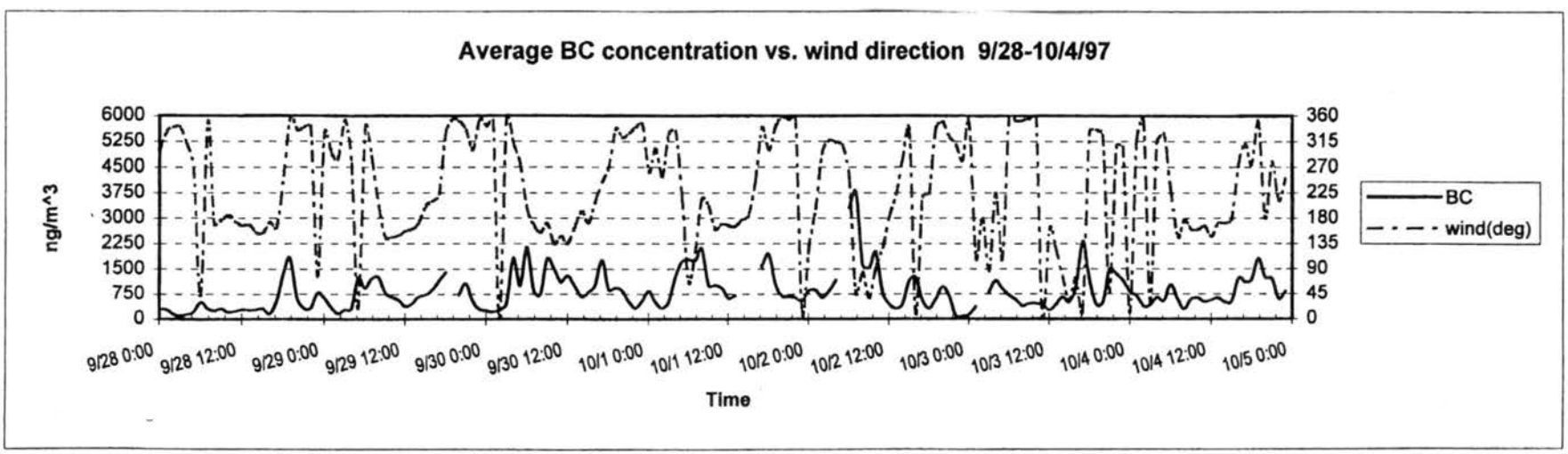

Figure D.3.19 Timeline of BC concentrations and wind direction.

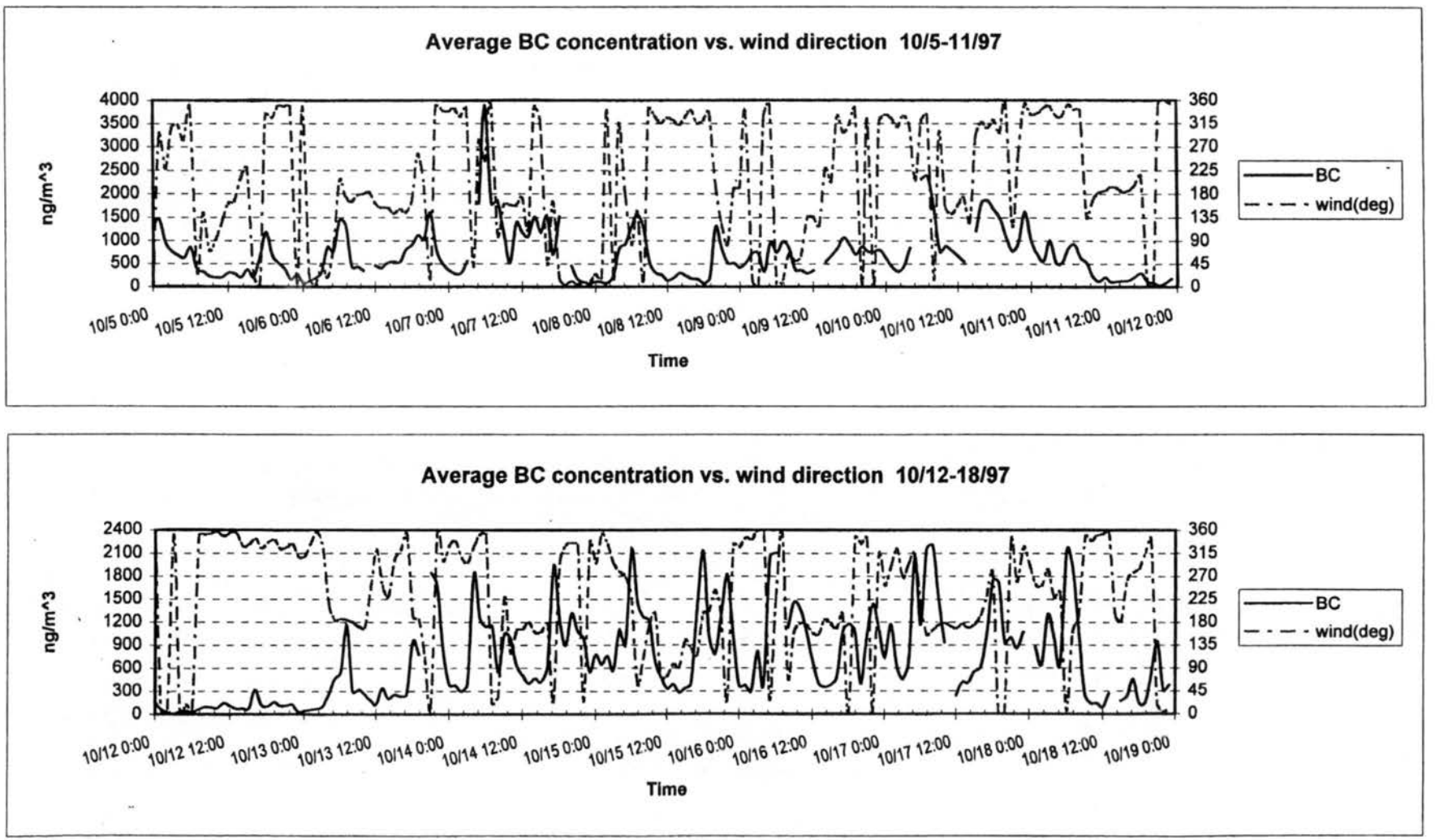

Figure D.3.20 Timeline of BC concentrations and wind direction.

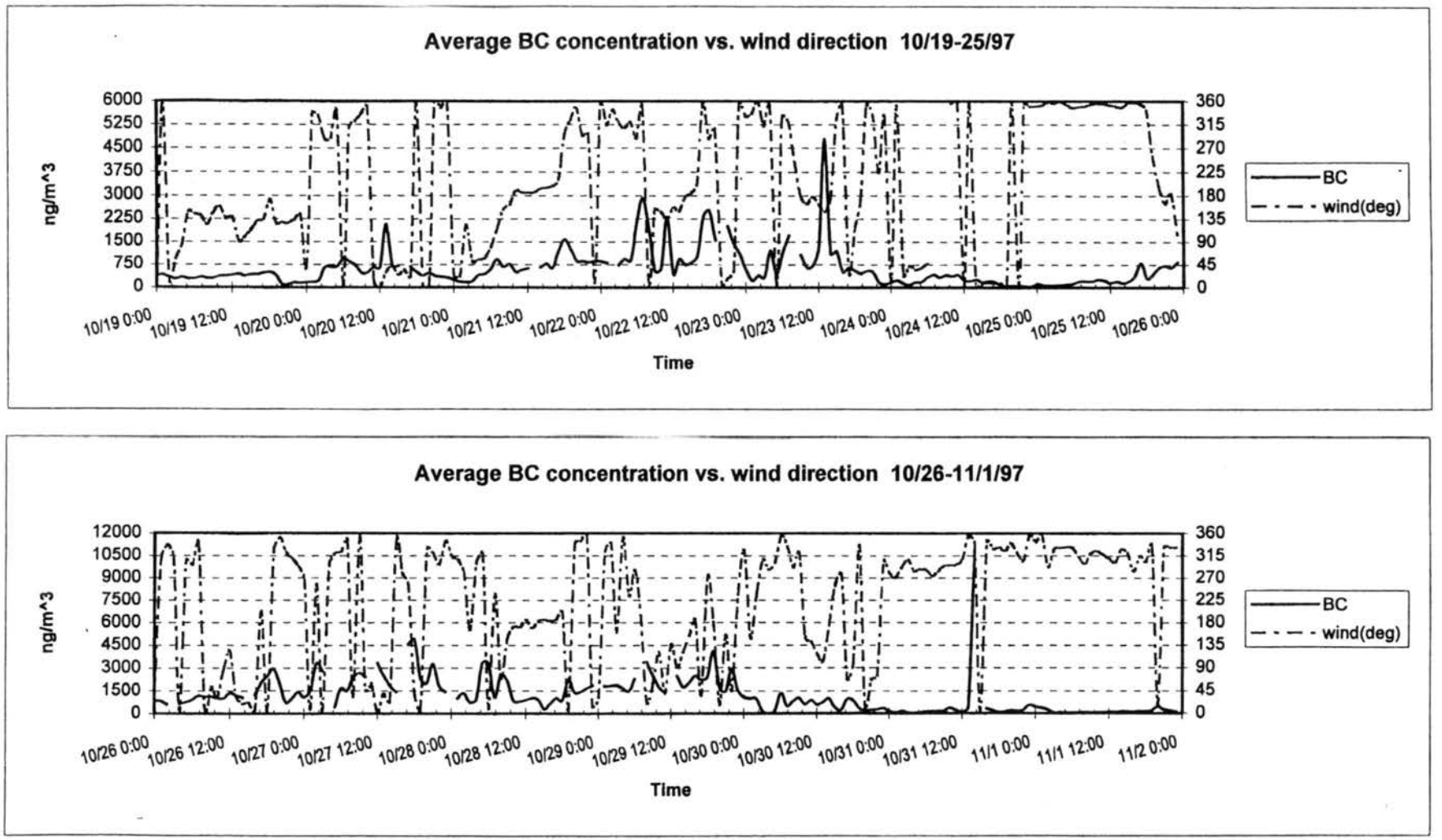

Figure D.3.21 Timeline of BC concentrations and wind direction.

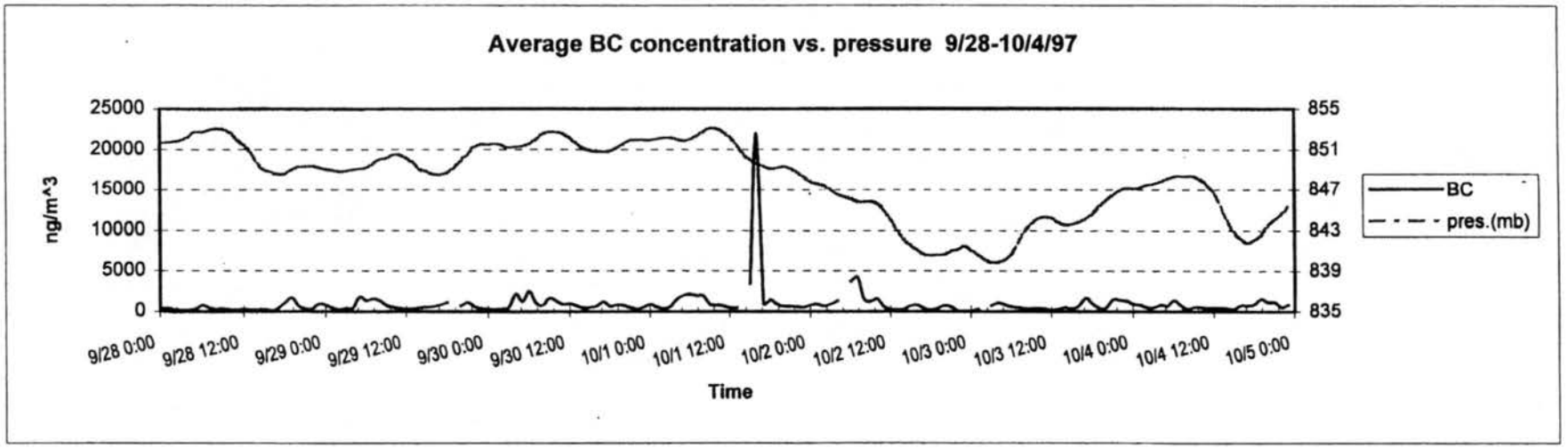

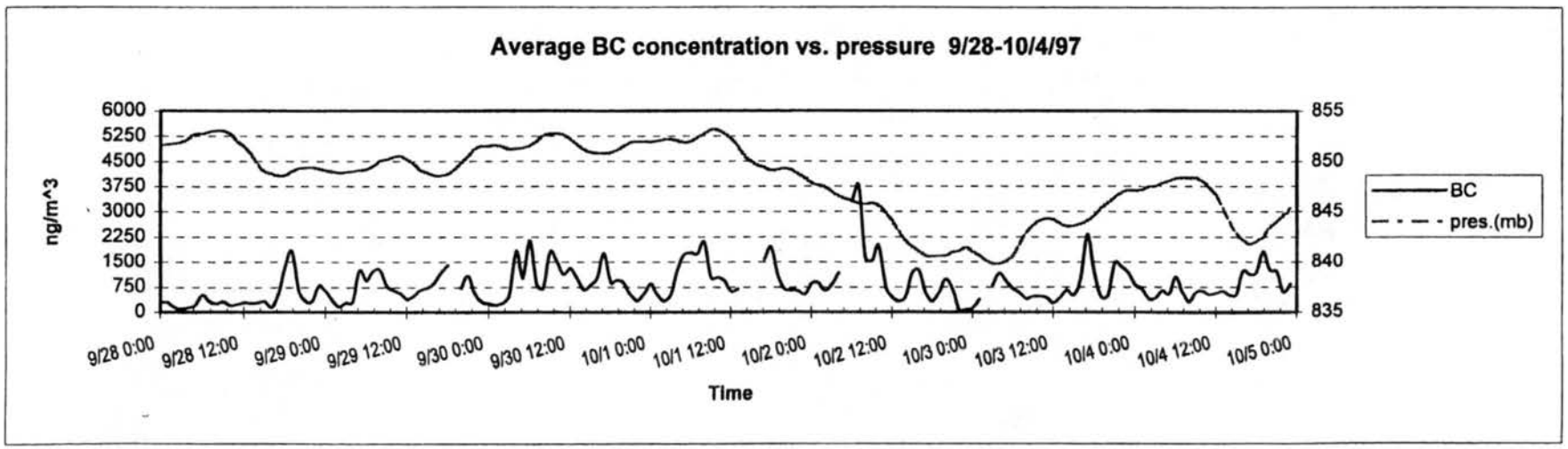

Figure D.3.22 Timeline of BC concentrations and pressure.

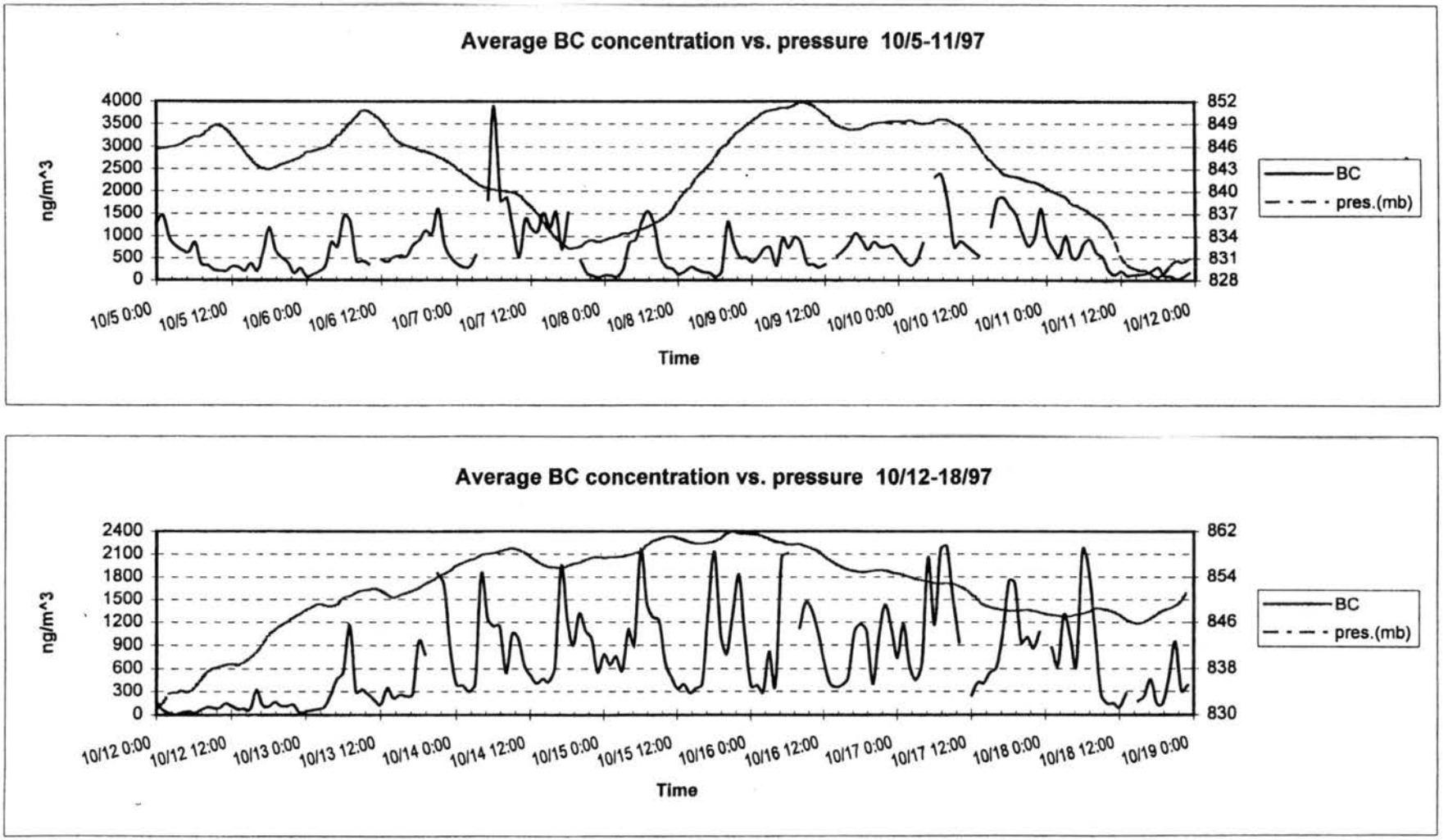

Figure D.3.23 Timeline of BC concentrations and pressure.

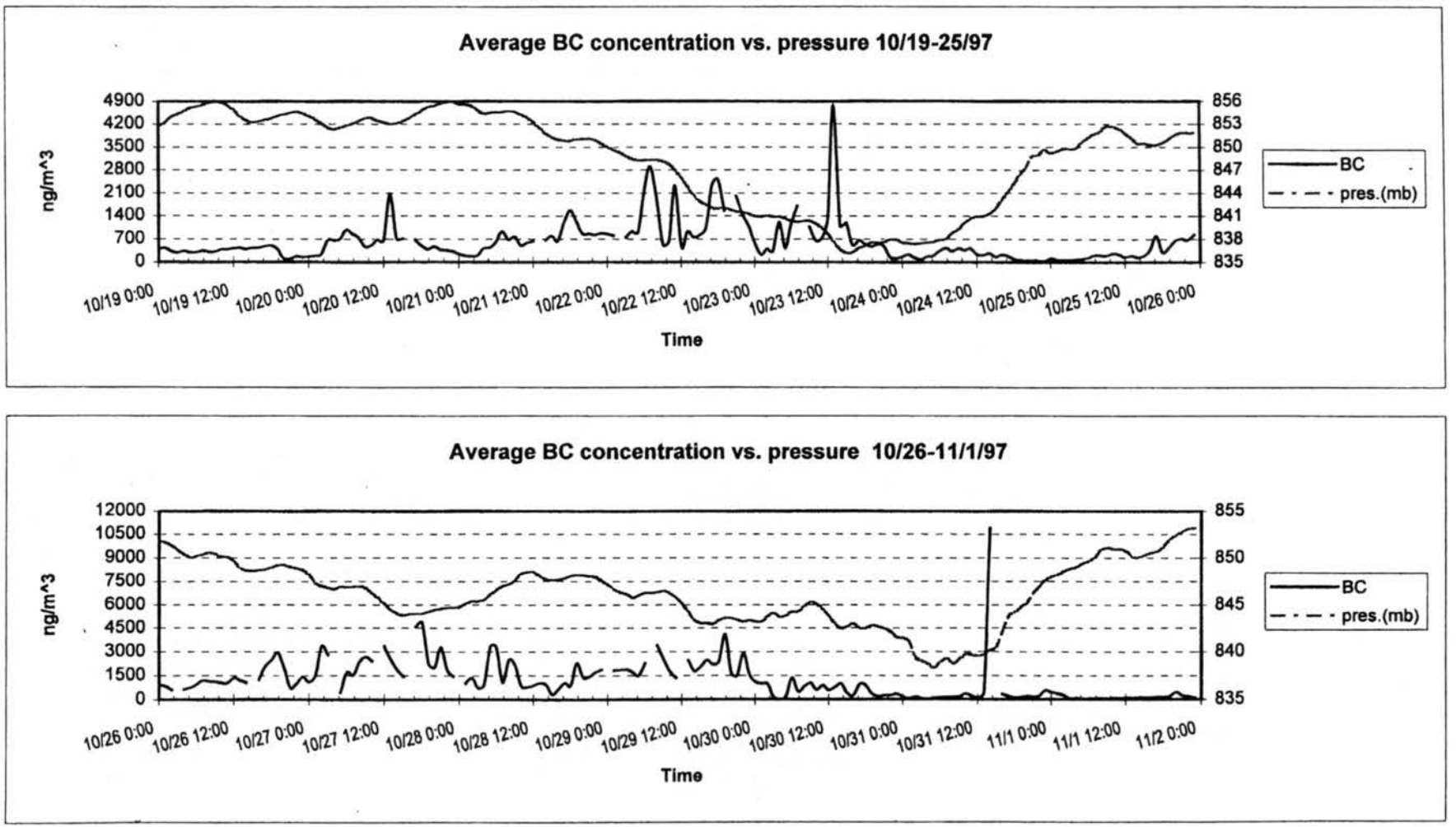

Figure D.3.24 Timeline of BC concentrations and pressure.

APPENDIX E

BC and CO concentrations

Figure E.1 – Figure E.12 show the weekly timelines of BC and CO concentrations for June – October, 1997. The timelines show the two variables track each other reasonably well. BC concentrations are plotted in ng/m^3 (left axis) and CO concentrations are shown in ppm * 10 (right axis).

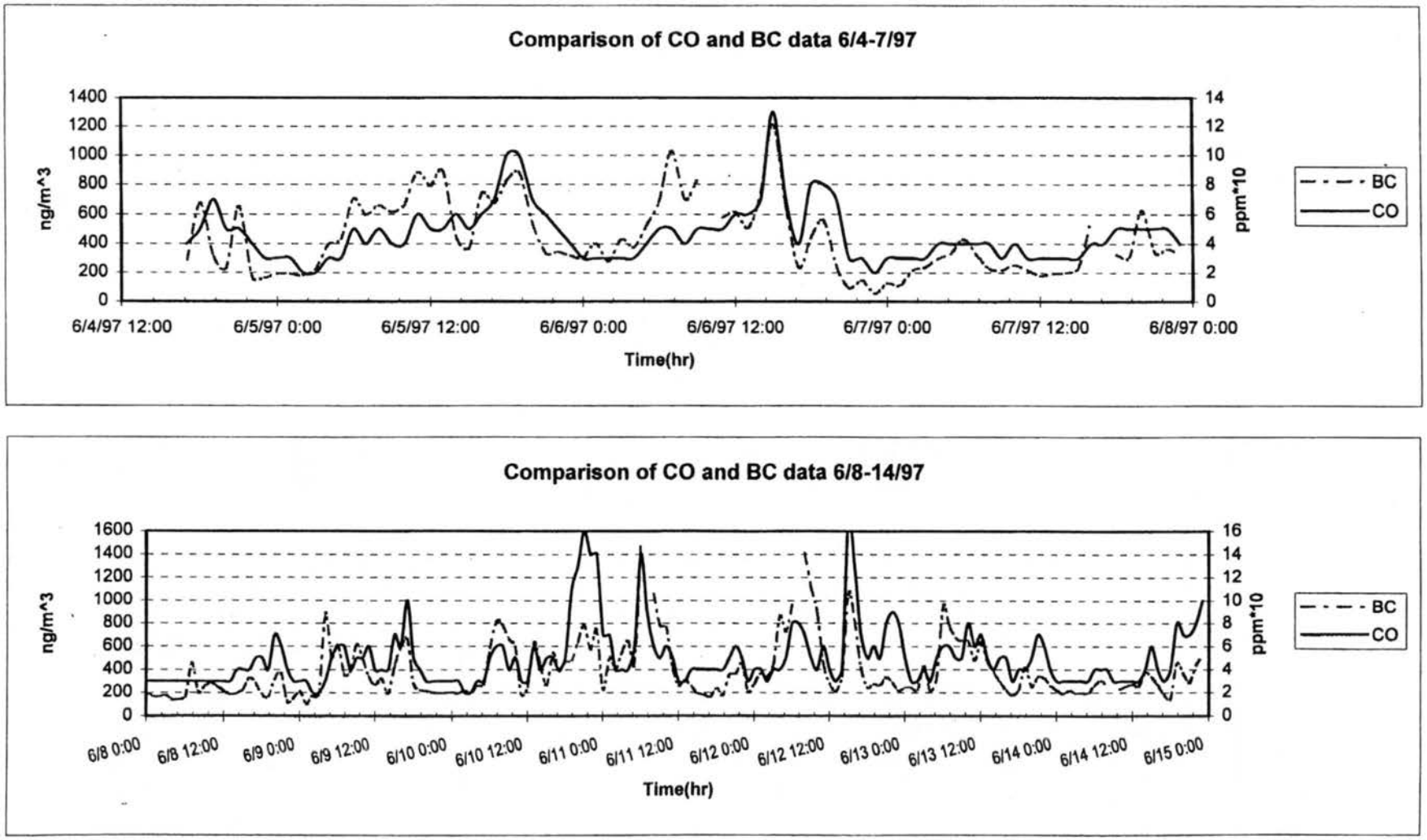

Figure E.1 BC and CO concentration time-lines.

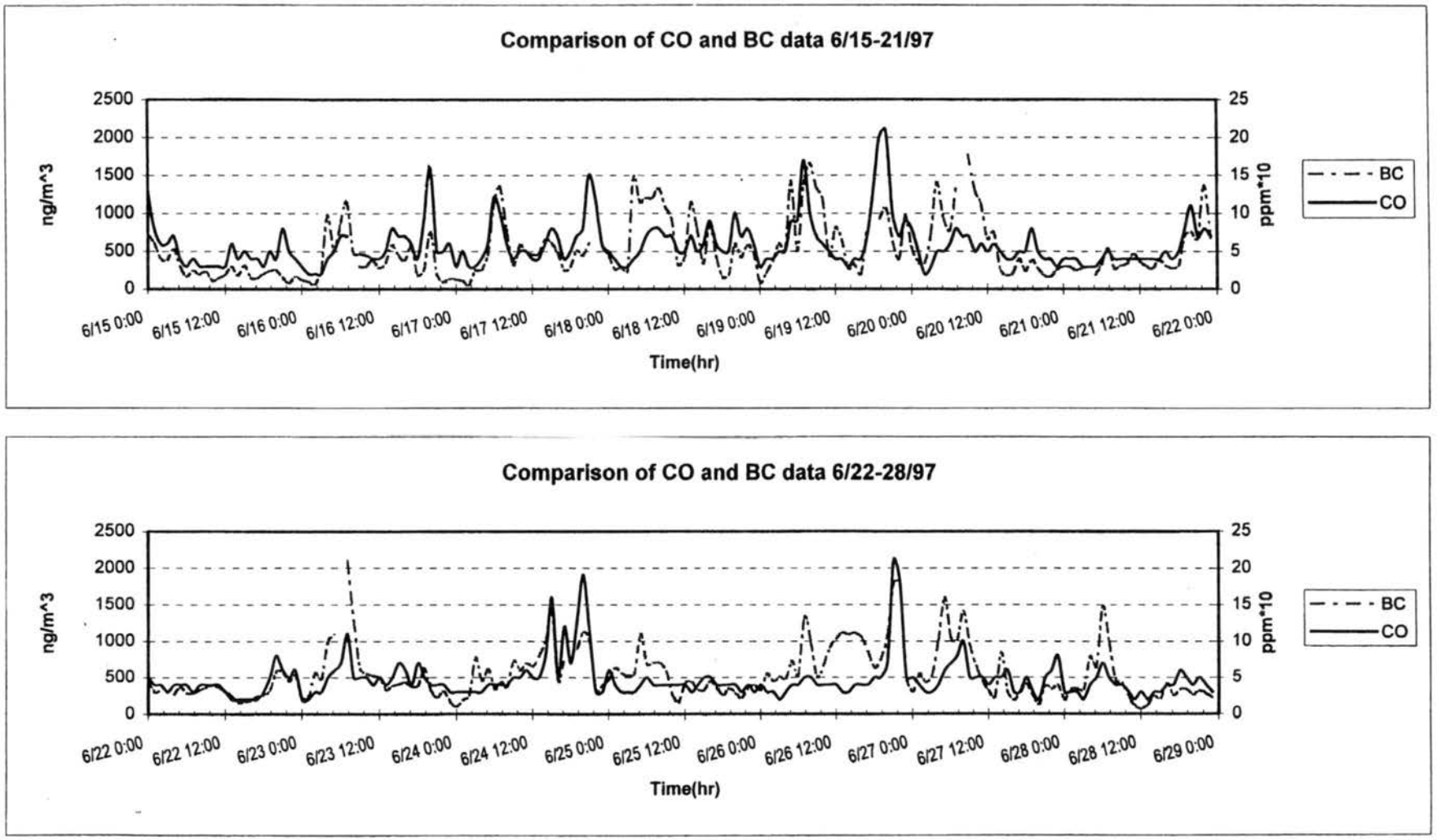

Figure E.2 BC and CO concentration time-lines.

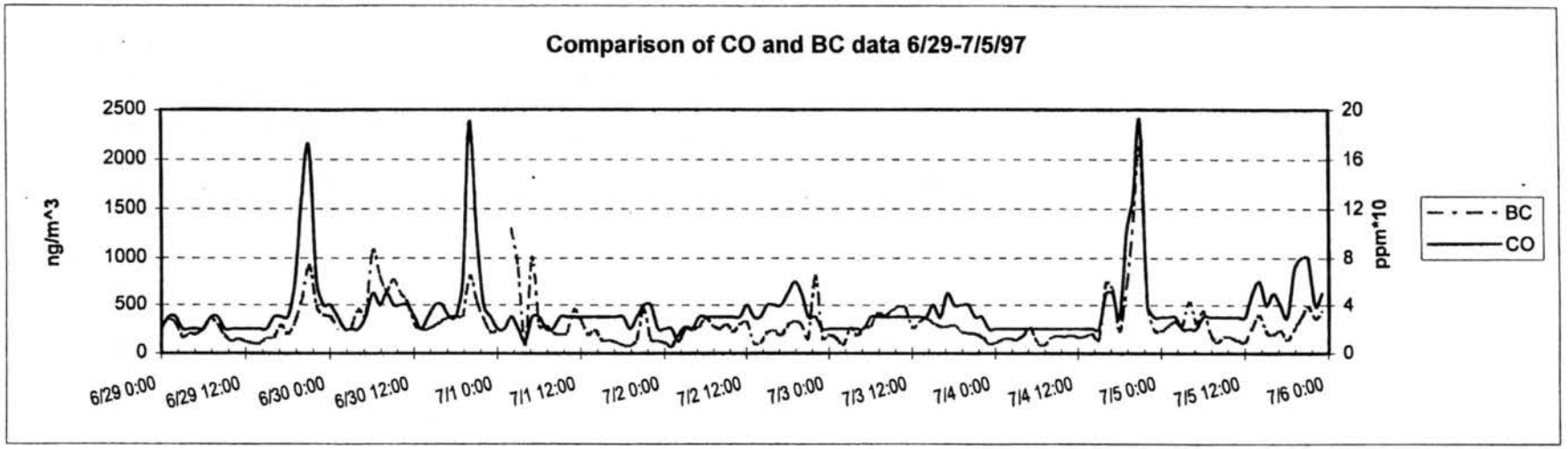

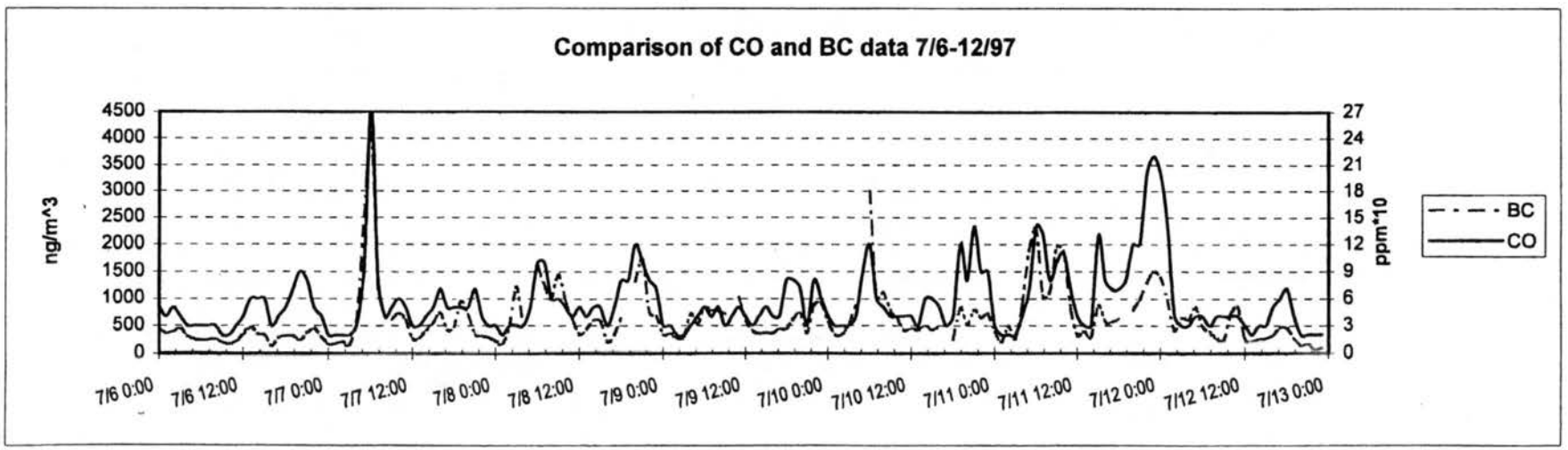

Figure E.3 BC and CO concentration time-lines.

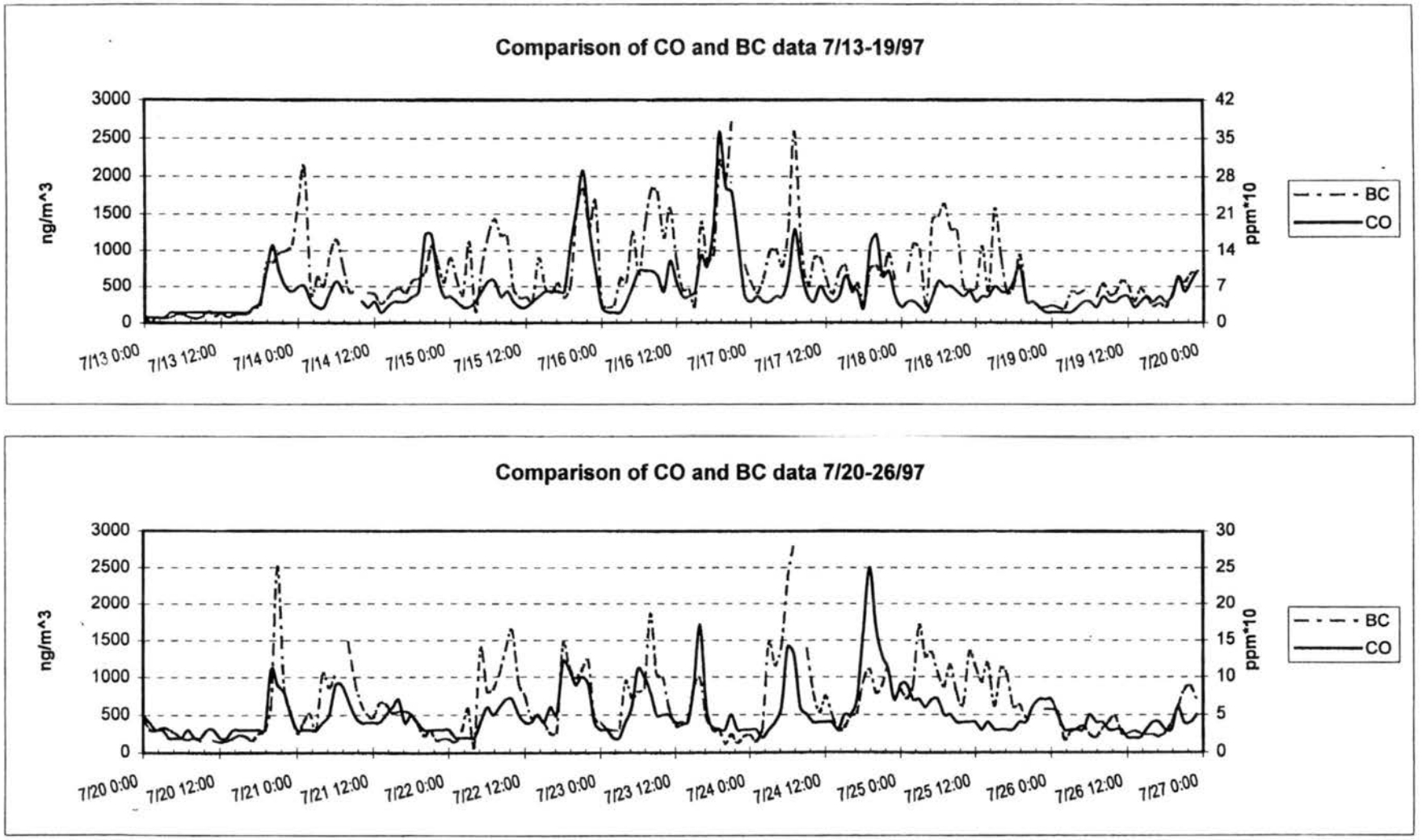

Figure E.4 BC and CO concentration time-lines.

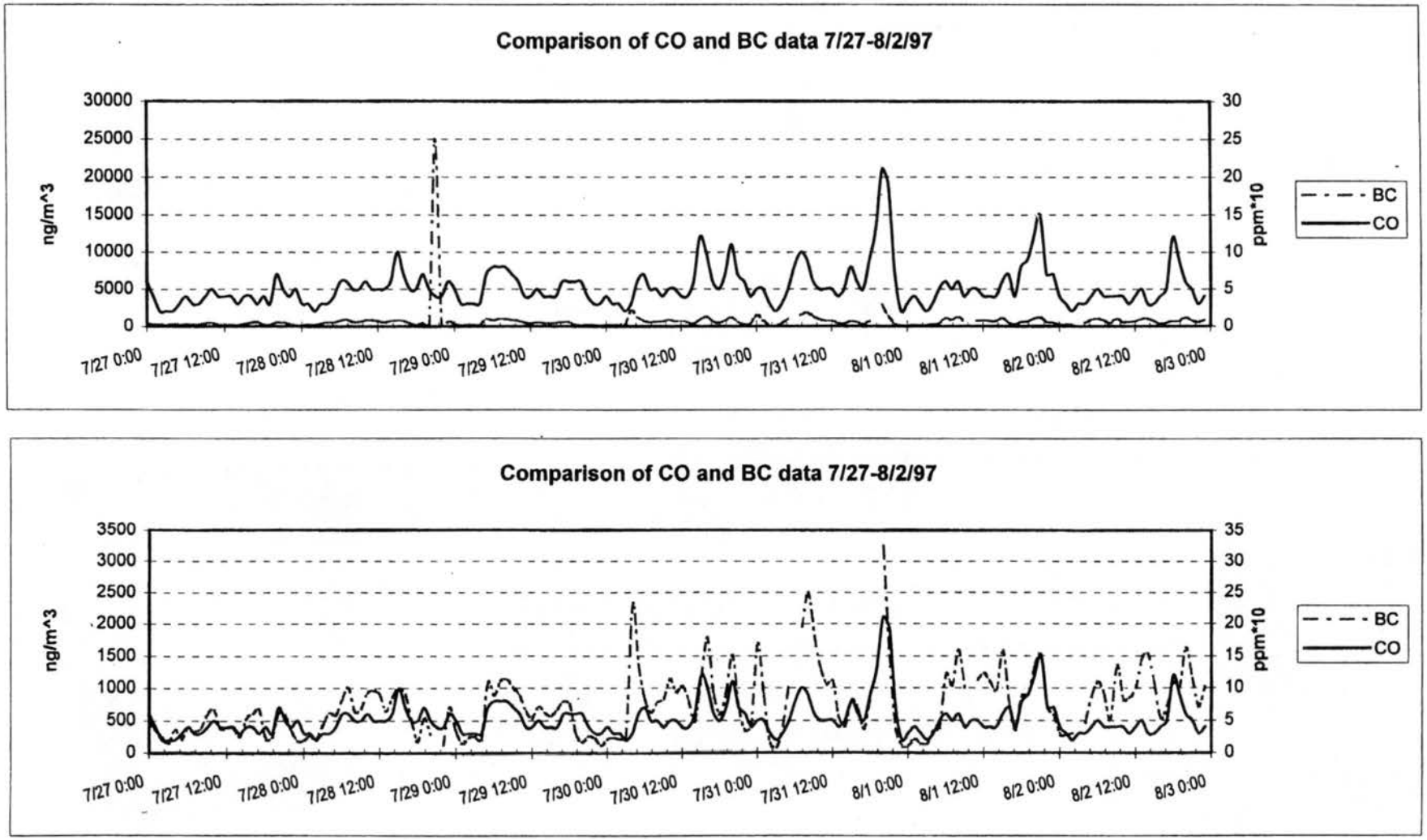

Figure E.5 BC and CO concentration time-lines.

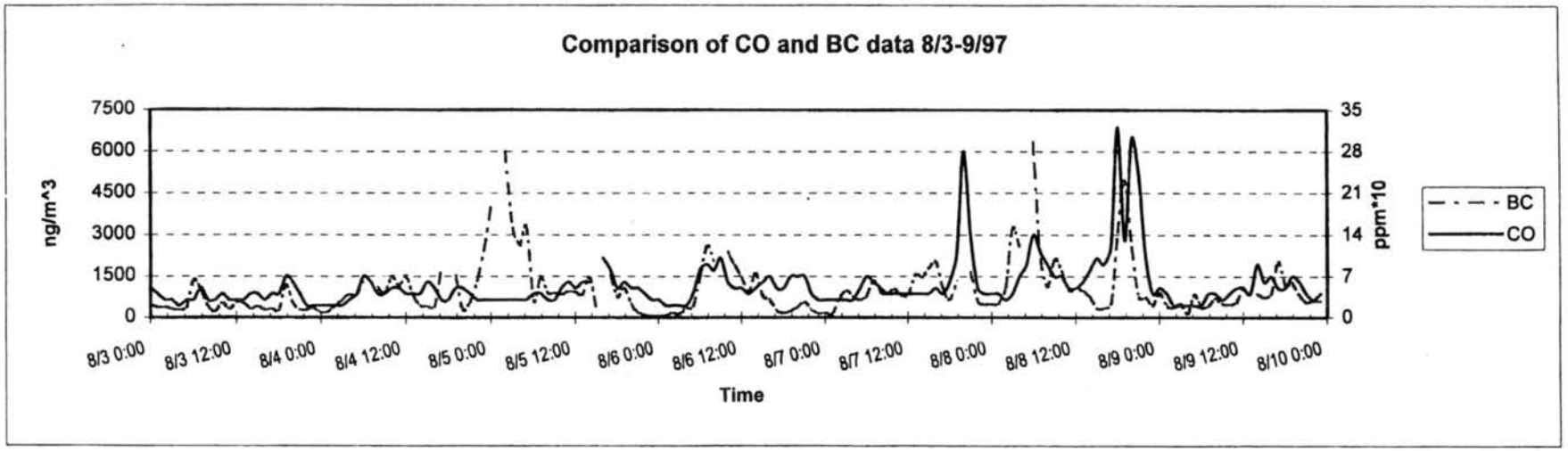

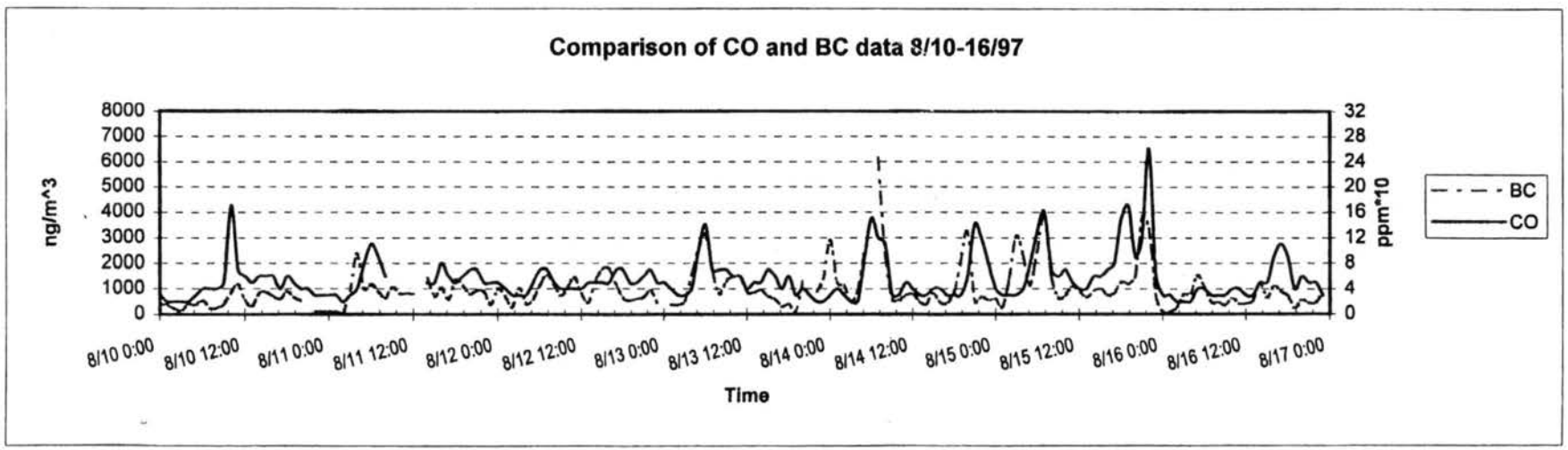

Figure E.6 BC and CO concentration time-lines.

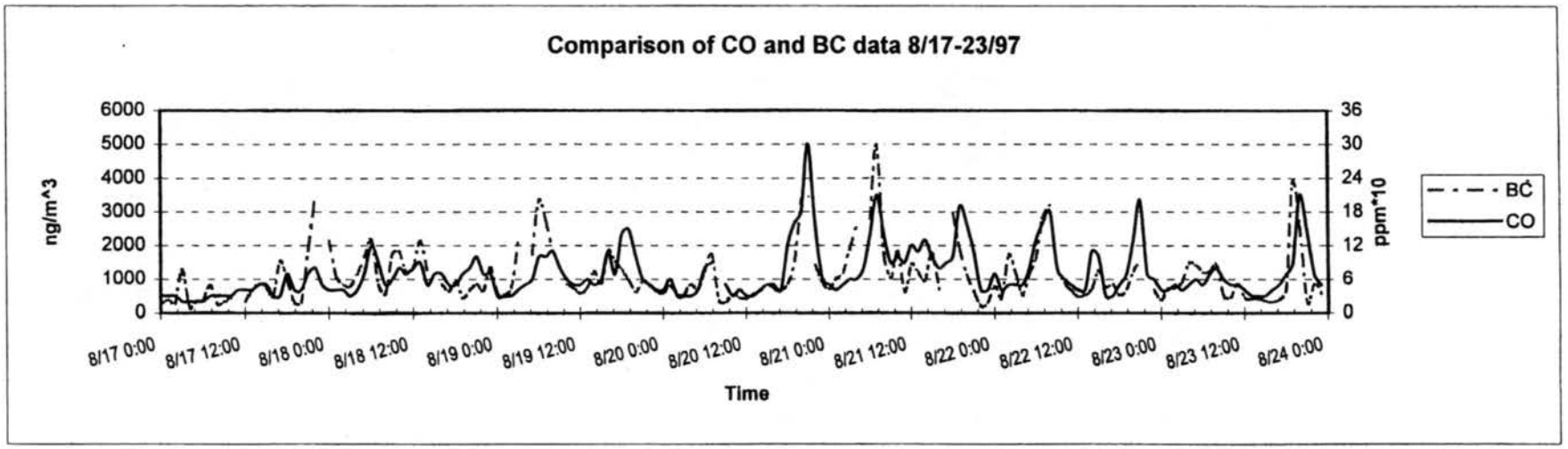

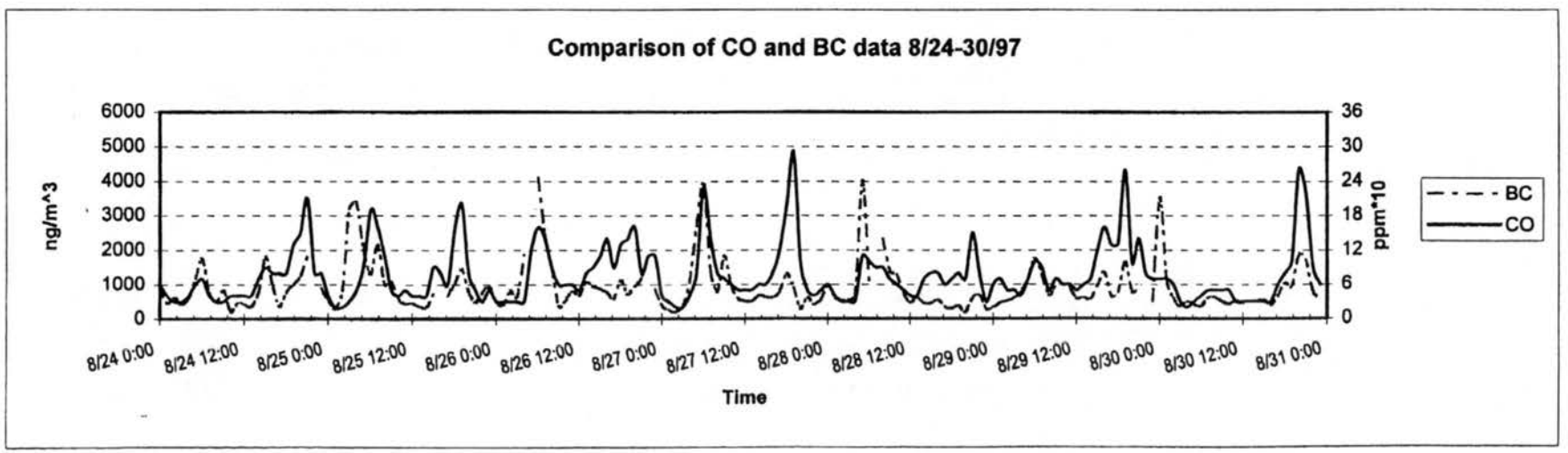

Figure E.7 BC and CO concentration time-lines.

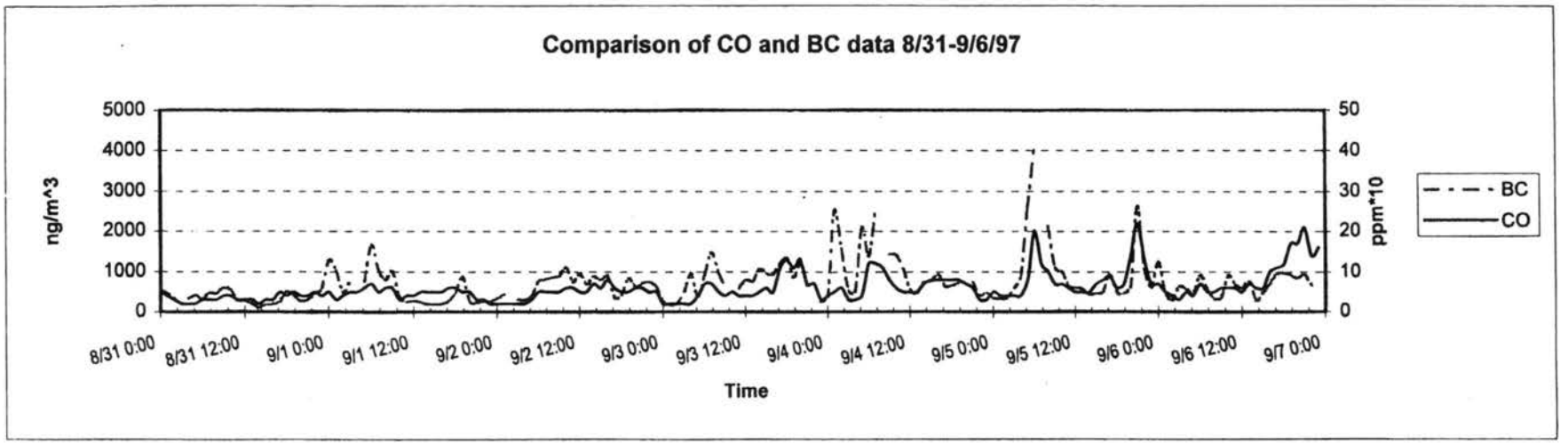

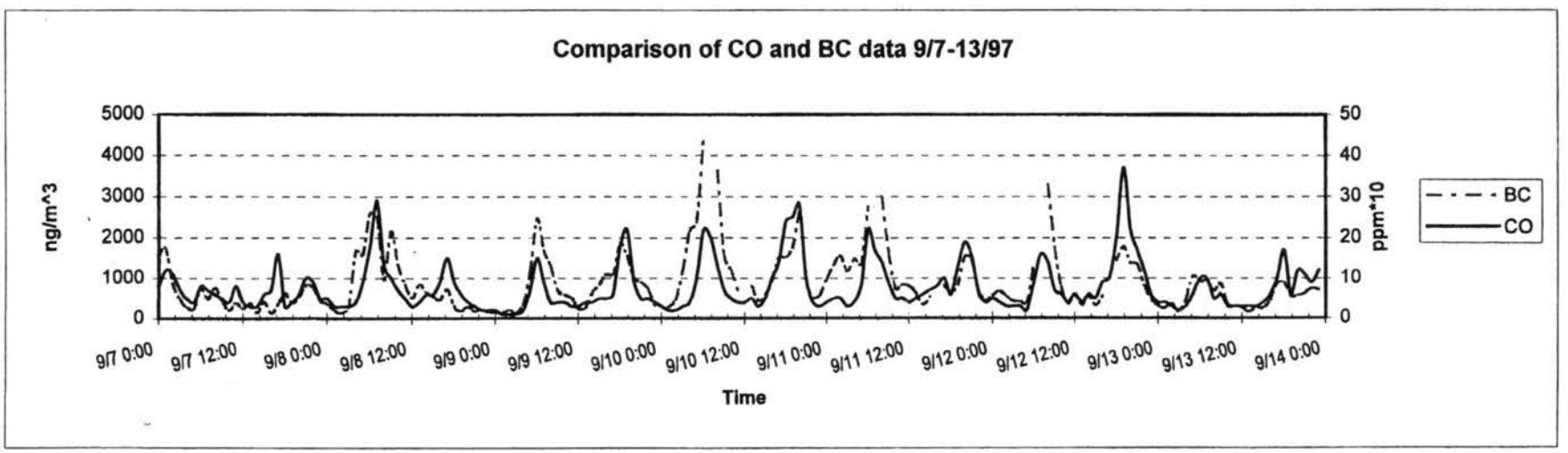

Figure E.8 BC and CO concentration time-lines.

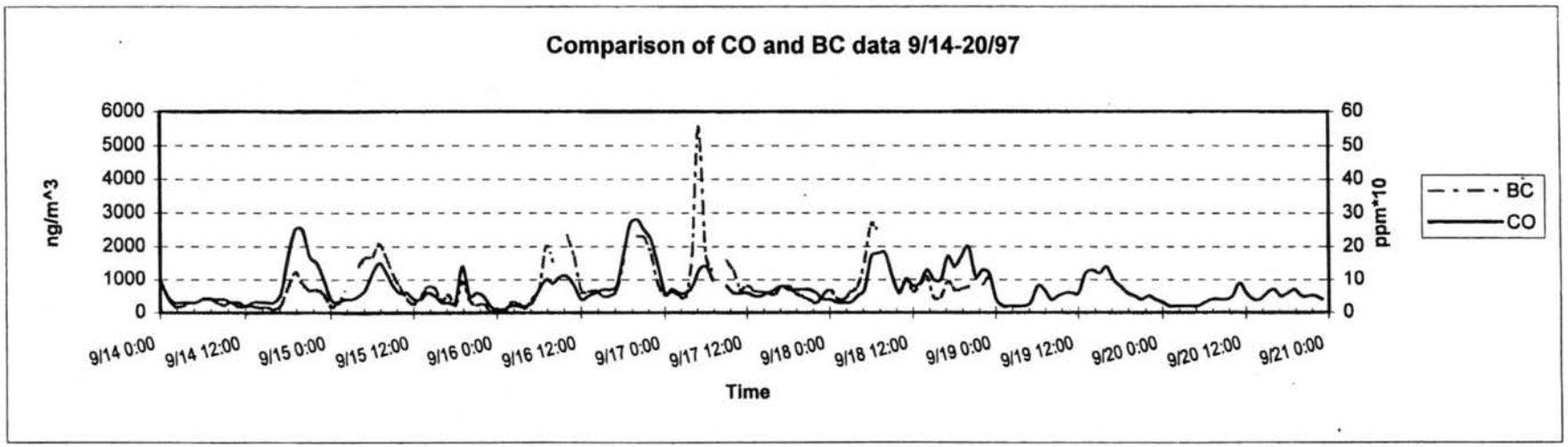

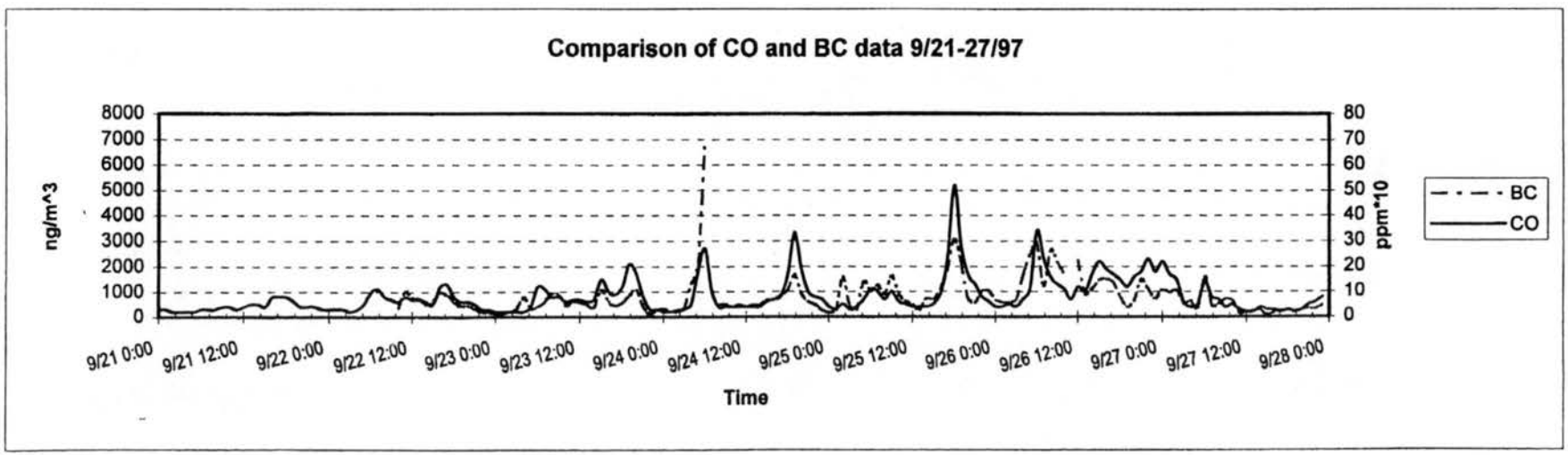

Figure E.9 BC and CO concentration time-lines.

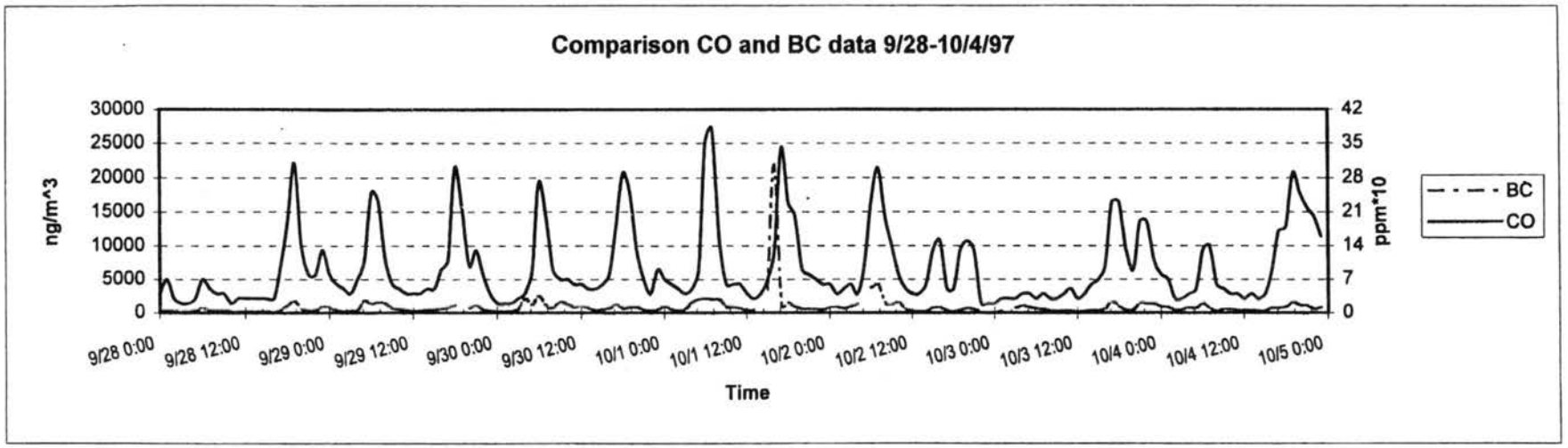

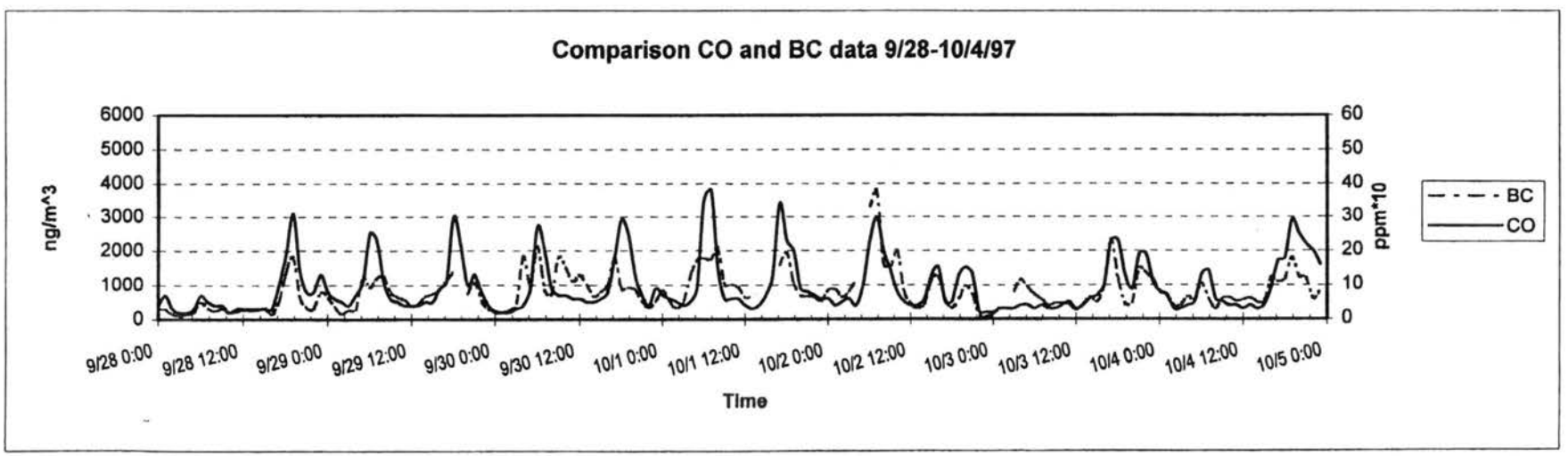

Figure E.10 BC and CO concentration time-lines.

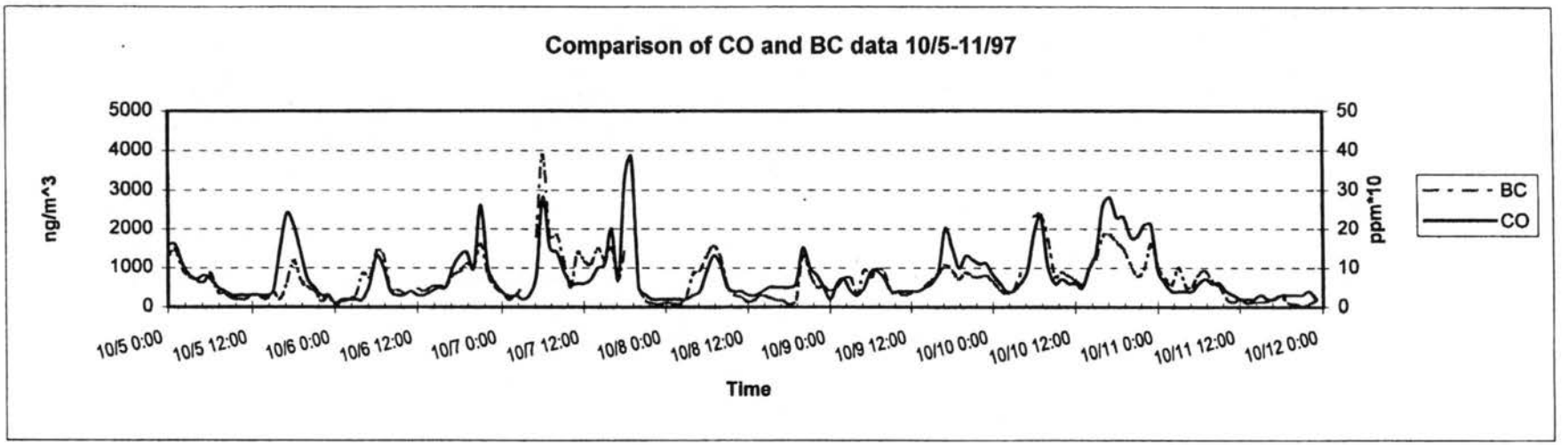

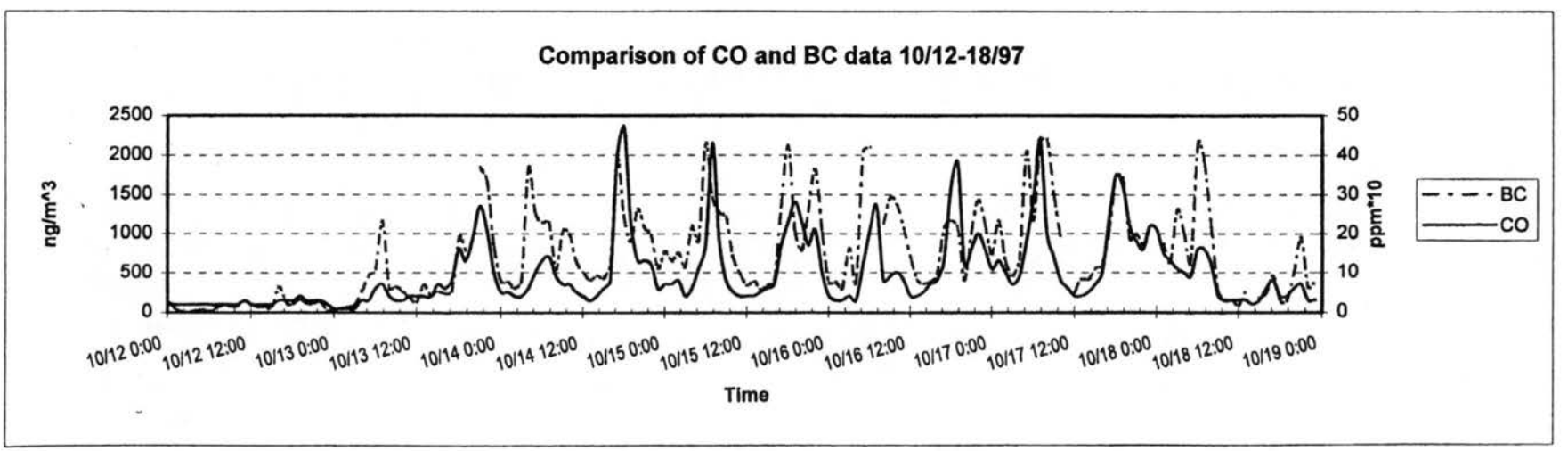

Figure E.11 BC and CO concentration time-lines.

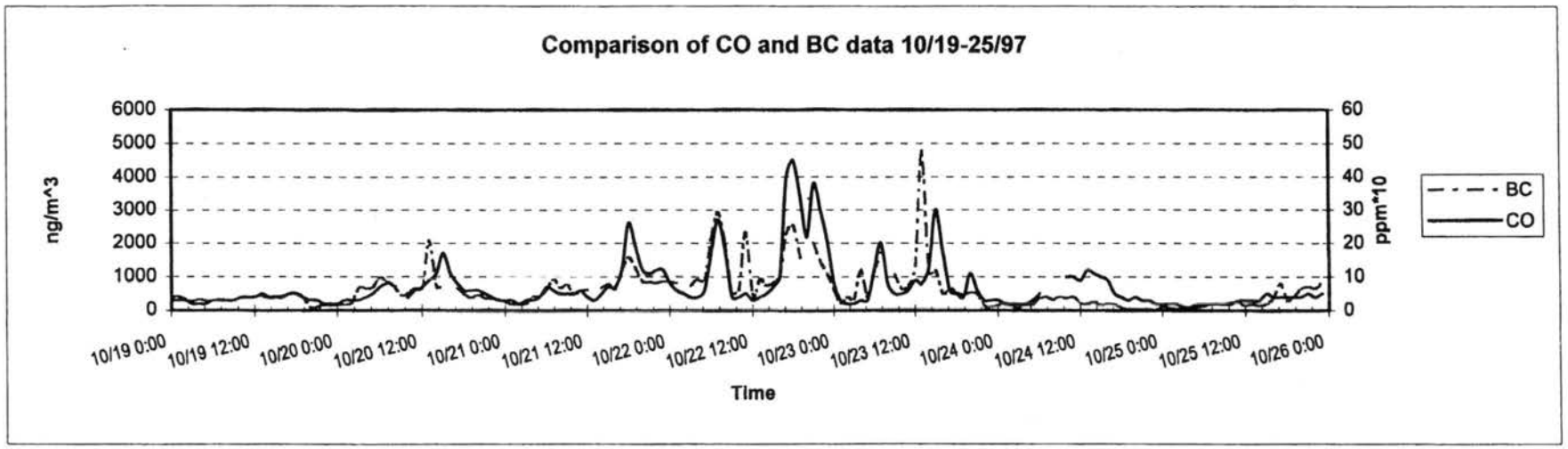

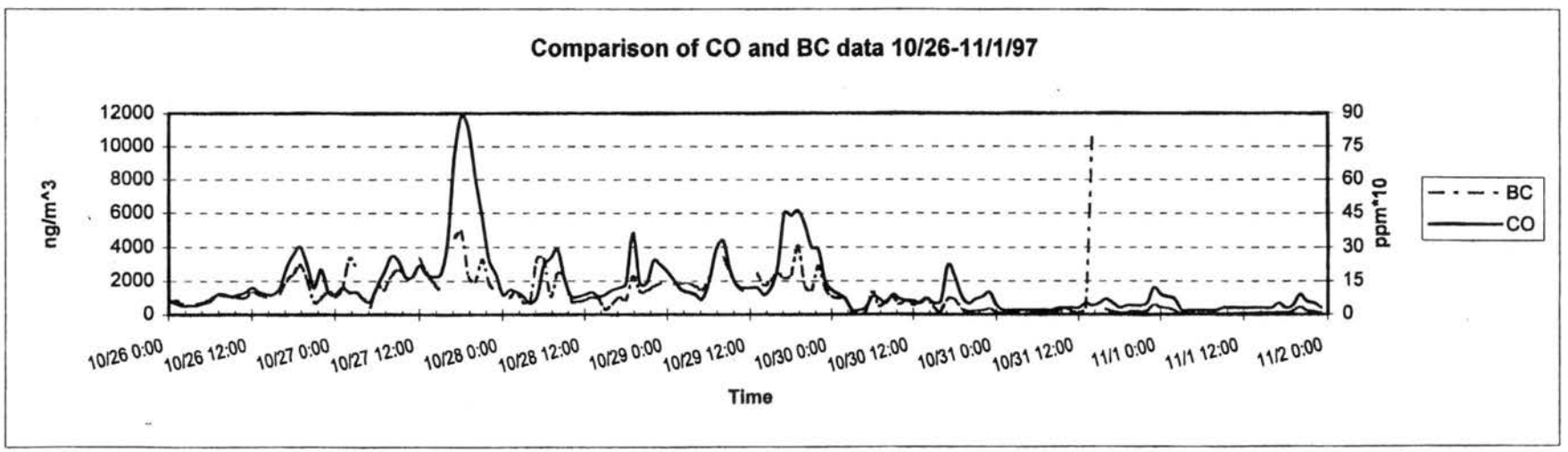

Figure E.12 BC and CO concentration time-lines.

APPENDIX F

Optical Particle Counter (OPC) concentrations

Figure F.1 – F.9 show the weekly timelines of OPC concentrations for June – September, 1997. There is no October data as the instrument was being repaired and calibrated. The figures show the peaks in the OPC timelines occur later than the BC and CN peaks shown in figure 17. The plots also show different patterns from day to day.

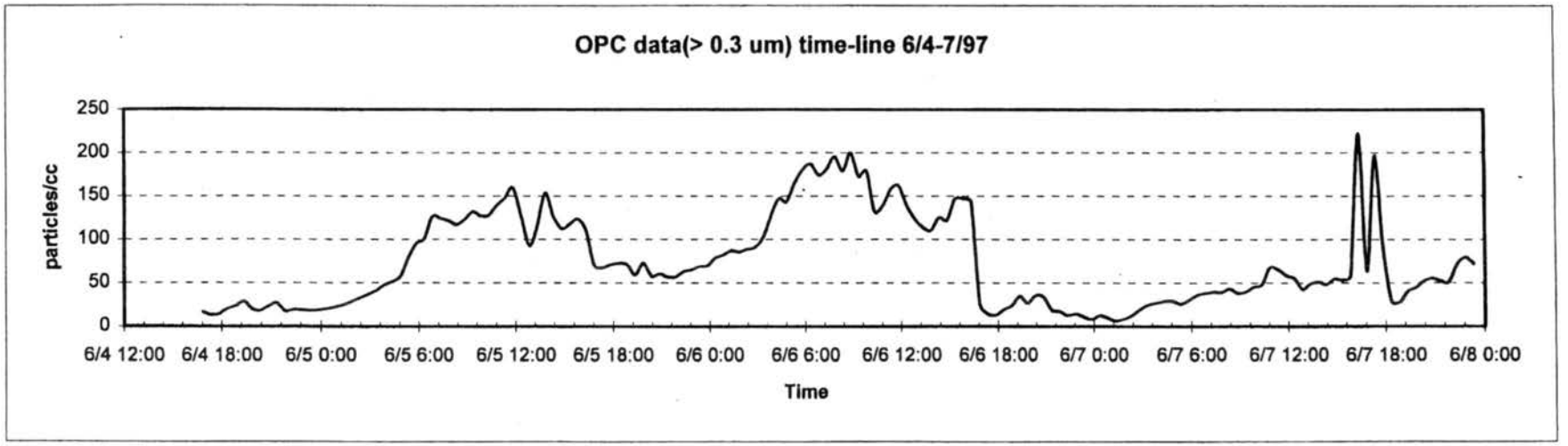

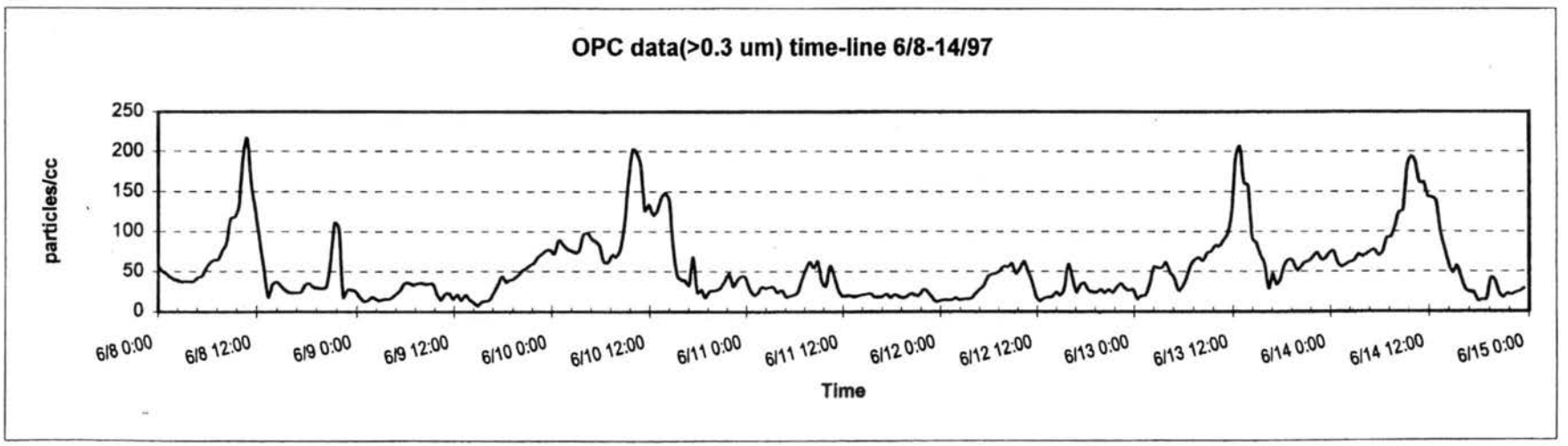

Figure F.1 OPC concentration time-lines.

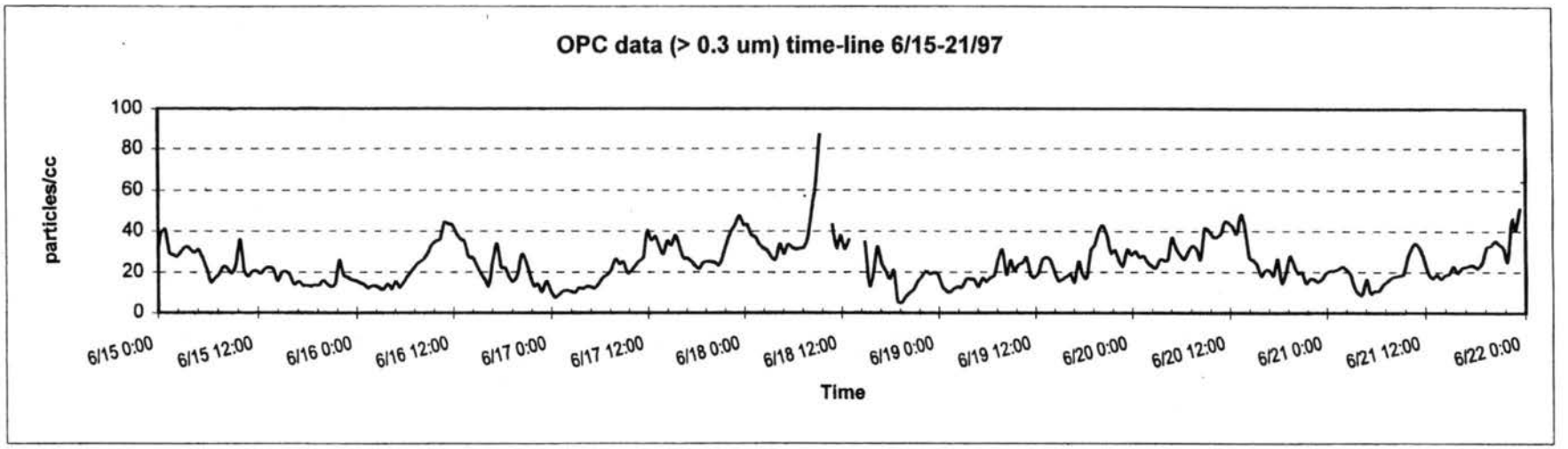

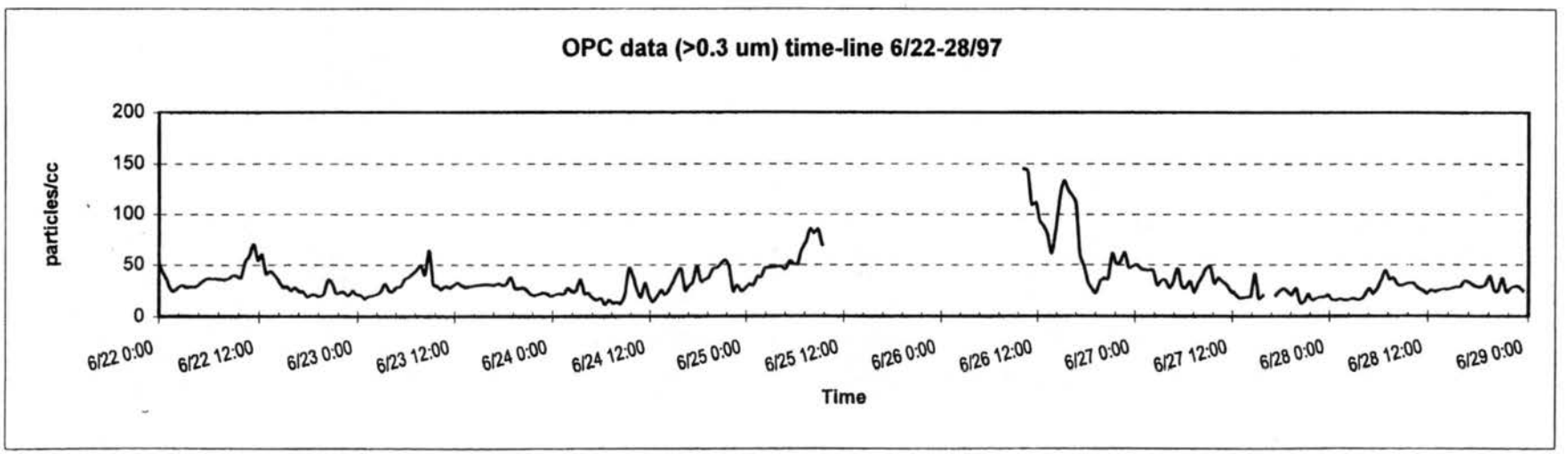

Figure F.2 OPC concentration time-lines.

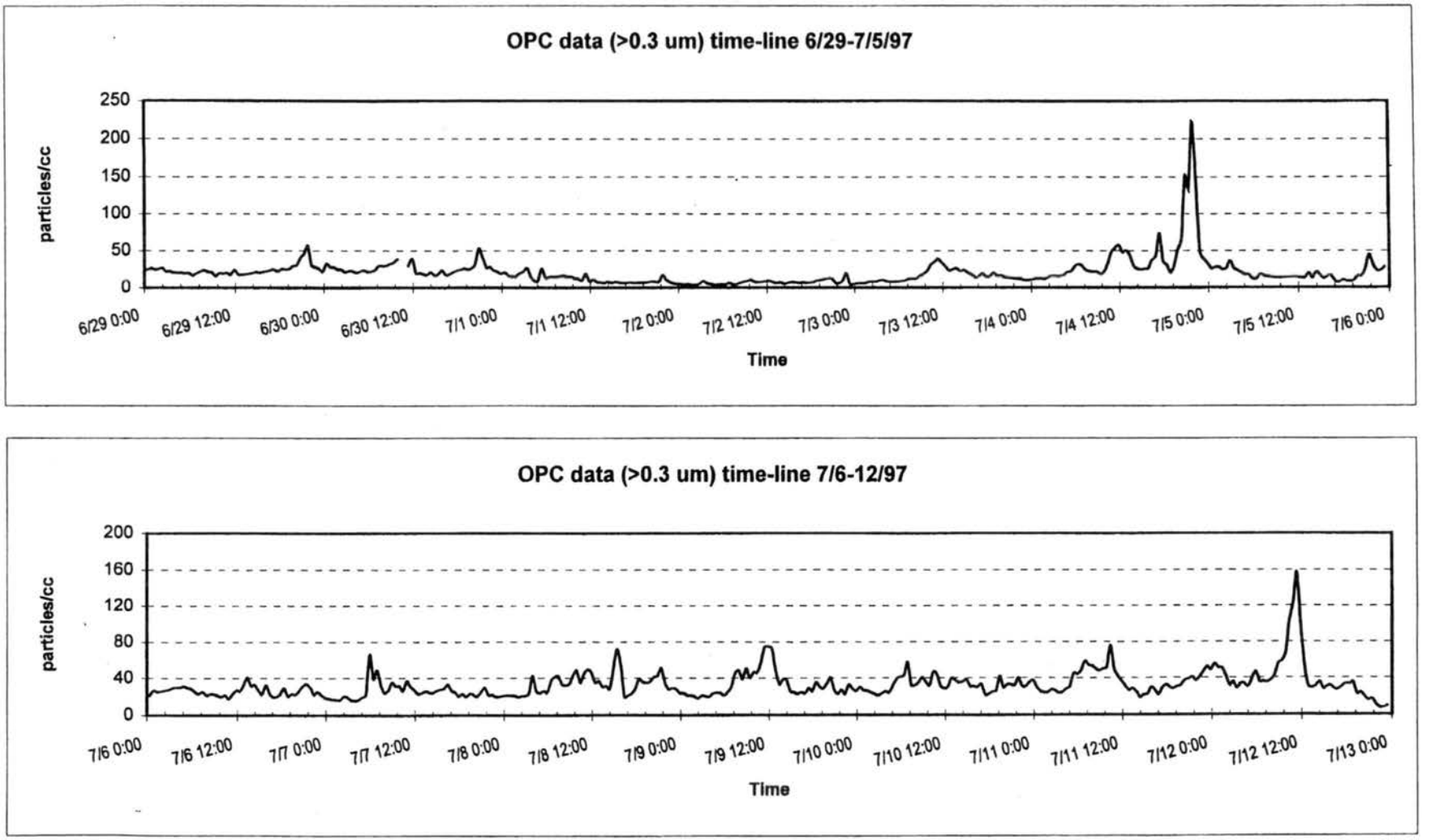

Figure F.3 OPC concentration time-lines.

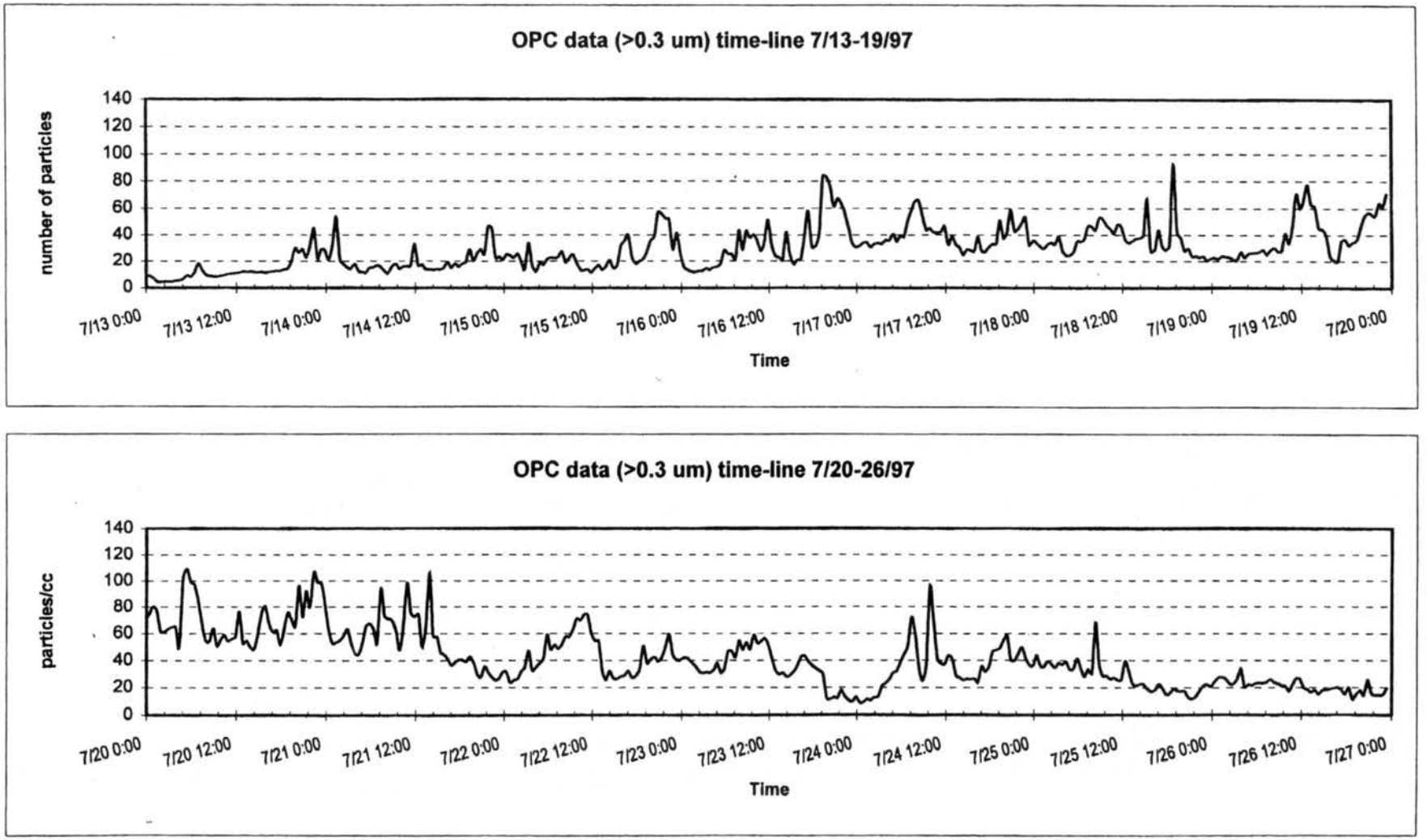

Figure F.4 OPC concentration time-lines.

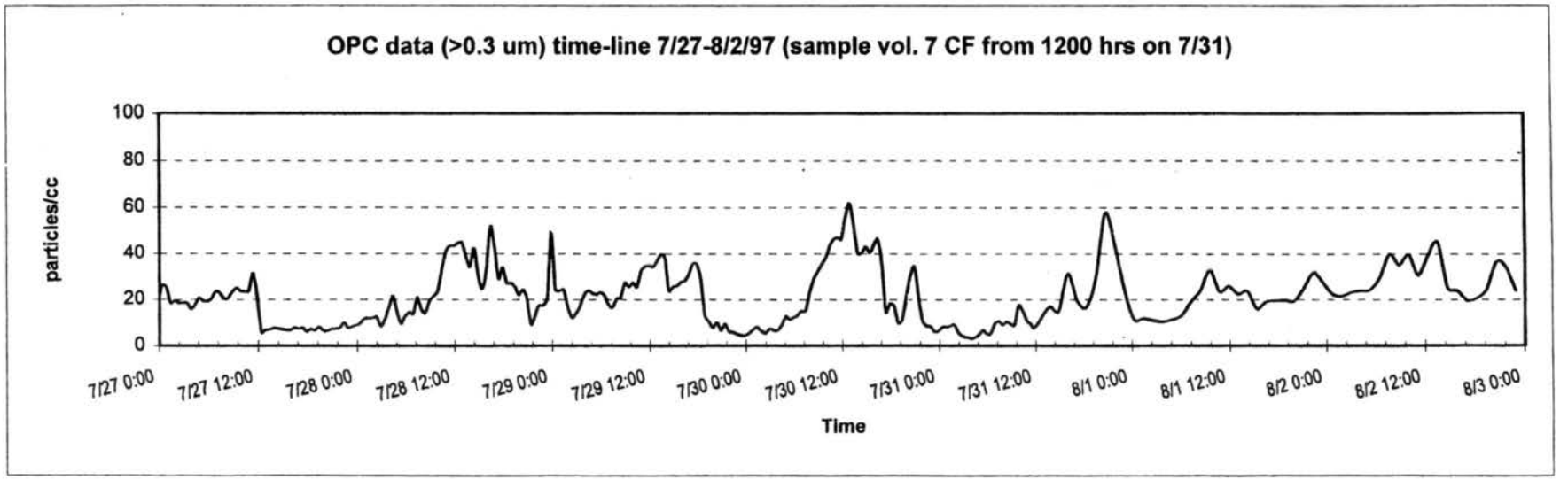

Figure F.5 OPC concentration time-lines.

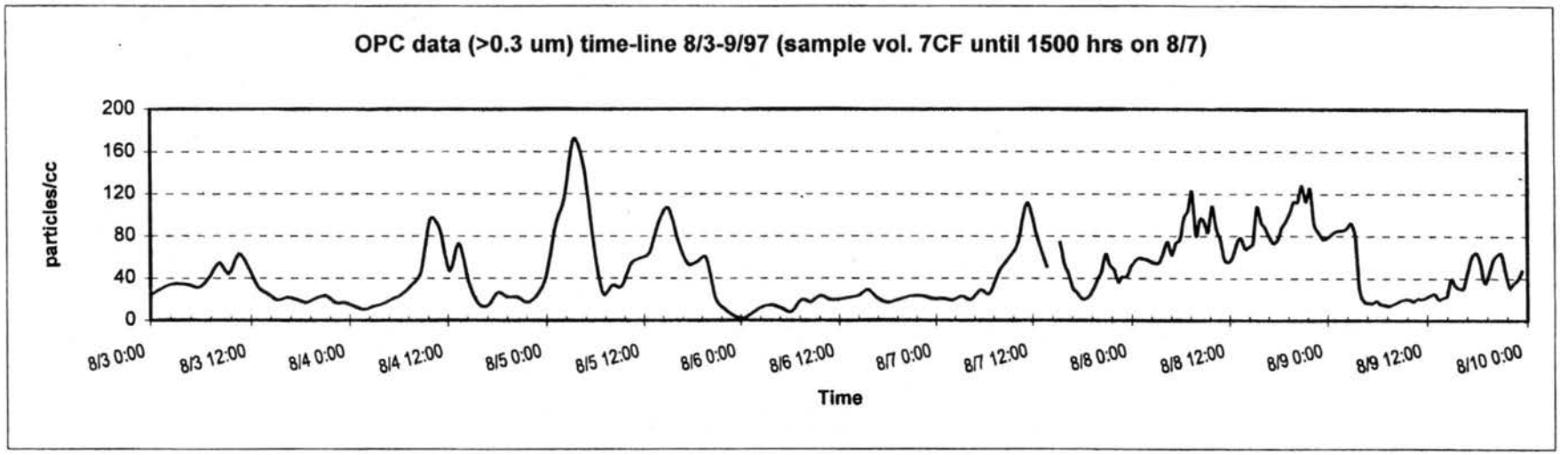

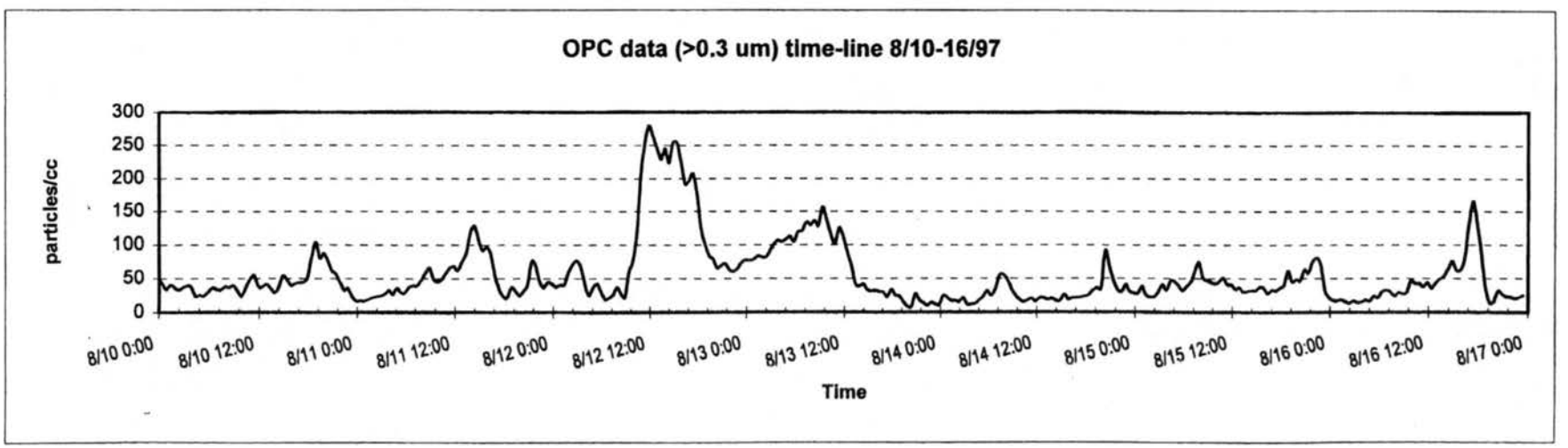

Figure F.6 OPC concentration time-lines.

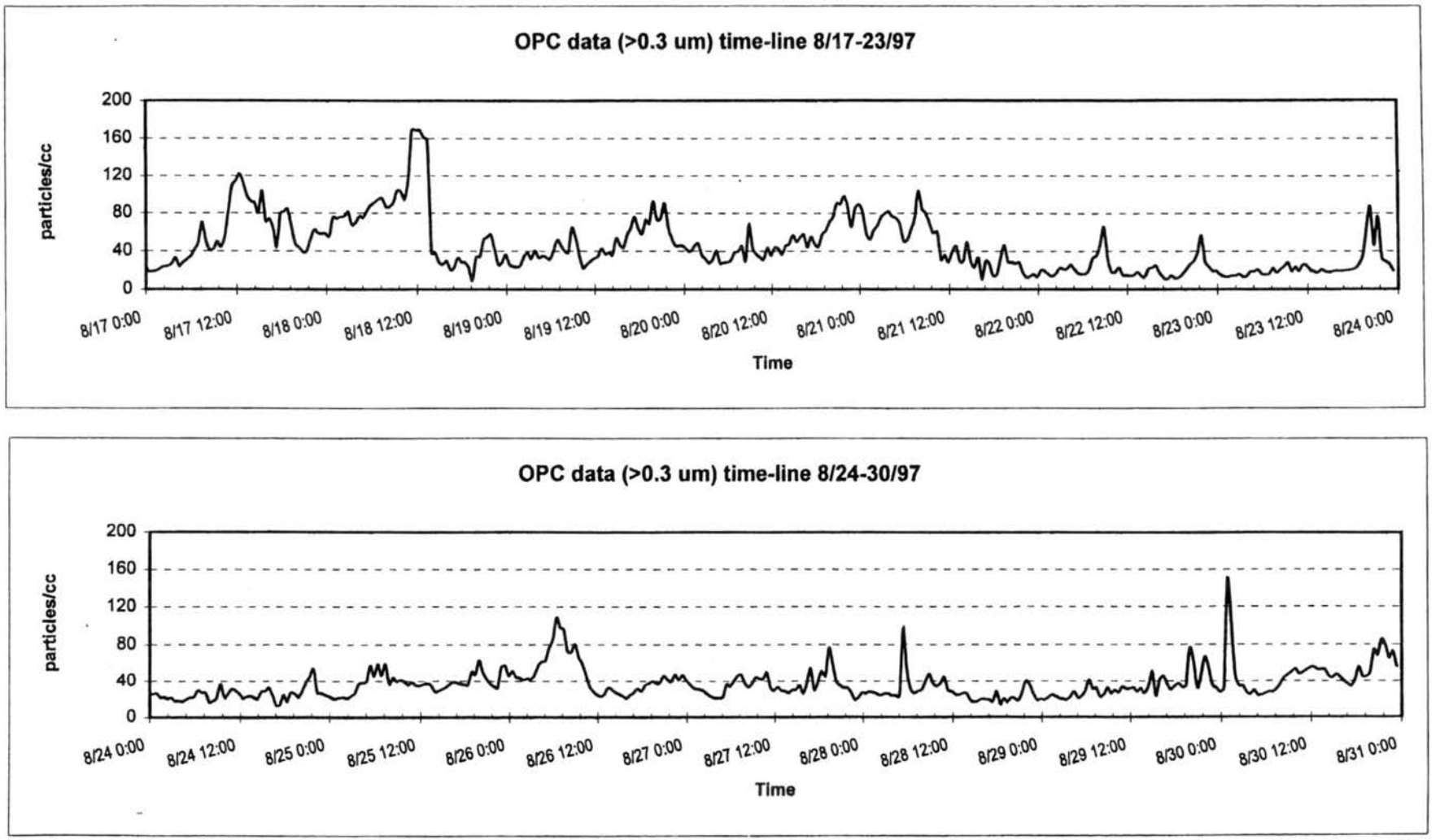

Figure F.7 OPC concentration time-lines.

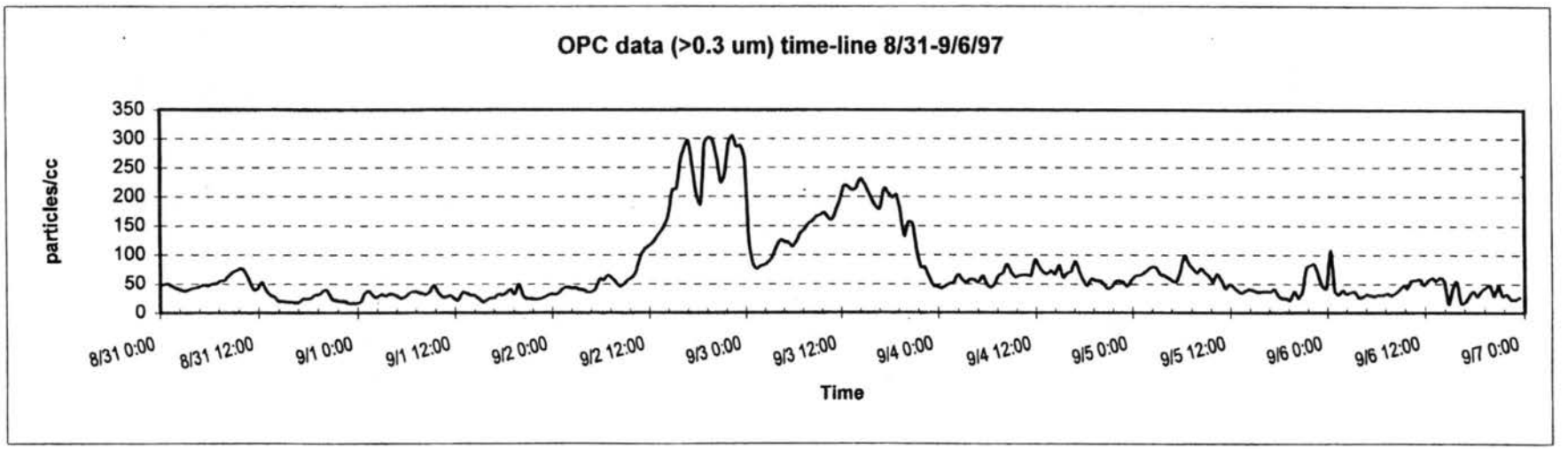

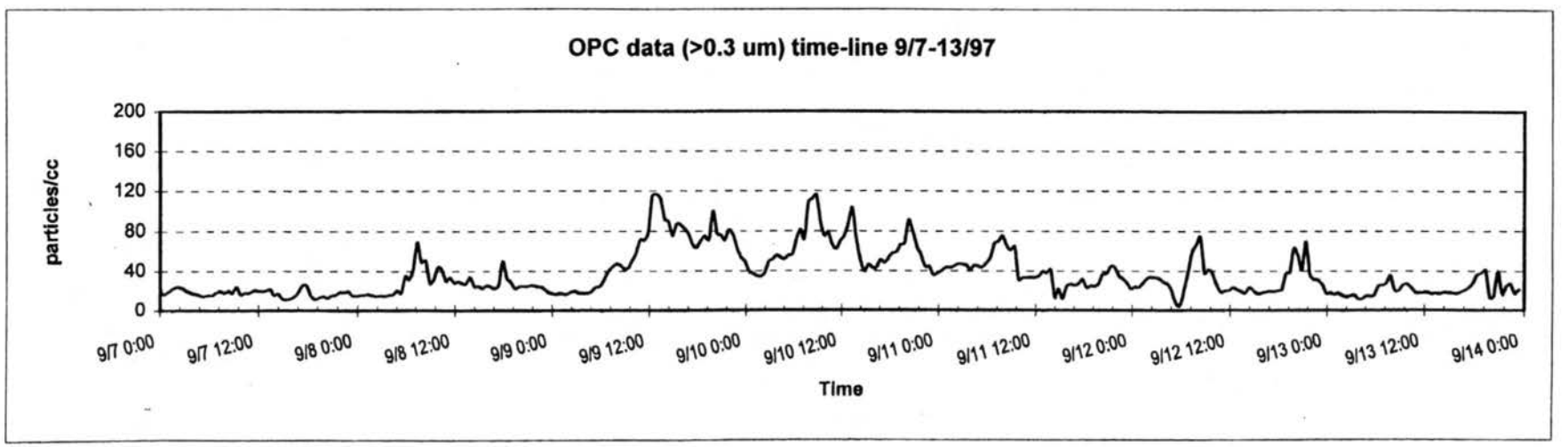

Figure F.8 OPC concentration time-lines.

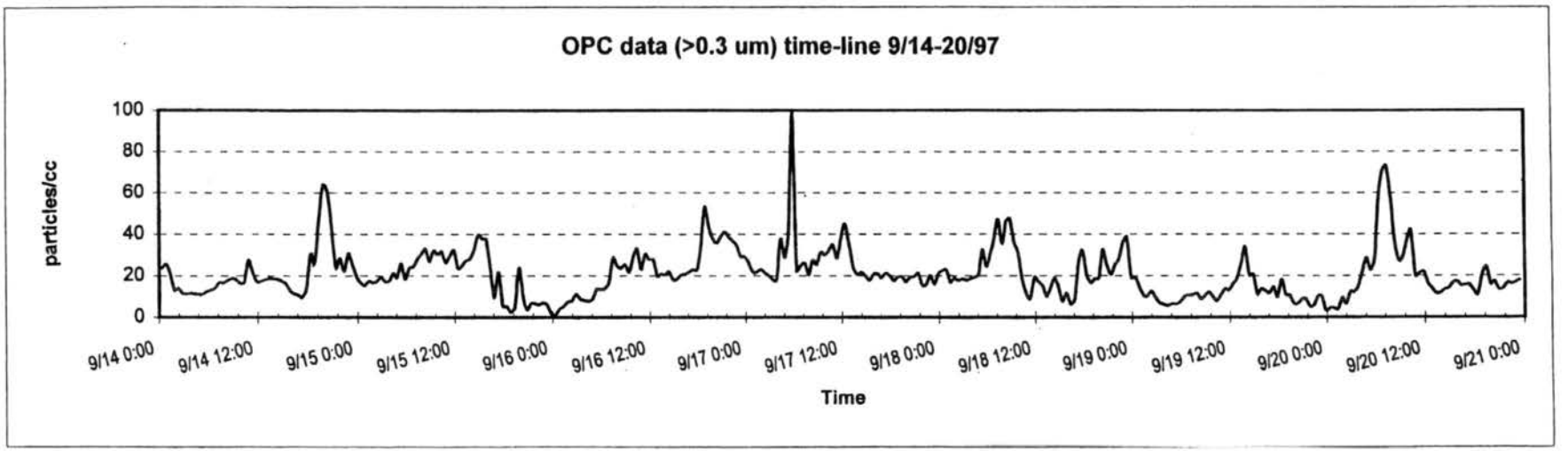

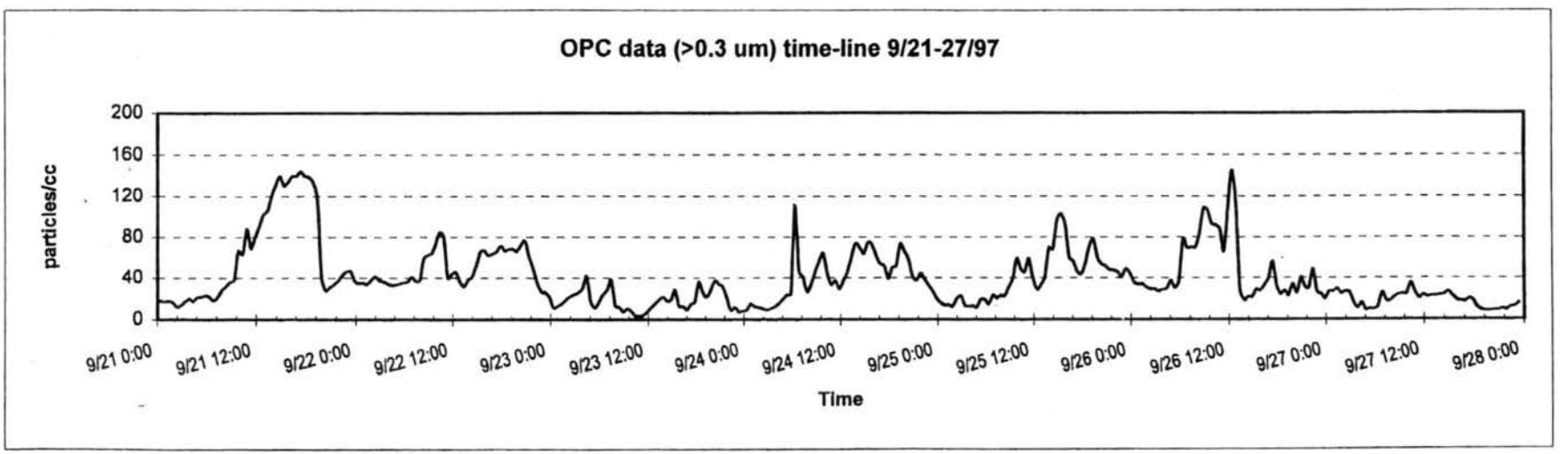

Figure F.9 OPC concentration time-lines.

APPENDIX G

BC concentrations

Figure G.1 – G.12 show the weekly timelines of BC concentrations for June – October ,1997. The timelines show clearly the morning and late afternoon/evening peaks associated with vehicle traffic.

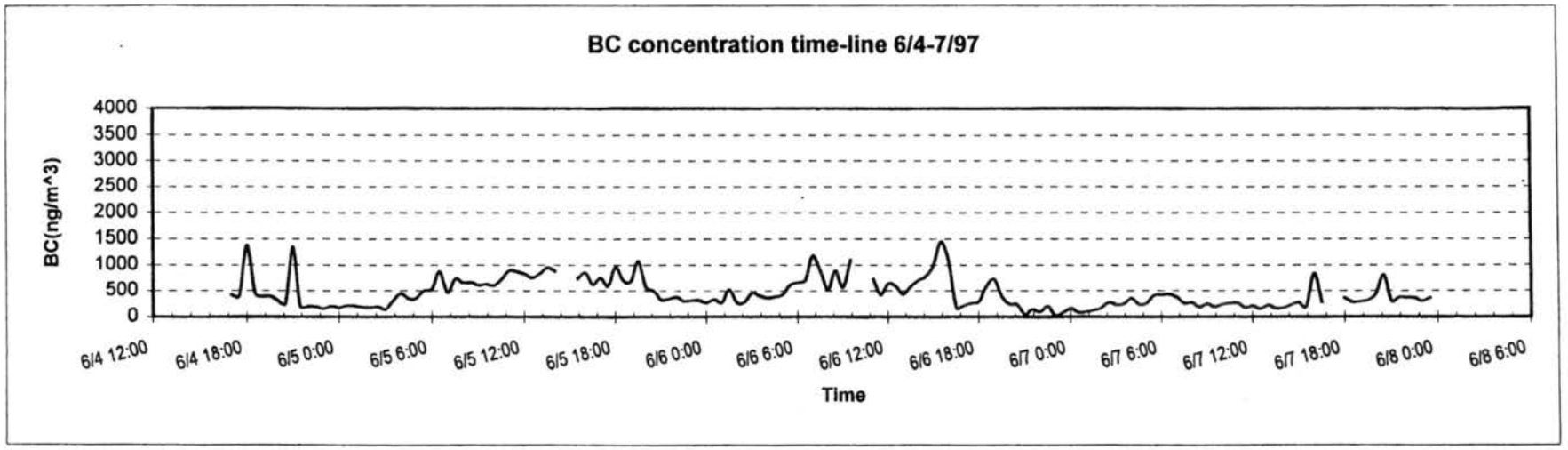

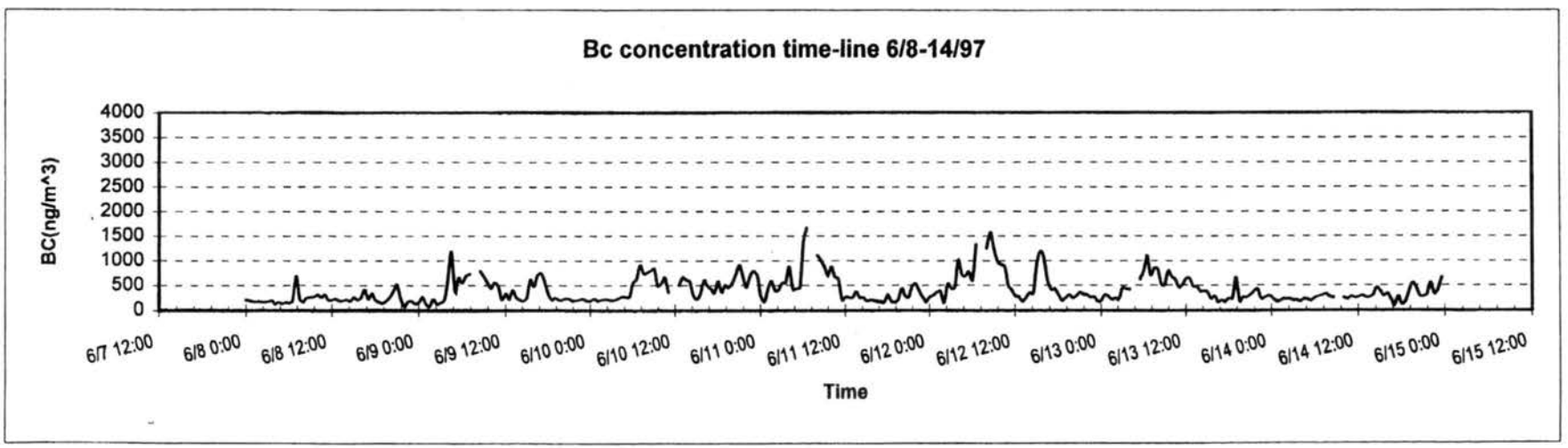

Figure G.1 BC concentration time-lines

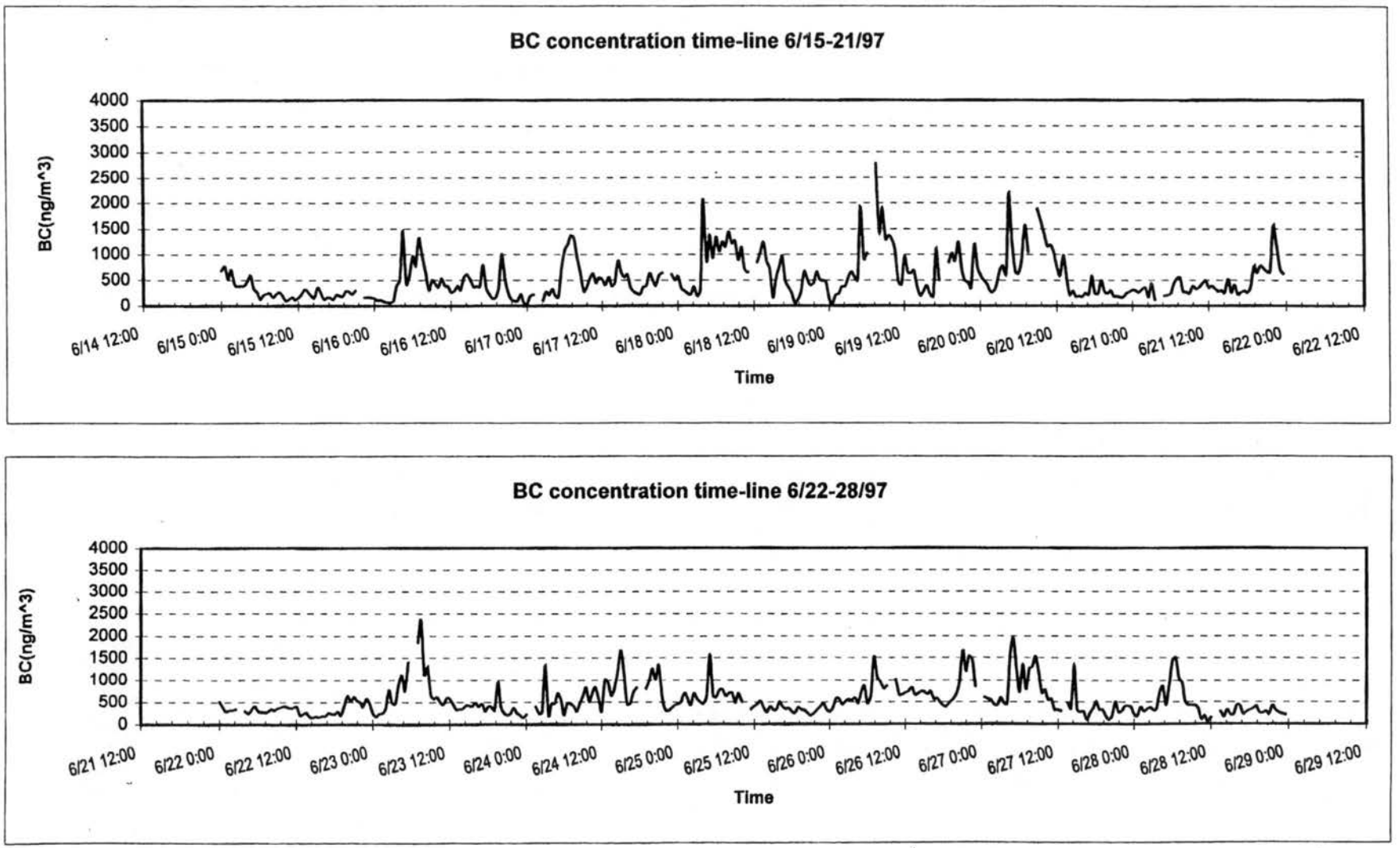

Figure G.2 BC concentration time-lines

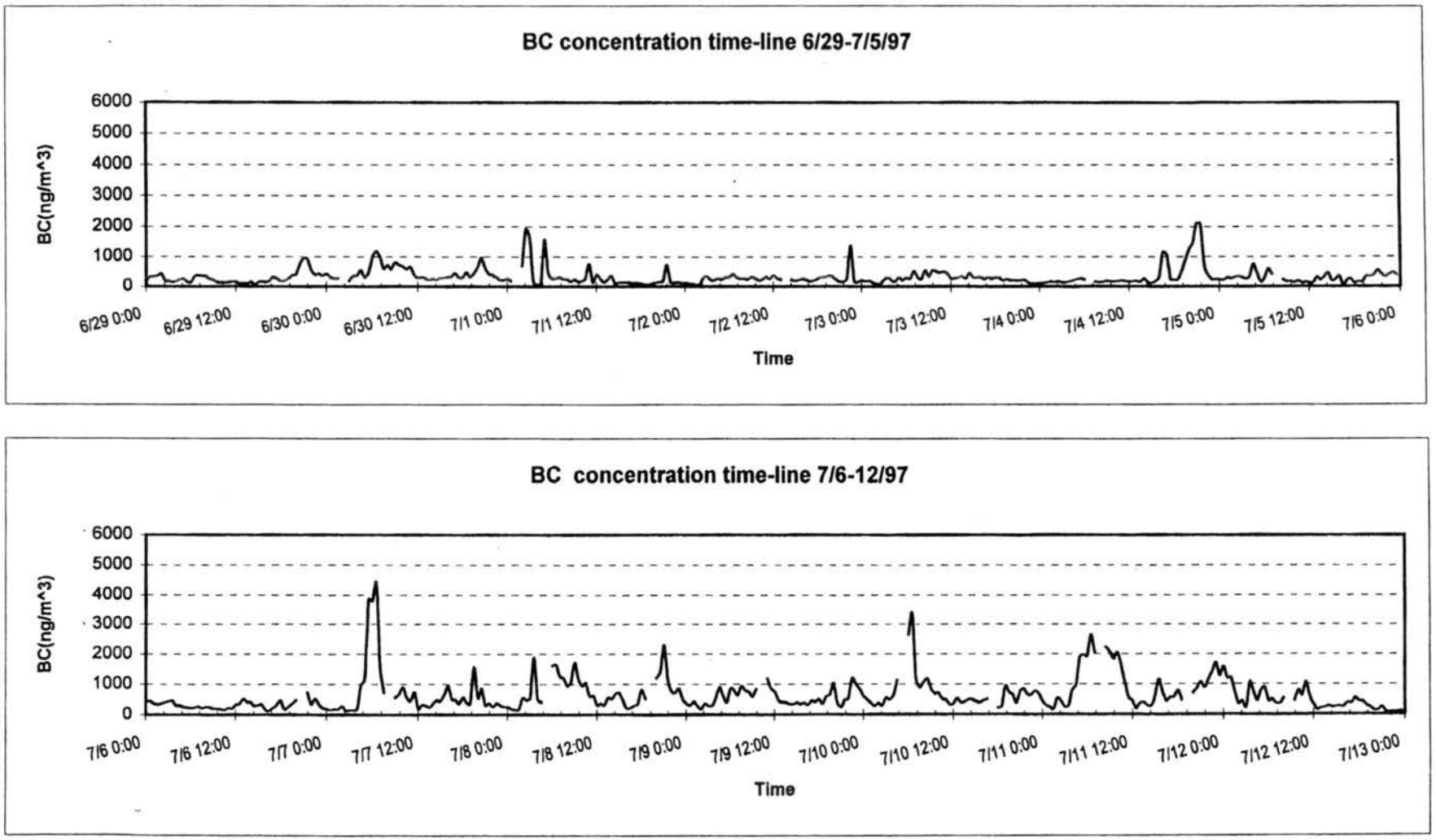

Figure G.3 BC concentration time-lines

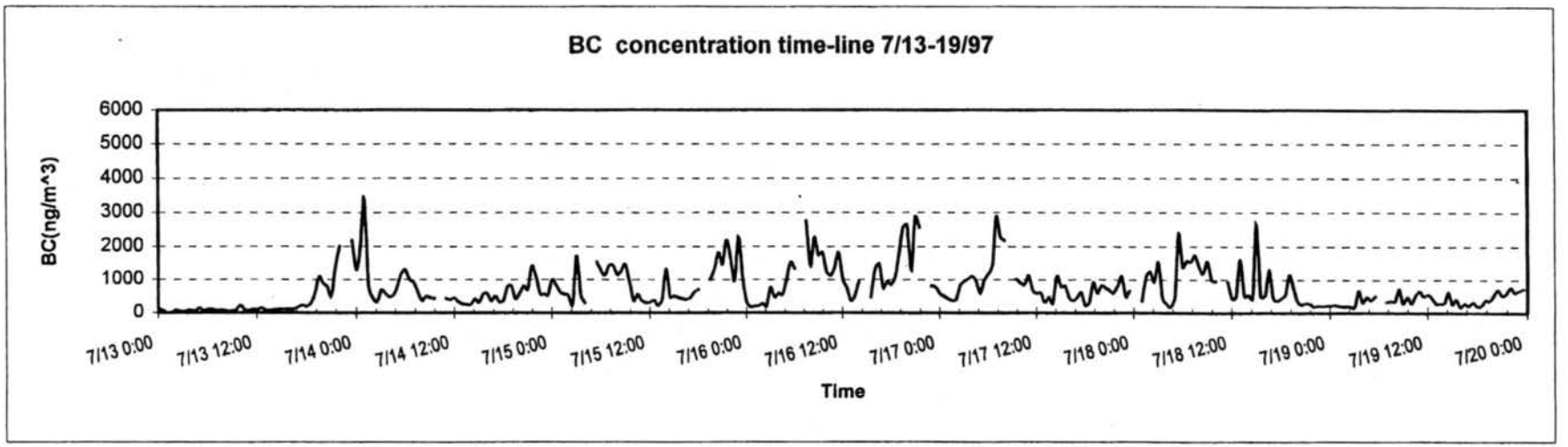

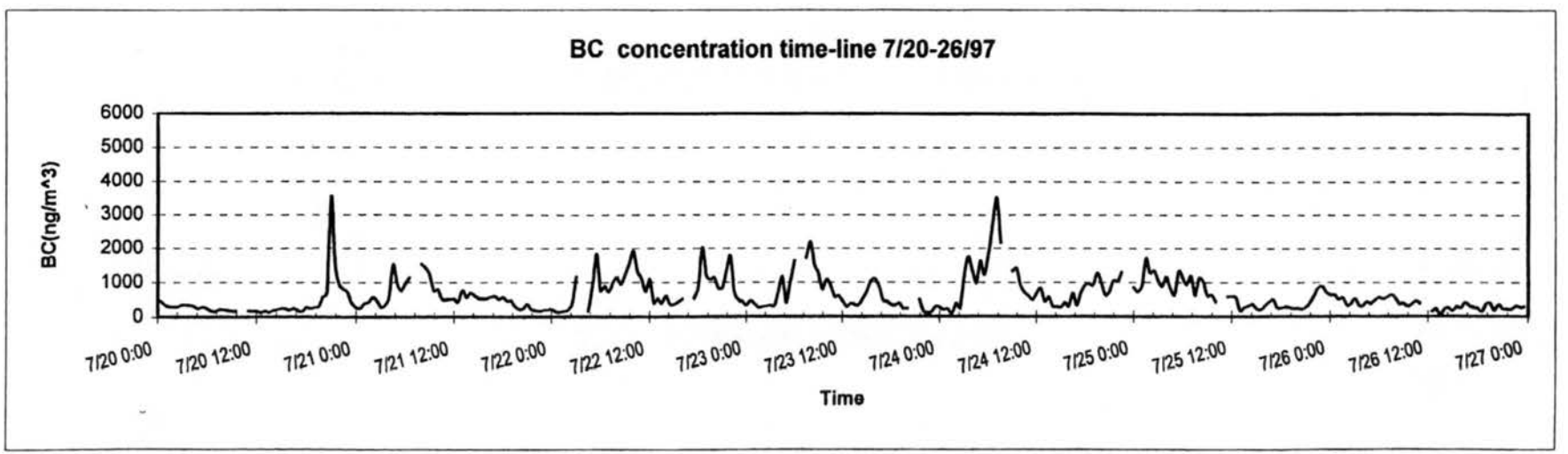

Figure G.4 BC concentration time-lines

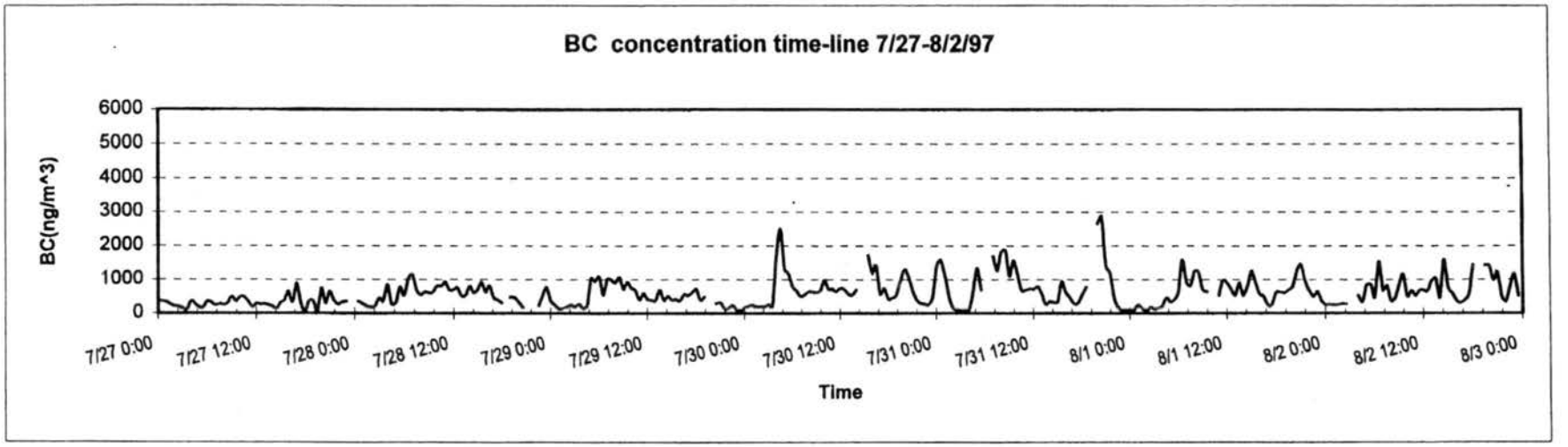

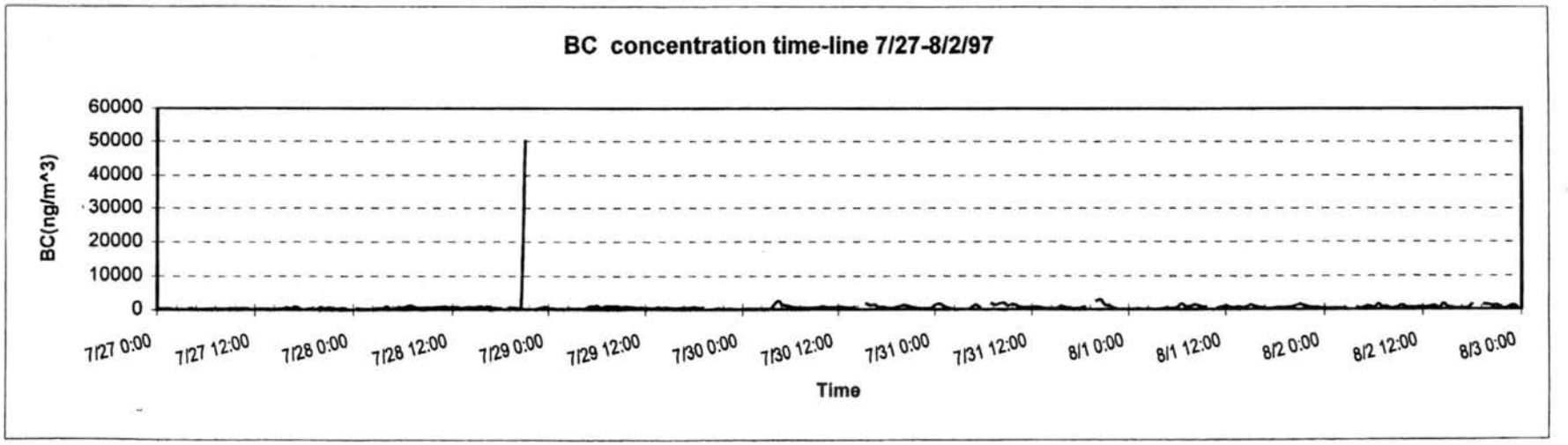

Figure G.5 BC concentration time-lines

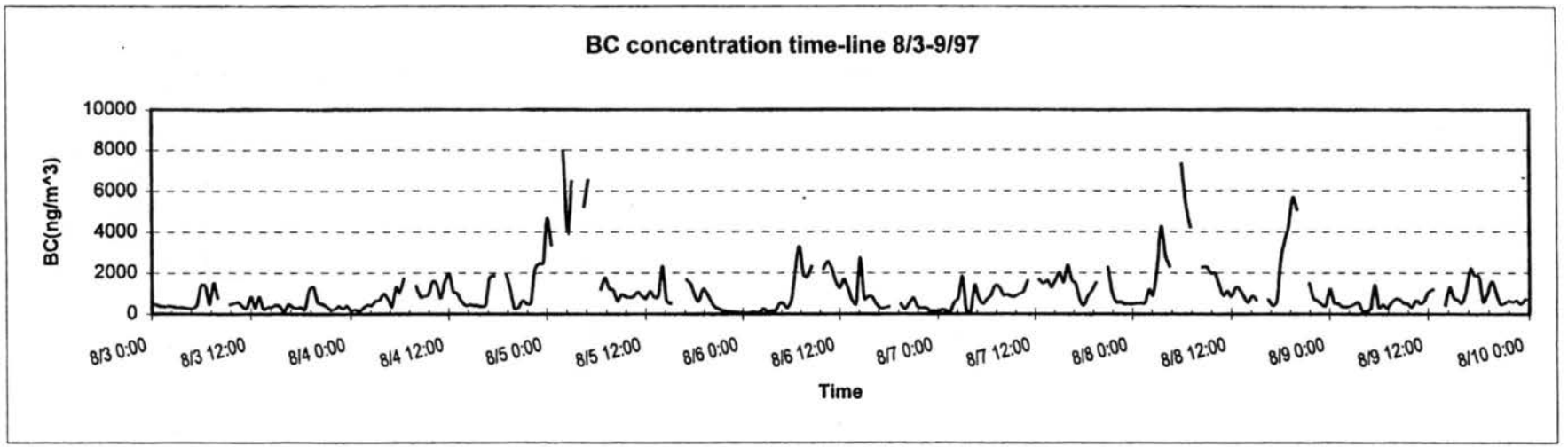

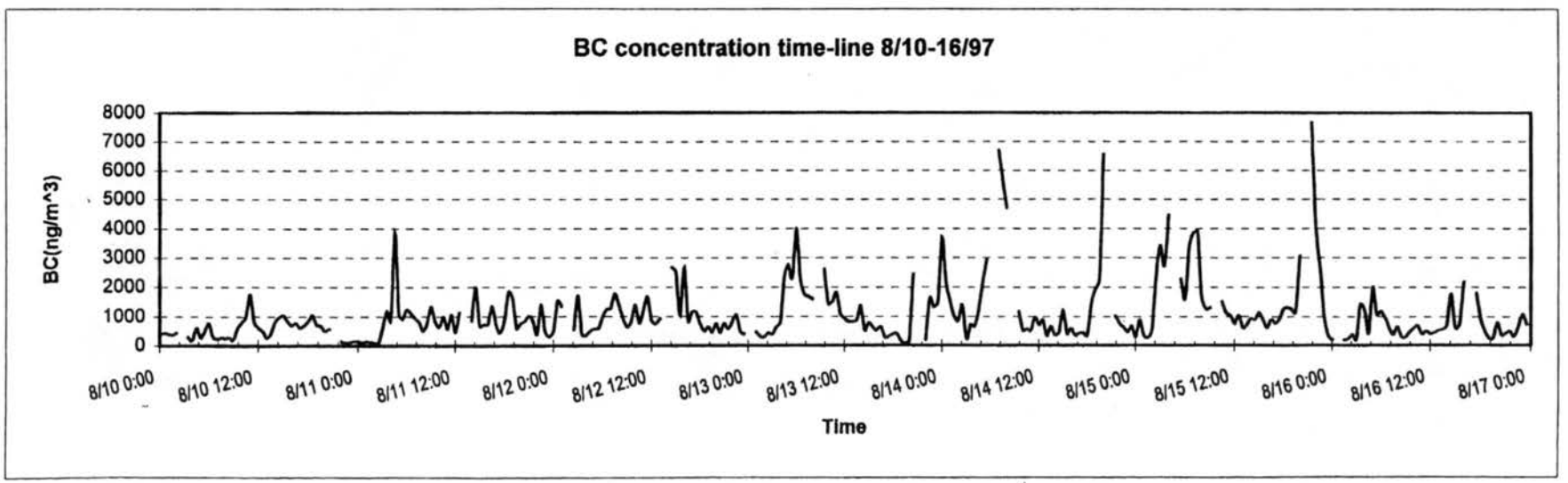

Figure G.6 BC concentration time-lines

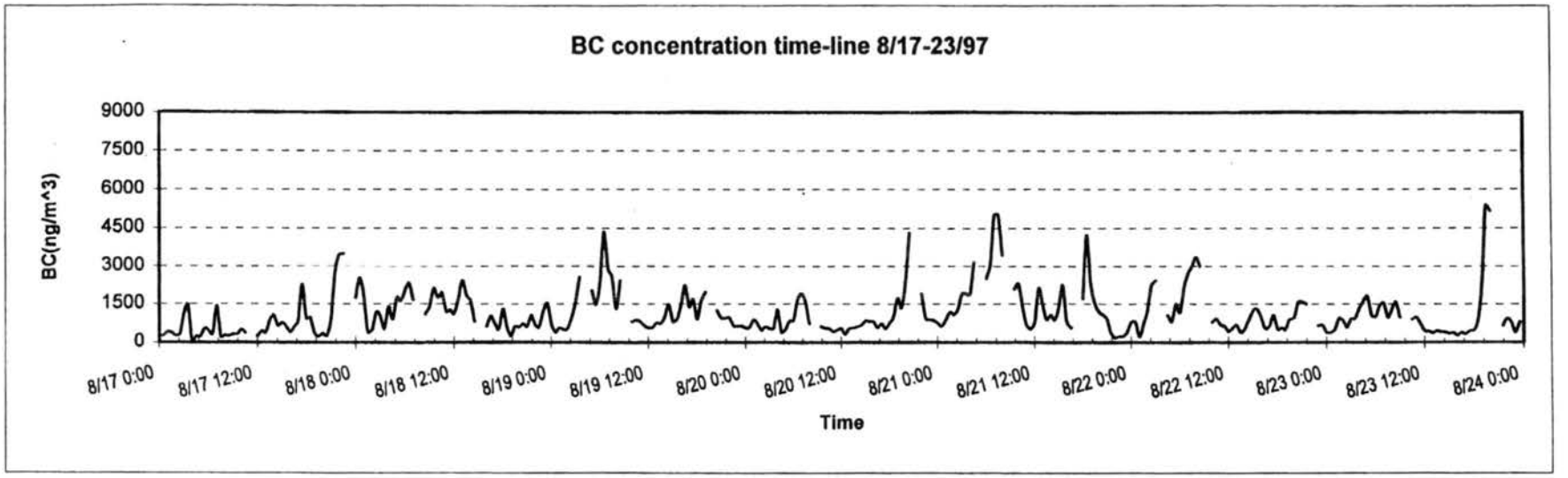

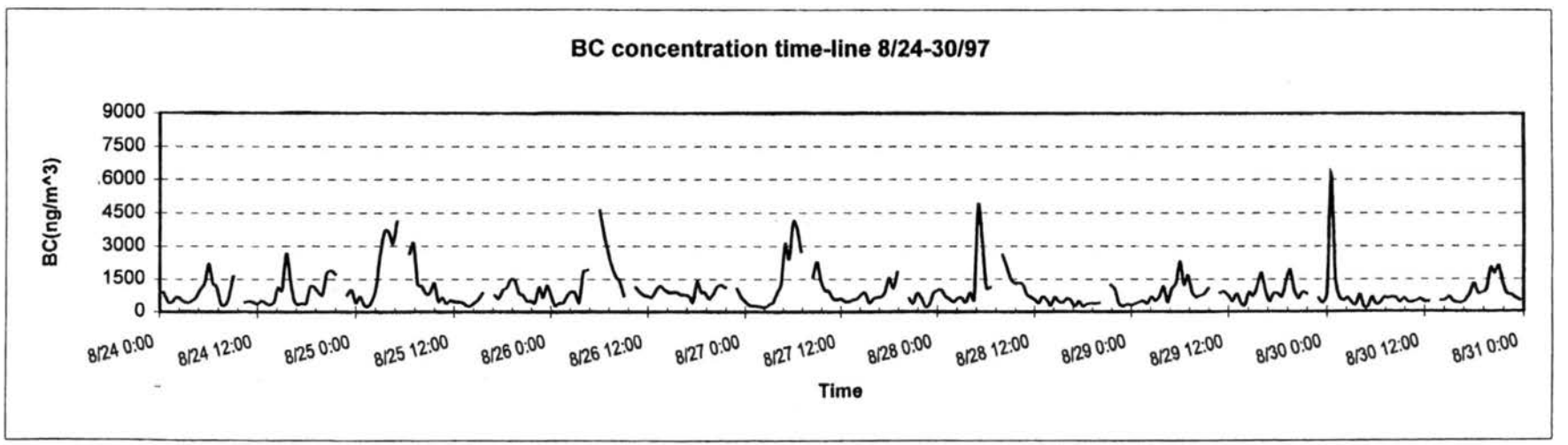

Figure G.7 BC concentration time-lines

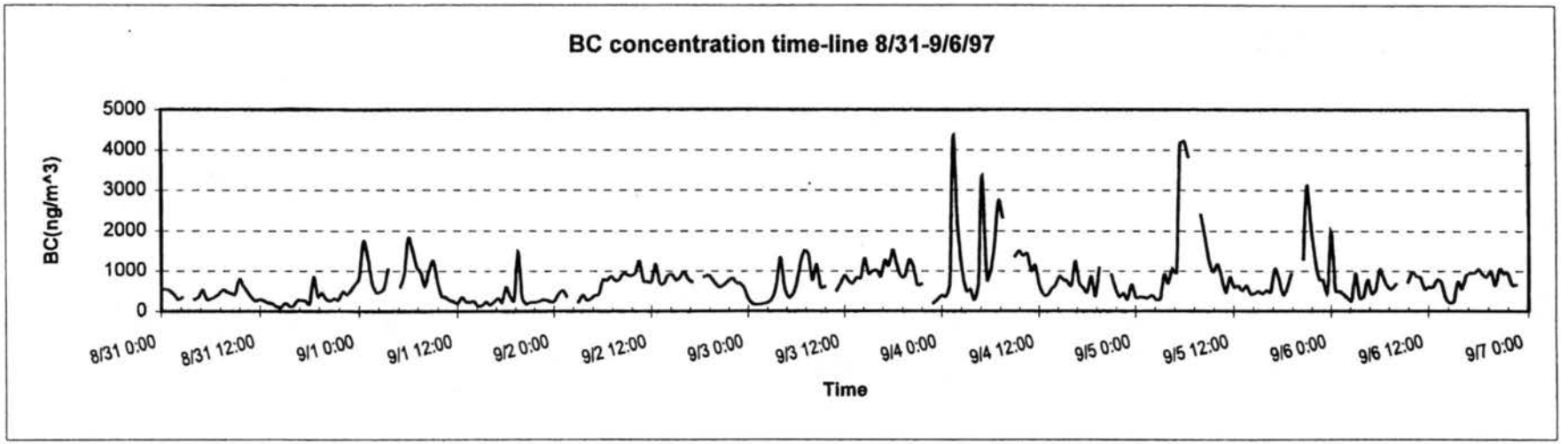

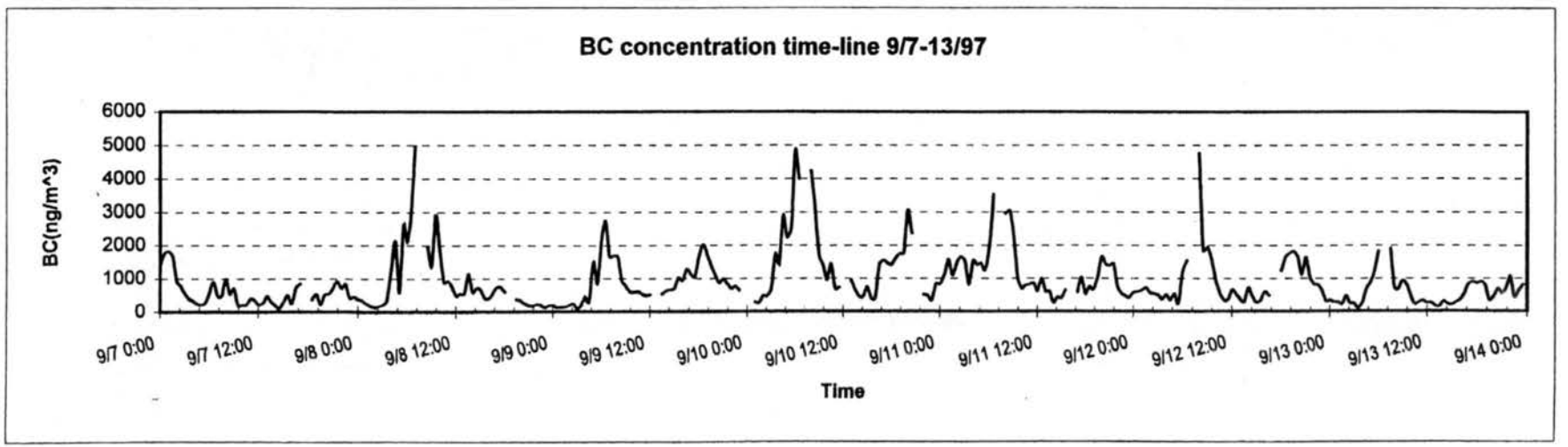

Figure G.8 BC concentration time-lines

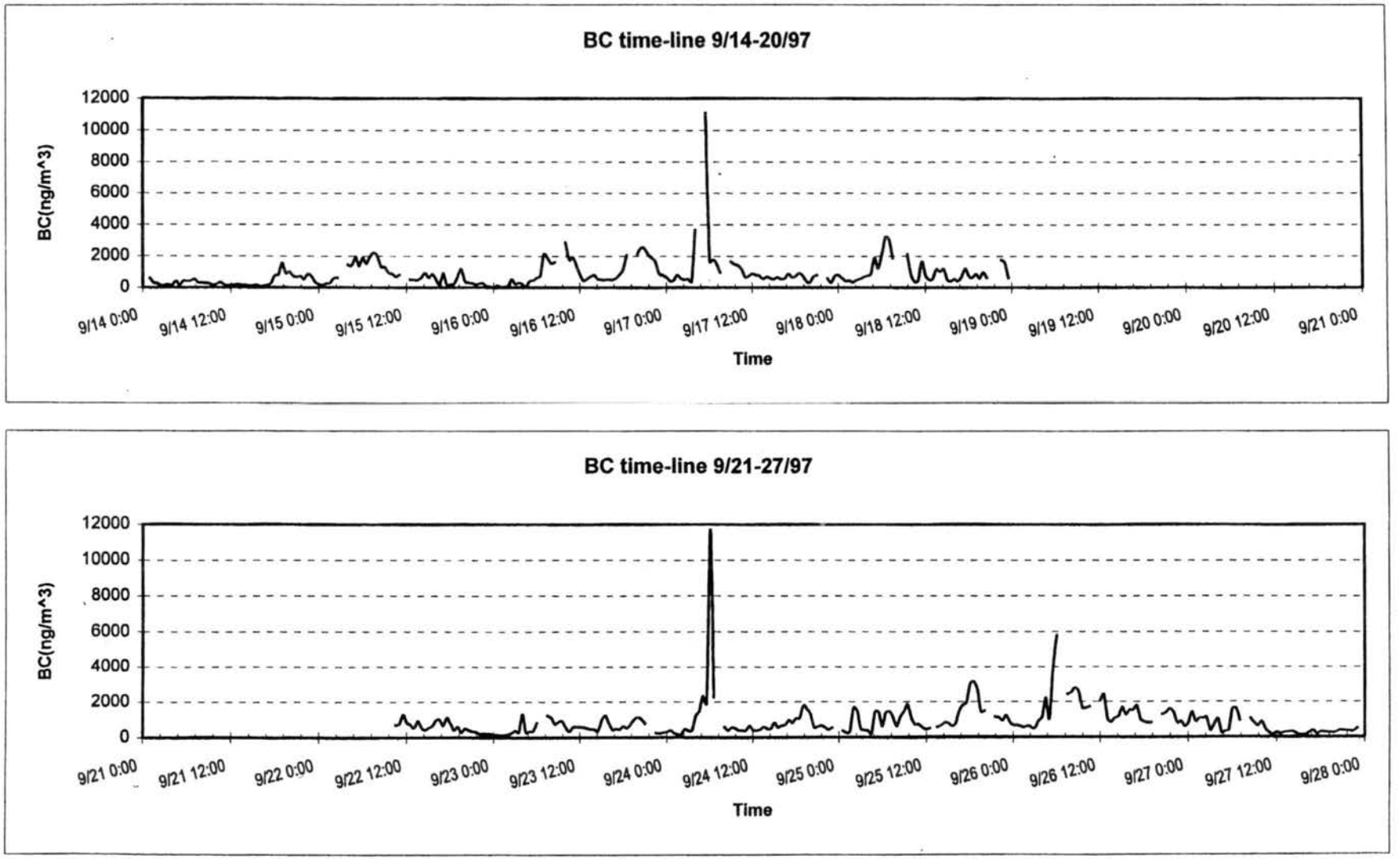

Figure G.9 BC concentration time-lines

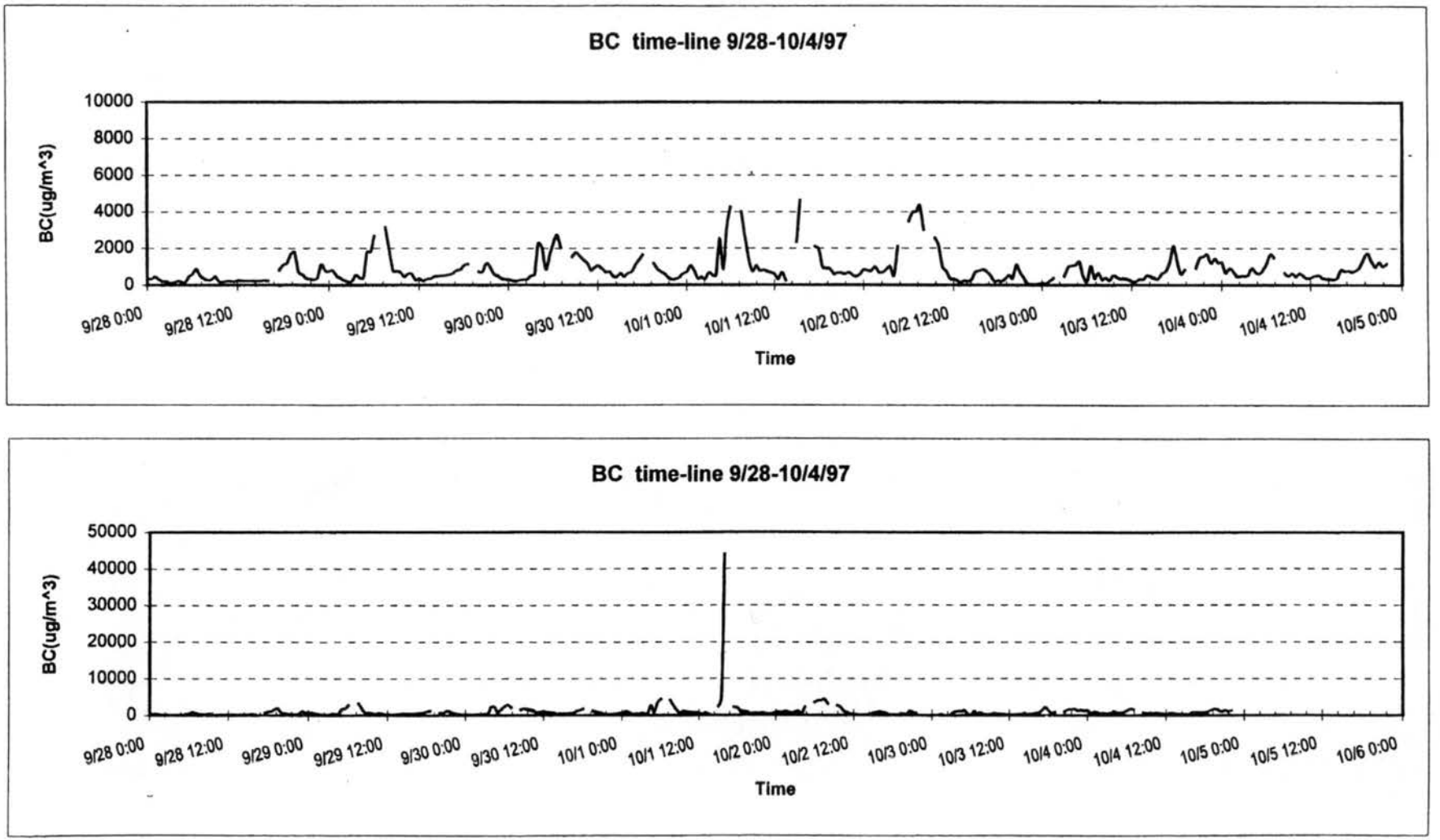

Figure G.10 BC concentration time-lines

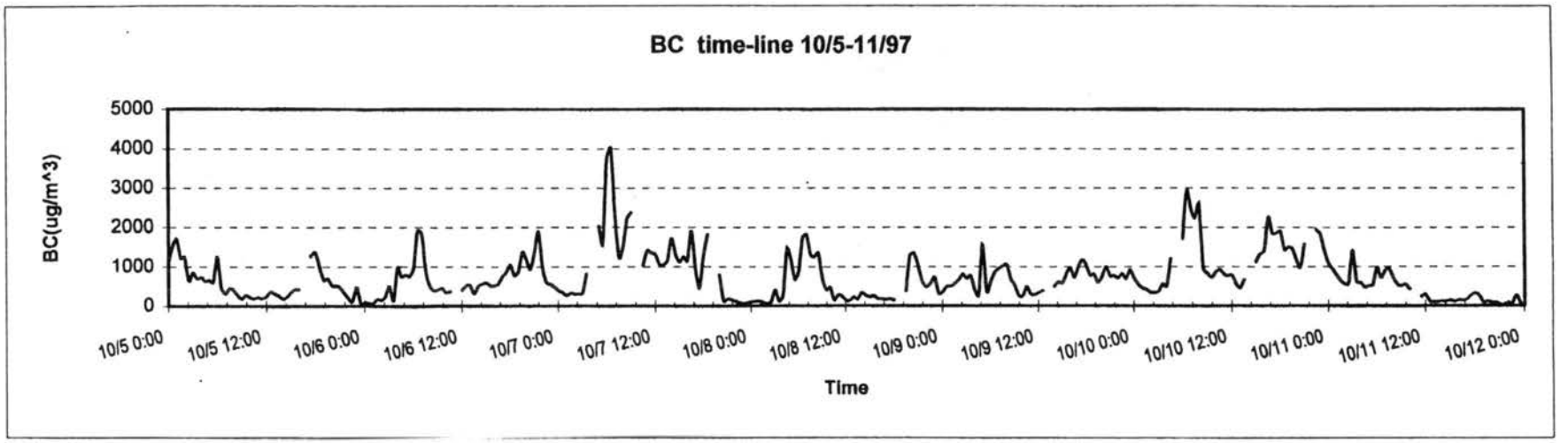

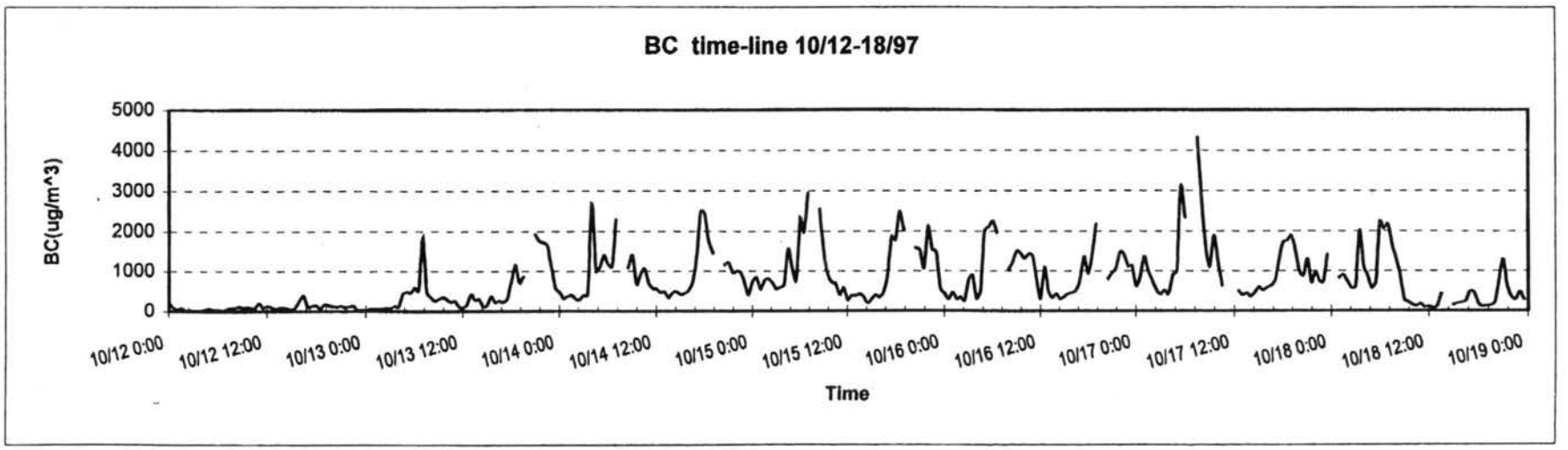

Figure G.11 BC concentration time-lines

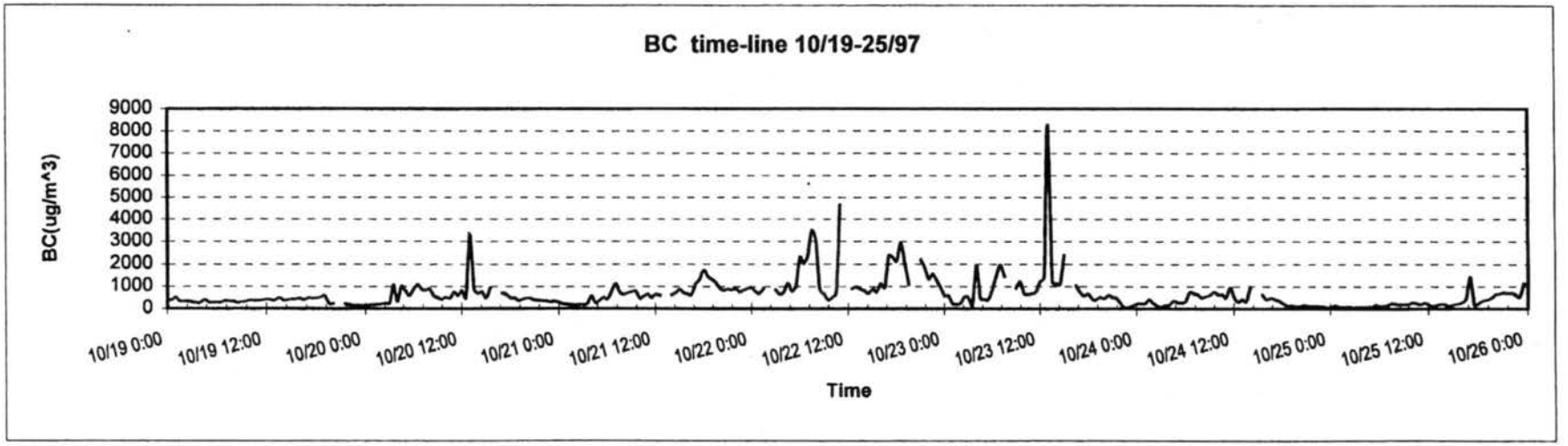

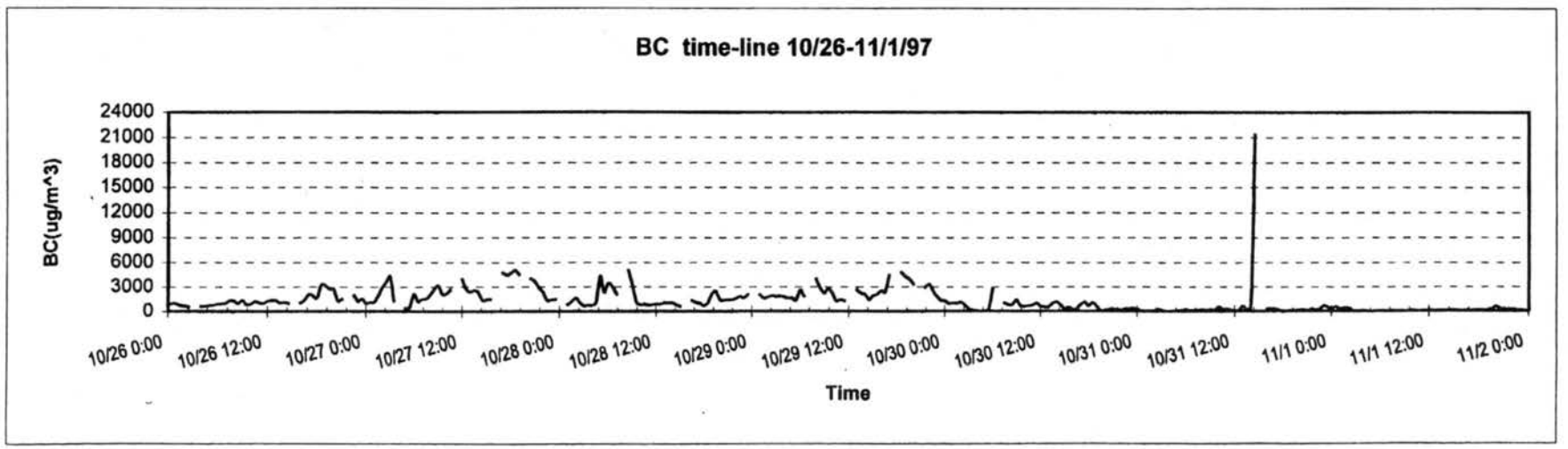

Figure G.12 BC concentration time-lines